UNIVERSITAT ROVIRA I VIRGILI

Departament de Química Física i Inorgànica

NEW CHIRAL LIGANDS IN ASYMMETRIC CATALYSIS. APPLICATION IN STABILIZATION OF METAL NANOPARTICLES

Memòria presentada per

M. Rosa Axet Martí

Tarragona, Desembre 2005

La Prof. Dra. CARMEN CLAVER CABRERO, Catedràtica del Departament de Química Física i Inorgànica de la Facultat de Química de la Universitat Rovira i Virgili i el Prof. Dr. SERGIO CASTILLÓN MIRANDA, Catedràtic del Departament de Química Analítica i Química Orgànica de la Facultat de Química de la Universitat Rovira i Virgili,

CERTIFIQUEN:

Que la memòria que porta per títol "New chiral ligands in asymmetric catalysis. Application in stabilization of metal nanoparticles", que presenta M. Rosa Axet Martí per a obtenir el grau de Doctora en Química, ha estat realitzada sota la nostra direcció en els corresponents departaments de la Universitat Rovira i Virgili.

Tarragona, Desembre de 2005

Prof. Dra. Carmen Claver Cabrero Prof. Dr. Sergio Castillón Miranda

Contents

Chapter 1

General Introduction

The demand for chiral compounds in pharmaceuticals, agrochemicals and the flavours and fragrance industry, has encouraged the development of methods for synthesizing such compounds. Three basic strategies make it possible to produce enantiomerically pure compounds: a) the use of naturally occurring optically active molecules as building blocks, b) optical resolution via resolving agents and c) asymmetric synthesis. Asymmetric synthesis is commonly used to prepare chiral compounds. The basic principle of this method is to form a new chiral center under the influence of a chiral group. Asymmetric catalysis is part of this preparative method and makes it possible to transform an achiral substrate into a chiral product using catalytic amounts of the complexes which contain the chiral information. Homogeneous catalysis involves a catalytic system in which the substrates for a reaction and the catalyst components are brought together in one phase, most often the liquid phase, where the catalyst is usually a metal complex modified with ligands. So ligand effects are extremely important in homogeneous catalysis by metal complexes. In enantioselective homogeneous metal catalysis the design of new ligands is, perhaps, the most crucial step to achieve the highest levels of reactivity and selectivity.

1.1 Carbohydrate derivative ligands in asymmetric catalysts

Carbohydrates are prominent members of the "chiral pool". They have been widely used as chiral templates for synthesizing enantiomerically pure organic compounds through stereoselective transformations (the *chiron* approach).[1, 2] Carbohydrates have been used as synthons to obtain chiral ligands for catalysis although this issue had been explored very little until very recently.[3-5] Because of the high degree of functionalisation of the carbohydrates and the presence of several stereogenic centers, these compounds are an attractive starting materials for synthesizing chiral ligands. The presence of the hydroxyl groups make it possible to easily introduce phosphorus moieties such as phosphinites, phosphonites or phosphites. Since the first ligands derived from carbohydrates were reported in the 1970s,[6-8]

much effort has been focused on this area. Ligands derived from carbohydrates have been successfully applied to a variety of catalytic reactions.[3-5]

The most frequently studied reaction is, perhaps, asymmetric hydrogenation. Phosphine ligands synthesised from carbohydrates, which are the most common ligands used in asymmetric hydrogenation, are mainly DIOP derivatives, phospholanes (related to DUPHOS) or carbohydrate-based ligands. Another successful family of carbohydrate derivative ligands applied in asymmetric hydrogenation is phosphinite ligands. This sort of ligands have a pyranoside backbone, are derived from inexpensive D-glucose, and are one of the most studied phosphinite ligands. Diphosphinite ligands with a furanoside backbone, with C_1- and C_2-symmetry, have been used as ligands in asymmetric hydrogenation showing excellent results.[9-15] Other kinds of ligands with a carbohydrate backbone — phosphoroamidite, S-donor and other heterodonor ligands, such as phosphine-phosphite or phosphine-phosphoroamidite— have also been successfully applied to this reaction.[3-5]

The asymmetric hydroformylation reaction has also been studied using carbohydrate derivative ligands. High enantioselectivities were obtained in the asymmetric hydroformylation of various substrates with a series of tunable furanoside diphosphite ligands synthesised in our group, which are among the best reported in this reaction. Diphosphinite ligands with a pyranoside backbone were also applied to rhodium-catalysed asymmetric hydroformylation showing moderate to good enantioselectivities. Carbohydrate derivative ligands have been successfully used in other catalytic reactions, such as asymmetric allylic substitution, asymmetric 1,4- and 1,2-addition and the asymmetric Heck reaction, among others.[3-5]

Concerning the research carried out in our laboratories, series of carbohydrate derivative ligands, with C_1-symmetry and C_2-symmetry, have been developed. These ligands make it possible to introduce several modifications and systematically study how the electronic and steric properties, and the configuration of the stereocenters affect the catalysis. (Figure 1.1).

The most studied ligands are those with a furanoside structure and C_1-symmetry, which have been applied to a variety of catalytic reactions. Recently, a new series of diphosphinite ligands with C_2-symmetry has been synthesised in our group. These ligands can also be easily modulated by introducing various phosphorus moieties or substituents into the furanoside ring or changing the configuration of some of the stereocenters (Figure 1.1). These diphosphinite ligands have been successfully applied to the asymmetric hydrogenation of prochiral olefins.[16]

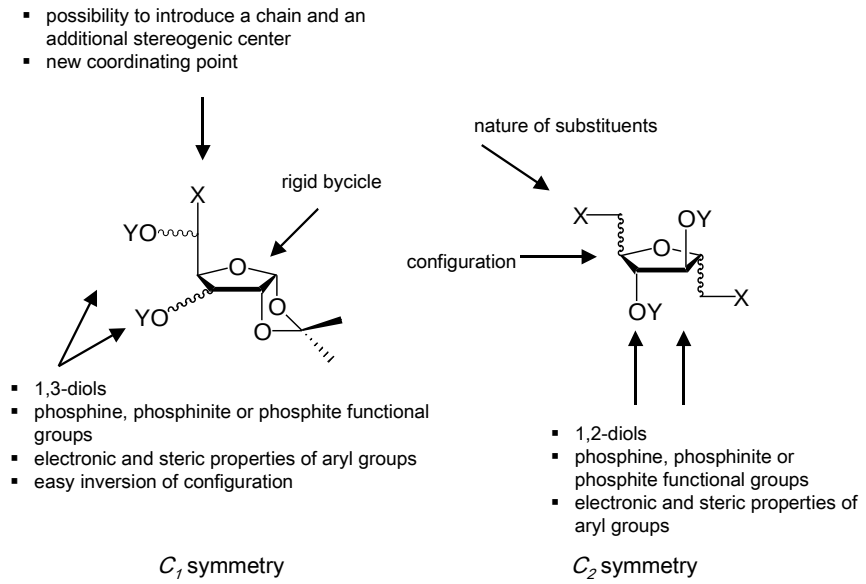

Figure 1.1. Possible modifications in ligands with a furanoside backbone

Figure 1.2 summarizes the best results obtained when these ligands have been applied to such catalytic reactions as asymmetric hydrogenation, asymmetric hydroformylation, palladium-allylic alkylation and copper-catalysed asymmetric 1,4-addition. The most studied reaction with these ligands is the asymmetric hydrogenation reaction. Phosphines,[17] phosphites,[18-20] phosphine-phospite[21] or phosphinite[16, 22] ligands and heterodonor ligands such as thioether-phosphite ligands[23] have been proved to be efficient ligands in this reaction (see Figure 1.2). A series of diphosphite ligands (for instance, ligands **9d** and **10c**, Figure 1.2) derived from D-glucose have provided excellent enantioselectivities in rhodium-

catalysed asymmetric hydroformylation.[18, 19, 24, 25] Other reactions such as palladium-allylic alkylation[20, 26-29] and copper-catalysed asymmetric 1,4-addition[30-37] have been studied with various carbohydrate derivative ligands with excellent results.

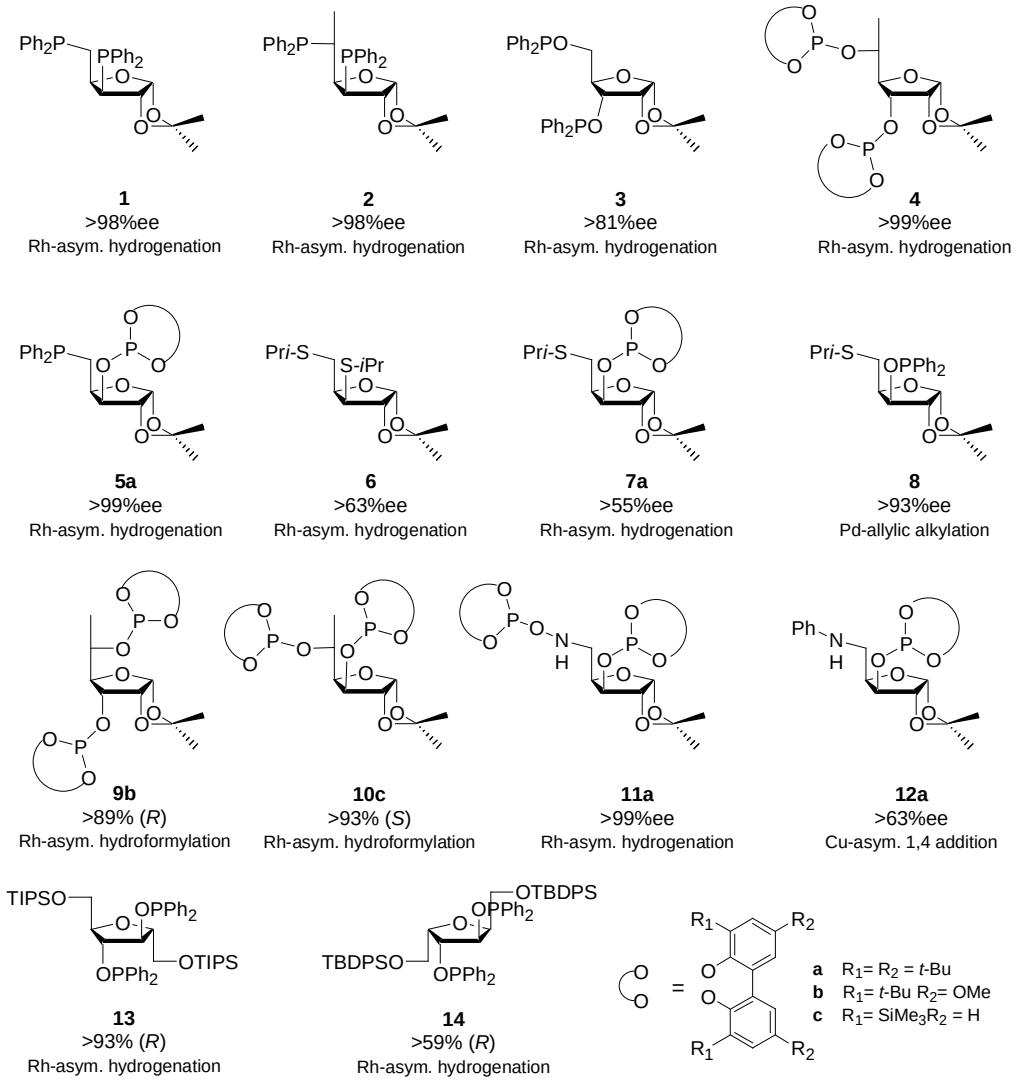

Figure 1.2. Enantioselectivities obtained in various catalytic reactions with tunable ligands derived from carbohydrates[3, 5]

As has been mentioned above, these compounds, most of them with C_1-symmetry, xylose and glucose derivative have been successfully applied as ligands in metal-catalysed asymmetric reactions. However, C_2-symmetry ligands have been much less studied. In this context, one of the aims of this thesis is to synthesize new carbohydrate derivative ligands with C_2-symmetry and apply them to rhodium-catalysed asymmetric hydroformylation and hydrogenation reactions.

The configuration of the sterocenters and the substituents in the tetrahydrofuran ring in ligands **13** and **14** have an important effect on the enantioselectivity in the rhodium-catalysed asymmetric hydrogenation of enamidoesters. Therefore, we decided to synthesise a new series of C_2-symmetry diphosphite ligands, **15** and **16** (Figure 1.3), with the same backbone as the previously reported diphosphinites (see Figure 1.2, ligands **13** and **14**) in order to test whether a similar effect is also produced in the hydroformylation reaction with rhodium-diphosphite catalytic systems. Diphosphite ligands **15** and **16** have been synthesised from D-glucosamine and D-glucitol, respectively. For comparative purposes diphosphite ligands **17**, without substituents in the tetrahydrofuran ring, have also been prepared.

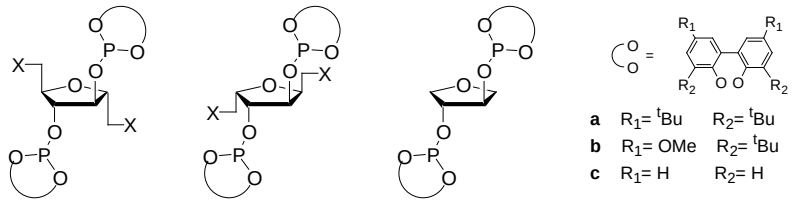

15 X= OTBDPS
15' X= H

16 X= OTBDPS
16' X= H

17

Figure 1.3. New diphosphite ligands derived from carbohydrates

1.2 Metal nanoparticles in catalysis

Interest in the catalytic properties of transition metal colloids has recently begun to increase. This is due to the very large specific surface area of the metal nanoparticles, which means that a large number of metal atoms are available to the

substrates.[38] Metal nanoparticles have been proven to be efficient and selective catalysts for reactions which are also catalysed by molecular complexes such as olefin hydrogenation or C-C coupling reactions. They can also be used for reactions which are not catalysed, or poorly catalysed, by molecular species such as aromatic hydrocarbons.[38-44] Recently, metal nanoparticles have been applied to enantioselective catalysts for reactions such as hydrogenation[45-50] or allylic alkylation.[51]

Palladium nanoparticles synthesised by the organometallic approach[52, 53] have been applied to the palladium-catalysed asymmetric allylic alkylation of rac-3-acetoxy-1,3-diphenyl-1-propene with dimethyl malonate.[51] They were synthesised by decomposing $[Pd_2(dba)_3]$ by H_2 (3 bar) at room temperature in THF in the presence of diphosphite ligand **18** (Figure 1.4). The application of these palladium nanoparticles in this reaction led to an enantiomeric excess of >95% in the product with high kinetic resolution in the substrate (89% ee in the remaining substrate).

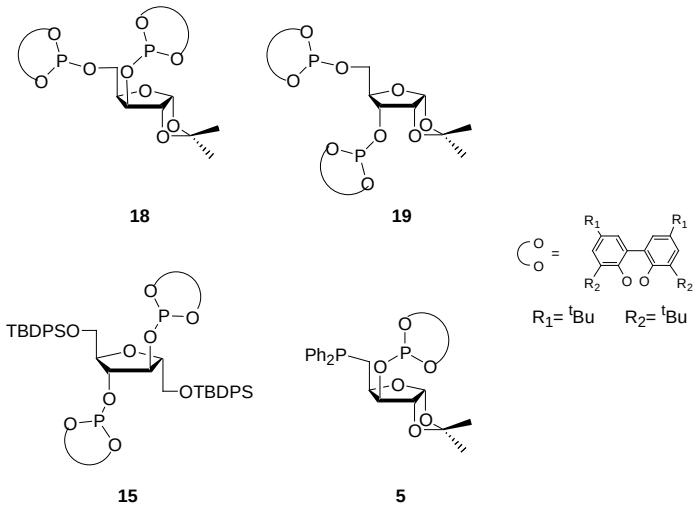

Figure 1.4. Ligands derived from carbohydrates

In this context we decided to apply other carbohydrate derivative ligands to stabilise palladium nanoparticles (Figure 1.4). Palladium nanoparticles are prepared with ligands **5**, **15**, and **19** (Figure 1.4), in order to apply them as the catalyst in

the asymmetric allylic alkylation reaction. We extended this method to other metals such as ruthenium and rhodium, the nanoparticles of which were synthesised in the presence of diphosphite **18** and **15**.

1.3 Scope and outline of the thesis

This thesis deals with the development and application of diphosphite ligands derived from carbohydrates to rhodium-catalysed asymmetric hydroformylation and hydrogenation reactions. The use of various carbohydrate derivative ligands as stabilisers of metal nanoparticles is also studied.

The synthesis and the characterisation of the series of diphosphite ligands **15**-**17** is described in Chapter 2. The results of the asymmetric hydroformylation of styrene and related vinyl arenes is also described. High pressure NMR studies of $[RhH(CO)_2(L)]$ (L:diphosphite) under catalytic conditions reveal detailed information about the coordination behaviour of these diphosphite ligands. The respective cationic rhodium complexes of diphosphite ligands are prepared and characterised to be used in the hydrogenation of methyl acetamidoacrylate.

Chapter 3 discusses the use of diphosphite chiral ligands in the rhodium-catalysed hydroformylation of allylbenzene and propenylbenzene. The hydroformylation of these substrates, easily available from biomass, enables the facile synthesis of aldehydes that are useful in the perfume and pharmaceutical industry.

Chapter 4 describes the novel application of carbohydrate derivative ligands as stabilisers of metal nanoparticles. Rhodium, platinum and ruthenium nanoparticles are prepared by the organometallic approach.

1.6 References

[1] S. Hanessian, *Total Synthesis of Natural Products: The Chiron Approach*, Pergamon Press., Oxford, **1983**.

[2] K. Totani, K. I. Takao, K. I. Tadano, *Synlett* **2004**, 2066.

[3] S. Castillón, C. Claver, Y. Díaz, *Chem. Soc. Rev.* **2005**, *34*, 702.

[4] M. Diéguez, O. Pàmies, C. Claver, *Chem. Rev.* **2004**, *104*, 3189.
[5] M. Diéguez, O. Pàmies, A. Ruiz, Y. Diaz, S. Castillón, C. Claver, *Coord. Chem. Rev.* **2004**, *248*, 2165.
[6] R. Jackson, D. J. Thompson, *J. Organomet. Chem.* **1978**, *159*.
[7] W. R. Cullen, Y. Sugi, *Tetrahedron Lett.* **1978**, *19*, 1635.
[8] G. Descotes, D. Lafont, D. Sinou, *J. Organomet. Chem.* **1978**, *150*.
[9] T. A. Ayers, T. V. RajanBabu, *U.S. Patent 5510507* **1996**.
[10] T. V. RajanBabu, T. A. Ayers, A. L. Casalnuovo, *J. Am. Chem. Soc.* **1994**, *116*, 4101.
[11] T. V. RajanBabu, T. A. Ayers, G. A. Halliday, K. K. You, J. C. Calabrese, *J. Org. Chem.* **1997**, *62*, 6012.
[12] R. Selke, *React. Kinet. Catal. Lett.* **1979**, *10*, 135.
[13] R. Selke, *J. Organomet. Chem.* **1989**, *370*, 249.
[14] R. Selke, H. Pracejus, *J. Mol. Catal.* **1986**, *37*, 213.
[15] R. Selke, M. Schwarze, H. Baudisch, I. Grassert, M. Michalik, G. Oehme, N. Stoll, B. Costisella, *J. Mol. Catal.* **1993**, *84*, 223.
[16] M. Aghmiz, A. Aghmiz, Y. Diaz, A. Masdeu-Bulto, C. Claver, S. Castillón, *J. Org. Chem.* **2004**, *69*, 7502.
[17] M. Diéguez, O. Pàmies, A. Ruiz, S. Castillón, C. Claver, *Tetrahedron: Asymmetry* **2000**, *11*, 4701.
[18] M. Diéguez, O. Pàmies, A. Ruiz, C. Claver, *New J. Chem.* **2002**, *26*, 827.
[19] O. Pàmies, G. Net, A. Ruiz, C. Claver, *Tetrahedron: Asymmetry* **2000**, *11*, 1097.
[20] M. Diéguez, A. Ruiz, C. Claver, *J. Org. Chem.* **2002**, *67*, 3796.
[21] M. Diéguez, O. Pàmies, G. Net, A. Ruiz, C. Claver, *Tetrahedron: Asymmetry* **2001**, *12*, 3441.
[22] E. Guimet, M. Diéguez, A. Ruiz, C. Claver, *Tetrahedron: Asymmetry* **2004**, *15*, 2247.
[23] E. Guimet, M. Diéguez, A. Ruiz, C. Claver, *J. Chem. Soc., Dalton Trans.* **2005**, 2557.
[24] M. Diéguez, O. Pàmies, A. Ruiz, S. Castillón, C. Claver, *Chem. Commun.* **2000**, 1607.
[25] M. Diéguez, O. Pàmies, A. Ruiz, C. Claver, S. Castillón, *Chem. Eur. J.* **2001**, *7*, 3086.
[26] E. Guimet, M. Diéguez, A. Ruiz, C. Claver, *Inorg. Chim. Acta* **2005**, *358*, 3824.
[27] M. Diéguez, O. Pàmies, C. Claver, *Adv. Synth. Catal.* **2005**, *347*, 1257.
[28] O. Pàmies, G. P. F. van Strijdonck, M. Diéguez, S. Deerenberg, G. Net, A. Ruiz, C. Claver, P. C. J. Kamer, P. van Leeuwen, *J. Org. Chem.* **2001**, *66*, 8867.
[29] M. Diéguez, S. Jansat, M. Gomez, A. Ruiz, G. Muller, C. Claver, *Chem. Commun.* **2001**, 1132.
[30] E. Guimet, M. Diéguez, A. Ruiz, C. Claver, *Tetrahedron: Asymmetry* **2005**, *16*, 2161.
[31] O. Pàmies, G. Net, A. Ruiz, C. Claver, *Tetrahedron: Asymmetry* **1999**, *10*, 2007.

[32] M. Diéguez, S. Deerenberg, O. Pàmies, C. Claver, P. van Leeuwen, P. Kamer, *Tetrahedron: Asymmetry* **2000**, *11*, 3161.

[33] O. Pàmies, M. Diéguez, G. Net, A. Ruiz, C. Claver, *Tetrahedron: Asymmetry* **2000**, *11*, 4377.

[34] O. Pàmies, G. Net, A. Ruiz, C. Claver, S. Woodward, *Tetrahedron: Asymmetry* **2000**, *11*, 871.

[35] M. Diéguez, A. Ruiz, C. Claver, *Tetrahedron: Asymmetry* **2001**, *12*, 2861.

[36] M. Diéguez, A. Ruiz, C. Claver, *Tetrahedron: Asymmetry* **2001**, *12*, 2895.

[37] M. Diéguez, O. Pàmies, G. Net, A. Ruiz, C. Claver, *J. Mol. Catal. A: Chem.* **2002**, *185*, 11.

[38] A. Roucoux, J. Schulz, H. Patin, *Chem. Rev.* **2002**, *102*, 3757.

[39] J. D. Aiken, R. G. Finke, *J. Am. Chem. Soc.* **1999**, *121*, 8803.

[40] J. D. Aiken III, R. G. Finke, *J. Mol. Catal. A: Chem.* **1999**, *145*, 1.

[41] M. A. El-Sayed, *Acc. Chem. Res.* **2001**, *34*, 257.

[42] H. Bonnemann, R. M. Richards, *Eur. J. Inorg. Chem.* **2001**, 2455.

[43] J. Dupont, G. S. Fonseca, A. P. Umpierre, P. F. P. Fichtner, S. R. Teixeira, *J. Am. Chem. Soc.* **2002**, *124*, 4228.

[44] J. A. Widegren, R. G. Finke, *J. Mol. Catal. A: Chem.* **2003**, *191*, 187.

[45] J. U. Kohler, J. S. Bradley, *Langmuir* **1998**, *14*, 2730.

[46] H. Bonnemann, G. A. Braun, *Chem. Eur. J.* **1997**, *3*, 1200.

[47] J. U. Kohler, J. S. Bradley, *Catal. Lett.* **1997**, *45*, 203.

[48] H. Bonnemann, G. A. Braun, *Angew. Chem. Int. Ed.* **1996**, *35*, 1992.

[49] M. Studer, H. U. Blaser, C. Exner, *Adv. Synth. Catal.* **2003**, *345*, 45.

[50] X. B. Zuo, H. F. Liu, D. W. Guo, X. Z. Yang, *Tetrahedron* **1999**, *55*, 7787.

[51] S. Jansat, M. Gomez, K. Philippot, G. Muller, E. Guiu, C. Claver, S. Castillon, B. Chaudret, *J. Am. Chem. Soc.* **2004**, *126*, 1592.

[52] K. Philippot, B. Chaudret, *C. R. Chimie* **2003**, *6*, 1019.

[53] B. Chaudret, *C. R. Physique* **2005**, *6*, 117.

Chapter 2

Carbohydrate derivative diphosphite ligands in asymmetric catalysis

Abstract. *The synthesis of new modular diphosphite chiral ligands with C_2-symmetry and carbohydrate backbone* ***74-76*** *is reported. Rhodium complexes [Rh(cod)(L)]BF_4 (L:* ***74-76****) have also been synthesised. The application of this new series of diphosphite ligands in asymmetric rhodium-catalysed hydroformylation of prochiral olefins provides high regioselectivities and moderate enantioselectivities. The application in rhodium-catalysed hydrogenation of methyl acetamidoacrylate with rhodium complexes provides low activities and low enantioselectivities. In both processes the asymmetric induction strongly depends on the structure of the ligand, behaviour that had been previously observed in diphosphinite ligands with the same carbohydrate backbone.*

2.1 Introduction

2.1.1 Carbohydrate derivative ligands in asymmetric catalysts

In enantioselective homogeneous metal catalysis the design of new ligands is, perhaps, the most crucial step to achieve highest levels of reactivity and selectivity. One of the simplest ways of obtaining chiral ligands is to transform or derivatize natural chiral compounds, thus making optical-resolution procedures unnecessary. In recent decades, carbohydrates have been widely used as chiral synthons for the synthesis of enantiomerically pure compounds.[1] A variety of structures can be obtained from carbohydrates, mainly pyranoses and furanoses, through well-established procedures (Scheme 2.1). Because hydroxyl groups are present, phosphinite, phosphonite, and phosphite functional groups are easily introduced so that they can be used as ligands in metal-catalysed reactions.[2, 3] Carbohydrate derivative ligands have been used in a wide range of catalytic asymmetric reactions with excellent results. This kind of ligands have many advantages: they are readily available, they are highly functionalised, and they have several stereogenic centers. These properties make it possible to synthesise a series of chiral ligands -the electronic and steric factors of which can be systematically varied by introducing different functionalities. These series can be screened in the search for high activities and selectivities in many catalytic reactions. One of the limitations of the ligands prepared from the chiral pool is that only one enantiomer is accessible. However, this limitation can be partially overcome by using the so-called pseudo-enantiomer ligands.[4-6]

Because of the presence of hydroxyl groups in the carbohydrate skeleton, phosphinite, phosphonite and phosphite ligands are the most common ligands synthesised from carbohydrates. However, ligands containing other phosphorus moieties, such as phospines and phosphoroamidites, or other donor atoms such as sulfur or nitrogen, have also been reported. All these ligands were synthesised from various sugars including xylose, glucose, galactose, mannitol and trehalose among others.[4-6]

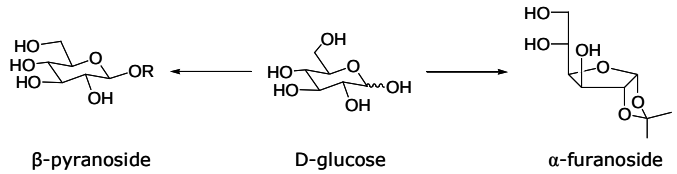

Scheme 2.1. Pyranoside and furanoside structures obtained from D-glucose

The first chiral ligands derived from carbohydrates were reported in the 1970s by Sinou and Descotes[7] who synthesised monophosphines **1** and **2** and diphosphine **3** (Figure 2.1) from D-xylose and D-glucose. They were all tested in asymmetric rhodium-catalysed hydrogenation, they obtained an enantiomeric excess of 85%with Rh/**3** catalytic system in the hydrogenation of α-acetamidocinnamic and α-actamidoacrylic acids. In the same year, Cullen[8] and Thompson[9] reported the first diphosphinite derived from glucose with a pyranoid skeleton **4**, and Thompson described the first diphosphinite derived from xylose with a furanoid skeleton **5** (Figure 2.1). They also studied the application of these ligands in asymmetric hydrogenation and their work led to a new family of ligands, which turned out to be highly efficient for chiral induction in several metal-catalysed processes.

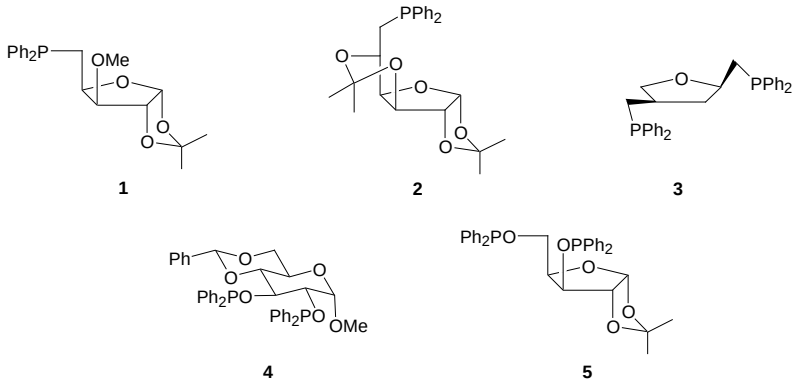

Figure 2.1. First chiral ligands prepared from carbohydrates

Ligands derived from carbohydrates have been applied to many homogeneous catalytic reactions. Asymmetric hydrogenation of different substrates, C=C or C=N double bonds, is the most studied reaction with this sort of ligands, mainly

bidentate phosphorus ligands. Asymmetric hydroformylation, allylic substitution and 1,4 addition reactions have also been widely studied with carbohydrate derivative ligands. The use of these ligands in such other asymmetric reactions as asymmetric 1,2 addition, the Heck reaction, hydroboration, hydrosilylation or cyclopropanation, has also been reported.[4-6]

2.1.2 Hydroformylation reaction

Hydroformylation is an important and extensively studied process for the functionalization of carbon-carbon bonds. In this process, alkenes are converted into aldehydes by reaction with CO/H_2 via the addition of a formyl group to the double carbon-carbon bond (Scheme 2.2).[10-16]

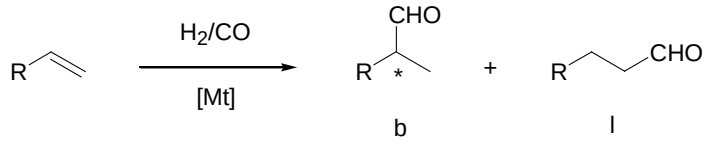

Scheme 2.2. Hydroformylation reaction

The regioselectivity of the reaction is the ratio between the branched (b) and linear (l) aldehydes. Linear aldehydes are the desired products in the hydroformylation of long chain alkenes, because they make it possible to synthesise alcohols, which are used as intermediates for detergents and plasticizers.[10]

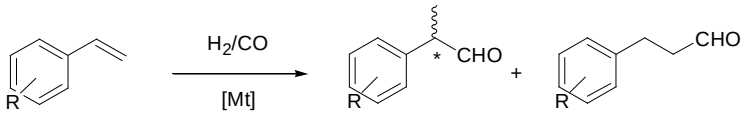

Scheme 2.3. Asymmetric hydroformylation of vinylarenes

In the asymmetric hydroformylation, however, the branched aldehydes are the product of interest.[11-13] Chiral aldehydes are important intermediates for the preparation of fine chemicals, such as flavours, fragrances, pharmaceuticals and agrochemicals.[11, 17, 18] Considerable attention has been paid to the

hydroformylation of vinylarenes (Scheme 2.3): the branched aldehyde (*S*)-2-phenylpropanal is of great interest because it is the key step in a straightforward route to synthesising enantiomerically pure non-steroidal anti-inflammatory drugs (Figure 2.2).

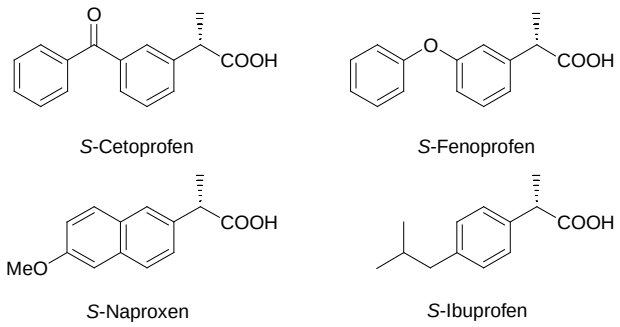

Figure 2.2. Enantiomerically anti-inflammatory drugs produced via asymmetric hydroformylation

Mechanism

The accepted mechanism of the hydroformylation reaction of olefins is illustrated in Figure 2.3. It was proposed by Heck[19-21] and it corresponds to Wilkinson's so-called dissociative mechanism.[22-24]

The starting material, $[RhHCO(PPh_3)_3]$ **6**, under CO pressure forms the complexes **7ee** and **7ea**, the ligands of which are coordinated in equatorial-equatorial position (**ee**) or in equatorial-axial position (**ea**).

The dissociation of one equatorial ligand (L or CO) leads to the square planar complexes **8c** and **8t**, with phosphines in *cis* (c) or *trans* (t). The association of ethene give complexes **9**, which undergo a migratory insertion to give square-planar alkyl complexes **10**. Complex **10** can undergo β-hydride elimination which leads to isomerisation when alkenes higher than ethene are used, or it can react with CO to form trigonal bipyramidal complexes **11**. Thus, under low CO pressure more isomerisation may be expected. At low temperatures (<70ºC) and a sufficiently high CO pressure (>10 bar), the insertion reaction is usually irreversible

and so the regioselectivity of the hydroformylation of α-alkenes is determined at this point also. Acyl complexes **12** are formed by a second migratory insertion in complexes **11**. The acyl complexes can react with CO to give saturated acyl intermediates **13**, which have been observed spectroscopically, or they can react with H_2 to give the aldehyde and intermediates **8**. The reaction with H_2 involves an oxidative addition and a reductive elimination. Dirhodium species such as **14** are formed at low hydrogen and high rhodium concentrations and can be regenerated as active species with H_2.[25, 26]

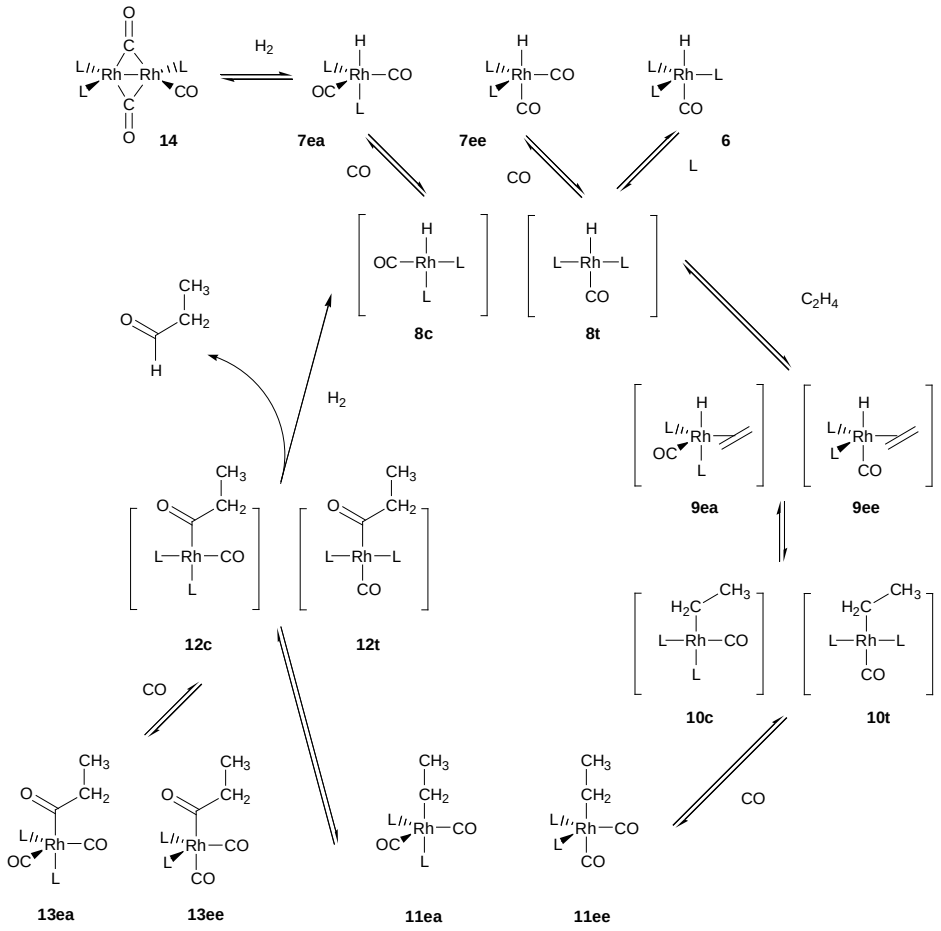

Figure 2.3. Simplified mechanism for the hydroformylation of ethene (L: PPh_3)[14]

Ever since the hydroformylation reaction was discovered in 1938 by Otto Roelen,[27, 28] who used cobalt carbonyl as catalyst, the process has been evolving even the asymmetric version. In the 1970s transition metal complexes based on rhodium and platinum were used as catalysts in asymmetric hydroformylation. The Pt/diphosphine catalyst yielded high enantioselectivities, but low chemo- and regioselectivities,[29, 30] while the Rh/diphosphine catalyst provided high activities and regioselectivities, but low enantioselectivities.[31]

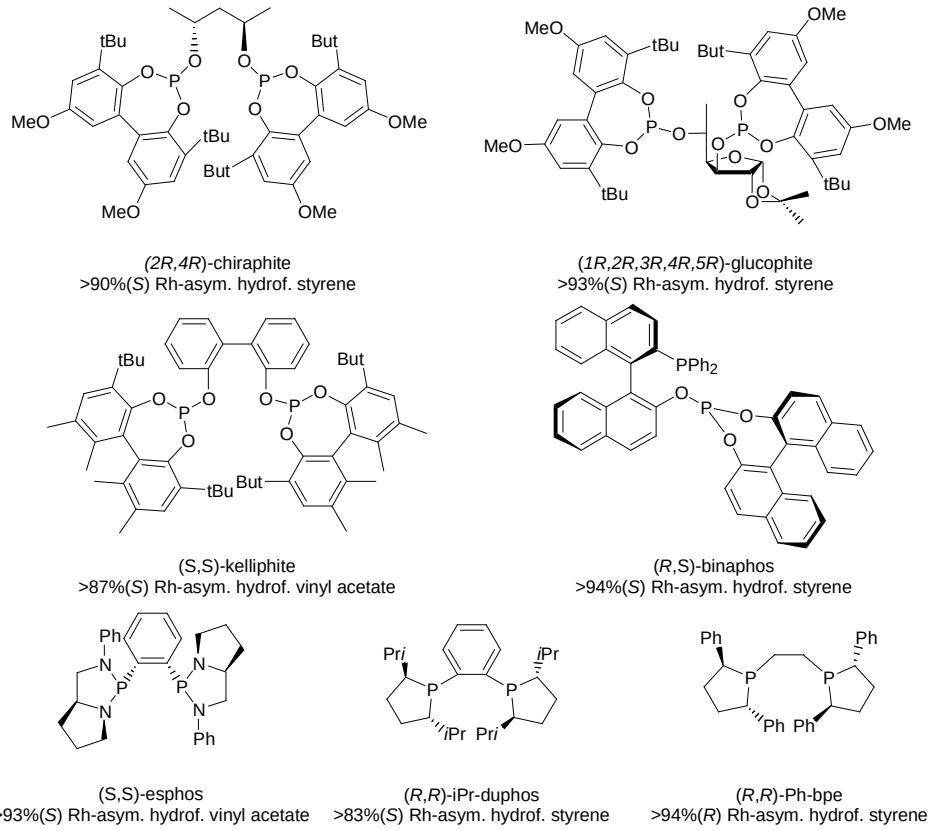

Figure 2.4. Chiral ligands that have been successfully applied in asymmetric hydroformylation reactions

In the last decade, Rh/diphosphite and Rh/phosphine-phosphite catalysts have shown high activities, regioselectivities and enantioselectivities. Results have been best with diphosphite ligands such as (2*R*,4*R*)-chiraphite,[32, 33] glucophite,[34-36] and

(*S*,*S*)-kelliphite,[37, 38] and phosphine-phosphite ligands, (*R*,*S*)-binaphos and related ligands.[39, 40] Recently, such other ligands as diazaphospholidine, (*S*,*S*)-esphos,[41, 42] and phospholanes, (R,R)-Me-duphos and (R,R)-iPr-bpe,[43] have been successfully applied to rhodium-catalysed asymmetric hydroformylation showing high enantioselectivities in various substrates (see Figure 2.4).

2.1.2.1 Diphosphite ligands in asymmetric hydroformylation

Chiral diphosphite ligands with C_2-symmetry

The first reports on asymmetric hydroformylation using diphosphite ligands revealed no asymmetric induction.[44] Takaya and co-workers, in 1992, reported enantioselectivities up to 50% in the asymmetric hydroformylation of vinyl acetate using chiral diphosphite ligands with a binaphthyl backbone.[45] In the same year, enantioselectivities up to 90% in the asymmetric hydroformylation of various alkenes were patented by Babin and Whiteker at Union Carbide, with diphosphite ligands **21a-c** derived from (2*R*,4*R*)-pentane-2,4-diol (Figure 2.5).[32] The results showed that bulky substituents at the *ortho*-positions of the biphenyl moieties (**21a**,**b**) led to better regio- and enantioselectivities than when there were no substituents (**21c**). The presence of methoxy groups in the *para*-positions of the biphenyl moieties **21b** always produced better enantioselectivities than those with *tert*-butyl groups in *para*-position **21a**.

Optically pure diols are useful building blocks for the synthesis of chiral diphosphite ligands. Ligands **15c**, **16c** and **17a**,**c** (Figure 2.5) were synthesised from commercially available optically pure 1,2 and 1,4 diols. These ligands were used in the asymmetric hydroformylation of styrene in mild conditions and the regioselectives were high (>95%) and enantioselectivities low (20% ee) with the most bulky diphosphite **17c**. The less bulky and more flexible diphosphites hardly produced enantioselectivity.[46]

van Leeuwen and co-workers studied how the length of the bridge of diphosphites **18a**, **19a-b**, **20a-b**, **21a-c** and **23b** affected in the hydroformylation reaction (Figure 2.5).[47] They also observed that bulky substituents at the *ortho*-positions of

the biphenyl moieties were necessary for obtaining better enantioselectivities, and the methoxy groups in *para*-positions of the biphenyl moieties enhanced the enantioselectivity (Table 2.1, entries 6 *vs*. 7). Because bulky substituents in the biphenyl moieties significantly affect the catalyst performance, they synthesised ligands based on 2,4-pentanediol **21** where the steric hindrance increased when bulky substituents **21d-m** were introduced.[33, 48] Bulky groups Si(*t*-Bu)$(CH_3)_2$ and Si$(CH_2CH_3)_3$ did not improve the enantiomeric excess. The steric bulk in the *ortho*-positions was optimal with the trimethylsilyl substituent **21d** (Table 2.1, entry 10).

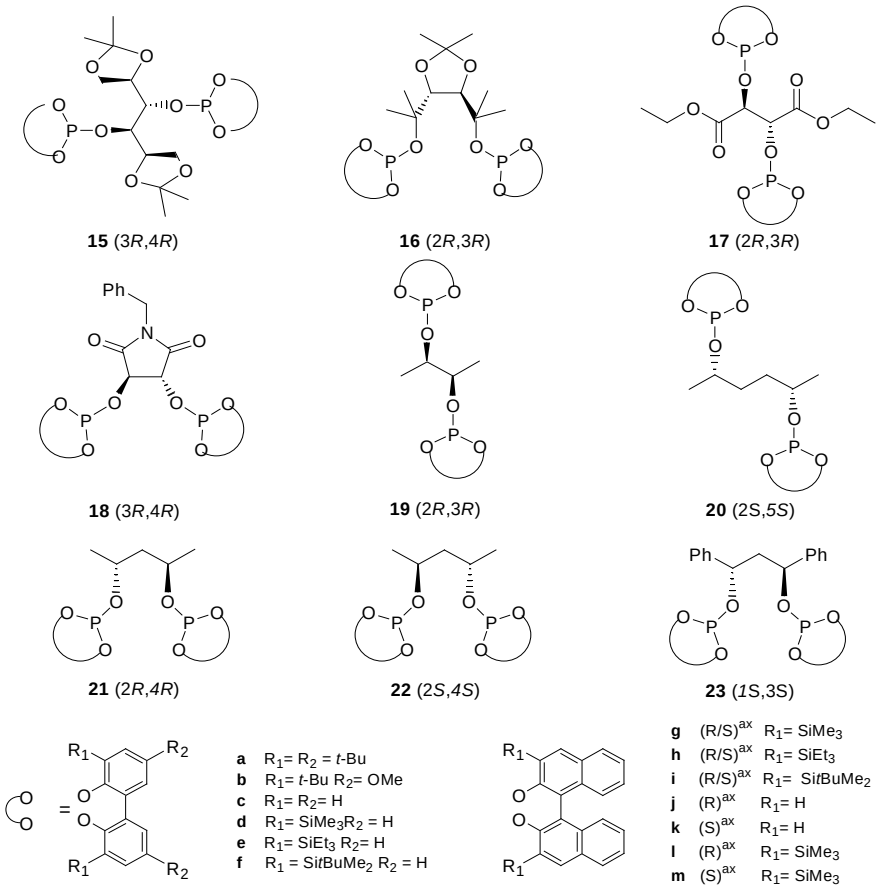

Figure 2.5. Chiral diphosphite ligands with C_2-symmetry

They found an interesting connection between the enantiomeric excess and the structure of the diphosphite. Enantiomeric excesses are highest for the backbones of the diphosphites based on (2*R*,4*R*)-pentane-2,4-diol, **21** and **23** (Table 2.1, entries 7 and 14), which form eight-membered rings in the catalyst. The enantioselectivities were low for the diphosphites based on (2*S*,5*S*)-hexane-2,5-diol **20**, which form nine-membered rings in the catalyst (Table 2.1, entry 5), and moderate for the backbones of the diphosphites based on (2*R*,3*R*)-butane-2,3-diol, **19**, which form seven-membered rings when coordinates to the rhodium (Table 2.1, entry 2). In most cases, when the ligands are based on (*R*,*R*) diols the (*S*)-aldehyde is predominantly formed. If the configuration is inverted at the chiral carbon atoms, C-2 and C-5 in the (2*S*,5*S*)-hexane-2,5-diol, the (*R*)-aldehyde is predominantly formed.

Table 2.1. Hydroformylation of styrene with chiral rhodium diphosphite catalysts[33, 47, 48]

Entry	Diphosphite	T (ºC)	TOF[b]	% Conversion[c]	% 2-phenyl propanal	% ee
1	**19a**	40	66	74	93	19 (*S*)
2	**19b**	40	177[d]	99	92	25 (*S*)
3	**19b**	25	31	40	93	34 (*S*)
4	**20a**	40	19	26	93	1 (*R*)
5	**20b**	40	19	26	92	7 (*R*)
6	**21a**	40	113	89	96	50 (*S*)
7	**21b**	40	207[d]	98	94	67 (*S*)
8	**21c**	40	117	81	80	11 (*R*)
9	**21d**	40	45	21	89	67 (*S*)
10	**21d**[e]	25	9	26[d]	93	87 (*S*)
11	**21g**	25	14	20	91	47 (*S*)
12	**21m**[e]	25	17	38	88	69 (*S*)
13	**23b**	40	165	99	90	47 (*S*)
14	**23b**	25	40	45	95	62 (*S*)

styrene: 13.3 mmol, CO/H_2=10 bar, styrene:Rh=421:1, P:Rh=2.5:1 [b]mol/molRh.h determined after 2h of reaction by GC, [c]of styrene after 5h., [d] after 1h of reaction, [e] styrene:Rh=1000:1, P:Rh=2.2:1 TOF mol/molRh.h determined after 1h of reaction by GC, conversion of styrene after 24 h.

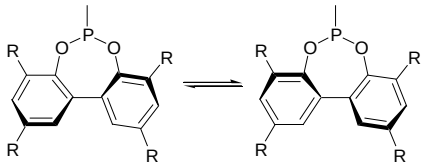

Figure 2.6. Atropoisomerism in biphenyl moieties

Diphosphite ligands containing biphenyl moieties have a low energy barrier for interconversion in atropoisomers, which could lead to the formation of several diastereomers (Figure 2.6). However, the rotation around the biphenyl axis of the diphosphite ligands containing bulky substituents in the biphenyl moieties is hindered. In the rhodium system with diphosphite ligands **21** it was observed that introducing chiral binaphthyl moieties instead of bulky substituted biphenyl led to similar results (Table 2.1, entries 7, 9 and 12). This indicated that the biphenyl moiety adopted one preferable configuration when coordinates to the rhodium.[14, 33]

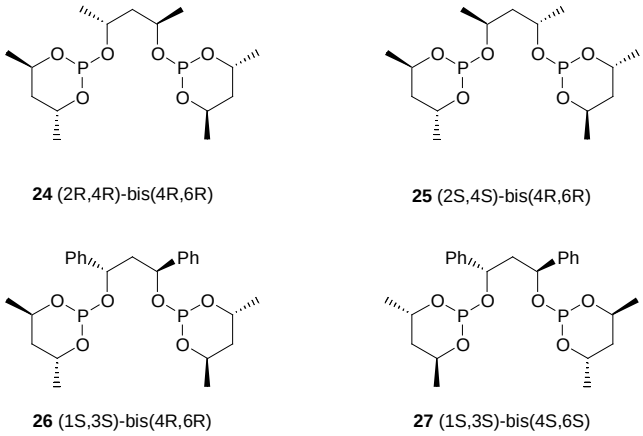

Figure 2.7. Diphosphite chiral ligands

Bakos et al. prepared ligands **24** to **27** (Figure 2.7).[49, 50] These ligands led to active rhodium systems, and are considerably affected by chiral cooperativity between the stereocenters. Enantioselectivities were no higher than 24%.[49] Ligands **28**-**31** (Figure 2.8) based on binaphthol were used in rhodium asymmetric

hydroformylation. These ligands have shown good regioselectivities in 2-phenylpropanal (up to 87%) and low-to-moderate enantioselectivities (up to 37% ee).[50, 51]

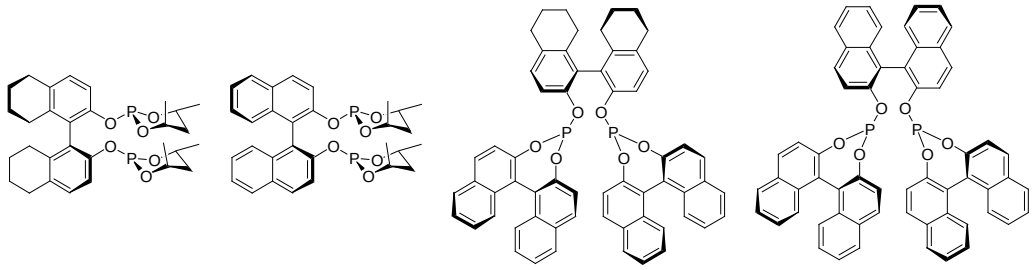

28a *S*-bis (4*R*,6*R*)
28b *R*-bis (4*R*,6*R*)

29a *S*-bis (4*R*,6*R*)
29b *R*-bis (4*R*,6*R*)

30a *S*-bis (*S*)
30b *R*-bis (*S*)

31a *S*-bis (*S*)
31b *R*-bis (*S*)

Figure 2.8. Diphosphite ligands based on binaphthol

Chiral diphosphite ligand **32** (Figure 2.9) which contains a spiro backbone in the bridge and forms a complex with an eight-membered ring, has also been used in the rhodium-catalysed asymmetric hydroformylation of styrene and related vinyl arenes. Regioselectivities were high and enantioselectivities moderate to good enantioselectivities (up to 70%).[52] Bayón et al. [53] reported the first example of chiral macrocyclic diphosphite ligands **33** (Figure 2.9). They provided good enantioselectivities (up to 76%), but moderate regioselectivities to the branched aldehyde (up to 83%)

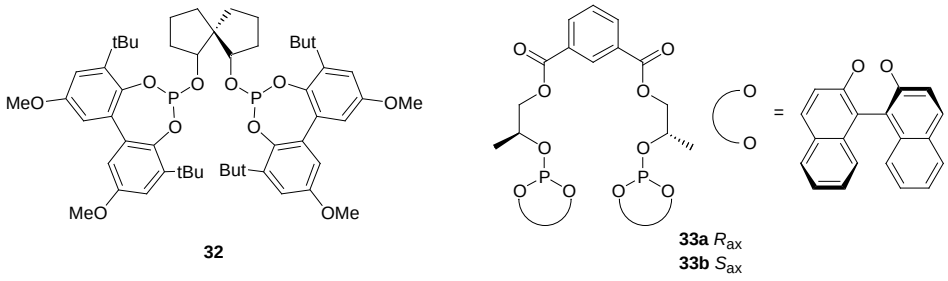

32

33a R_{ax}
33b S_{ax}

Figure 2.9. Diphosphite chiral ligands

Recently, the rhodium-catalysed hydroformylation of allyl cyanide and vinyl acetate with (*S,S*)-kelliphite **34** provided high enantioselectivities, up to 75% and 87%, respectively.[37, 38]

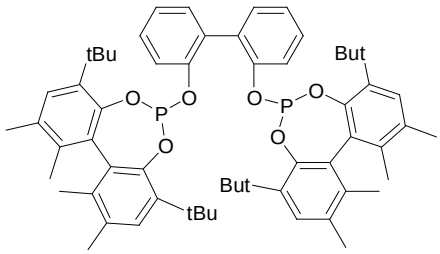

34

Figure 2.10. (*S*,*S*)-kelliphite diphosphite chiral ligand

Chiral diphosphite ligands derived from carbohydrates

Phosphite functional groups can be easily introduced into carbohydrate backbones because of the presence of hydroxyl groups. The first report in this field, by van Leeuwen et al. in 1995,[54] showed the potential of this type of backbone (providing enantioselectivities up to 65% in rhodium-catalysed hydroformylation of styrene). In 1998, Selke and co-workers tested a series of diphosphite ligands **35** (Figure 2.11), with a β-D-glucopyranoside backbone, in the rhodium-catalysed asymmetric hydroformylation of vinyl acetate, allyl acetate and *p*-methoxystyrene.[55] In general, regioselectivities in branched product were good (>90%) and enantioselectivities were low to moderate (up to 36%).

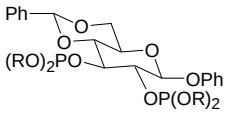

35

Figure 2.11. Diphosphite ligands with β-D-glucopyranoside backbone

Tunable furanoside diphosphite ligands **36**-**41** (Figure 2.12) derived from carbohydrates have been developed in our group, which have been successfully applied in rhodium-catalysed asymmetric hydroformylation.[34-36, 56] They have

shown excellent enantioselectivities (up to 93%) and regioselectivities (up to 98%) under mild conditions (Table 2.2). It has been found that a) a methyl substituents must be present in C-5 enantioselectivities are to be high (Table 2.2, entries 1 and 2 *vs*. entries 4 and 10), b) the enantioselectivity is influenced by a cooperative effect between stereocenters C-3 and C-5: ligands **38** and **41** provide better enantioselectivities than ligands **39** and **40** (Table 2.2, entries 4 and 10 *vs.* entries 6 and 8), c) the absolute configuration of the product is governed by the configuration of the stereogenic center C-3: ligands **36**, **38** and **40** gave (*S*)-2-phenylpropanal and ligands **37**, **39** and **41** gave (*R*)-2-phenylpropanal (Table 2.2, entries 1, 4 and 8 *vs*. entries 2, 6 and 10) and d) the substituents of the biphenyl moieties have an influence: when methoxy or trimethylsilyl groups are present enantioselectivities were better (Table 2.2, entries 3, 4 and 12).

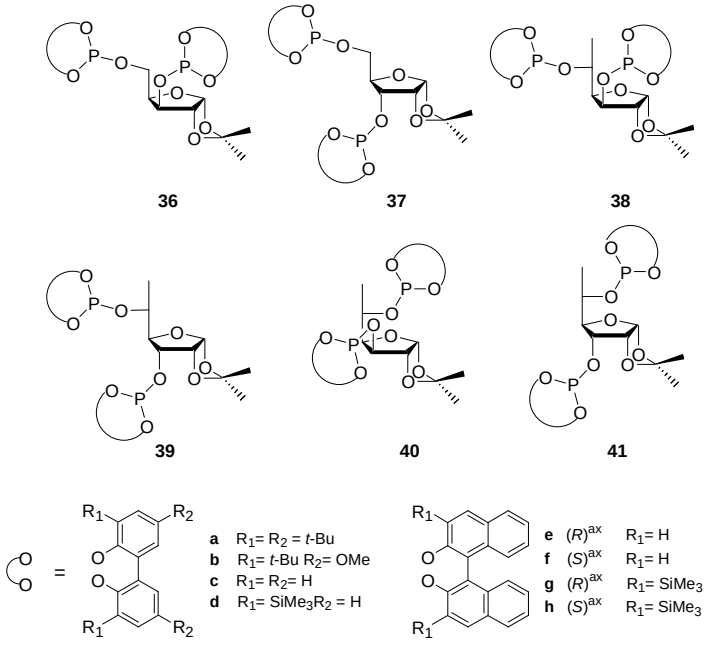

Figure 2.12. Tunable furanoside diphosphite ligands derived from carbohydrates

In summary, diphosphite ligands **36**-**41** derived from carbohydrates provided excellent regio- and enantioselectivities in the asymmetric hydroformylation of vinyl arenes, and gave one of the best enantioselectivities in this reaction. Recently,

good enantioselectivities and excellent regioselectivities have been achieved in the rhodium-catalysed asymmetric hydroformylation of 2,5- and 2,3-dihydrofuran using diphosphite ligands **36a** and **38a**. When diphosphite ligand **38a** was used in both substrates enantioselectivities were high (up to 75%).[57]

Table 2.2. Hydroformylation of styrene with chiral rhodium diphosphite **36**-**41**[a][34-36, 56]

Entry	Ligand	TOF[b]	% 2-phenyl propanal[c]	% ee
1	**36b**	5	97	60 (S)
2	**37b**	5	97	61 (R)
3	**38a**	19	98.4	74 (S)
4	**38b**	18	98.6	90 (S)
5	**39a**	14	97.1	46 (R)
6	**39b**	13	97.2	58 (R)
7	**40a**	15	97.4	52 (S)
8	**40b**	12	97.6	64 (S)
9	**41a**	16	98.7	76 (R)
10	**41b**	17	98.3	89 (R)
11	**39d**	10	98.1	62 (R)
12	**38d**	11	98.8	93 (S)

[a] [Rh(acac)(CO)2]=0.0135 mmol; ligand/Rh=1.1; substrate/Rh=1000; Toluene=15 mL; PH2=CO =10 bar; T =20 ºC; PCO/PH2 =0.5. [b]TOF in mol styreneXmol Rh^{-1}x h^{-1} determined after 1 h reaction time.[c] Regioselectivity for 2-phenylpropanal.

2.1.2.2 Phosphine-phosphite ligands in asymmetric hydroformylation

Binaphos and related ligands

The first report on asymmetric hydroformylation using phosphine-phosphite ligands was by Takaya and co-workers in 1993.[58] They developed the (*R*,*S*)-Binaphos ligand **42** (Figure 2.13) in order to combine the high enantioselectivity obtained with diphosphines such as BINAP in asymmetric hydrogenation, with the apparently efficient coordination of the phosphite moiety. (*R*,*S*)-Binaphos ligand **42** (Figure 2.13) provided higher enantioselectivities (up to 95%) than other C_2-symmetry diphosphine or diphosphite ligands in asymmetric hydroformylation of a wide variety of substrates. They have reported a wide range of structural variations (Figure 2.13).[39, 59-61] They observed that: a) the configuration of the binaphthyl bridge governs the sense of the enantioselectivity, b) the enantioselectivities are

enhanced when the configuration of the binaphthyl moieties are opposite and c) the substituents of the aryl groups also positively affect the enantioselectivity (see Figure 2.13).

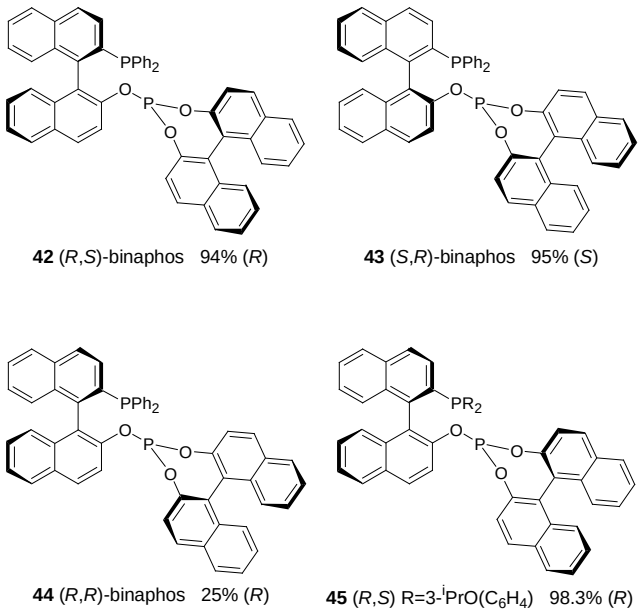

42 (*R*,*S*)-binaphos 94% (*R*) **43** (*S*,*R*)-binaphos 95% (*S*)

44 (*R*,*R*)-binaphos 25% (*R*) **45** (*R*,*S*) R=3-^{i}PrO(C_6H_4) 98.3% (*R*)

Figure 2.13. Binaphos and related ligands. Enantioselectivities obtained in asymmetric hydroformylation of styrene.

Other phosphine-phosphite ligands

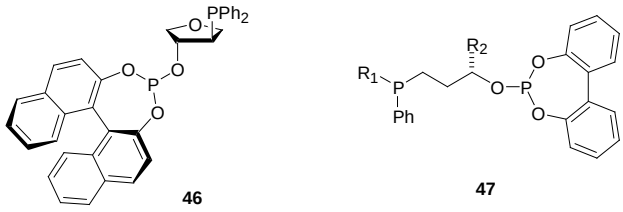

46 **47**

Figure 2.14. Chiral phosphine-phosphite ligands

Börner et al.[62] developed a series of phosphine-phosphite ligands with furanoside backbones. They observed enantioselectivities up to 40% in the rhodium-catalysed

asymmetric hydroformylation of vinyl acetate with ligand **46** (Figure 2.14). van Leuween et al. [63] reported a series of phosphine-phosphite ligands **47** (Figure 2.14), and obtained enantioselectivities up to 62% in the rhodium-catalysed asymmetric hydroformylation of styrene.

Our group[64] has also developed a series of phosphine-phosphite ligands. These ligands, with carbohydrate backbone **48** (Figure 2.15), showed low-to-moderate enantioselectivities in the rhodium-catalysed asymmetric hydroformylation of styrene (up to 49%).

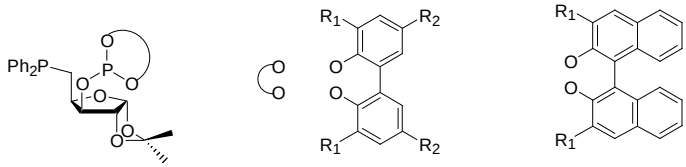

Figure 2.15. Phosphine-phosphite ligands with furanoside backbone

2.1.2.3 Characterisation of $[RhH(CO)_2(L)]$ intermediates. Structure versus stability and enantioselectivity.

The solution structures of the trigonal bipyramidal $[RhH(CO)_2(L)]$ (L: bidentate ligand) complexes, which are the resting states in the hydroformylation reaction, have been widely studied.[14] The species are generally formed from the $[Rh(acac)(CO)_2]$ complex by adding one equivalent of bidentate ligand, under syngas pressure. The complexes are generally assumed to have a trigonal bipyramidal structure with two possible isomeric structures: the ligand coordinated in an equatorial-equatorial (**ee**) or an equatorial-axial (**ea**) fashion (Figure 2.16).

The structure can be elucidated by high pressure IR and NMR data. ^{31}P and ^{1}H NMR spectroscopy combined with IR studies establish a relation between the results from catalysis, the coordination mode of the diphosphites to the rhodium and the stability of these species. In the carbonyl region of the infrared spectrum the vibrations of the **ee** and **ea** complex can be easily distinguished. The **ee** complexes

show absorptions around 2015 and 2075 cm^{-1}, whereas the **ea** complexes show absorptions around 1990 and 2030 cm^{-1}, when diphosphite ligands are analysed. The ^{31}P NMR gives additional information. In the complexes with **ee** coordination, the phosphorus atoms coordinated in the equatorial plane, have small phosphorus to hydrogen coupling constants (<10Hz), whereas the coupling constant of a *trans* coordinated phosphite, **ea** complex, has a large phosphorus to hydrogen coupling constant of 180-200 Hz. The phosphorus to phosphorus coupling constants are much larger for the **ee** (around 250 Hz) than for the **ea** complex (usually 70 Hz).[14]

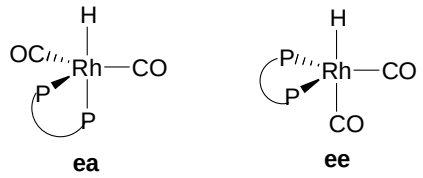

Figure 2.16. Equatorial-equatorial (**ee**) and equatorial-axial (**ea**) rhodium hydride dicarbonyl diphosphite

Several studies have observed that the phosphorus atoms of the **ee** and **ea** complexes show fluxional behaviour at room temperature, which can be halted at low temperatures. It has been suggested that the exchange process of the phosphorus donor atoms of the **ee** and **ea** complexes proceeds by the low energy rearrangement mechanism described by Meakin (Figure 2.17).[65, 66]

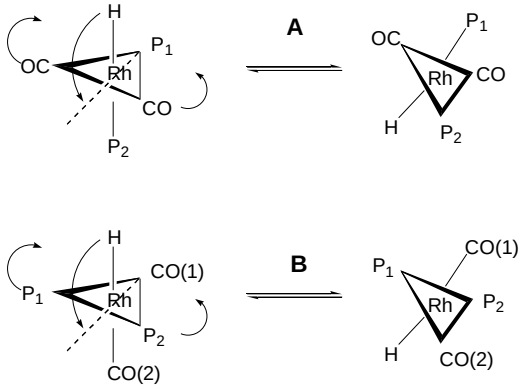

Figure 2.17. A: equatorial-axial phosphorus exchange. B: equatorial-equatorial phosphorus exchange.[65, 66]

A simultaneous bending motion of the hydride and carbonyl ligands takes place in the hydridorhodium diphosphite complexes with **ea** coordination (Figure 2.17A). However, for **ee** coordinated diphosphite complexes a motion of the hydride and the equatorial phosphite function is responsible for the exchange (Figure 2.17B). The latter process is expected to be more difficult than the former, which explains the higher fluxionality of the **ea** coordinating complexes.

van Leuween and co-workers[47, 48] established a correlation between the structure of the ligand, the coordination mode in the trigonal bipyramidal hydridorhodium diphosphite complexes and the selectivity of the process. They observed that seven-membered chelate rings (ligands **19a-b**, Figure 2.5) generally give equatorial-axial coordination, while eight- and nine-membered chelate rings (ligands **21a-b** and **20a-b**, respectively, Figure 2.5) preferably coordinate bis-equatorially to rhodium. The highest enantiomeric excesses were observed with relatively stable complexes of **21a-b** and **23b**, which form eight-membered rings and coordinate bis-equatorial to rhodium. Ligand **20a-b**, which forms nine-membered rings coordinated in **ee** fashion formed rather unstable complexes giving lower enantiomeric excesses than ligands **21** and **23**. The enantiomeric excess were lowest with ligands **19a-b**, which coordinated in a **ea** fashion in the more fluxional $[RhH(CO)_2(L)]$ complexes. However, ligand **18a**, which forms a seven-membered ring, coordinated in **ee** fashion, when an **ea** coordination was expected. This could be due to the rigid tartarimide backbone of the diphosphite.

Our group has also used high pressure IR spectroscopy and NMR techniques to characterize the rhodium complexes formed under hydroformylation conditions with diphosphites **36-41** (Figure 2.12).[35, 36] It has been observed that enantioselectivities were generally highest with ligands with a strong **ee** coordination preference, while an equilibrium of species with **ee** and **ea** coordination modes considerably reduced the enantiomeric excess.

The study of Binaphos **42** ligand (which shows enantioselectivities up to 90% in the hydroformylation reaction) under hydroformylation conditions revealed that Binaphos coordinates in an equatorial-axial mode with the phosphite moiety in axial position.[39, 67] However, correlations have been made between the $[RhH(CO)_2(L)]$

complex structure and the selectivity of the hydroformylation reaction, they are not always straightforward.

2.1.3 Hydrogenation reaction

Metal-catalysed asymmetric hydrogenation to reduce prochiral olefins, ketones and imines using molecular hydrogen is one of the most efficient asymmetric catalytic methods for synthesising chiral compounds (Scheme 2.4). This process has been widely used in stereoselective organic synthesis and some processes have found industrial applications.[13, 68, 69]

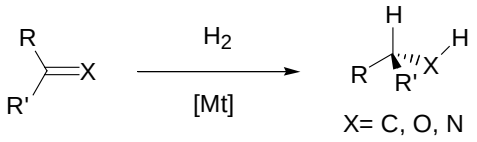

Scheme 2.4. Asymmteric hydrogenation of prochiral compounds

The asymmetric hydrogenation of ketones makes it possible to synthesise chiral secondary alcohols; ruthenium is the most widely used metal source, followed in lesser extent by rhodium. The asymmetric hydrogenation of C=N double bonds allows to obtain chiral amines; rhodium and ruthenium are the most studied metal sources, but the most of the recent effort has focused on iridium. The hydrogenation of carbon-carbon bonds is widely used: for example, the hydrogenation of α-dehydroaminoacid derivatives and enamides make it possible to synthesise aminoacids and amines, which are useful intermediates for the pharmaceutical and agrochemical industries. The hydrogenation of α-dehydroaminoacid derivatives is a typical reaction for testing new chiral ligands.[13, 68, 69]

Mechanism

The mechanism for the rhodium-catalysed hydrogenation of methyl-α-acetamidocinnamate, depicted in Figure 2.18, was proposed by Landis and Halpern.[70] The catalytic cycle consists on two coupled diastereoisomeric manifolds.

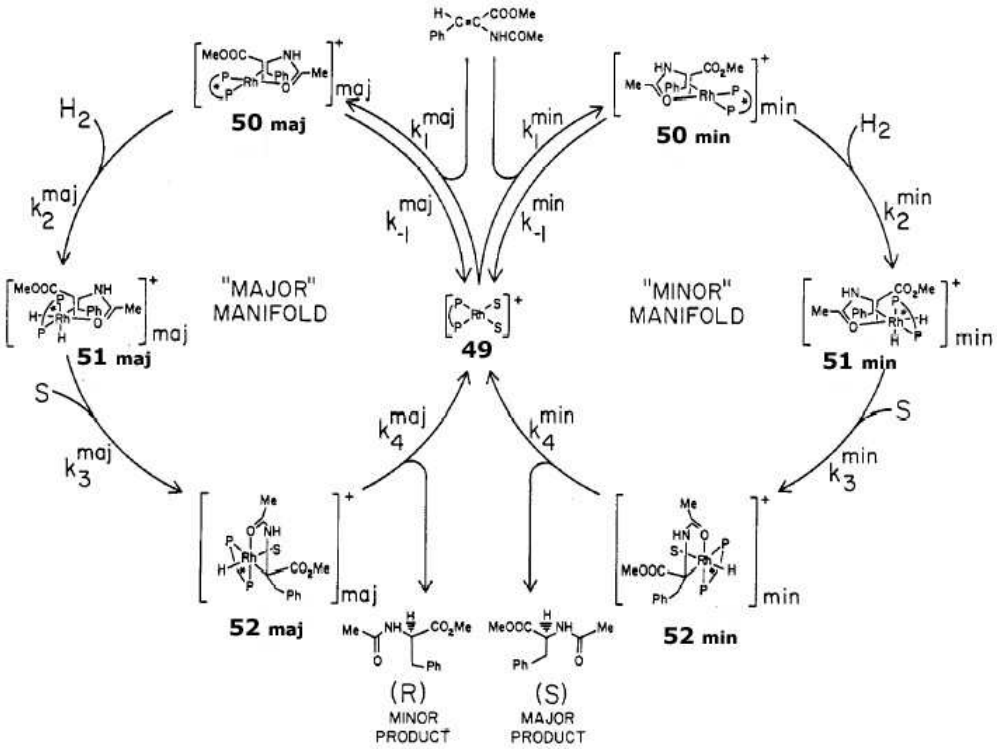

Figure 2.18. Mechanistic scheme for the $[Rh(dipamp)]^+$-catalysed hydrogenation of methyl-α-acetamidocinnamate[70]

The square planar Rh(I) complex **49** containing the coordinated diphosphine and two molecules of solvent is the starting species of the catalytic cycle. Next, the substrate displaces the two molecules of solvent to form two diastereoisomeric adducts, **50maj** and **50min**, where the substrate is coordinated as a bidentate ligand. The irreversible oxidative addition of hydrogen gives the octahedral *cis*-dihydridorhodium complexes **51**. The insertion of the olefin into one of the Rh-H bonds produces the two diastereomeric alkyl complexes **52**. Next, by reductive elimination, the enatiomeric forms of the product are formed and the catalytic active species **49** regenerated. It is accepted that the oxidative addition of hydrogen is the rate- and enantioselective determining step. The reactivity of the minor diastereomer **50min** is much higher than that of the major diastereomer **50maj**, so the minor isomer becomes the determining product.

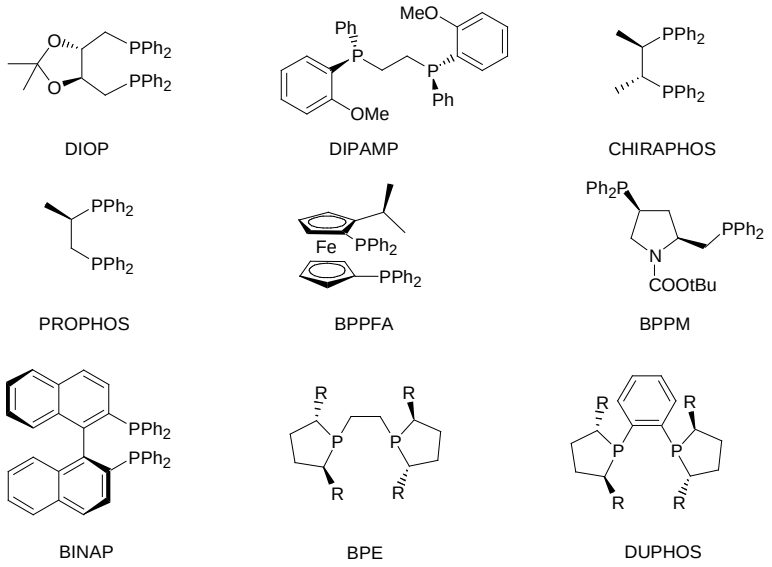

Figure 2.19. Chiral ligands that have been successfully applied in asymmetric hydrogenation reactions[71]

The first contributions to asymmetric hydrogenation were made by Knowles[72] and Horner,[73] who replaced the triphenyl phosphine of Wilkinson's catalyst, $[RhCl(PPh_3)_3]$,[74] with chiral monophosphines. Later Kagan[75] reported the diphosphine ligand DIOP (Figure 2.19), which was successfully applied in asymmetric hydrogenation. Knowles[76-78] reported the use of the diphosphine ligand DIPAMP ((1*R*,2*R*)-(-)-Bis[(2-methoxyphenyl)phenylphosphino]ethane) (Figure 2.19) in this reaction, and because of its high catalytic efficiency was employed in the industrial production of L-Dopa. Since then, a thousand other successful chiral diphosphorus ligands have been developed: for example Chiraphos and Prophos developed by Bonisch, Kumada's ferrocene ligand BPPFA and Achiwa's BPPM, among others (Figure 2.19).[71] In the 1980s Noyori and co-workers reported the Ru/BINAP ((1,1'-Binaphthalene-2,2'-diyl)bis(diphenylphosphine)) catalyst, which is efficient catalyst for hydrogenation of various substrates.[79, 80] In the past decade such phosphorus ligands as DUPHOS and BPE developed by Burk and co-workers, showed efficient catalytic properties for the asymmetric hydrogenation of various substrates.[81, 82]

Nowadays, many chiral ligands, mainly phosphorus donor ligands have been successfully applied to asymmetric hydrogenation.[13, 68, 69, 71] Carbohydrate derivative ligands have also been successfully applied in this reaction.[4-6]

2.1.3.1 Carbohydrate derivative ligands in asymmetric hydrogenation reaction

Diphosphine ligands

Diphosphine ligands derived from carbohydrates are mainly related to DIOP and DUPHOS ligands. Ligands **53** and **54**[83-85] (Figure 2.20) increased the rigidity of the conformational flexibility of the seven-member chelate ring in the DIOP ligand by introducing methyl groups in the α positions of the phosphine groups, and ligands **55** and **56**[86] by introducing a conformationally rigid 1,4-dioxane backbone. These ligands led to high enantioselectivities (>99%) in the rhodium-catalysed hydrogenation of aryl enamides.

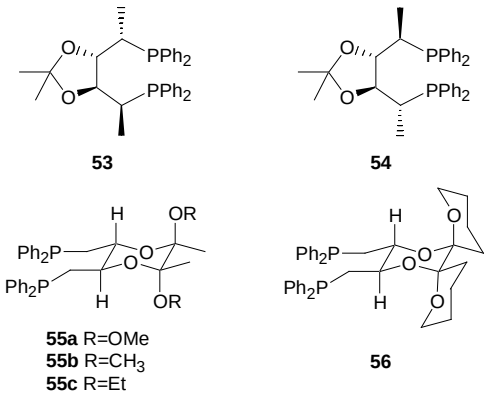

Figure 2.20. Diphosphine ligands related to DIOP

Ligands related to DUPHOS and BPE are mainly derived from D-mannitol (Figure 2.21). Diphospholanes **57**, **58a-c** and **59**, developed by Holz and co-workers[87] and Zhang and co-workers,[88-90] which introduced various substituents in α and β positions, provided high enantioselectivities (between 93-99%). Rieger and co-workers[91] studied the effect of the substituents in the α position, **58b-f**. The

results showed that methyl and ethyl substituents led to best results. Diphospholanes **60** and **61** (Figure 2.21) have also been applied to the rhodium-catalysed asymmetric hydrogenation of various substrates and enantioselectivities have been high (up to 99%).[92] Other ligands with phospholane moieties derived from D-mannitol **62** were applied in the rhodium-catalysed asymmetric hydrogenation of several itaconates leading to enantioselectivities between 80 to 95%.[93]

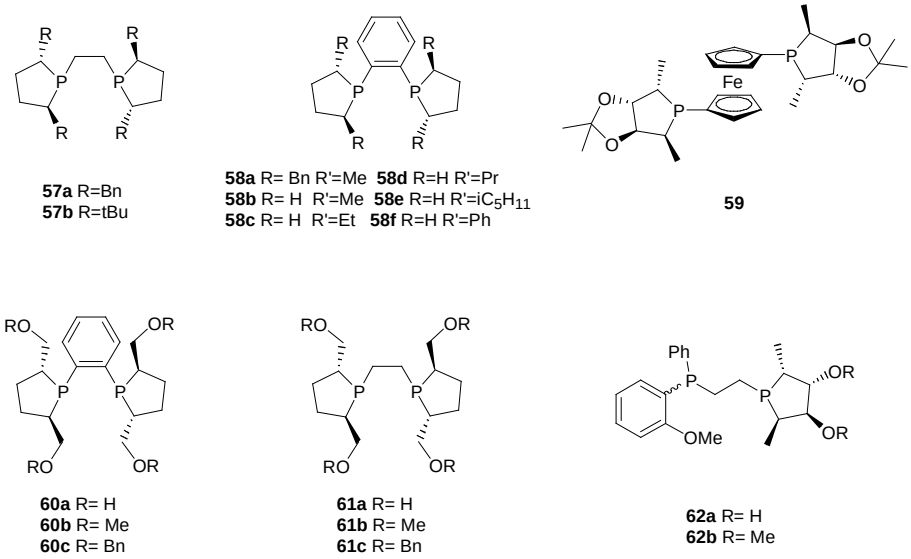

Figure 2.21. Diphosphine ligands

Recently, our group prepared diphosphines **63-65** with a furanoside backbone (Figure 2.22).[94] These ligands showed high enantioselectivities in the rhodium-catalysed asymmetric hydrogenation of α, β-unsaturated carboxylic acids.

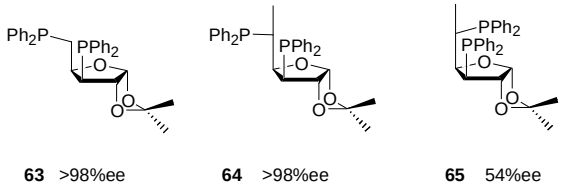

Figure 2.22. Diphosphine ligands with furanoside backbone

The introduction of a methyl group in the C-5 position (ligands **64** and **65** *vs*. ligand **63**) increases activity and its configuration has a strong influence on the enantioselectivity. While catalysts based on ligand **64** showed high enantioselectivities (98%ee), ligand **65,** with a different configuration in this stereocenter, showed a lower enantioselectivity (54% ee) (see Figure 2.22).

Diphosphinite ligands

As has been mentioned above, the first chiral ligands derived from carbohydrates with phosphinite moieties were reported by Cullen[8], Thompson[9], Selke[95] and Descotes.[96] Cullen and Thompson synthesised a ligand derived from glucose with a pyranoid skeleton **4**, and Thompson described the first diphosphinite derived from xylose with a furanoid skeleton **5** (Figure 2.1). The ligands with a pyranoside backbone were applied in the asymmetric hydrogenation of dehydroamino acid derivatives.

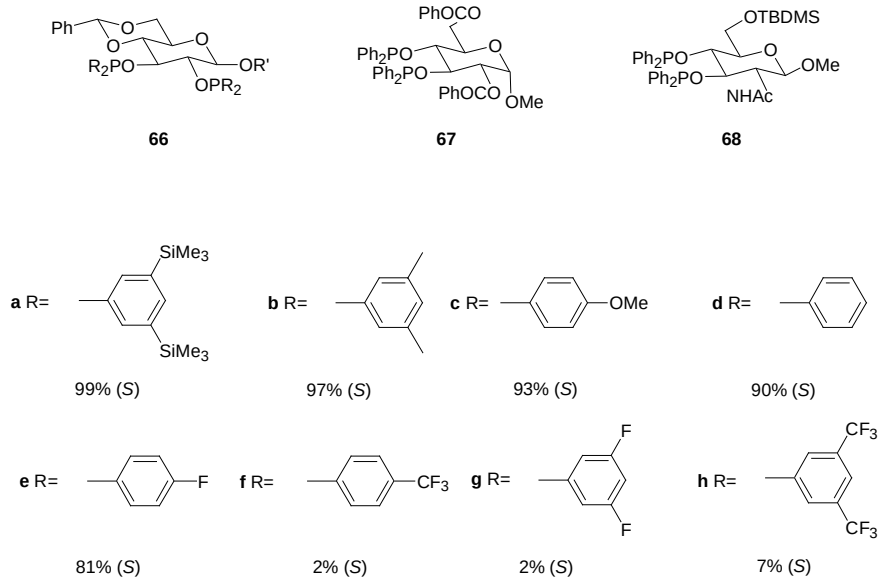

Figure 2.23. Diphosphinite ligands with pyranoside backbone. Enantioselectivities in the hydrogenation of methyl α-acetamidocinnamate

Ligand series **66** showed enantioselectivities above 96%. Selke and co-workers[95, 97-99] studied the effect of the substituents R' (R'= Me, Ph, Bn; R=Ph) (see Figure 2.23), while RajanBabu and co-workers studied the electronic and steric effects of the substituents of the phenyl groups by introducing various diphosphinite groups in the same backbone (R'=Ph, see Figure 2.23).[100-102] In all cases, the (*S*)-enantiomer of the hydrogenated product was obtained and the enantioselectivity was strongly influenced by the substituents of the phenyl groups. The electron-rich diphosphinite ligands increased the enantioselectivities, whereas the electron-deficient ligands decreased them. The same group prepared ligands **67** and **68**, which can be considered as pseudo-enantiomers of ligand **66**. [100-102] These ligands provided the (*R*)-enantiomer of the hydrogenated product, while ligand **66** provided the (*S*)-enantiomer, and showing that the electron-rich diphosphinite enhanced the enantioselectivity.

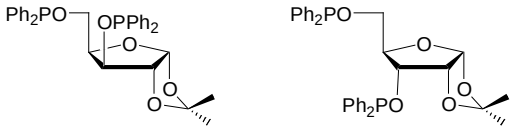

5 **69**

Figure 2.24. Diphosphinite ligands with furanoside backbone.

Our group[103] synthesised diphosphinite ligand **69**. Its configuration in carbon 3 is different to that previously described for diphosphinite ligand **5** by Thompson (Figure 2.24).[9] The use of these ligands, **69** and **5**, in rhodium- and iridium-catalysed hydrogenation showed that the results are strongly influenced by the metal and the ligand used. Ligand **5** showed better results with iridium-based catalysis (>78%ee) and ligand **69** with rhodium-based catalysis (>81%ee). These diphosphinite ligands, **5** and **69**, have also been used in a variety of catalytic reactions, asymmetric Rh-hydroformylation[104], asymmetric Cu-1,4 addition[105] and asymmetric Pd-allylic alkylation[106], and enantioselectivities have been low to moderate.

Recently, diphosphinites **70a–d** and **71a–d** (Figure 2.25) have been prepared from D-glucosamine and D-glucitol.[107] These new series of diphosphinite ligands with

C_2-symmetry were used in the rhodium-catalysed hydrogenation of methyl acetamidoacrylate, methyl acetamidocinnamate and dimethyl itaconate. Catalytic systems containing the ligand **70b** afforded the best results with enatioselectivities of 93% in the hydrogenation of methyl acetamidoacrylate. Ligand **72**, which does not contain substituents at positions 2 and 5 of the tetrahydrofuran ring only gave a 22% of enantioselectivity. This indicates that the stereogenic centers which are not directly bonded to the coordinating atoms have a strong influence on the selectivity. Substituents X in **70** and **71** (Figure 2.25) also affect the stereoselectivity. The enantioselectivities were lower for the dimethyl itaconate than for the other substrates but the configuration of the major enantiomer, when ligands **70a** and **71a** were used, unexpectedly seems to be determined by the configuration of substituents at carbons 2 and 5.

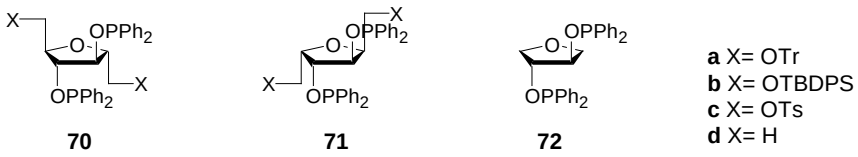

Figure 2.25. Diphosphinite ligands developed by our group

Diphosphite ligands

Diphosphite ligands have been successfully used in the asymmetric hydrogenation of prochiral olefins. The first application of these ligands in this reaction was reported by Reetz and co-workers with ligands **73** derived form D-mannitol. These ligands were applied in the rhodium-catalysed hydrogenation of prochiral olefins providing high enantioselectivities (up to 98%).[108]

Tunable diphosphite chiral ligands **36**-**41** (Figure 2.12, see above), which have been applied successfully in the hydroformylation reaction of vinyl arenes, were used as ligands in rhodium-catalysed asymmetric hydrogenation. They were developed in our group,[35, 56, 109] and showed high enantioselectivities (>99%). The enantiomeric excesses were strongly influenced by the configuration of the ligands, which was also the case in the hydroformylation reaction.

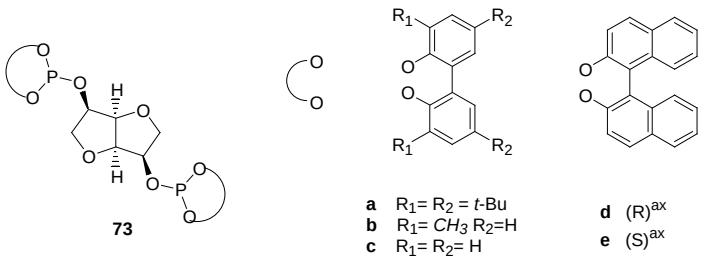

Figure 2.26. *C*$_2$-symmetry diphosphite chiral ligands developed by Reetz

Objective

The carbohydrate derivative ligands synthesised in our group have been successfully applied in several asymmetric catalytic reactions. We emphasise the results obtained in the asymmetric hydroformylation of vinyl arenes with *C*$_1$-symmetry diphosphites derived from carbohydrates, **36-41** (Figure 2.12, see above), which are one of the best reported in the literature.[34-36, 56] The application of these ligands to the asymmetric hydrogenation of prochiral olefins also led to excellent results.[35, 56, 109]

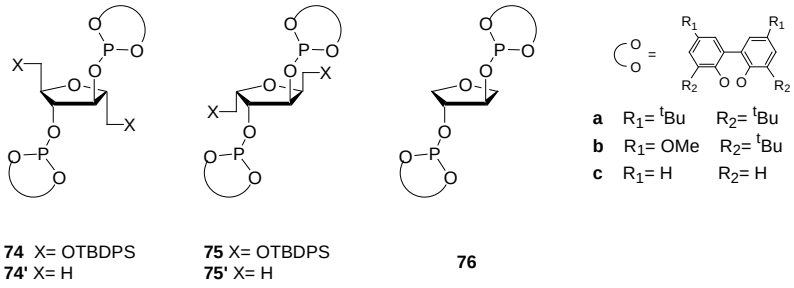

Figure 2.27. New series of *C*$_2$-symmetry diphosphite ligands **74**-**76**

Since it has been shown that additional sterocenters in ligands **70, 71** (Figure 2.25) lead to a considerably higher enantioselectivity in the hydrogenation of enamidoesters in comparison than the reference compound **72**, and given that, until now, the diphosphites derived from 1,2-diols provided moderate enantiomeric

excess in the asymmetric hydroformylation of styrene, we decided to synthesise a new series of C_2-symmetry diphosphite ligands, **74**-**76** (Figure 2.27), with the same backbone as the previously reported diphosphinites **70** and **71** (see Figure 2.25) in order to test whether a similar effect was also produced in the hydroformylation reaction with a rhodium-diphosphite catalytic system.[107]

These diphosphites can also be modified by changing the substituents of the phosphorus moieties, the nature of the substituents and the configuration at positions 2 and 5. We shall use these ligands to synthesise their rhodium cationic complexes. This new series of chiral ligands **74-76** will be applied in the rhodium-asymmetric hydroformylation reaction of vinyl arenes. We also report the application of the rhodium cationic complexes that contain chiral ligands **74-76** in the hydrogenation of methyl acetamidoacrylate.

2.2 Results and discussion

2.2.1 Synthesis of diphosphite ligands with carbohydrate backbone

2.2.1.1 Synthesis of 2,5-anhydro-D-mannitol derivative ligands 74a-c and 74'a,b

Phosphorus ligands **74** and **74'** can be prepared from 2,5-anhydro-D-mannitol (**78**), which in turn can be prepared from D-glucosamine (**77**) in a straightforward manner (Scheme 2.5). Treating **77** with sodium nitrite gives the diazonium salt which undergoes a ring contraction reaction to give the tetrahydrofuran aldehyde derivative. This aldehyde is in equilibrium with its hydrate. The reduction of the aldehyde/hydrate mixture with sodium borohydride provides tetrol **78** in 82% yield (Scheme 2.5).[110-112]

To study the effect of the groups at positions 2 and 5 we prepared the diols **80** and **80'** from the tetrol **78** (Scheme 2.6). The primary alcohols in **78** were protected by reaction with *tert*-butyldiphenylchlorosilane (TBDPSCl) to afford the diol **80**. To obtain the diol **80'** with a methyl group at positions 2 and 5, the primary alcohols of

78 were selectively ditosylated[113] to give diol **79**, which was then treated with $LiAlH_4$ to afford compound **80'** (Scheme 2.6).[113]

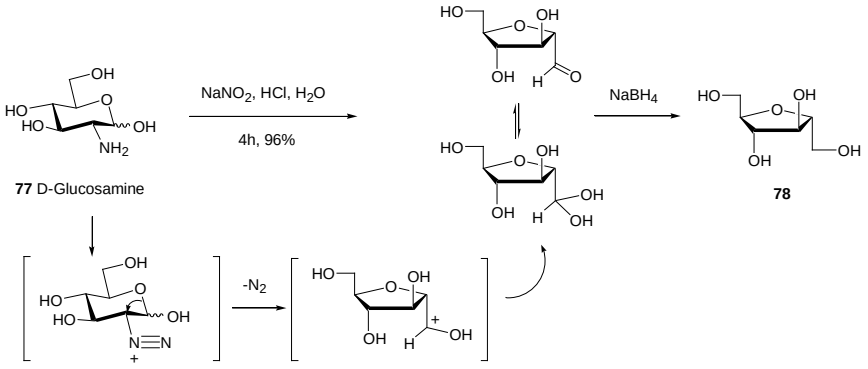

Scheme 2.5. Synthesis of 2,5-anhydro-D-mannitol **78**

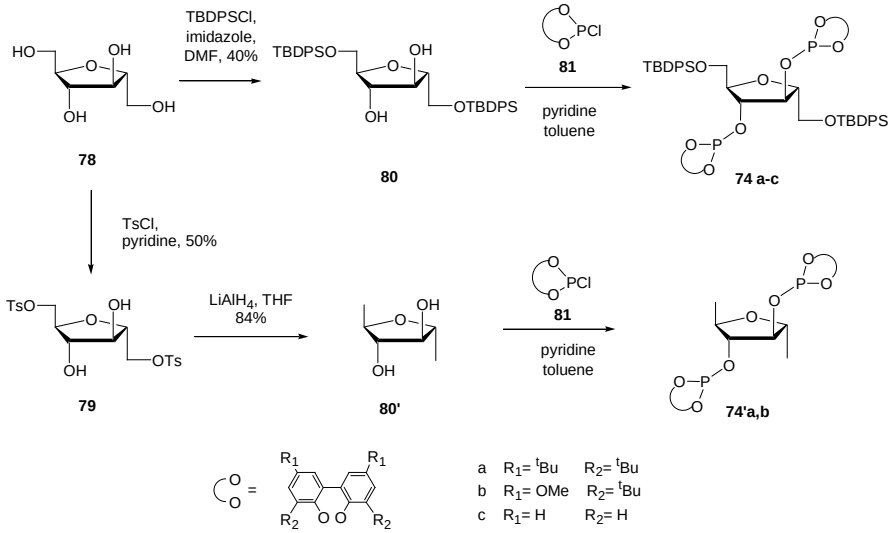

Scheme 2.6. Synthesis of 2,5-anhydro-D-mannitol derivative ligands **74a**-**c** and **74'a**, **b**

The diols **80** were treated with the corresponding phosphorochloridite **81**, which had been previously synthesised by standard procedures,[46, 114] to give the corresponding diphosphites **74a-c** and **74'a**,**b** in moderate to good yields (31-72%) (Scheme 2.6).

2.2.1.2 Synthesis of 2,5-anhydro-L-iditol derivative ligands 75a,b and 75'a,b

To study the effect of the configuration of carbons 2 and 5, ligands **75** and **75'** were prepared from 2,5-anhydro-L-iditol **84**. Tetrol **84** was obtained from D-glucitol **82** following a reported procedure (Scheme 2.7).[115, 116] The yield was only 5%, similar to previously reported yields, but this procedure allows **84** to be easily obtained from a very accessible nonexpensive starting material in a multigram scale.

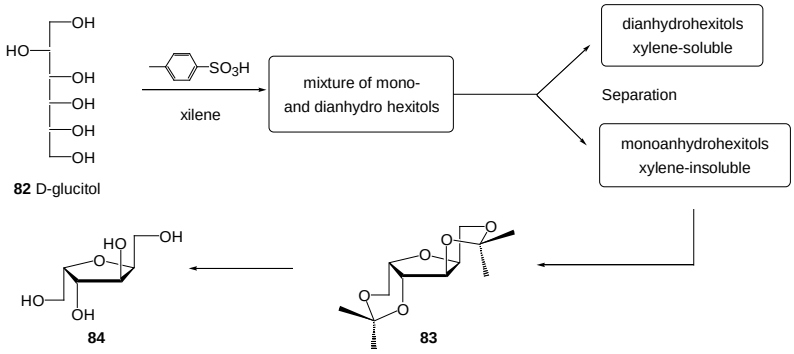

Scheme 2.7. Synthesis of 2,5-anhydro-L-iditol **84**

We also prepared diols **86** and **86'** (Scheme 2.8) in a similar way to **80** and **80'**. The diols **86** were then treated with the corresponding phosphorochloridite **81**, synthesised *in situ* by standard procedures,[46, 114] to give the corresponding diphosphites **75a**,**b** and **75'a**,**b** in moderate to good yields (32-92%) (Scheme 2.8).

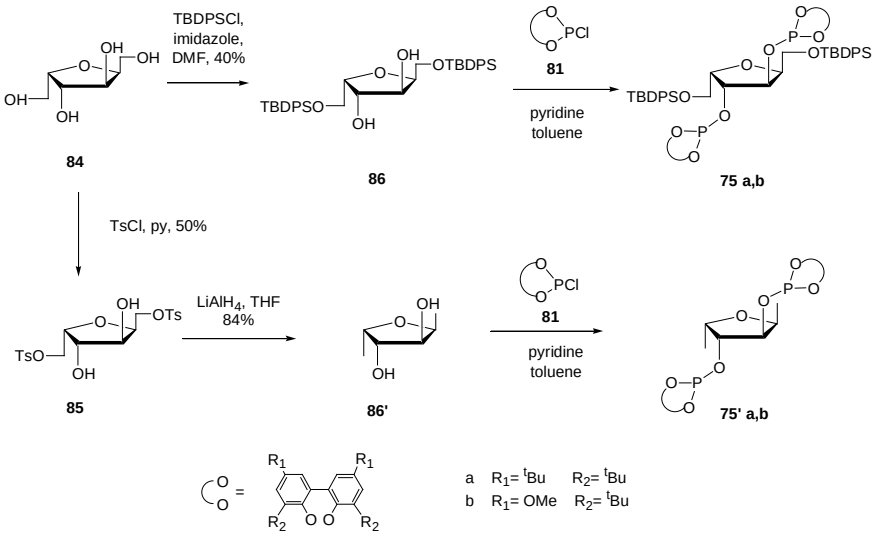

Scheme 2.8. Synthesis of 2,5-anhydro-L-iditol derivative ligands **75a**, **b** and **75'a**, **b**

2.2.1.3 Synthesis of (3*R*,4*R*)-3,4–dihydroxytetrahydrofuran derivative ligands 76a, b

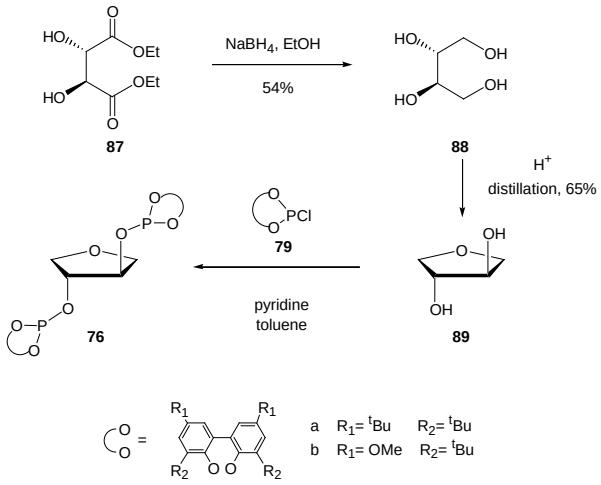

Scheme 2.9. Synthesis of (3*R*,4*R*)-3,4–dihydroxytetrahydrofuran derivative ligands **76a**, **b**

In order to compare the effect of the stereocenters 2 and 5, we prepared the diphosphite ligands **76a**, **b** which do not contain substituents in these positions. They were synthesised from diol (3*R*, 4*R*)-3,4–dihydroxytetrahydrofuran.[117] The diol **89** was prepared from (2*S*,3*S*)-diethyl tartrate in two steps. The reaction of **87** with $NaBH_4$ affords tetrol **88**, which was distilled in the presence of catalytic amounts of *p*-toluenesulfonic acid to afford **89** in moderate yields. The treatment of **89** with phosphorochloridite **81**, synthesised *in situ* by standard procedures,[46, 114] gives the corresponding diphosphites **76a**,**b** in moderate to good yields (29-75%) (Scheme 2.9).

2.2.1.4 Structural elucidation of diphosphites 74-76

The structure of diphosphite ligands **74**-**76** was determined by one-dimensional ^{1}H, ^{13}C and ^{31}P NMR. The signals were unequivocally assigned by the bidimensional techniques COSY and HSQC. We also determined the crystal structure of diphosphite ligand **74a** by X-ray diffraction.

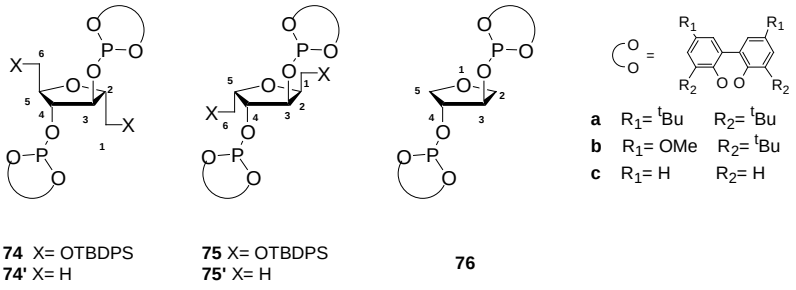

Figure 2.28. C_2-symmetry diphosphite ligands derived from carbohydrares

Ligands **74a**-**c**, **74'a**, **b**, **75a**, **b**, **75'a**, **b** and **76a**, **b**, as well as their alcohol precursors, showed simple ^{1}H and ^{13}C NMR spectra, characteristic of compounds with a C_2-symmetry.

The $^{31}P\{^{1}H\}$ NMR spectrum of ligands **74**-**76** showed only one signal between 140 and 147 ppm, characteristic of a phosphite function. The ^{1}H NMR spectra of ligands **74**-**76** showed signals corresponding to the second order protons H2/H5 and H3/H4

so coupling constants cannot be directly measured in the spectra. These second order spectra are derived from the existence of protons that are chemically but not magnetically equivalent, which give rise to spin systems AA'BB'$X_2X'_2$ for compounds **74-75** and AA'BB'$X_3X'_3$ for compounds **74'-75'**.

The ^{1}H NMR spectra of ligands **74**-**76** showed three different regions. We observed the aromatic protons between 6.58 and 7.83 ppm, the methynic and methylenic protons bonded to oxygen and the methyl protons of the methoxy groups (for **b** ligands) at lower chemical shifts (3.38-5.20 ppm), and finally the signals of the protons of the *tert*-butyl and methyl groups in the area between 1.46 and 1.06 ppm.

In the ^{1}H NMR spectra of ligands **74** and **75**, with OTBDPS groups, we observed four signals corresponding to methynic and methylenic protons. H1/H6, H1'/H6' appeared in the range 3.38 to 3.67 ppm for ligands **74** and between 3.79-3.98 ppm for ligands **75**. Protons H2/H5 appeared around 4.0 ppm for ligands **74** and around 4.4 ppm for ligands **75**. Protons H3/H4 appeared near 5.1 ppm in ligands **74** and **75**.

The ^{1}H NMR spectra of ligands **74'** and **75'**, with methyl substituents in carbons 2 and 5, showed two signals between 4.07 and 4.70 ppm corresponding to methynic protons. Protons H2/H5 appeared at 4.07 and 4.31 for ligands **74'** and at 4.12 and 4.26 for ligands **75'**. Protons H3/H4 appeared at 4.56 and 4.65 for ligands **74'** and at 4.63 and 4.73 for ligands **75'**. The methyl substituents in carbons 2 and 5, appeared as a doublet with chemical shifts of 1.09 to 1.29 ppm and coupling constants between 6.2-6.6 Hz.

The ^{1}H NMR spectra for ligand **76** presents three signals in the same area corresponding to protons H2/H5, H2'/H5' and H3/H4. The methylenic protons H2/H5 and H2'/H5' appeared in the range 3.84 to 3.96 ppm while the methynic protons H3/H4 apperared around 4.8 ppm (see Table 2.3).

The ^{13}C NMR spectrum of ligands **74-76** showed aromatic carbons in the range 155-122 ppm, the signal of *tert*-butyl groups appeared at 35-31 ppm and the

methoxy groups of ligands **b** showed chemical shifts around 55 ppm. The ^{13}C NMR spectrum of ligands **74** and **75** showed chemical shifts around 63 ppm for C1, while C2 appeared in the range 79.7 to 82.9 ppm and C3 in the range 79.9 to 79.5 ppm. For ligands **74'** and **75'** C1 appeared in the range 14.3 to 18.5 ppm, while C2 showed chemical shifts between 75.2 and 79.9 ppm and C3 between 80.0 and 85.4 ppm. Ligands **76** showed to signals in this area, C2 appeared around 72 ppm and C3 at 79.1 ppm (Table 2.4).

Table 2.3. ^{1}H and $^{31}P\{^{1}H\}$ NMR ($CDCl_3$) chemical shifts of compounds **74**–**76**

Diphosphite	Ph	H_1	$H_{1'}$	H_2	H_3	CH_3	OCH_3	$C(CH_3)_3$	^{31}P
74a	7.64–7.00	3.60	3.38	3.96	5.20	0.93	-	1.43-1.20	143.85
74b	7.65–6.58	3.67	3.53	4.05	5.14	0.98	3.81, 3.74	1.42, 1.35	144.54
74c	7.66–7.06	3.76	3.72	4.14	5.16	0.99	-	-	146.70
74'a	7.41, 7.15	1.06	-	4.07	4.56	-	-	1.46-1.33	143.03
74'b	7.08–6.82	1.29	–	4.31	4.65	–	3.90	1.55, 1.53	142.45
75a	7.65–7.17	3.85	3.79	4.30	4.56	0.96	-	1.45–1.28	147.47
75b	7.83–6.85	3.98	3.98	4.47	5.14	0.94	4.00, 3.96	–	146.72
75'a	7.42, 7.16	1.09	–	4.12	4.63	–	-	1.46–1.33	146.95
75'b	6.96, 6.68	1.16	–	4.26	4.70	–	3.79, 3.77	1.42, 1.40	146.07
76a	7.42, 7.16	-	-	3.84, 3.69[a]	4.82	-	-	1.46–1.34	141.50
76b	7.00, 6.74	-	-	3.96, 3.85[a]	4.85	-	3.83	1.47, 1.43	140.97

[a] ppm chemical shift of $H_{2'}$.

Table 2.4. $^{13}C\{^{1}H\}$ NMR ($CDCl_3$) chemical shifts of compounds **74**–**76**

Diphosphite	Ph	C_1	C_2	C_3	OCH_3	$C(CH_3)_3$	$C(CH_3)_3$
74a	146.3–124.1	62.5	82.5	79.5	-	35.4– 34.5, 19.2	31.6–31.3, 26.8
74b	155.5–112.6	62.6	82.9	79.6	55.5, 55.4	35.7–35.6, 19.5	31.5–31.3, 27.5
74c	146.7–121.3	63.1	83.4	79.9	-	19.5	27.0
74'a	146.5–124.2	18.5	79.5	85.4	-	35.4–34.6	31.5–31.1
74'b	155.6–112.7	18.3	79.9	85.4	55.5, 55.4	35.3	31.0, 30,8
75a	146.5–124.1	62.9	79.7	77.8	-	35.4–34.6, 19.2	31.5–31.1, 26.8
75b	156.0–112.9	62.7	80.0	77.7	55.5, 55.4	35.3, 35.3, 19.2	31.2, 31.0, 26.1
75'a	146.5–124.1	14.3	75.2	80.0	-	35.4–34.6	31.5–31.2
75'b	155.6–112.8	15.0	75.2	80.2	55.5, 55.4	35.4– 5.3	31.0
76a	146.6–124.2	-	72.3	79.1	-	35.4–34.6	31.5–31.1
76b	155.6–112.8	-	72.3	79.1	55.5, 55.5	35.3, 35.2	30.9, 30.9

Monocrystals of **74a** suitable for X-ray diffraction were obtained by slow diffusion of hexane into a CH_2Cl_2 solution of the ligand. The structure of **74a** was unambiguously revealed by single crystal X-ray diffraction. The ligand crystallizes as a solvate with two molecules of n-hexane in the elementary cell. The central five-membered ring O1-C1-C2-C3-C4 has a twisted conformation. The measured compound crystallizes as a racemic twin (74:16).

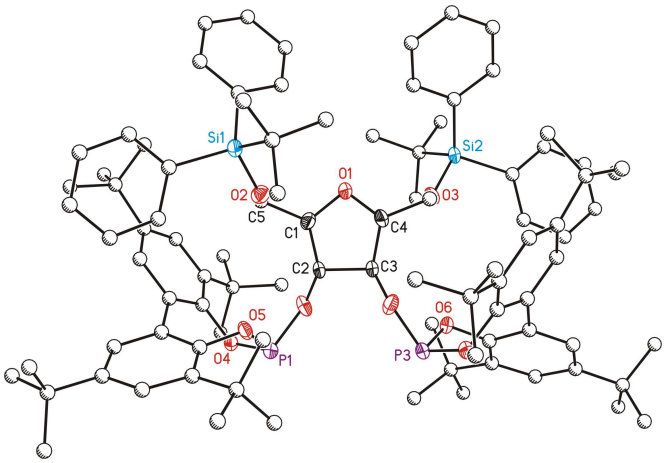

Figure 2.29. Structure model (ellipsoids at 50 % probability level) of ligand **74a**. Counterions, solvates and hydrogen atoms have been omitted for the sake of clarity. Selected bond distances and angles are given in Tables 1 and 2 of the appendix.

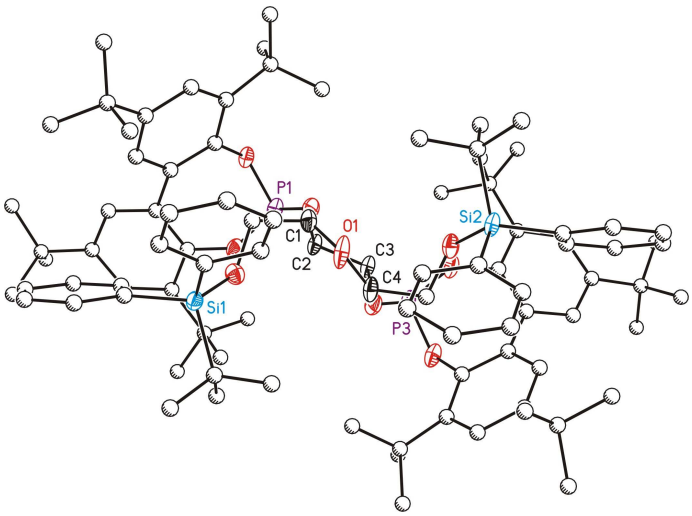

Figure 2.30. Structure model showing a lateral view of the molecule **74a**.

2.2.2 Synthesis of rhodium complexes

2.2.2.1 Synthesis of rhodium complexes [Rh(cod)(L)]BF_4

Rhodium complexes [Rh(cod)(L)]BF_4, L: diphosphite ligand, **90**-**92** were prepared by reacting [Rh(cod)$_2$]BF_4 with ligands **74a-c**, **74'a-b**, **75a**, **75'a** and **76a**,**b**, respectively. All complexes were isolated as coloured solids and were stable in air (Scheme 2.10).

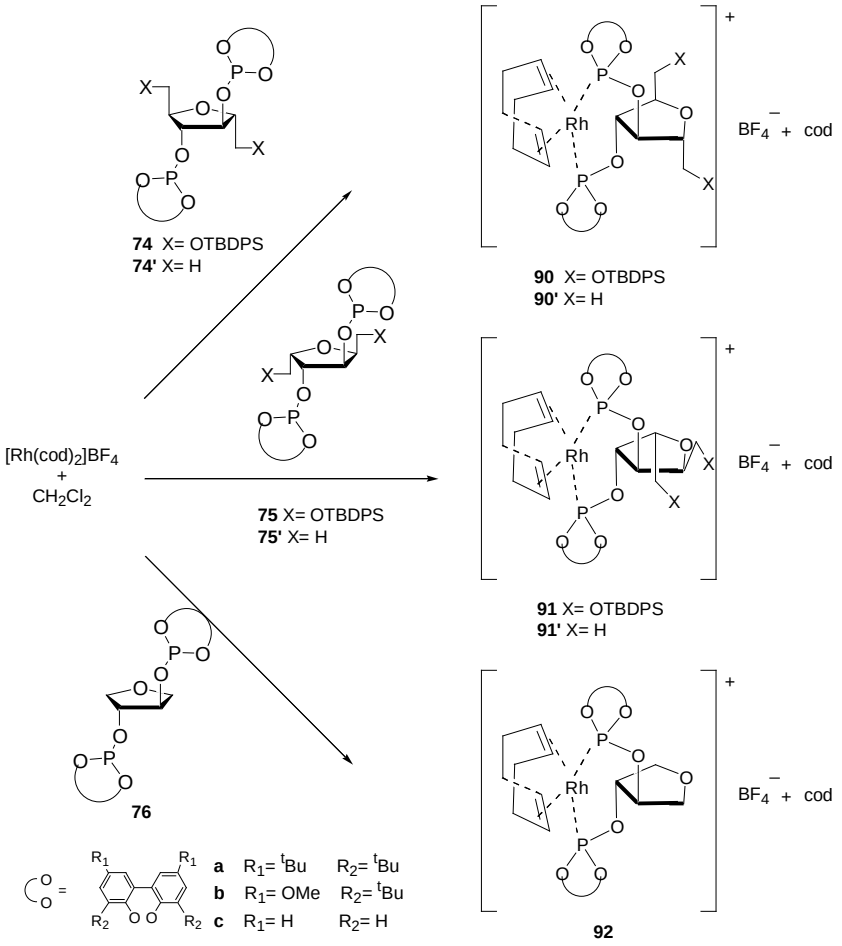

Scheme 2.10. Synthesis of cationic rhodium complexes

2.2.2.2 Structural elucidation of rhodium complexes [Rh(cod)(L)]BF_4

The structure of the rhodium complexes **90-92** was elucidated by NMR spectroscopic techniques. Tables 2.5 and 2.6 summarise the ^{1}H, ^{13}C and ^{31}P NMR data. The signals were unequivocally assigned by the bidimensional techniques COSY and HSQC. We also determined the crystal structure of rhodium complexes **90a** and **91'a** by X-ray diffraction.

Table 2.5. ^{1}H and $^{31}P\{^{1}H\}$ NMR ($CDCl_3$) chemical shifts of complexes **90-92**

Rh	Ph	H_1	$H_{1'}$	H_2	H_3	CH_3	OCH_3	$C(CH_3)_3$	CH	CH_2	^{31}P
90a	7.62–6.87	3.52	2.82	3.73	5.69	0.89	-	1.65-1.14	5.88, 4.92	2.34–2.00	129.35
90b	7.51–6.54	3.59	3.10	3.87	5.72	0.98	3.93, 3.66	1.71, 1.47	5.81, 4.96	2.45–2.05	129.85
90c	7.54–7.18	3.85	3.57	4.12	5.68	0.95	-	-	5.68	2.50–2.09	136.71
90'a	7.60, 7.06	0.84	-	3.84	5.78	-	-	1.76-1.32	4.87	2.32–1.94	128.38
90'b	7.22–6.71	1.03	–	3.96	5.98	–	3.97, 3.92	1.84, 1.57	5.85, 5.00	2.44–2.05	128.65
91a	7.51–7.13	3.44	3.44	3.89	4.66	0.96	-	1.51–1.25	5.67, 5.34	2.36-2.05	126.62
91'a	7.58, 7.09	0.86	–	4.13	5.49	–	-	1.76–1.34	5.85, 5.00	2.34–2.01	127.97
92a	7.61, 7.08	-	-	4.13, 3.72[a]	5.51	-	-	1.75–1.36	5.51, 4.65	2.21, 2.07	127.85
92b	7.13, 6.62	-	-	4.07, 3.66[a]	5.53	-	3.87, 3.83	1.71, 1.48	5.64, 4.80	2.26–1.82	129.36

[a] ppm chemical shift of $H_{2'}$.

The NMR spectra of the complexes at 25 °C show that they have C_2-symmetry in solution. In the $^{31}P\{^{1}H\}$ NMR spectrum, only one signal appeared between 127 and 136 ppm ($J_{P\text{-}Rh}$ =253-256 Hz). The chemical shift and coupling constant values are

in agreement with those observed for structurally related cationic diphosphite rhodium complexes.[56] The chemical shifts of the ^{1}H NMR and ^{13}C NMR (Table 2.5 and 2.6, respectively) where similar to those of the free ligands, and 1,5-cyclooctadiene showed two groups of signals between 4.65 and 5.88 ppm, and between 1.94 and 2.34 ppm for the methynic groups and methylenic groups, respectively.

The mononuclearity of the complexes was confirmed by MALDI spectra, which in all cases showed molecular ions corresponding to the cation $[Rh(cod)(L)]^{+}$ (L= **74a-c**, **74'a-b**, **75a**, **75'a** and **76a**,**b**).

Table 2.6. $^{13}C\{^{1}H\}$ NMR ($CDCl_3$) chemical shifts of complexes **90**–**92**

Rh	Ph	C_1	C_2	C_3	OCH_3	$C(CH_3)_3$	$C(CH_3)_3$	CH	CH_2
90a	149.4–125.2	60.7	78.6	77.4	-	36.0–34.6, 19.4	32.9–31.1, 26.8	112.9, 103.5	30.6, 29.7
90b	157.2–113.8	61.2	76.6	77.2	56.0, 55.4	36.1, 35.6, 19.4	32.9, 31.6, 26.7	112.8, 103.7	31.1, 29.4
90c	148.0–121.4	62.3	79.1	80.1	-	19.3	26.8	110.8, 110.1	30.4, 29.8
90'a	149.4–125.4	17.9	72.6	84.2	-	35.8–34.8	32.6–31.3	112.4, 103.6	30.6, 29.6
90'b	157.1–114.1	18.1	72.7	85.3	55.9, 55.7	35.8, 35.5	32.4, 31.5	112.2, 103.2	30.8, 29.6
91a	149.6–125.4	63.1	80.9	74.7	-	35.6–34.8, 19.2	32.3–31.4, 26.8	112.8, 103,4	30.3, 29.7
91'a	149.2–125.3	16.1	71.0	81.5	-	35.8–34.7	32.4–31.3	111.8, 104.2	30.1, 29.6
92a	149.7–125.6	-	67.9	80.1	-	35.8–34.7	32.7–31.3	112.6, 103.2	30.5, 29.5
92b	157.3–114.2	-	68.1	80.3	56.2, 55.3	36.1, 35.7	32.7, 31.6	113.6, 103.8	30.8, 30.1

Monocrystals of the complexes [Rh(cod)(**74a**)]BF_4 (**90a**) and [Rh(cod)(**75'a**)]BF_4 (**91'a**), suitable for X-ray diffraction, were obtained by slow diffusion of hexane into a CH_2Cl_2 solution of the complex.

Compound [Rh(cod)(**74a**)]BF_4, **90a**, crystallizes as a cation together with a BF_4^- anion (Figure 2.31 and 2.32), a disordered water molecule and two disordered positions of dichloromethane. The rhodium atom is coordinated in a slightly distorted square planar geometry with a mean deviation from the plane of 0.101 Å. The distances between the metal atom and the centers of the double bonds at the cyclooctadiene rings are A: 2.169 Å and 2.183 Å. The five-membered ring C1-C2-O3-C3-C4 has a twisted conformation. The measured compound crystallizes in a pure chiral structure.

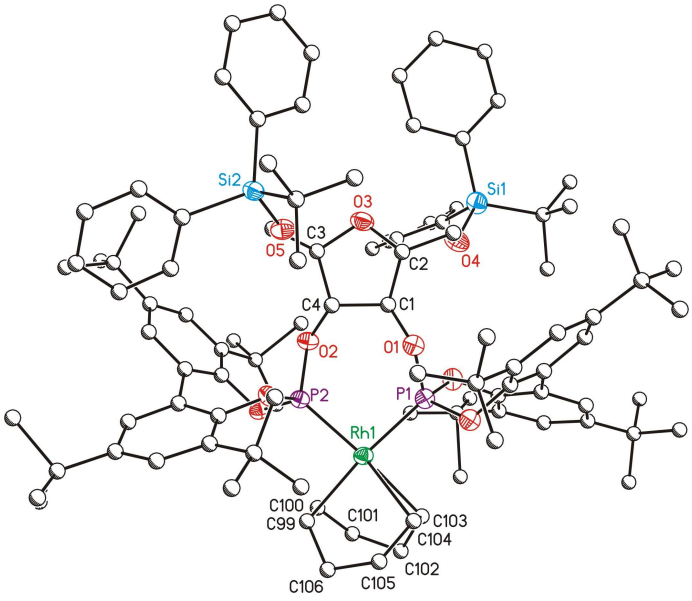

Figure 2.31. Structure model (ellipsoids at 50 % probability level) of [Rh(cod)(**74a**)]BF_4, **90a**. Counterions, solvates and hydrogen atoms have been omitted for the sake of clarity. Selected bond distances and angles are given in Tables 3 and 4 of the appendix.

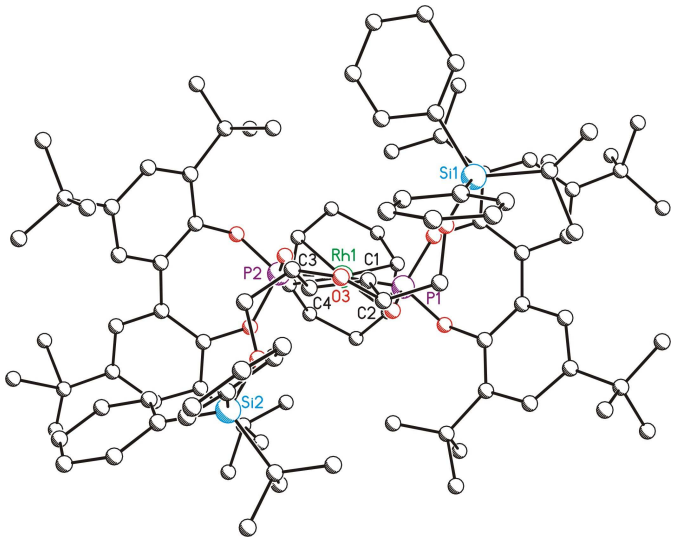

Figure 2.32. Structure model showing a lateral view of the complex [Rh(cod)(**74a**)]BF_4, **90a**.

Compound [Rh(cod)(**75'a**)]BF_4 (**91'a**) crystallizes with two independent cations in the elementary cell (Figure 2.33 to 2.36). The crystal cell also contains two anions of BF_4^- and four disordered positions of dichloromethane molecules. The independently obtained cationic structures have different conformations. In molecule A, the five-membered ring C1-C2-O1-C3-C4 has a twisted conformation and in molecule B the same ring has an envelope conformation. The seven-membered ring formed by the metal atom also shows different folding in molecules A and B. For molecule B, the folding of this seven-membered ring is more pronounced. In both molecules the rhodium atom is coordinated in a slightly distorted square planar geometry. In molecule A, the mean deviation from the plane is 0.041 Å and in molecule B the mean deviation from plane is 0.081 Å. The distances between the metal atom and the centers of the double bonds at the cyclooctadiene rings are in molecule A: 2.221 Å and 2.196 Å and in molecule B: 2.254 Å and 2.259 Å. The measured compound crystallizes in a pure chiral structure.

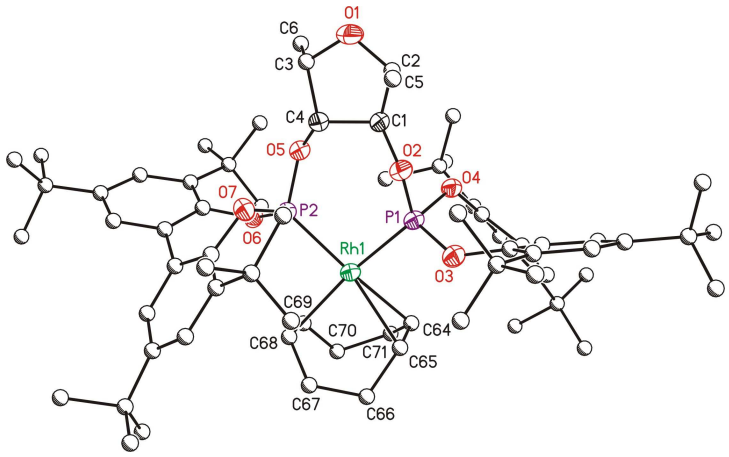

Figure 2.33. Structure model (ellipsoids at 50 % probability level) of [Rh(cod)(**75'a**)]BF_4, **91'a**, molecule A. Counterions, solvates and hydrogen atoms have been omitted for the sake of clarity. Selected bond distances and angles are given in Tables 5 and 6 of the appendix.

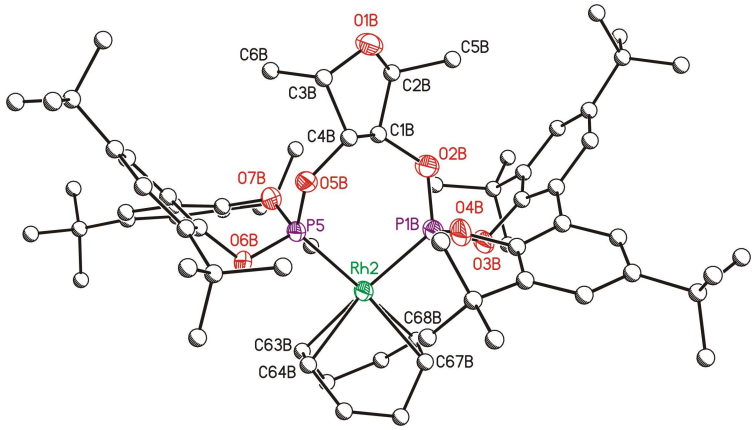

Figure 2.34. Structure model (ellipsoids at 50 % probability level) of [Rh(cod)(**75'a**)]BF_4, **91'a**, molecule B. Counterions, solvates and hydrogen atoms have been omitted for the sake of clarity. Selected bond distances and angles are given in Tables 5 and 6 of the appendix

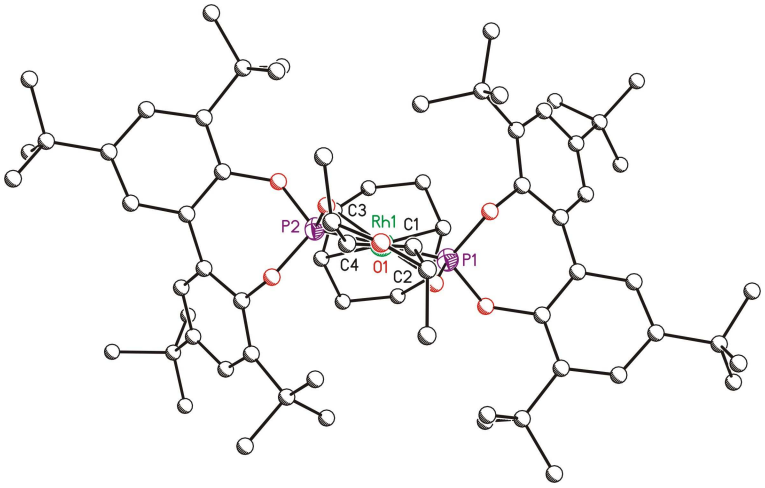

Figure 2.35. Structure model showing a lateral view of the [Rh(cod)(**75'a**)]BF_4, **91'a**, molecule A.

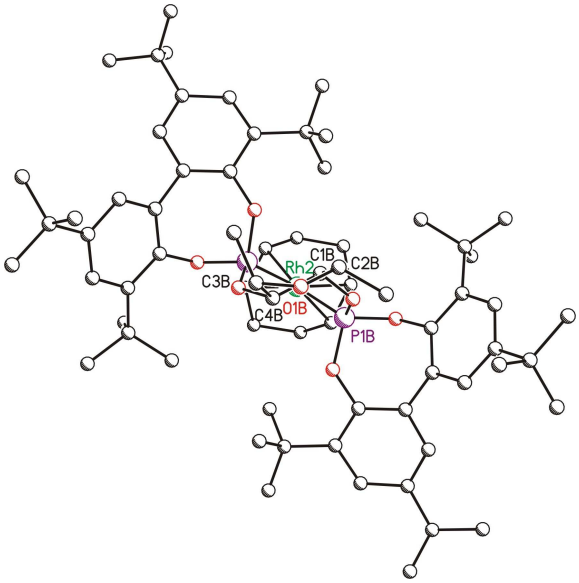

Figure 2.36. Structure model showing a lateral view of the [Rh(cod)(**75'a**)]BF_4, **91'a**, molecule B.

Although there are not many X-ray structures of rhodium complexes with carbohydrate ligands, the rhodium distances are similar to those of the previously described X-ray structure of rhodium-diphosphinite complex, **71d** (Figure 2.25), where diphosphinite ligand has the same furanoside backbone.[107]

2.2.3 Hydroformylation of styrene and related prochiral olefin

The chiral diphosphites **74-76** were used in the rhodium-catalysed asymmetric hydroformylation of styrene. The catalyst was prepared *in situ* by adding first the diphosphite ligand to a solution of $[Rh(acac)(CO)_2]$ (acac=acetylacetonate), and then the substrate. The results of the asymmetric hydroformylation of styrene are given in Tables 2.7 and 2.8. Neither hydrogenated nor polymerised products were observed. The effects of different reaction parameters were investigated for catalytic precursors containing diphosphite ligands **74** to **76**. The reaction parameters were in the range 60ºC to 25ºC of temperature, 20 bar (CO/H_2=1/1) to 30 bar (CO/H_2=1/2) of pressure and a rhodium/ligand ratio between 1/1 to 1/4.

We optimised the conditions with ligands **74a-c** and **74'a**,**b** (Table 2.7). We observed that when the Rh/L ratio was 1:2 the enantioselectivity increased and the activity decreased (Table 2.7, entry 3 *vs* entry 4, entries 7 and 9 *vs* 8 and 11, entries 14-15 *vs* 16-17, and entry 18 *vs* 19). This is because at low Rh/L ratios $[RhH(CO)_4]$ is formed, which is a highly active achiral hydroformylation catalyst.[14] A rhodium/ligand ratio of 1/4 did not enhance the regioselectivity or the enantioselectivity (Table 2.7, entries 11-12).

The effect of the partial pressure of hydrogen was also studied. We observe no improvement in the activity, the regioselectivity or the enantioselectivity when the hydrogen pressure was increased to 20 bar ($P_{CO/H2}$= 1/2) (Table 2.7, entries 4-5 and 9-10). The fact that the activity did not increase when the partial pressure of H_2 was increased suggests that the rate determining step is not the hydrogenolysis but the alkene coordination.

Lower temperatures led to a decrease in the activities (Table 2.7, entries 7 *vs*. 11 or 16 *vs*. 17), thus we needed 48 hours at 25ºC of temperature to have comparable conversions than the obtained at 40ºC for 15 hours. In some cases a slight increase in the enantioselectivities (Table 2.7, entries 2 to 4) was also observed.

Table 2.7. Styrene hydroformylation with diphosphites **74-76**[a]

Entry	L	Rh/L	t (h)	T (ºC)	% conversion[b]	% regioselec.[c]	%ee
1	**74a**	1/1	15	60	99	78	20 (*S*)
2	**74a**	1/2	15	40	57	96	41 (*S*)
3	**74a**	1/1	48	25	>99	93	20 (*S*)
4	**74a**	1/2	48	25	77	97	46 (*S*)
5	**74a** [d]	1/2	48	25	85	97	42 (*S*)
6	**74b**	1/1	15	60	99	79	24 (*S*)
7	**74b**	1/1	15	40	99	88	28 (*S*)
8	**74b**	1/2	15	40	64	93	30 (*S*)
9	**74b**	1/1	48	25	>99	95	30 (*S*)
10	**74b** [d]	1/1	48	25	99	94	25 (*S*)
11	**74b**	1/2	48	25	97	93	39 (*S*)
12	**74b**	1/4	48	25	61	95	37 (*S*)
13	**74c**	1/1	15	60	99	79	0
14	**74'a**	1/1	15	40	99	93	4 (*R*)
15	**74'a**	1/1	48	25	98	95	4 (*R*)
16	**74'a**	1/2	15	40	98	93	14 (*R*)
17	**74'a**	1/2	48	25	96	97	12 (*R*)
18	**74'b**	1/1	15	40	98	92	5 (*R*)
19	**74'b**	1/2	15	40	98	94	19 (*R*)

[a]Substrate/Rh=200, styrene 2.7 mmol, [Rh(acac)$(CO)_2$] 0.0135mmol P=20 bar, 15 ml toluene Pco/H_2=1 [b] % conv. Styrene determined by G.C.[c] % 2-fenylpropanal [d] Pco= 10 PH_2=20

For comparative purposes, the rest of the ligands were tested under conditions that gave the optimum compromise between enantioselectivities and reaction rates; that is a ligand to rhodium ratio of 2, a total pressure of 20 bar of synthesis gas with a P_{CO}/P_{H2} ratio of 1 and a temperature of 40 ºC. The results are given in Table 2.8.

The comparison of the different catalysts that incorporate ligands derived from mannitol **74**, iditol **75** and dihydroxytetrahydrofuran **76**, showed that those that contain ligands **74a**,**b** and **75a**,**b** have slightly higher activity than those containing the reference ligands **76a**,**b** (Table 2.8, entries 1, 2 and 5, 6 *vs*. 9, 10). More

curious and difficult to explain are the results obtained with the catalytic systems Rh/**74'a**, **b**, which are much more actives, and Rh/**75'a**,**b**, which are the least actives (Table 2.8, entries 3, 4 and 7, 8). Ligands **74'a**,**b** and **75'a**,**b** have a methyl group at positions 2 and 5 of the tetrahydrofuran backbone, and are less crowded than ligands **74a**,**b** and **75a**,**b**, which have a OTBDPS group, but more hindered than ligands **76a**,**b** which have no substituents at these positions. In all cases, the regioselectivity in the branched aldehyde was higher than 90%, and in several cases it was higher than 95%. This values are in agreement with those obtained with diphosphite ligands containing biphenyl moieties. .[14, 16, 56]

Table 2.8. Styrene hydroformylation with diphosphite **74-76**[a]

Entry	L	% conversion[b]	% regioselec.[c]	%ee
1	**74a**	57	96	41 (*S*)
2	**74b**	64	93	30 (*S*)
3	**74'a**	98	93	14 (*R*)
4	**74'b**	98	94	19 (*R*)
5	**75a**	57	95	22 (*R*)
6	**75b**	40	98	43 (*R*)
7	**75'a**	33	96	17 (*S*)
8	**75'b**	25	94	18 (*S*)
9	**76a**	43	>99	26 (*R*)
10	**76b**	38	94	34 (*R*)

[a]Substrate/Rh=200, Rh/L=0.5, styrene 2.7 mmol, [Rh(acac)$(CO)_2$] 0.0135mmol, P=20 bar, 15 ml toluene Pco/H_2=1, temp=40ºC, reaction time: 15 hours [b] % conv. Styrene determined by G.C.[c] % 2-fenylpropanal [d] Pco= 10 PH_2=20

If we compare the results obtained with ligands **74a** and **74b** with **74c** (Table 2.7, entries 1, 6 and 13) we observe that they have similar the activities and regioselectivities but no enantioselectivity was observed with ligand **74c**. This indicates that bulky substituents need to be in the *ortho*-positions of the biphenyl moieties if asymmetric induction is to be obtained. This behaviour was also observed in other diphosphite ligands with the same biphenyl moieties.[14, 16, 56] Introducing a methoxy group into ligands **74-76** (ligands **b**) at the *para*-positions

of biphenyl moieties increased the enantioselectivity. Nevertheless, the activity for ligands **74b-76b** was slightly lower than for the corresponding **74a-76a** (see for instance Table 2.8, entries 5 *vs*. 6). Similar behaviour has also been observed in other carbohydrate derivative diphosphite ligands.[14, 16, 56] Ligands **74a**, **b** are an exception, since when ligand **74b** was used the activity was higher and the enantioselectivity lower than with ligand **74a**.

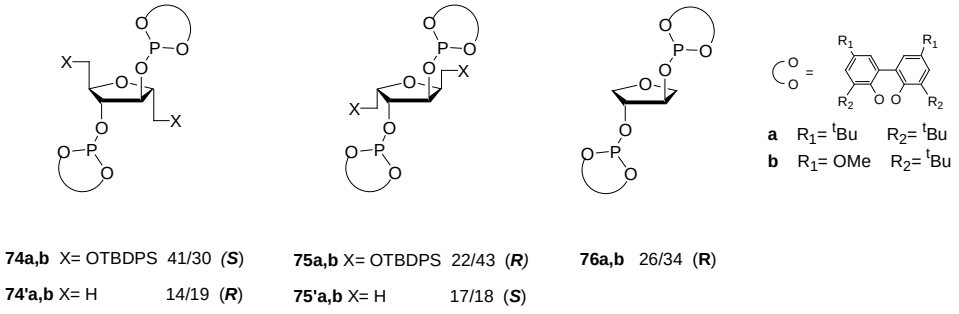

Figure 2.37. Values of enantioselectivity and configuration of the major enantiomer obtained in the hydroformylation of styrene using Rh/**74**-**76** catalytic systems

In general the enantiomeric excess obtained with ligands **74-76** was always moderate and the absolute values obtained with the catalytic systems Rh/**74a**,**b**-**75a**,**b** were in the same range as those obtained with Rh/**76a**,**b**. However, we observed that the configuration of the stereocenters at positions 2,5 of the tetrahydrofuran backbone and the substituents of these positions had a strong effect on the sense of the asymmetric induction (Table 2.8).

In general, as has been mentioned above, the enantioselectivities were higher when the bulky substituents in the chains were at positions 2 and 5. This is the case of ligands **74a**,**b** and **75a**,**b** (where X= OTBDPS, Table 2.8, entries 1 and 6) (Figure 2.37), in comparison with ligands **76** (Table 2.8, entries 9 and 10). The enantioselectivities were poorest when ligands had a methyl group in positions 2 and 5, **74'a**,**b** and **75'a**,**b** (Table 2.8, entries 3, 4 and 7, 8, respectively). This tendency that has already been mentioned for ligands **74** and **74'**, is also observed in ligands **75** and **75'**.

However, what is noteworthy is the fact that the configuration of the major enantiomer obtained is governed by both the substituents and the configuration of the remote stereocenters at positions 2 and 5 (Table 2.8, Figure 2.37). Thus, taking ligand **76**, which has no substituents at positions 2 and 5, as a reference ligand it can be observed that when **75** was used as the ligand the enantioselectivity increased slightly to afford the major enantiomer with the same configuration as **76**. Curiously, ligand **74**, which differs from **75** only in the configuration of the stereogenic centers at positions 2 and 5, preferentially gave the opposite enantiomer.

The behaviour of ligands **74'** and **75'** is also curious. From the point of view of the influence of the chains at positions 2,5, they would be expected to provide results intermediates between **74**, **75** and **76**. However, **75'** gave an enantiomeric excess lower than **75** and **76**, but preferentially afforded the opposite enantiomer. Similarly, **74'** also gave a lower enantioselectivity than **74**, and the opposite enantiomer was also the major one. Thus, the configuration of the major enantiomer is inverted by changing the group at positions 2 and 5, but more significantly because the effect is more important, when change the configuration at positions 2 and 5.

This behaviour has already been observed in the asymmetric hydrogenation reaction of enamidoesters with diphosphinite ligands **70-72** (Figure 2.25) which have a similar structure.[107] We are currently exploring the reasons for this behaviour, and although we have not yet an explanation for that, it can be suggested that the influence of the remote stereocenters on the sense of the chiral induction can be due to the influence of the chains at positions 2 and 5, in the conformation on the biphenyl moieties, which are ultimately responsible for the chirality transfer. It is known that the rotation around the biaryl axis of the diphosphite ligands containing bulky substituents in the biaryl moieties is hindered and that the biphenyl moiety preferentially adopts one configuration (see Figure 2.6).[14, 33]

Finally, we applied the diphosphite ligand **74a** in the rhodium-catalysed hydroformylation of various substituted vinyl arenes. The results are summarised in Table 2.9.

Table 2.9. Hydroformylation of different vinyl arenes with diphosphite **74a**[a]

Entry	Substrate	% conv[b]	% regioselec.[c]	%ee
1	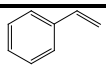	57	96	41 (*S*)
2	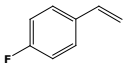	60	97	49 (*S*)
3	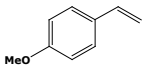	34	96	60 (*S*)
4	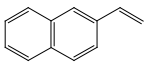	96	94	18 (*S*)

[a]Substrate/Rh=200, Rh/L=0.5,substrate 2.7 mmol, $[Rh(acac)(CO)_2]$ 0.0135mmol P=20 bar,15 ml toluene Pco/H_2=1, temp=40ºC, reaction time: 15 hours [b] % conv. substrate determined by G.C.[c] % branched aldehyde

The presence of a fluoro substituent in the *para*-position of the substrate (Table 2.9, entry 2) did not affect the activity or the regioselectivity. If we compare the results with those obtained in the hydroformylation of styrene (Table 2.9, entry 1), a slight increase in the enantioselectivity (41%ee *(S)* to 49%ee *(S)*) is observed. When a methoxy group is introduced in the *para*-position the enantioselectivity is enhanced to 60%ee *(S)* (Table 2.9, entry 3), but the activity is lower. Unexpectedly, the hydroformylation of 2-vinylnaphthalene with diphosphite **74a** evolved with high activity but very low enantioselectivity, 18%ee *(S)* (Table 2.9, entry 4). In all cases, the sense of the asymmetric induction was the same. We can conclude that introducing various substituents in the *para*-position of the substrate, which changes not only its electronic but also its steric properties, affects the conversion and the enantioselectivity. When a methoxy group is introduced in the *para*-position the activity decreases whereas the enantioselectivity is enhanced. The opposite behaviour is observed in the asymmetric hydroformylation of 2-vinylnaphthalene. The literature describes some examples in which the rhodium-catalysed hydroformylation of *p*-methoxystyrene provided higher enantioselectivities than other vinylarenes such as styrene, 2-vinylnaphthalene and

p-fluorostyrene .[104, 118, 119] However, the enantioselectivities obtained with the other ones depended on the ligand used and no correlation was found.

2.2.4 High pressure NMR study

The hydridorhodium diphosphite complexes $[RhH(CO)_2(L)]$ (L: bidentate ligand) are generally considered as the resting state in the hydroformylation reaction.[32, 33, 39, 40] They are generally assumed to have a trigonal-bipyramidal structure. Two isomeric structures of these complexes, with a coordinated bidentate ligand, can be formed (Figure 2.38). The bidentate ligand can coordinated in an equatorial-equatorial (**ee**) or in equatorial-axial (**ea**) fashion. The presence of only one active diastereoisomeric hydridorhodiumcarbonyl species with bidentate ligands is presumably the key of an efficient control of the chirality transfer.[14]

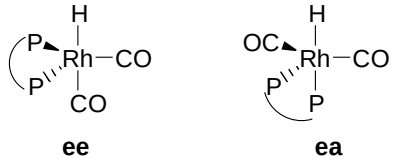

Figure 2.38. Equatorial-equatorial (**ee**) and equatorial-axial (**ea**) $[RhH(CO)_2(L)]$ species.

In our previous study of the hydroformylation reaction with ligands **74**-**76** we used $[Rh(acac)(CO)_2]$ as catalyst precursor. We therefore used the same compound as starting material in our study on the evolution of this precursor in the presence of diphosphite ligand under the reaction conditions. Under typical hydroformylation conditions, [Rh(acac)(L)] complexes transform to trigonal bipyramidal hydridorhodium diphosphites (Scheme 2.11). For this study we used high pressure-NMR spectroscopy.

[Rh(acac)(L)] complexes were prepared by adding one equivalent of diphosphite ligand to the rhodium precursor $[Rh(acac)(CO)_2]$. For [Rh(acac)(L)] species chemical shifts around 140 ppm have been reported with rhodium-phosphorus coupling constants close to 300 Hz when L is a diphosphite.[47, 48] Intermediate

complexes [Rh(acac)(CO)(L)] can also be formed under hydroformylation conditions. They have slightly lower chemical shifts than [Rh(acac)(L)] complexes with a rhodium-phosphorus coupling constants close to 290 Hz.[47, 48] Under typical hydroformylation conditions, [Rh(acac)(L)] complexes undergo transformation to trigonal bipyramidal hydridorhodium diphosphites in which the diphosphite ligand coordinates in an **ee** or **ea** fashion. The complexes with **ee** (equatorial-equatorial) coordination show small phosphorus-hydrogen coupling constants (<10Hz), whereas the coupling constant of a *trans* coordinated phosphite, **ea** (equatorial-axial) complex, shows a large phosphorus-hydrogen coupling constant of 180-200 Hz. The phosphorus-phosphorus coupling constants are much larger for the **ee** complex (around 250 Hz) than for the **ea** complex (usually 70 Hz). [14, 47, 48, 54]

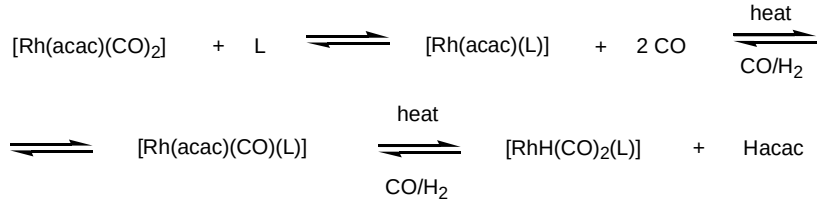

Scheme 2.11. Formation of $[RhH(CO)_2(L)]$ from $[Rh(acac)(CO)_2]$ and diphosphite (L)

The initial solution of $[Rh(acac)(CO)_2]$ and diphosphite ligand (**74**-**76**) in toluene-d_8 was analysed by ^{31}P and ^{1}H NMR. Then the NMR tube was pressurised with syngas (20 bar) and heated at 80ºC for 30 minutes, hydroformylation conditions, and the spectra of ^{31}P and ^{1}H NMR were then recorded. Finally the NMR tube was shaken for 15 h at 80ºC and the ^{31}P and ^{1}H NMR spectra were again recorded.

When ligands **74a** and **74b** were added to a solution of $[Rh(acac)(CO)_2]$ in toluene-d_8, the colour changed immediately and in ^{31}P NMR spectrum showed the presence of a doublet assigned to [Rh(acac)(L)] (L=**74a**, **74b**) species (Figure 2.39a). After the NMR tube was pressurized and heated for 30 minutes, the presence of a new doublet in the ^{31}P NMR spectrum indicated that a new species had formed (Figure 2.39b). Maintaining the solution under hydroformylation conditions the [Rh(acac)(L)] for 15 h, all species completely evolved to this new species (Figure

2.39c), which it was assigned to be [RhH(CO)$_2$(L)] on the basis of ^{31}P and ^{1}H spectrum (see later structural elucidation). No traces of intermediate species [Rh(acac)(CO)(L)] or other species were detected.

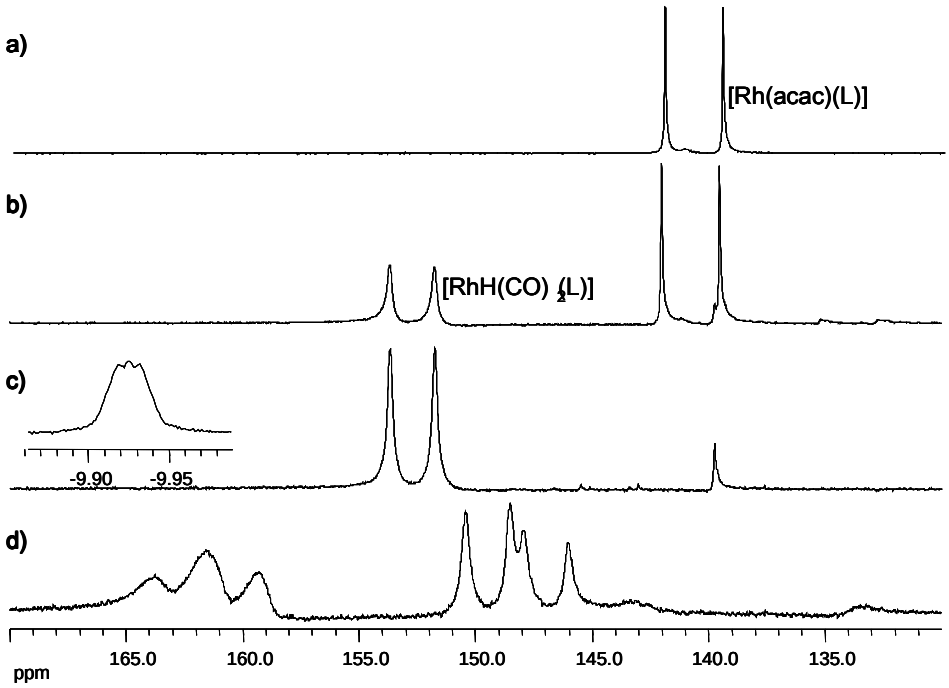

Figure 2.39. ^{1}H and ^{31}P{^{1}H} NMR spectra of the evolution of the precursor [Rh(acac)(CO)$_2$] in the presence of ligand **74a**, under hydroformylation conditions (80ºC and 20 bar of syn gas) in toluene-d$_8$. a) [Rh(acac)(**74a**)] at room temperature, b) after 30 minutes under hydroformylation conditions c) after 15 h under hydroformylation conditions, spectrums collected at room temperature and d) after 15 h under hydroformylation conditions, spectrum collected at –100ºC.

The study that started from [Rh(acac)(CO)$_2$] and used ligands **74'a**, **75a**, **75'a** and **76a** showed a different behaviour than for ligands **74a** and **74b** because intermediate species [Rh(acac)(CO)(L)] were observed. As was observed for ligands **74a** and **74b**, when ligands **74'a**, **75'a** and **76a** were added to the solution of [Rh(acac)(CO)$_2$] in toluene-d$_8$ a fast change of colour and displacement of CO were observed and the ^{31}P NMR spectrum also showed a doublet that was characteristic of the [Rh(acac)(L)] (L= **74'a**, **75'a** and **76a**) species (Figures 2.40a and 2.41a and b). However, in the case of diphosphite ligand **75a**, for which the displacements of CO and the change in colour were also observed, the ^{31}P NMR

spectrum showed a mixture of [Rh(acac)(CO)(L)], where **75a** coordinated in a bidentate fashion, and traces of another complex were ligand was coordinated in a monodentate fashion (Figure 2.40a). The $^{31}P\{^{1}H\}$ NMR chemical shifts (in ppm) and the coupling constants (in Hertzs) of these species are summarised in Table 2.10.

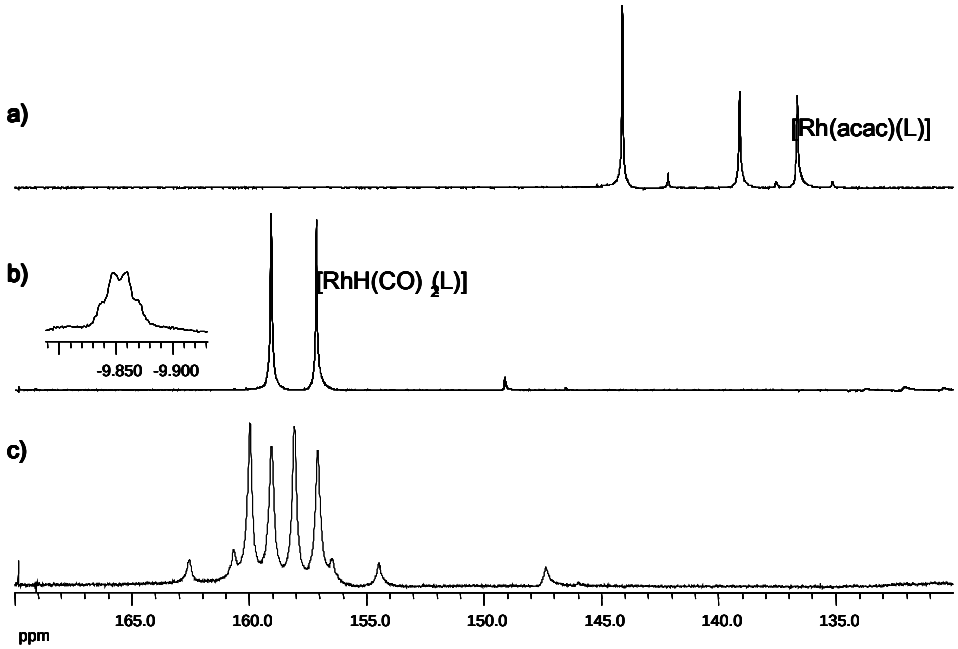

Figure 2.40. ^{1}H and $^{31}P\{^{1}H\}$ NMR spectra of the evolution of the precursor $[Rh(acac)(CO)_2]$ in the presence of ligand **75a**, under hydroformylation conditions (80ºC and 20 bar of syn gas) in toluene-d_8. a) [Rh(acac)(**75a**)] at room temperature, b) after 15 h under hydroformylation conditions, spectrums collected at room temperature and c) after 15 h under hydroformylation conditions, spectrum collected at –80ºC.

After a reaction time of 15 hours and shaking at the desired temperature, the solution was analysed at room temperature. In all cases stable $[RhH(CO)_2(L)]$ complexes were obtained exclusively, since a doublet was observed in ^{31}P NMR around 155 ppm with a rhodium-phosphorus coupling constant near 230 Hz; small amounts of the phosphonate signal was observed around 10 ppm. In the ^{1}H NMR spectrum we detected the signal for the hydride around –10 ppm (Figures 2.39c, 2.40b and 2.41c).

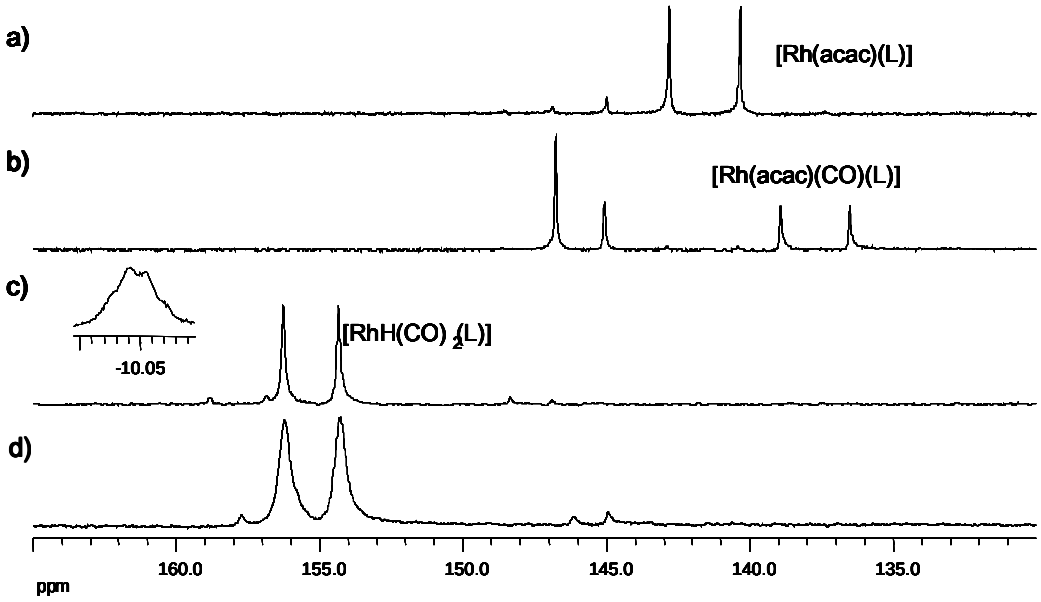

Figure 2.41. ^{1}H and $^{31}P\{^{1}H\}$ NMR spectra of the evolution of the precursor $[Rh(acac)(CO)_2]$ in the presence of ligand **76a**, under hydroformylation conditions (80ºC and 20 bar of syn gas) in toluene-d_8. a) [Rh(acac)(**76a**)] at room temperature, b), after a short period of time under hydroformylation conditions, d) after 15 h under hydroformylation conditions, spectrums collected at room temperature and d) after 15 h under hydroformylation conditions, spectrum collected at –80ºC.

Structural assignments

The $^{31}P\{^{1}H\}$ NMR chemical shifts (in ppm) and the coupling constants (in Hertzs) of complexes [Rh(acac)(L)] and [Rh(acac)(CO)(L)] are summarised in Table 2.10. The [Rh(acac)(L)] complexes showed chemical shifts in the range 140 to 147 ppm with $^{1}J_{Rh-P}$ coupling constants around 300 Hz. The bidentate [Rh(acac)(CO)(L)] species showed doublets between 133.71 and 137.97 ppm with $^{1}J_{Rh-P}$ coupling constants around 295 Hz; when the ligand coordinates in a monodentate fashion we detected a singlet between 141.72 and 146.76 ppm, near the signal of the free ligand, and a doublet between 135.47 and 137.76 ppm with $^{1}J_{Rh-P}$ coupling constants around 295 Hz.

Table 2.10. $^{31}P\{^{1}H\}$ NMR data for [Rh(acac)(L)] and [Rh(acac)(CO)(L)]complexes[a]

Ligand	[Rh(acac)(L)][b]		[Rh(acac)(CO)(L)][b]	
	$\delta(^{31}P)$[b]	$^{1}J_{Rh-P}$[c]	$\delta(^{31}P)$[b]	$^{1}J_{Rh-P}$[c]
74a	140.78 (d)	301.4	-	-
74b	141.29 (d)	300.3	-	-
74'a	141.14 (d)	299.5	133.71 (d) 141.72 (s), 135.47 (d)	296.3 293.9
75a	-	-	137.86 (d) 142.16 (s), 136.34 (d)	299.13 290.75
75'a	141.55 (d)	300.1	146.76 (s), 137.70 (d)	291.60
76a	147.12 (d)	294.1	137.97 (d) 143.82(s), 137.76 (d)	295.85 294.12

[a]Prepared in toluene-d_8 by adding 1.1 equivalents of ligand to $[Rh(acac)(CO)_2]$ solution. [b] ^{31}P and ^{1}H NMR spectra recorded in toluene-d_8 using High-pressure NMR. Chemicals shifts δ in ppm multiplicity) [c] Coupling constants in Hz.

Table 2.11 shows selected data obtained for the $[RhH(CO)_2(L)]$ (L:**74**–**76**) complexes, which showed somewhat broadened doublets at room temperature in the $^{31}P\{^{1}H\}$ NMR spectra. These broad signals suggest a fluxional process on the NMR time scale.[33] The doublets appeared between 152.70 and 158.09 ppm showing a $^{1}J_{Rh-P}$ coupling constants in the range 230.0 to 234.1 Hz. These large $^{1}J_{Rh-P}$ coupling constants indicate that the ligands coordinate in an equatorial-equatorial fashion in the trigonal-bipyramidal hydridorhodiumcarbonyl species.[14, 47, 48, 54] In the ^{1}H NMR spectrum we detected the signal for the hydride around –10 ppm. The $^{1}J_{Rh-H}$ coupling constants were in the range of 2.0 to 3.8 Hz and the $^{2}J_{P-H}$ coupling constants were between 2.0 and 9.0 Hz. These small phosphorus-hydrogen coupling constants (<10Hz) mean that the hydride signal appears as a quadruplet in most cases, except for the complex with ligand **74a** where the really small coupling constants revealed a broad signal, and for the complex with ligand **76a** where a double triplet was observed in the hydride region. This comfirms the a *cis* relationship between the phosphorus and the hydrogen atom bonded to the rhodium. Large $^{1}J_{Rh-P}$ coupling constants around 235 Hz, and small $^{2}J_{P-H}$ coupling

constants have been reported for diphosphite ligands which coordinate in an equatorial-equatorial fashion in the hydridorhodium species.[14, 47, 48, 54]

Table 2.11. Selected ^{1}H and $^{31}P\{^{1}H\}$ NMR data for $[RhH(CO)_2(L)]$ complexes[a]

Ligand	$\delta(^{31}P)$[b]	$\delta(^{1}H)$[b]	$^{1}J_{Rh-P}$[c]	$^{1}J_{Rh-H}$[c]	$^{2}J_{P-H}$[c]
74a	152.70 (d)	-9.93 (br t)	231.9	2.0	2.0
74b	155.33 (d)	-9.91 (q)	230.0	3.4	3.9
74'a	155.43 (d)	-10.14 (q)	231.6	2.7	3.8
75a	158.09 (d)	-9.85 (q)	233.6	2.9	3.1
75'a	155.27 (d)	-10.05 (q)	234.1	3.8	3.9
76a	156.40 (d)	-10.24 (dt)	232.6	3.4	9.0

[a]Prepared in toluene-d_8 by adding 1.1 equivalents of ligand to $[Rh(acac)(CO)_2]$ solution, 15 h. at 80ºC and 20 bar of syn gas. [b] ^{31}P and ^{1}H NMR spectra recorded in toluene-d_8 using High-pressure NMR. Chemicals shifts δ in ppm (multiplicity) [c] Coupling constants in Hz.

Low temperature studies

As a consequence of the C_2-symmetry, phosphorus atoms are equivalent in the free ligand. However, this is not the case in hydridorhodiumcarbonyl diphosphite complexes, because even when both phosphorus atoms are coordinated in an equatorial-equatorial fashion to the rhodium the complex has C_1-symmetry. The fact that only one doublet is observed in the $^{31}P\{^{1}H\}$ NMR spectrum, means that either the chemical shifts of both atoms accidentally coincide or that they exchange rapidly on the NMR time scale.[14, 47, 48, 54] We studied the hydridorhodiumcarbonyl species at low temperature under hydroformylation conditions. Table 2.12 summarizes selected ^{1}H and $^{31}P\{^{1}H\}$ NMR data for $[RhH(CO)_2(L)]$ complexes at low temperature.

We detected that the behaviour of these species strongly depends on the structure of the diphosphite ligands. Complexes $[RhH(CO)_2(L)]$ where L: **74a**, **74b** and **74'a**, derived from 2,5-anhydro-D-mannitol, showed the same behaviour. When the

temperature decreased we observed line broadening in the $^{31}P\{^{1}H\}$ NMR and in the hydride region of the ^{1}H NMR. The signals of the $^{31}P\{^{1}H\}$ NMR for complexes $[RhH(CO)_2(L)]$, where L: **74a** and **74'a**, were resolved at –100ºC (see Figure 2.39d). We observed two double doublets in the $^{31}P\{^{1}H\}$ NMR spectrum: one signal appeared around 160 ppm, and the other around 150 ppm. The coupling constants, $^{1}J_{Rh-P1}$ around 270 Hz and $^{1}J_{Rh-P2}$ around 230 Hz, and $^{2}J_{P-P}$ around 300 Hz, indicated that the ligand was coordinated in an equatorial-equatorial fashion to the complex. The hydride region in the ^{1}H NMR spectrum was not resolved showing a line broadening at this temperature.

Table 2.12. Selected ^{1}H and $^{31}P\{^{1}H\}$ NMR data for $[RhH(CO)_2(L)]$ complexes at low temperature[a]

Ligand	δ(^{31}P)[b]		$^{1}J_{Rh-P1}$[c]	$^{1}J_{Rh-P2}$[c]	$^{2}J_{P-P}$[c]	T/ºC
74a	161.56 (dd)	148.21 (dd)	270.9	230.2	302.2	-100
74b	153.92 (broad)			Unresolved		- 80
74'a	164.42 (dd)	153.62 (dd)	269.3	232.6	305.1	-100
75a	160.30 (dd)	156.75 (dd)	230.1	240.4	314.2	-80
75'a	157.49 (broad d)		238.6		-	-100
76a	158.68 (broad d)		233.5		-	-80

[a]Prepared in toluene-d_8 by adding 1.1 equivalents of ligand to $[Rh(acac)(CO)_2]$ solution, 15 h. at 80ºC and 20 bar of syn gas. [b] ^{31}P and ^{1}H NMR spectra recorded in toluene d_8 using High-pressure NMR. Chemicals shifts δ in ppm (multiplicity) [c] Coupling constants in Hz.

For the $[RhH(CO)_2($**75a**$)]$ complex, where diphosphite ligand **75a** is derived from 2,5-anhydro-L-iditol, the decrease in the temperature also led to line broadening in the $^{31}P\{^{1}H\}$ NMR and the hydride region on the ^{1}H NMR. The $^{31}P\{^{1}H\}$ NMR was resolved at –80ºC, we observed an eight-line spectrum for phosphorus atoms. These was due to an ABX system where $^{1}J_{Rh-P1}$ and $^{1}J_{Rh-P2}$ were very close, 230 and 240 Hz, and the signals appeared at 160.30 and 156.75 ppm with a phosphorus-phosphorus coupling constant of 314.2 Hz (see Figure 2.40c). These coupling constants indicated an equatorial-equatorial coordination mode.

In the variable temperature study of the hydridorhodiumdicarbonyl complexes with ligands **75'a** and **76a** we observed only a slight broadening of the doublet at –80ºC (Figure 2.41d). This indicates that the fluxional process at this temperature does not halt completely, which indicates a lower-energy-barrier in this process than the ligands **74a**, **74b**, **74'a** and **75a**.

These new carbohydrate derivative ligands **74-76** were expected to show an equatorial-axial coordination mode in the trigonal bipyramidal hydridorhodium dicarbonyl species since they form a seven-membered chelate ring when they coordinate to the rhodium, as usual as observed in ligands which form seven-membered rings coordinate mainly in **ea** fashion.[47, 48, 120] However, this is not the case for ligands **74-76**, which coordinate in an **ee** fashion (corroborated by large $^{1}J_{Rh-P}$ and $^{2}J_{P-P}$ coupling constants and small $^{2}J_{P-H}$ coupling constants, observed in the NMR spectrum). This behaviour may be due to the rigidity of the ligands, and the presence of the tetrahydrofuran backbone could favour this coordination. A reported ligand derived from *N*-benzyltartarimide,[47] which forms a seven-membered ring when it coordinates to the rhodium and has a backbone composed by five-membered ring (diphosphite **18a**, see Figure 2.5), also coordinates in an equatorial-equatorial mode. Even when the ligands coordinated in an equatorial-equatorial mode, the enantioselectivities obtained with these ligands in asymmetric the hydroformylation reaction were moderate or low. [47]

2.2.5 Rhodium-catalysed hydrogenation of methyl acetamidoacrylate

In order to know how complexes $[Rh(cod)(L)]BF_4$ **90-92** behave in asymmetric hydrogenation, we tested them as catalyst precursors in the hydrogenation of methyl acetamidoacrylate in a multireactor (Scheme 2.12). The results are summarised in Table 2.13.

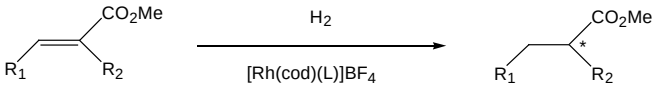

R_1 = H, R_2 = NHCOMe

Scheme 2.12. Hydrogenation of methyl acetamidoacrylate with $[Rh(cod)((L)]BF_4$ catalytic system

Table 2.13 summarizes the results obtained in the hydrogenation of methyl acetamidoacrylate with [Rh(cod)(L)]BF_4 complexes **90-92** using dichloromethane or dichloromethane/methanol (2/1) as a solvent, rhodium/subtrate ratio=100 at 10 bar of H_2 pressure and at room temperature. We also decided to use a mixture of dichloromethane and methanol as the solvent in order to improve the activity and selectivity of the system, since in Rh/diphosphite asymmetric hydrogenation it was observed that these solvents improve the results.[35, 56, 109]

Table 2.13. Hydrogenation of methyl acetamidoacrylate with [Rh(L)(cod)]BF_4 complexes **90-92**[a]

Entry	Ligand	solvent	conv. (%)	TOF (h^{-1})	% ee
1	**74a**	CH_2Cl_2	7	0.5	0
2	**74a**[b]	CH_2Cl_2	61	4.1	10 (*R*)
3	**74a**	CH_2Cl_2/CH_3OH	41	2.7	45 (*R*)
4	**74b**	CH_2Cl_2	6	0.4	8 (*R*)
5	**74c**	CH_2Cl_2	>99	-	57 (*R*)
6	**74c**	CH_2Cl_2/CH_3OH	21	1.4	0
7	**74'a**	CH_2Cl_2	21	1.4	16 (*R*)
8	**74'a**[b]	CH_2Cl_2	59	3.9	19 (*R*)
9	**74'a**	CH_2Cl_2/CH_3OH	24	1.6	3 (*R*)
10	**74'b**	CH_2Cl_2	74	4.9	34 (*R*)
11	**74'b**	CH_2Cl_2/CH_3OH	20	1.3	11 (*R*)
12	**75a**	CH_2Cl_2	81	5.4	0
13	**75a**	CH_2Cl_2/CH_3OH	16	1.1	3 (*S*)
14	**75'a**	CH_2Cl_2	20	1.3	6 (*S*)
15	**75'a**	CH_2Cl_2/CH_3OH	21	1.4	0
16	**76a**	CH_2Cl_2	26	1.7	13 (*R*)
17	**76a**	CH_2Cl_2/CH_3OH	29	1.9	7 (*R*)
18	**76b**	CH_2Cl_2	17	1.1	6 (*R*)
19	**76b**	CH_2Cl_2/CH_3OH	38	2.5	0

[a]Conditions:2.5 ml, Rh: $2.5x10^{-6}$ mol, Rh/substrate: 1/100, room temperature, $P(H_2)$: 10 bar. [b]Conditions: 5 ml, Rh: $5x10^{-6}$ mol, Rh/substrate: 1/100, room temperature, $P(H_2)$: 50 bar.

Activities were low for all thecomplexes tested, and a reaction time of at least 15 h was required to attain full conversion in the best cases. The most active catalytic system was the one with ligand **74c** (Table 2.13, entry 5). The enantioselectivities

were also poor, and results were also best with the catalytic system [Rh(cod)(**74c**)]BF_4. Ligand **74c** has no substituents in the biphenyl moieties, and this may explain the higher activity of the catalytic system containing this ligand. The enantiomeric excesses obtained show that substitution in the biphenyl moieties has a negative effect on the enantioselectivity. This has previously been observed for related xylose derivatives with bulky diphosphites.[121]

The results depend on the solvent used, and were very different in some cases depending on whether the solvent was dichloromethane or a dichloromethane/methanol mixture. When the dichloromethane/methanol mixture was used the [Rh(cod)(**74c**)]BF_4 system provided the racemic mixture, while in dichloromethane the enantioselectivity was 57% (Table 2.13, entries 5, 6). A similar tendency was observed for ligand **74'b**. However, when ligand **74a** was used the enantioselectivity increased significantly in this mixture of solvents (Table 2.13, entries 1, 3). With ligands **74a**, **75a**, **75'a**, **76a** and **76b** the effect was not important or was slightly negative. However, the conversion was generally lower in dichoromethane/methanol than in dichloromethane, with the exception of [Rh(cod)(**74a**)]BF_4, which may be due to the instability of the ligands in methanol. An increase in hydrogen pressure enhanced the conversion but had a little effect on the enantioselectivity (Table 2.13, entries 2 and 8 vs. 1 and 7).

As far as the influence of the substituents at positions 2 and 5 is concerned, [Rh(cod)(L)]BF_4 complexes with ligands **74** gave better results than with ligands **75** and **76**. The major enantiomer, when the enantiomeric excesses were substantial, was always *R*.

The previously described diphosphinite ligands, with the same furanoside backbone (Figure 2.25),[107] showed very high activities (total conversion in 5 minutes at 1 bar of H_2 pressure and room temperature) in the asymmetric hydrogenation of methyl acetamido acrylate, whereas the related diphosphite ligands **74-76** showed lower activities in more drastic conditions (10 bar of pressure and room temperature). This may be due to the greater steric hindrance of the diphosphite ligands (ligand **74c**, without substituents in the biphenyl moieties, showed higher activities than the rest of the related diphosphites) and also to the fact that the

diphosphite ligands are less basic than the diphosphinite ligands, since greater basicity favours the oxidative addition of hydrogen which is the rate- and enantioselective determining step of this reaction. On the other hand, in all cases the enantioselectivity of the Rh/diphosphite systems was much lower than the corresponding Rh/diphosphinite system.

2.3 Conclusions

New diphosphite ligands (**74-76**) with C_2-symmetry and a tetrahydrofuran backbone have been synthesised in moderate to good yields starting from D-glucosamine, D-glucitol and (2*S*,3*S*)-diethyl tartrate. Rhodium cationic complexes containing diphosphite ligands of general formula [Rh(cod)(L)]BF_4, (L= **74a**-**c**, **74'a**,**b**, **75a**, **75'a** and **76a**-**b**) were prepared by reacting [Rh(cod)$_2$]BF_4 with the respective ligands. Monocrystals of diphosphite ligand **74a** and rhodium cationic complexes [Rh(cod)(**74a**)]BF_4 **90a** and [Rh(cod)(**75'a**)]BF_4 **91'a**, suitable for X-ray diffraction were obtained. The structure of **74a**, **90a** and **91'a** could be proved unambiguously by single crystal X-ray diffraction.

This new family of diphosphite ligands has been applied to the rhodium-catalysed asymmetric hydroformylation of styrene and related substituted vinyl arenes. High regioselectivities to the branched aldehyde and moderate enantioselectivities were obtained. The configuration and substitution of the remote stereocenters at positions 2 and 5 of the tetrahydrofuran ring were observed to have a considerable influence on the enantioselectivity. The most significant result is that the configuration of the major isomer obtained in the hydroformylation reaction can be controlled by changing the configuration of these stereocenters.

The intermediate species in hydroformylation with diphosphite ligands **74a**, **74b**, **74'a**, **75a**, **75'a** and **76a** were studied by high pressure-NMR spectroscopy. These species were prepared *in situ* under hydroformylation conditions, observing that the formation of the hydridorhodiumcarbonyl specie was very slow. The small $^2J_{P\text{-}H}$ coupling constants (2.0 to 9.0 Hz) and the large $^1J_{Rh\text{-}P}$ coupling constants (230.0 to 234.1 Hz) indicate that the ligands coordinate in an equatorial-equatorial fashion in the trigonal-bypiramidal hydridorhodiumcarbonyl species. The low temperature

study of the hydridorhodiumcarbonyl species under hydroformylation conditions detected that the phosphorous atoms were non equivalent, which proved the C_1-symmetry of these complexes.

Rhodium complexes were tested in the asymmetric hydrogenation of methyl acetamidoacrylate. The conversions and the enantioselectivities were low and mainly influenced by the substitution in the biphenyl moiety and by the configuration of the remote centres at positions 2 and 5 of the tetrahydrofuran ring.

2.4 Experimental section

General methods

All syntheses were performed by using standard Schlenk techniques under argon atmosphere. Solvents were purified by standard procedures. Compounds **78**-**80**, **82**-**86**, **88** and **89** [107] and phosphorochloridites [46, 114] were prepared by methods described previously. All other reagents were used as commercially available. Elemental analyses were performed on a Carlo Erba EA-1108 instrument. ^{1}H, $^{13}C\{^{1}H\}$ and $^{31}P\{^{1}H\}$ NMR spectra were recorded on a Varian Gemini 400 MHz spectrometer. Chemical shifts are relative to $SiMe_4$ (^{1}H and ^{13}C) as internal standard or H_3PO_4 (^{31}P) as external standard. All NMR spectral assignments were determined by COSY and HSQC spectra. Gas chromatographic analyses were run on a Hewlett-Packard HP 5890A instrument (split/splitless injector, J&W Scientific, HP-5, 25 m column, internal diameter 0.25 mm, film thickness 0.33 mm, carrier gas: 150 kPa He, F.I.D. detector) equipped with a Hewlett-Packard HP3396 series II integrator. Hydroformylation reactions were carried out in a Berghof 100 ml. stainless steel autoclave. Enantiomeric excesses of hydroformylation reaction were measured after oxidation of the aldehydes to the corresponding carboxylic acids on a Hewlett-Packard HP 5890A gas chromatograph (split/splitless injector, J&W Scientific, FS-Cyclodex β-I/P 50 m column, internal diameter 0.2 mm, film thickness 0.33 mm, carrier gas: 100 kPa He, F.I.D. detector). Absolute configuration was determined by comparing of retention times with optically pure (*S*)-(+)-2-phenylpropionic and (*R*)-(-)-2-phenylpropionic acids. Hydrogenation reactions were carried out in a Parr 450 ml multiple reaction vessel autoclave.

Conversion and enantiomeric excesses of the reaction crude were measured on a Hewlett-Packard HP 5890A gas chromatograph (split/splitless injector, J&W Scientific, Permabond L-Chirasil-Val, 25 m. column, internal diameter 0.25 mm., carrier gas: 100 kPa He, F.I.D. detector).

Crystal structure determination was carried out using a Bruker-Nonius diffractometer equipped with a APPEX 2 4K CCD area detector, a FR591 rotating anode with $Mo_{K\alpha}$ radiation, Montel mirrors as monochromator and a Kryoflex low temperature device (T = 100 K). Fullsphere data collection omega and phi scans. Programs used: Data collection Apex2 V. 1.0-22 (Bruker-Nonius 2004), data reduction Saint + Version 6.22 (Bruker-Nonius 2001) and absorption correction SADABS V. 2.10 (2003). Crystal structure solution was achieved using direct methods as implemented in SHELXTL Version 6.10 (Sheldrick, Universtität Göttingen (Germany), 2000) and visualized using XP program. Missing atoms were subsequently located from difference Fourier synthesis and added to the atom list. Least-squares refinement on F2 using all measured intensities was carried out using the program SHELXTL Version 6.10 (Sheldrick, Universtität Göttingen (Germany), 2000). All non hydrogen atoms were refined including anisotropic displacement parameters.

Synthesis of the ligands

General procedure for synthesizing diphosphites from the corresponding diols. [107]

To a solution of the diol (0.5 mmol), which is previously azeotropically dried with toluene (3x1 ml), in dry and degassed toluene (5 ml) was added dry pyridine (2.0 mmol). After the mixture was cooled to 0 ºC was slowly added to a solution of phosphoroclorohidrite (2.2 mmol), synthesised *in situ* by standard procedure,[46, 114] in dry and degassed toluene (6 ml) and dry pyridine (2.2 mmol). The mixture was allowed to rise room temperature and stirred overnight. The mixture was then

filtered to eliminate the pyridine salts, and the filtrate was concentrated to dryness. The white foam was purified by chromatographic techniques.

3,4-Bis-*O*-[(3,3',5,5'-tetra-*tert*-butyl-1,1'-biphenyl-2,2'-diyl)phosphite]-1,6-di-*O*-(*tert*-butyl-diphenylsilyl)-2,5-anhydro-D-mannitol (74a)

The synthesis of **74a** was carried out in accordance with the general procedure from 0.3 g (0.47 mmol) of diol **80** in 5 ml of dry and degassed toluene and 0.2 ml (2.4 mmol) of dry pyridine. This solution was slowly added to a solution of 2.1 mmol of the corresponding phosphorochlorhydrite formed *in situ*, dissolved in 6 ml of toluene and 0.2 ml (2.4 mmol) of pyridine. The mixture was stirred overnight, the salts were filtered and the white foam was purified by flash column chromatography (eluent: toluene Rf=0.9) to afford 0.22 g (31 %) of **74a** as a white solid. $[\alpha]^{25}_{D}$ +76.72º (CH_2Cl_2, *c* 1.005); ^{1}H NMR ($CDCl_3$, 400 MHz) δ 7.64-7.00 (m, 28H, aromatic), 5.20 (s broad, 2H, H3), 3.96 (s broad, 2H, H2), 3.60 (m, 2H, H1), 3.38 (m, 2H, H1'), 1.43 (s, 18H, *o*-C($C\underline{H}_3$)$_3$), 1.37 (s, 18H, *p*-C($C\underline{H}_3$)$_3$'), 1.35 (s, 18H, *p*-C($C\underline{H}_3$)$_3$), 1.20 (s, 18H, *o*-C($C\underline{H}_3$)$_3$'), 0.93 (s, 18H, C($C\underline{H}_3$)$_3$); ^{13}C NMR ($CDCl_3$, 100.6 MHz) δ 146.30-124.1 (aromatic), 82.5 (C2), 79.5 (broad, C3), 62.5 (C1), 35.4 (*o*-$\underline{C}(CH_3)_3$), 35.3 (*o*-$\underline{C}(CH_3)_3$'), 34.7 (*p*-$\underline{C}(CH_3)_3$), 34.5 (*p*-$\underline{C}(CH_3)_3$'), 31.6 (*o*-C($\underline{C}H_3$)$_3$), 31.4 (*p*-C($\underline{C}H_3$)$_3$), 31.3 (*o*-C($\underline{C}H_3$)$_3$'), 26.7 (C($\underline{C}H_3$)$_3$), 19.2 ($\underline{C}(CH_3)_3$); ^{31}P NMR ($CDCl_3$, 161.97 MHz) δ 143.85 (s). Anal. Calcd. for $C_{94}H_{126}O_9P_2Si_2$: C, 74.37; H, 8.37. Found: C, 74.27; H, 9.16.

74a. X-ray Crystallography.

Crystals of **74a** were obtained by slow diffusion of hexane into a solution of **74a** in dichloromethane. Empirical formula: $C_{42.40}$ $H_{61.60}$ $O_{3.80}$ $P_{0.80}$ $Si_{0.80}$, Formula weight: 679.36, Temperature: 100(2) K, Wavelength: 0.71073 Å, Crystal system: Monoclinic, Space group: $P2_1$, Unit cell dimensions: a=14.6938(11) Å, a=90°, b=24.842(2) Å, b=109.112(2)°, c=15.0146(12) Å, g=90°, Volume: 5178.6(7) Å^3, Z:5, Density (calculated): 1.089 Mg/m^3, Absorption coefficient: 0.118 mm^{-1}, F(000): 1848, Crystal size: 0.40 x 0.40 x 0.40 mm^3, Theta range for data collection: 2.81 to 36.88°, Index ranges: -24 ≤ h ≤ 23, -41 ≤ k ≤ 41, -13 ≤ l ≤ 25,

Reflections collected: 86383, Independent reflections: 46995 [R(int) = 0.0401], Completeness to theta = 36.88°: 96.3 % , Absorption correction:SADABS (Bruker-Nonius), Refinement method: Full-matrix least-squares on F^2, Data / restraints / parameters: 46995 / 1 / 1125, Goodness-of-fit on F^2: 1.018, Final R indices [I>2sigma(I)]: R1 = 0.0719, wR2 = 0.2001, R indices (all data): R1 = 0.0933, wR2 = 0.2190, Absolute structure parameter: 0.16(5), Largest diff. peak and hole: 1.050 and -0.584 e.$Å^{-3}$

The ligand crystallizes as a solvate with two molecules of n-hexane in the elementary cell. The measured compound crystallizes as a razemic twin (74:16). Selected bond distances and angles are given in Table 1 and 2 of the appendix.

3,4-Bis-*O*-[(3,3'-di-*tert*-butyl-,5,5'-dimethoxy-1,1'-biphenyl-2,2'-diyl)phosphite]-1,6-di-*O*-(*tert*-butyl-diphenylsilyl)-2,5-anhydro-D-mannitol (74b)

The synthesis of **74b** was carried out in accordance with the general procedure from 0.3 g (0.47 mmol) of diol **80** in 5 ml of dry and degassed toluene and 0.2 ml (2.4 mmol) of dry pyridine. This solution was slowly added to a solution of 2.1 mmol of the corresponding phosphorochlorhydrite formed *in situ*, dissolved in 6 ml of toluene and 0.2 ml (2.4 mmol) of pyridine. The mixture was stirred overnight, the salts were filtered and the white foam was purified by flash column chromatography (eluent: toluene Rf=0.75) to afford 0.28 g (42 %) of **74b** as a white solid. $[\alpha]^{25}_{D}$ +58.71º (CH_2Cl_2, *c* 0.402); ^{1}H NMR ($CDCl_3$, 400 MHz) δ 7.65-6.58 (m, 28H, aromatic), 5.14 (broad, 2H, H3), 4.05 (m broad, 2H, H2), 3.81 (s, 6H, *p*-OC$\underline{H}_3$'), 3.74 (s, 6H, *p*-OC$\underline{H}_3$), 3.67 (m, 2H, H1), 3.53 (m, 2H, H1´), 1.42 (s, 18H, *o*-C(C$\underline{H}_3)_3$'), 1.35 (s, 18H, *o*-C(C$\underline{H}_3)_3$), 0.98 (s, 18H, C(C$\underline{H}_3)_3$). ^{13}C NMR ($CDCl_3$, 100.6 MHz) δ 155.5-112.6 (aromatic), 82.9 (C2), 79.6 (broad C3), 62.7 (C1), 55.5 (*p*-O$\underline{C}H_3$'), 55.4 (*p*-O$\underline{C}H_3$), 35.7 (*o*-$\underline{C}(CH_3)_3$'), 35.6 (*o*-$\underline{C}(CH_3)_3$), 31.5 (*o*-C($\underline{C}H_3)_3$'), 31.3 (*o*-C($\underline{C}H_3)_3$), 27.5 (C($\underline{C}H_3)_3$), 19.5 ($\underline{C}(CH_3)_3$); ^{31}P NMR ($CDCl_3$, 161.97 MHz) δ 144.54 (s). Anal. Calcd. for $C_{82}H_{102}O_{13}P_2Si_2$: C, 69.66; H, 7.27. Found: C, 69.30; H, 7.96.

3,4-Bis-*O*-[(1,1'-biphenyl-2,2'-diyl)phosphite]-1,6-di-*O*-(*tert*-butyl-diphenylsilyl)-2,5-anhydro-D-mannitol (74c)

The synthesis of **74c** was carried out in accordance with the general procedure from 0.25 g (0.40 mmol) of diol **80** in 2.5 ml of dry and degassed toluene and 0.1 ml (1.6 mmol) of dry pyridine. This solution was slowly added to a solution of 1.6 mmol of the corresponding phosphorochlorhydrite formed *in situ*, dissolved in 4 ml of toluene and 0.1 ml (1.6 mmol) of pyridine. The mixture was stirred overnight, the salts were filtered and the white foam was purified by flash column chromatography (eluent: hexane/ethyl acetate 100:2 Rf=0.6) to afford 0.21 g (50 %) of **74b** as a white solid. $[\alpha]^{25}_{D}$ +0.61º (CH_2Cl_2, *c* 0.330); ^{1}H NMR ($CDCl_3$, 400 MHz) δ 7.66-7.06 (m, 28H, aromatic), 5.16 (m broad, 2H, H3), 4.13 (m broad, 2H, H2), 3.76 (m, 2H, H1), 3.72 (m, 2H, H1'), 0.99 (s, 18H, C(C$\underline{H}_3)_3$); ^{13}C NMR ($CDCl_3$, 100.6 MHz) δ 146.7-121.3 (aromatic), 83.4 (C2), 79.9 (broad C3), 63.1 (C1), 27.0 (C($\underline{C}H_3)_3$), 19.5 ($\underline{C}(CH_3)_3$) ^{31}P NMR ($CDCl_3$, 161.97 MHz) δ 146.70 (s). Anal. Calcd. for $C_{62}H_{62}O_9P_2Si_2$: C, 69.64; H, 5.84. Found: C, 69.44; H, 6.01.

3,4-Bis-*O*-[(3,3',5,5'-tetra-*tert*-butyl-1,1'-biphenyl-2,2'-diyl)phosphite]-1,6-dideoxy-2,5-anhydro-D-mannitol (74'a)

The synthesis of **74'a** was carried out in accordance with the general procedure from 0.15 g (1.14 mmol) of diol **80'** in 10 ml of dry and degassed toluene and 0.5 ml (5.7 mmol) of dry pyridine. This solution was slowly added to a solution of 4.6 mmol of the corresponding phosphorochlorhydrite formed *in situ*, dissolved in 12 ml of toluene and 0.5 ml (5.7 mmol) of pyridine. The mixture was stirred overnight, the salts were filtered and the white foam was purified by flash column chromatography (eluent: toluene Rf=0.9) to afford 0.84 g (72 %) of **74'a** as a white solid. $[\alpha]^{25}_{D}$ +65.81º (CH_2Cl_2, *c* 1.006); ^{1}H NMR ($CDCl_3$, 400 MHz) δ 7.41 (m, 4H, aromatic), 7.15 (m, 4H, aromatic), 4.56 (m broad, 2H, H3), 4.07 (m, broad, 2H, H2), 1.46 (s, 18H, C($\underline{C}H_3)_3$'), 1.43 (s, 18H, C($\underline{C}H_3)_3$), 1.34 (s, 18H, C($CH_3)_3$'), 1.33 (m, 18H, C($\underline{C}H_3)_3$') 1.06 (d, 6H, $J_{1,2}$ = 6.6 Hz, H1); ^{13}C NMR ($CDCl_3$, 100.6 MHz) δ 146.5-124.2 (aromatic), 85.4 (broad C3), 79.5 (C2), 35.4 (*o*-$\underline{C}(CH_3)_3$), 35.34 (*o*-$\underline{C}(CH_3)_3$'), 34.6 (*p*-$\underline{C}(CH_3)_3$), 34.6 (*p*-$\underline{C}(CH_3)_3$'), 31.5 (*o*-C($\underline{C}H_3)_3$), 31.2 (*o*-

C($\underline{C}H_3)_3$'), 31.1 (*p*-C($\underline{C}H_3)_3$), 18.5 (CH_3, C1) ^{31}P NMR ($CDCl_3$, 161.97 MHz) δ 143.03 (s). Anal. Calcd. for $C_{62}H_{90}O_7P_2$: C, 73.78; H, 8.99. Found: C, 74.02; H, 8.98.

3,4-Bis-*O*-[(3,3'-di-*tert*-butyl-,5,5'-dimethoxy-1,1'-biphenyl-2,2'-diyl)phosphite]-1,6-dideoxy-2,5-anhydro-D-mannitol (74'b)

The synthesis of **74'b** was carried out in accordance with the general procedure from 0.15 g (1.14 mmol) of diol **80'** in 10 ml of dry and degassed toluene and 0.5 ml (5.7 mmol) of dry pyridine. This solution was slowly added to a solution of 4.6 mmol of the corresponding phosphorochlorhydrite formed *in situ*, dissolved in 12 ml of toluene and 0.5 ml (5.7 mmol) of pyridine. The mixture was stirred overnight, the salts were filtered and the white foam was purified by flash column chromatography (eluent: toluene Rf=0.9) to afford 0.4 g (42 %) of **74'b** as a white solid. $[\alpha]^{25}_D$ +20.39º (CH_2Cl_2, *c* 0.466); ^{1}H NMR ($CDCl_3$, 400 MHz) δ 7.08 (m, 4H, aromatic), 6.82 (m, 4, aromatic), 4.65 (m, 2H, H3), 4.31 (m, 2H, H2), 3.90 (s, 12H, *p*-OCH_3), 1.55 (s, 18H, *o*-C($CH_3)_3$'), 1.53 (s, 18H, *o*-C($CH_3)_3$), 1.29 (d, 6H, , $J_{1,2}$ = 6.6 Hz, H1); ^{13}C NMR ($CDCl_3$, 100.6 MHz) δ 155.6-112.7 (aromatic), 85.4 (broad, C3), 79.9 (C2), 55.5 (*p*-O$\underline{C}H_3$'), 55.4 (*p*-O$\underline{C}H_3$), 35.3 (*o*-$\underline{C}(CH_3)_3$), 31.0 (*o*-C($\underline{C}H_3)_3$'), 30.8 (*o*-C($\underline{C}H_3)_3$) 18.3 (CH_3, C1); ^{31}P NMR ($CDCl_3$, 161.97 MHz) δ 142.45 (s). Anal. Calcd. for $C_{50}H_{66}O_{11}P_2$: C, 66.36; H, 7.35. Found: C, 66.49; H, 7.96.

3,4-Bis-*O*-[(3,3',5,5'-tetra-*tert*-butyl-1,1'-biphenyl-2,2'-diyl)phosphite]-1,6-di-*O*-(*tert*-butyl-diphenylsilyl)-2,5-anhydro-L-iditol (75a)

The synthesis of **75a** was carried out in accordance with the general procedure from 0.25 g (0.40 mmol) of diol **86** in 2.5 ml of dry and degassed toluene and 0.1 ml (1.6 mmol) of dry pyridine. This solution was slowly added to a solution of 1.6 mmol of the corresponding phosphorochlorhydrite formed *in situ*, dissolved in 4 ml of toluene and 0.1 ml (1.6 mmol) of pyridine. The mixture was stirred overnight, the salts were filtered and the white foam was purified by flash column chromatography (eluent: toluene Rf=0.9) to afford 0.25 g (42 %) of **75a** as a white solid. $[\alpha]^{25}_D$ -8.72º (CH_2Cl_2, *c* 0.390); ^{1}H NMR ($CDCl_3$, 400 MHz) δ 7.17-7.65 (m, 28H, aromatic), 5.07 (s broad, 2H, H3), 4.26 (m broad, 2H, H2), 3.85 (m, 2H, H1), 3.79 (m, 2H, H1'), 1.45 (s, 18H, *o*-C($C\underline{H}_3)_3$), 1.34 (s, 18H, *o*-C($C\underline{H}_3)_3$), 1.31 (s,

18H, *p*-C(C$\underline{H}_3$)$_3$), 1.28 (s, 18H, *p*-C(C$\underline{H}_3$)$_3$'), 0.96 (s, 18H, C(C$\underline{H}_3$)$_3$); ^{13}C NMR ($CDCl_3$, 100.6 MHz) δ 146.5-124.1 (aromatic), 79.7 (C2), 77.8 (broad, C3), 62.9 (C1), 35.4 (*o*-$\underline{C}$(CH$_3$)$_3$'), 35.3 (*o*-$\underline{C}$(CH$_3$)$_3$), 34.6 (*p*-$\underline{C}$(CH$_3$)$_3$'), 34.6 (*p*-$\underline{C}$(CH$_3$)$_3$), 31.5 (*o*-$\underline{C}$(CH$_3$)$_3$'), 31.4 (*o*-$\underline{C}$(CH$_3$)$_3$), 31.1 (*p*-C($\underline{C}$H$_3$)$_3$'), 31.1 (*p*-C($\underline{C}$H$_3$)$_3$), 26.8 (C($\underline{C}$H$_3$)$_3$), 19.2 ($\underline{C}$(CH$_3$)$_3$); ^{31}P NMR ($CDCl_3$, 161.97 MHz) δ147.47 (s). Anal. Cald. For $C_{94}H_{126}O_9P_2Si_2$: C, 74.37; H, 8.37. Found: C,74.56 ; H, 8.28.

3,4-Bis-*O*-[(3,3'-di-*tert*-butyl-,5,5'-dimethoxy-1,1'-biphenyl-2,2'-diyl)phosphite]-1,6-di-*O*-(*tert*-butyl-diphenylsilyl)-2,5-anhydro-L-iditol (75b)

The synthesis of **75b** was carried out in accordance with the general procedure from 0.25 g (0.40 mmol) of diol **86** in 4 ml of dry and degassed toluene and 0.1 ml (1.6 mmol) of dry pyridine. This solution was slowly added to a solution of 1.6 mmol of the corresponding phosphorochlorhydrite formed *in situ*, dissolved in 4 ml of toluene and 0.1 ml (1.6 mmol) of pyridine. The mixture was stirred overnight, the salts were filtered and the white foam was purified by flash column chromatography (eluent: toluene Rf=0.6) to afford 0.18 g (32 %) of **75b** as a white solid. $[\alpha]^{25}_D$ - 15.45º (CH_2Cl_2, *c* 1.100); ^{1}H NMR ($CDCl_3$, 400 MHz) δ 7.83-6.85 (m, 28H, Ph), 5.14 (m broad, 2H, H3), 4.47 (m broad, 2H, H2), 4.00 (s, 6H, *p*-OC$\underline{H}_3$), 3.96 (s, 6H, *p*-OC$\underline{H}_3$'), 3.98 (m, 4H, H1, H1'), 1.62 (s, 18H, *o*-C(C$\underline{H}_3$)$_3$), 1.50 (s, 18H, C(C$\underline{H}_3$)$_3$'), 1.18 (s, 18H, C(C$\underline{H}_3$)); ^{13}C NMR ($CDCl_3$, 100.6 MHz) δ 155.9-112.9 (aromatic), 80.0 (C2), 77.7 (broad, C3), 62.7 (C1), 55.5 (*p*-O$\underline{C}$H$_3$), 55.4 (p-O$\underline{C}$H$_3$'), 35.3 (*o*-$\underline{C}$(CH$_3$)$_3$), 35.3 (*o*-$\underline{C}$(CH$_3$)$_3$'), 31.2 (*o*-C($\underline{C}$H$_3$)$_3$), 31.0 (*o*-C($\underline{C}$H$_3$)$_3$'), 26.0 (C($\underline{C}$H$_3$)$_3$), 19.2 ($\underline{C}$(CH$_3$)$_3$); ^{31}P NMR ($CDCl_3$, 161.97 MHz) δ 146.72 (s). Anal. Calcd. for $C_{82}H_{102}O_{13}P_2Si_2$: C, 69.66; H, 7.27. Found: C, 69.15 ; H 7.91

3,4-Bis-*O*-[(3,3',5,5'-tetra-*tert*-butyl-1,1'-biphenyl-2,2'-diyl)phosphite]-1,6-dideoxy-2,5-anhydro-L-iditol (75'a)

The synthesis of **75'a** was carried out in accordance with the general procedure from 0.075 g (0.57 mmol) of diol **86'** in 5 ml of dry and degassed toluene and 0.25 ml (2.9 mmol) of dry pyridine. This solution was slowly added to a solution of 2.3 mmol of the corresponding phosphorochlorhydrite formed *in situ*, dissolved in 6 ml

of toluene and 0.25 ml (2.9 mmol) of pyridine. The mixture was stirred overnight, the salts were filtered and the white foam was purified by flash column chromatography (eluent: toluene Rf=0.9) to afford 0.53 g (92 %) of **75'a** as a white solid. $[\alpha]^{25}_{D}$ -8.53º (CH_2Cl_2, *c* 1.160); ^{1}H NMR ($CDCl_3$, 400 MHz) δ 7.42 (m, 4H, aromatic), 7.16 (m, 4H, aromatic), 4.63 (m broad, 2H, H3), 4.12 (m, broad, 2H, H2), 1.46 (s, 18H, *o*-C($C\underline{H}_3)_3$), 1.44 (s, 18H, *o*-C($C\underline{H}_3)_3$'), 1.34 (s, 18H, *p*-C($C\underline{H}_3)_3$), 1.33 (s, 36H, *p*-C($C\underline{H}_3)_3$'), 1.09 (d, 6H, , $J_{1,2}$ = 6.2 Hz, H1); ^{13}C NMR ($CDCl_3$, 100.6 MHz) δ 146.5-124.1 (aromatic), 80.0 (C3 $J_{C,P}$ = 11.3), 75.2 (broad C2), 35.4 (*o*-$\underline{C}(CH_3)_3$'), 35.4 (*o*-$\underline{C}(CH_3)_3$), 34.6 (*p*-$\underline{C}(CH_3)_3$'), 34.6 (*p*-$\underline{C}(CH_3)_3$), 31.5 (*p*-C($\underline{C}H_3)_3$'), 31.3 (*o*-C($\underline{C}H_3)_3$), 31.2 (*o*-C($\underline{C}H_3)_3$), 14.9 (CH_3, C1) ^{31}P NMR ($CDCl_3$, 161.97 MHz) δ 146.95 (s). Anal. Cald. For $C_{62}H_{90}O_7P_2$: C, 73.78; H, 8.99. Found: C, 73.61 ; H, 9.43.

3,4-Bis-*O*-[(3,3'-di-*tert*-butyl-,5,5'-dimethoxy-1,1'-biphenyl-2,2'-diyl)phosphite]-1,6-dideoxy-2,5-anhydro-L-iditol (75'b)

The synthesis of **75'b** was carried out in accordance with the general procedure from 0.075 g (0.57 mmol) of diol **86'** in 5 ml of dry and degassed toluene and 0.25 ml (2.9 mmol) of dry pyridine. This solution was slowly added to a solution of 2.3 mmol of the corresponding phosphorochlorhydrite formed *in situ*, dissolved in 6 ml of toluene and 0.25 ml (2.9 mmol) of pyridine. The mixture was stirred overnight, the salts were filtered and the white foam was purified by flash column chromatography (eluent: toluene Rf=0.5) to afford 0.53 g (64 %) of **75'b** as a white solid. $[\alpha]^{25}_{D}$ -47.60º (CH_2Cl_2, *c* 0.775); ^{1}H NMR ($CDCl_3$, 400 MHz) δ 6.96 (m, 4H, aromatic), 6.68 (m, 4,aromatic), 4.70 (m, 2H, H3), 4.26 (m, 2H, H2), 3.79 (s, 6H, *p*-OCH_3'), 3.77 (s, 6H, *p*-OCH_3), 1.42 (s, 18H, *o*-C($CH_3)_3$'), 1.40 (s, 18H, *o*-C($CH_3)_3$), 1.16 (d, 6H, , $J_{1,2}$ = 6.4 Hz, H1); ^{13}C NMR ($CDCl_3$, 100.6 MHz) δ 155.7-112.8 (aromatic), 80.2 (m broad, C2), 75.2 (broad C3), 55.5 (*p*-O$\underline{C}H_3$'), 55.4 (*p*-O$\underline{C}H_3$), 35.4 (*o*-$\underline{C}(CH_3)_3$'), 35.3 (*o*-$\underline{C}(CH_3)_3$), 31.0 (C($\underline{C}H_3)_3$'), 15.0 (CH_3, C1); ^{31}P NMR ($CDCl_3$, 161.97 MHz) δ 146.07 (s). Anal. Cald. $C_{50}H_{66}O_{11}P_2$: C, 66.36; H, 7.35. Found: C, 66.32 ; H, 7.60 .

(3*R*,4*R*)-(-)-3,4-Bis-*O*-[(3,3',5,5'-tetra-*tert*-butyl-1,1'-biphenyl-2,2'-diyl)phosphite]-tetrahydrofuran (76a)

The synthesis of **76a** was carried out in accordance with the general procedure from 0.15 g (1.44 mmol) of diol **89** in 14 ml of dry and degassed toluene and 0.7 ml (5.7 mmol) of dry pyridine. This solution was slowly added to a solution of 5.7 mmol of the corresponding phosphorochlorhydrite formed *in situ*, dissolved in 15 ml of toluene and 0.7 ml (5.7 mmol) of pyridine. The mixture was stirred overnight, the salts were filtered and the white foam was purified by flash column chromatography (eluent: toluene Rf=0.9) to afford 1.00 g (75 %) of **76a** as a white solid. $[\alpha]^{25}_{D}$ –51.13º (CH_2Cl_2, *c* 1.105); ^{1}H NMR ($CDCl_3$, 400 MHz) δ 7.42 (m, 4H,aromatic), 7.16 (m, 4H, aromatic), 4.82 (m, 2H, H3), 3.84 (m, 2H, H2), 3.69 (m, 2H, H2'), 1.46 (s, 18H, *o*-C(CH_3)$_3$'), 1.41 (s, 18H, *o*-C($\underline{C}H_3$)$_3$), 1.35 (s, 18H, *p*-C(CH_3)$_3$'), 1.34 (s, 18H, *p*-C(CH_3)$_3$'); ^{13}C NMR ($CDCl_3$, 100.6 MHz) δ 146.6-124.2 (aromatic), 79.1 (broad, C3), 72.3 (broad, C2), 35.4 (*o*-$\underline{C}$(CH_3)$_3$'), 35.3 (*o*-$\underline{C}$(CH_3)$_3$), 34.6 (*p*-$\underline{C}$(CH_3)$_3$'), 31.5 (*o*-C($\underline{C}H_3$)$_3$'), 31.5 (*o*-C($\underline{C}H_3$)$_3$), 31.2 (*p*-C($\underline{C}H_3$)$_3$), 31.1 (*p*-C($\underline{C}H_3$)$_3$), ^{31}P NMR ($CDCl_3$, 161.97 MHz) δ 141.50 (s). Anal. Cald. $C_{60}H_{86}O_7P_2$: C, 73.44; H, 8.83. Found: C, 73.21 ; H, 8.88.

3,4-Bis-*O*-[(3,3'-di-*tert*-butyl-,5,5'-dimethoxy-1,1'-biphenyl-2,2'-diyl)phosphite] -tetrahydrofuran (76b)

The synthesis of **76b** was carried out in accordance with the general procedure from 0.15 g (1.14 mmol) of diol **89** in 10 ml of dry and degassed toluene and 0.5 ml (5.7 mmol) of dry pyridine. This solution was slowly added to a solution of 4.6 mmol of the corresponding phosphorochlorhydrite formed *in situ*, dissolved in 12 ml of toluene and 0.5 ml (5.7 mmol) of pyridine. The mixture was stirred overnight, the salts were filtered and the white foam was purified by flash column chromatography (eluent: toluene Rf=0.9) to afford 0.3 g (29 %) of **76b** as a white solid. $[\alpha]^{25}_{D}$ +19.95º (CH_2Cl_2, *c* 1.025); ^{1}H NMR ($CDCl_3$, 400 MHz) δ 7.00 (m, 4H, aromatic), 6.74 (m, 4, aromatic), 4.85 (m, 2H, H3), 3.96 (m, 2H, H1), 3.85 (m, 2H, H1), 3.83 (s, 12H, *p*-OCH_3), 1.47 (s, 18H, *o*-C(CH_3)$_3$'), 1.43 (s, 18H, *o*-C(CH_3)$_3$); ^{13}C NMR ($CDCl_3$, 100.6 MHz) δ 155.6-112.8 (aromatic), 79.1 (m, C3),

72.3 (C2), 55.5 (*p*-O<u>C</u>H$_3$), 55.5 (*p*-O<u>C</u>H$_3$), 35.3 (*o*-<u>C</u>(CH$_3$)$_3$'), 35.2 (*o*-<u>C</u>(CH$_3$)$_3$), 31.0 (*o*-C(<u>C</u>H$_3$)$_3$'), 30.9 (*o*-C(<u>C</u>H$_3$)$_3$); ^{31}P NMR ($CDCl_3$, 161.97 MHz) δ 140.97 (s). Anal. Calcd. for $C_{48}H_{62}O_{11}P_2$: C, 65.74; H, 7.13. Found: C, 64.91; H, 7.04.

Synthesis of rhodium complexes

General procedure for synthesizing [Rh(cod)(L)]BF_4, L=diphosphite

The complexes were prepared by adding 1.1 equivalents of diphosphinite ligand to a solution of [Rh(cod)$_2$]BF_4 in the minimum volume of CH_2Cl_2. The mixture was then stirred for 30 min, and the solvent was removed in vacuo. The residue was washed with dry hexane first and then with dry ether in order to remove the excess diphosphite and free cyclooctadiene.

[Rh(cod)(74a)]BF_4 (90a)

Beginning with 0.015 g (0.036 mmol) of [Rh(cod)$_2$]BF_4 in the minimum quantity of CH_2Cl_2, 0.060 g (0.040 mmol) of diphosphite **74a** and following the general procedure, 0.054 g (83%) of complex [Rh(cod)(**74a**)]BF_4 **90a** was obtained as a yellow solid. ^{1}H NMR ($CDCl_3$, 400 MHz) δ 7.62-6.87 (m, 28H, aromatic), 5.88 (s broad, 2H, C<u>H</u> (cod)), 5.69 (s broad, 2H, H3), 4.92 (s broad, 2H, C<u>H</u> (cod)), 3.73 (s broad, 2H, H2), 3.52 (d, 2H, H1), 2.82 (d, 2H, H1'), 2.34 (m broad, 4H, C<u>H</u>$_2$ (cod)), 2.26 (m broad, 2H, C<u>H</u>$_2$ (cod)), 2.00 (m broad, 4H, C<u>H</u>$_2$ (cod)), 1.67 (s, 18H, *o*-C(C<u>H</u>$_3$)$_3$'), 1.48 (s, 18H, *p*-C(C<u>H</u>$_3$)$_3$), 1.42 (s, 18H, *p*-C(C<u>H</u>$_3$)$_3$), 1.14 (s, 18H, *o*-C(C<u>H</u>$_3$)$_3$), 0.89 (s, 18H, C(C<u>H</u>$_3$)$_3$); ^{13}C NMR ($CDCl_3$, 100.6 MHz) δ 149.4-125.2 (aromatic), 112.9 (C<u>H</u> (cod)), 103.5 (C<u>H</u> (cod)), 78.6 (C2), 77.4 (broad, C3), 60.7 (C1), 36.0 (*o*-<u>C</u>(CH$_3$)$_3$'), 35.5 (*o*-<u>C</u>(CH$_3$)$_3$), 35.0 (*p*-<u>C</u>(CH$_3$)$_3$'), 34.6 (*p*-<u>C</u>(CH$_3$)$_3$), 32.9 (o-C(<u>C</u>H$_3$)$_3$'), 31.8 (o-C(<u>C</u>H$_3$)$_3$), 31.4 (p-C(<u>C</u>H$_3$)$_3$'), 31.1 (p-C(<u>C</u>H$_3$)$_3$), 30.6 (C<u>H</u>$_2$ (cod)), 29.7 (C<u>H</u>$_2$ (cod)), 26.8 (C(<u>C</u>H$_3$)$_3$), 19.4 (<u>C</u>(CH$_3$)$_3$); ^{31}P NMR ($CDCl_3$, 161.97 MHz) δ129.35 (d, $J_{P,\ Rh}$ = 254.4 Hz). Anal. Cald. $C_{102}H_{138}BF_4O_9P_2RhSi_2$: C, 67.46; H, 7.66. Found: C, 67.49; H, 10.93. MS (Maldi) *m/z* 1727.8 $[M]^+$, 1619.8 $[M\text{-(cod)}]^+$; HRMS (Maldi) calcd for $[C_{102}H_{138}O_9P_2RhSi_2]^+$ 1727.8410; found 1727.8404.

[Rh(cod)(74a)]BF_4 (90a). X-ray Crystallography.

Crystals of [Rh(cod)(**74a**)]BF_4 (**90a**) were obtained by slow diffusion of hexane into a solution of [Rh(cod)(**74a**)]BF_4 (**90a**) in dichloromethane. Empirical formula: C_{103} H_{140} B Cl_2 F_4 $O_{9.50}$ P_2 Rh Si_2, Formula weight: 1908.89, Temperature: 100(2) K, Wavelength: 0.71073 Å, Crystal system: Orthorhombic, Space group: $P2_12_12_1$, Unit cell dimensions: a=19.512(3) Å, a=90°, b=20.172(3) Å, b=90°,c=26.249(4) Å, g = 90°, Volume: 10332(3) $Å^3$, Z: 4, Density (calculated): 1.227 Mg/m^3, Absorption coefficient: 0.332 mm^{-1}, F(000): 4048, Crystal size: 0.20 x 0.10 x 0.04 mm^3, Theta range for data collection: 2.74 to 30.18°, Index ranges: -27 ≤ h ≤ 25, -28 ≤ k ≤ 28, -24 ≤ l ≤ 37, Reflections collected: 125396, Independent reflections: 30370 [R(int) = 0.0744], Completeness to theta = 30.18°: 99.3 % , Absorption correction: SADABS (Bruker-Nonius), Refinement method: Full-matrix least-squares on F^2, Data / restraints / parameters: 30370 / 14 / 1393, Goodness-of-fit on F^2: 1.013, Final R indices [I>2sigma(I)]:R1 = 0.0492, wR2 = 0.1139, R indices (all data): R1 = 0.0798, wR2 = 0.1283, Absolute structure parameter: -0.022(15), Largest diff. peak and hole: 1.185 and -0.973 e.$Å^{-3}$

Compound [Rh(cod)(**74a**)]BF_4 (**90a**) crystallizes as a cation together with a BF_4-anion, a disordered water molecule and two disordered positions of dichloromethane. The measured compound crystallizes in a pure chiral structure. Selected bond distances and angles are given in Tables 3 and 4 of the appendix.

[Rh(cod)(74b)]BF_4 (90b)

Beginning with 0.012 g (0.030 mmol) of [$Rh(cod)_2$]BF_4 in the minimum quantity of CH_2Cl_2 and 0.046 g (0.032 mmol) of diphosphite **74b** and following the general procedure, 0.030 g (61%) of complex [Rh(cod)(**74b**)]BF_4 **90b** was obtained as a yellow solid. ^{1}H NMR ($CDCl_3$, 400 MHz) δ 7.51-6.54 (m, 28H, aromatic), 5.81 (s broad, 2H, C<u>H</u> (cod)), 5.72 (s broad, 2H, H3), 4.96 (s broad, 2H, C<u>H</u> (cod)), 3.93 (s, 6H, *p*-OCH_3'), 3.87 (dt broad, 2H, H2), 3.66 (s, 6H, *p*-OCH_3), 3.59 (d, 2H, H1), 3.10 (d, 2H, H1'), 2.45 (m broad, 4H, C<u>H_2</u> (cod)), 2.31 (m broad, 2H, C<u>H_2</u> (cod)),

2.05 (m broad, 4H, C$\underline{H}_2$ (cod)), 1.71 (s, 18H, *o*-C(C$\underline{H}_3$)$_3$'), 1.47 (s, 18H, *p*-C(C$\underline{H}_3$)$_3$), 0.89 (s, 18H, C(C$\underline{H}_3$)$_3$); ^{13}C NMR ($CDCl_3$, 100.6 MHz) δ 157.2-113.8 (aromatic), 112.8 (C$\underline{H}$ (cod)), 103.7 (C$\underline{H}$ (cod)), 76.6 (C2), 77.2 (broad, C3), 61.2 (C1), 56.0 (*p*-O$\underline{C}$H$_3$'), 55.4 (*p*-O$\underline{C}$H$_3$),36.1 (*o*-$\underline{C}$(CH$_3$)$_3$'), 35.6 (*o*-$\underline{C}$(CH$_3$)$_3$), 32.9 (o-C($\underline{C}$H$_3$)$_3$'), 31.6 (o-C($\underline{C}$H$_3$)$_3$), 31.1 (C$\underline{H}_2$ (cod)), 29.4 (C$\underline{H}_2$ (cod)), 26.7 (C($\underline{C}$H$_3$)$_3$), 19.4 ($\underline{C}$(CH$_3$)$_3$); ^{31}P NMR ($CDCl_3$, 161.97 MHz) δ129.85 (d, $J_{P,\ Rh}$ = 254.8 Hz). Anal. Cald. $C_{90}H_{114}BF_4O_{13}P_2RhSi_2$: C, 63.15; H, 6.71. Found: C, 62.77; H, 6.87. MS (Maldi) *m/z* 1623.6 $[M]^+$, 1515.6 $[M\text{-}(cod)]^+$; HRMS (Maldi) calcd for $[C_{90}H_{114}O_{13}P_2RhSi_2]^+$ 1623.63282; found 1623.63228.

[Rh(cod)(74c)]BF$_4$ (90c)

Beginning with 0.025 g (0.061 mmol) of $[Rh(cod)_2]BF_4$ in 10 mL of CH_2Cl_2 and 0.074 g (0.067 mmol) of diphosphite **74c** and following the general procedure, 0.054 g (65%) of complex [Rh(cod)(**74c**]BF_4 **90c** was obtained as a pale yellow solid. ^{1}H NMR ($CDCl_3$, 400 MHz) δ 7.54–7.18 (m, 36H, aromatic), 5.68 (m broad, 4H, C$\underline{H}$ (cod)), 5.46 (s broad, 2H, H3), 4.12 (d broad, 2H, H2), 3.85 (d, 2H, H1), 3.57 (d, 2H, H1'), 2.50 (m broad, 4H, C$\underline{H}_2$ (cod)), 2.17 (m broad, 2H, C$\underline{H}_2$ (cod)), 2.09 (m broad, 2H, C$\underline{H}_2$ (cod)), 0.95 (s, 18H, C(C$\underline{H}_3$)$_3$); ^{13}C NMR ($CDCl_3$, 100.6 MHz) δ 148.0–121.4 (aromatic), 110.8 ($\underline{C}$H (cod)), 110.1 ($\underline{C}$H (cod)), 80.1 (broad, C3), 79.1 (C2), 62.3 (C1), 30.4 ($\underline{C}$H$_2$ (cod)), 29.8 ($\underline{C}$H$_2$ (cod)), 26.8 (C($\underline{C}$H$_3$)$_3$), 19.3 ($\underline{C}$(CH$_3$)$_3$); ^{31}P NMR ($CDCl_3$, 161.97 MHz) δ136.71 (d, $J_{P,\ Rh}$ = 249.7 Hz). MS (Maldi) *m/z* 1279.3 $[M]^+$, 1171.3 $[M\text{-}(cod)]^+$; HRMS (Maldi) calcd for $[C_{79}H_{74}O_9P_2RhSi_2]^+$ 1279.3402; found 1279.3396.

[Rh(cod)(74'a)]BF$_4$ (90'a)

Beginning with 0.025 g (0.062 mmol) of $[Rh(cod)_2]BF_4$ in the minimum quantity of CH_2Cl_2, 0.069 g (0.068 mmol) of diphosphite **74'a** and following the general procedure, 0.068 g (81%) of complex [Rh(cod)(**74'a**)]BF_4 **90'a** was obtained as a yellow solid. ^{1}H NMR ($CDCl_3$, 400 MHz) δ 7.60 (d, 2H, J= 1.9 Hz, aromatic), 7.48 (d, 2H, J= 1.9 Hz, aromatic), 7.19 (d, 2H, J= 1.9 Hz, aromatic), 7.06 (d, 2H, J= 1.9 Hz, aromatic), 5.78 (s broad, 2H, H3), 4.87 (s broad, 4H, C$\underline{H}$ (cod)), 3.85 (m broad, 2H, H2), 2.32 (m broad, 4H, C$\underline{H}_2$ (cod)), 2.20 (m broad, 2H, C$\underline{H}_2$ (cod)),

1.94 (m broad, 2H, C$\underline{H}_2$ (cod)), 1.76 (s, 18H, *o*-C(C$\underline{H}_3$)$_3$'), 1.51 (s, 18H, *p*-C(C$\underline{H}_3$)$_3$), 1.37 (s, 18H, *p*-C(C$\underline{H}_3$)$_3$), 1.32 (s, 18H, *o*-C(C$\underline{H}_3$)$_3$), 0.84 (d, 6H, $J_{1,2}$ = 6.0 Hz C(C$\underline{H}_3$)$_3$); ^{13}C NMR ($CDCl_3$, 100.6 MHz) δ 149.4-125.4 (aromatic), 112.4 (C$\underline{H}$ (cod)), 103.6 (C$\underline{H}$ (cod)), 84.2 (C3), 72.6 (C2), 35.8 (*o*-$\underline{C}$(CH$_3$)$_3$'), 35.6 (*o*-$\underline{C}$(CH$_3$)$_3$), 34.9 (*p*-$\underline{C}$(CH$_3$)$_3$'), 34.8 (*p*-$\underline{C}$(CH$_3$)$_3$), 32.6 (o-C($\underline{C}$H$_3$)$_3$'), 31.8 (o-C($\underline{C}$H$_3$)$_3$), 31.4 (p-C($\underline{C}$H$_3$)$_3$'), 31.3 (p-C($\underline{C}$H$_3$)$_3$), 30.6 (C$\underline{H}_2$ (cod)), 29.6 (C$\underline{H}_2$ (cod)), 17.9 (CH$_3$, C1); ^{31}P NMR ($CDCl_3$, 161.97 MHz) δ 128.38 (d, $J_{P,\ Rh}$ = 255.0 Hz). Anal. Cald. $C_{70}H_{102}BF_4O_7P_2Rh$: C, 64.32; H, 7.86. Found: C, 64.41; H, 8.26. MS (Maldi) *m/z* 1219.6 $[M]^+$, 1111.6 $[M\text{-}(cod)]^+$; HRMS (Maldi) calcd for $[C_{70}H_{102}O_7P_2Rh]^+$ 1219.6156; found 1219.6150.

[Rh(cod)(74'b)]BF$_4$ (90'b)

Beginning with 0.021 g (0.052 mmol) of $[Rh(cod)_2]BF_4$ in the minimum quantity of CH_2Cl_2, 0.050 g (0.055 mmol) of diphosphite **74'b** and following the general procedure, 0.047 g (76%) of complex [Rh(cod)(**74'b**)]BF_4 **90'b** was obtained as a yellow-orange solid. ^{1}H NMR ($CDCl_3$, 400 MHz) δ 7.22 (d, 2H, J= 2.5 Hz, aromatic), 7.10 (d, 2H, J= 2.6 Hz, aromatic), 6.84 (d, 2H, J= 2.5 Hz, aromatic), 6.71 (d, 2H, J= 2.7 Hz, aromatic), 5.85 (s broad, 2H, C$\underline{H}$ (cod)), 5.98 (s broad, 2H, H3), 5.00 (s broad, 2H, C$\underline{H}$ (cod)), 3.97 (s, 6H, *p*-OCH$_3$'), 3.96 (m, 2H, H2), 3.92 (s, 6H, *p*-OCH$_3$), 2.44 (m broad, 4H, C$\underline{H}_2$ (cod)), 2.35 (m broad, 2H, C$\underline{H}_2$ (cod)), 2.09 (m broad, 2H, C$\underline{H}_2$ (cod)), 1.84 (s, 18H, *o*-C(C$\underline{H}_3$)$_3$'), 1.57 (s, 18H, *o*-C(C$\underline{H}_3$)$_3$), 1.03 (d, 6H, $J_{1,2}$ = 6.0 Hz C(C$\underline{H}_3$)$_3$); ^{13}C NMR ($CDCl_3$, 100.6 MHz) δ 157.1-114.1 (aromatic), 112.2 (C$\underline{H}$ (cod)), 103.2 (C$\underline{H}$ (cod)), 85.3 (C3), 72.6 (C2), 55.9 (*p*-O$\underline{C}$H$_3$'), 55.7 (*p*-O$\underline{C}$H$_3$), 35.8 (*o*-$\underline{C}$(CH$_3$)$_3$'), 35.5 (*o*-$\underline{C}$(CH$_3$)$_3$), 32.4 (o-C($\underline{C}$H$_3$)$_3$'), 31.5 (o-C($\underline{C}$H$_3$)$_3$), 30.8 (C$\underline{H}_2$ (cod)), 29.6 (C$\underline{H}_2$ (cod)), 18.1 (CH$_3$, C1); ^{31}P NMR ($CDCl_3$, 161.97 MHz) δ 128.65 (d, $J_{P,\ Rh}$ = 254.1 Hz). MS (Maldi) *m/z* 1115.4 $[M]^+$, 1007.4 $[M\text{-}(cod)]^+$; HRMS (Maldi) calcd for $[C_{58}H_{78}O_{11}P_2Rh]^+$ 1115.4074; found 1115.4069.

[Rh(cod)(75a)]BF$_4$ (91a)

Beginning with 0.015 g (0.036 mmol) of $[Rh(cod)_2]BF_4$ in the minimum quantity of CH_2Cl_2, 0.062 g (0.041 mmol) of diphosphite **75a** and following the general procedure, 0.054 g (83%) of complex [Rh(cod)(**75a**)]BF_4 **91a** was obtained as a

yellow solid. ^{1}H NMR ($CDCl_3$, 400 MHz) δ 7.51-7.13 (m, 28H, aromatic), 5.67 (s broad, 2H, C<u>H</u> (cod)), 5.34(s broad, 2H, C<u>H</u> (cod)), 4.66 (s broad, 2H, H3), 3.89 (s broad, 2H, H2), 3.44 (s broad, 4H, H1), 2.36 (m broad, 4H, C<u>H</u>$_2$ (cod)), 2.23 (m broad, 2H, C<u>H</u>$_2$ (cod)), 2.05 (m broad, 4H, C<u>H</u>$_2$ (cod)), 1.51 (s, 18H, *o*-C(C<u>H</u>$_3$)$_3$'), 1.35 (s, 18H, *p*-C(C<u>H</u>$_3$)$_3$), 1.33 (s, 18H, *p*-C(C<u>H</u>$_3$)$_3$), 1.25 (s, 18H, *o*-C(C<u>H</u>$_3$)$_3$), 0.96 (s, 18H, C(C<u>H</u>$_3$)$_3$); ^{13}C NMR ($CDCl_3$, 100.6 MHz) δ 149.6-125.4 (aromatic), 112.8 (broad, C<u>H</u> (cod)), 103.4 (broad, C<u>H</u> (cod)), 80.9 (C2), 74.7 (broad, C3), 63.1 (broad, C1), 35.6 (*o*-<u>C</u>(CH$_3$)$_3$'), 35.3 (*o*-<u>C</u>(CH$_3$)$_3$), 34.8 (*p*-<u>C</u>(CH$_3$)$_3$), 32.3 (o-C(<u>C</u>H$_3$)$_3$), 31.4 (p-C(<u>C</u>H$_3$)$_3$), 30.3 (C<u>H</u>$_2$ (cod)), 29.7 (C<u>H</u>$_2$ (cod)), 26.8 (C(<u>C</u>H$_3$)$_3$), 19.2 (<u>C</u>(CH$_3$)$_3$); ^{31}P NMR ($CDCl_3$, 161.97 MHz) δ126.62 (d, $J_{P,\ Rh}$ = 258.7 Hz). MS (Maldi) *m/z* 1727.8 $[M]^+$, 1619.8 $[M\text{-(cod)}]^+$; HRMS (Maldi) calcd for $[C_{102}H_{138}O_9P_2RhSi_2]^+$ 1727.8410; found 1727.8404.

[Rh(cod)(75'a)]BF_4 (91'a)

Beginning with 0.025 g (0.062 mmol) of $[Rh(cod)_2]BF_4$ in the minimum quantity of CH_2Cl_2, 0.069 g (0.068 mmol) of diphosphite **75'a** and following the general procedure, 0.068 g (81%) of complex [Rh(cod)(**75'a**)]BF_4 **91'a** was obtained as a yellow solid. ^{1}H NMR ($CDCl_3$, 400 MHz) δ 7.58 (d, 2H, J= 1.9 Hz, aromatic), 7.48 (d, 2H, J= 1.9 Hz, aromatic), 7.15 (d, 2H, J= 1.9 Hz, aromatic), 7.09 (d, 2H, J= 1.9 Hz, aromatic), 5.85 (s broad, 2H, C<u>H</u> (cod)), 5,49 (s broad, 2H, H3), 5.00 (s broad, 2H, C<u>H</u> (cod)), 4.13 (m broad, 2H, H2), 2.34 (m broad, 4H, C<u>H</u>$_2$ (cod)), 2.10 (m broad, 2H, C<u>H</u>$_2$ (cod)), 2.01 (m broad, 2H, C<u>H</u>$_2$ (cod)), 1.73 (s, 18H, *o*-C(C<u>H</u>$_3$)$_3$'), 1.54 (s, 18H, *p*-C(C<u>H</u>$_3$)$_3$), 1.36 (s, 18H, *p*-C(C<u>H</u>$_3$)$_3$), 1.34 (s, 18H, *o*-C(C<u>H</u>$_3$)$_3$), 0.86 (d, 6H, $J_{1,2}$ = 6.5 Hz C(C<u>H</u>$_3$)$_3$); ^{13}C NMR ($CDCl_3$, 100.6 MHz) δ 149.2-125.3 (aromatic), 111.8 (C<u>H</u> (cod)), 104.2 (C<u>H</u> (cod)), 81.5 (C3), 71.0 (C2), 35.8 (*o*-<u>C</u>(CH$_3$)$_3$'), 35.4 (*o*-<u>C</u>(CH$_3$)$_3$), 34.8 (*p*-<u>C</u>(CH$_3$)$_3$'), 34.7 (*p*-<u>C</u>(CH$_3$)$_3$), 32.4 (o-C(<u>C</u>H$_3$)$_3$'), 31.6 (o-C(<u>C</u>H$_3$)$_3$), 31.3 (p-C(<u>C</u>H$_3$)$_3$'), 31.3 (p-C(<u>C</u>H$_3$)$_3$), 30.1 (C<u>H</u>$_2$ (cod)), 29.6 (C<u>H</u>$_2$ (cod)), 16.1 (CH$_3$, C1); ^{31}P NMR ($CDCl_3$, 161.97 MHz) δ 127.97 (d, $J_{P,\ Rh}$ = 253.9 Hz). Anal. Cald. $C_{70}H_{102}BF_4O_7P_2Rh$: C, 64.32; H, 7.86. MS (Maldi) *m/z* 1219.6 $[M]^+$, 1111.6 $[M\text{-(cod)}]^+$; HRMS (Maldi) calcd for $[C_{70}H_{102}O_7P_2Rh]^+$ 1219.6156; found 1219.6150.

[Rh(cod)(75'a)]BF_4 (91'a). X-ray Crystallography.

Crystals of [Rh(cod)(**75'a**)]BF_4 (**91'a**) were obtained by slow diffusion of hexane into a solution of [Rh(cod)(**75'a**)]BF_4 (**91'a**) in dichloromethane. Empirical formula: $C_{142.83}\,H_{209.35}\,B_2\,Cl_{5.67}\,F_8\,O_{14}\,P_4\,Rh_2$, Formula weight: 2854.67, Temperature: 100(2) K, Wavelength: 0.71073 Å, Crystal system: Orthorhombic, Space group: $P2_12_12_1$, Unit cell dimensions: a=19.1067(15) Å, a=90°, b=26.855(2) Å, b=90°, c=30.828(3) Å, g = 90°, Volume: 15818(2) $Å^3$, Z:4, Density (calculated):1.199 Mg/m^3, Absorption coefficient: 0.408 mm^{-1}, F(000): 6027, Crystal size: 0.20 x 0.04 x 0.02 mm^3, Theta range for data collection: 2.50 to 30.73°, Index ranges: -27 ≤ h ≤ 27, -37 ≤ k ≤ 38, -44 ≤ l ≤ 40, Reflections collected: 209015, Independent reflections: 48854 [R(int) = 0.0598], Completeness to theta = 30.73°: 99.3 %, Absorption correction: SADABS (Bruker-Nonius), Max. and min. transmission: 0.9919 and 0.9229, Refinement method: Full-matrix least-squares on F^2, Data / restraints / parameters: 48854 / 0 / 1644, Goodness-of-fit on F^2: 1.065, Final R indices [I>2sigma(I)]: R1 = 0.0674, wR2 = 0.1837, R indices (all data): R1 = 0.0880, wR2 = 0.1984, Absolute structure parameter: 0.000(18), Largest diff. peak and hole: 1.788 and -1.045 e.$Å^{-3}$

Compound [Rh(cod)(**75'a**)]BF_4 (**91'a**) crystallizes with two independent cations in the elementary cell. The crystal cell also contains two BF_4 anions and four disordered positions of dichloromethane molecules. The independently obtained cationic structures have different conformations. The measured compound crystallizes in a pure chiral structure. Selected bond distances and angles are given in Tables 5 and 6 of the appendix.

[Rh(cod)(76a)]BF_4 (92a)

Beginning with 0.025 g (0.062 mmol) of [$Rh(cod)_2$]BF_4 in the minimum quantity of CH_2Cl_2, 0.068 g (0.068 mmol) of diphosphite **74a** and following the general procedure, 0.059 g (75%) of complex [Rh(cod)(**74a**)]BF_4 **92a** was obtained as a yellow-orange solid. ^{1}H NMR ($CDCl_3$, 400 MHz) δ 7.61 (d, 2H, J= 1.9 Hz, aromatic),

7.50 (d, 2H, J= 1.9 Hz, aromatic), 7.21 (d, 2H, J= 1.9 Hz, aromatic), 7.08 (d, 2H, J= 1.9 Hz, aromatic), 5.51 (s broad, 2H, H3), 4.65 (s broad, 4H, C<u>H</u> (cod)), 4.13 (m, 2H, H2), 3.72 (t, 2H, H2'), 2.21 (m broad, 4H, C<u>H</u>$_2$ (cod)), 2.18 (m broad, 2H, C<u>H</u>$_2$ (cod)), 2.07 (m broad, 2H, C<u>H</u>$_2$ (cod)), 1.75 (s, 18H, *o*-C(C<u>H</u>$_3$)$_3$'), 1.53 (s, 18H, *p*-C(C<u>H</u>$_3$)$_3$), 1.38 (s, 18H, *p*-C(C<u>H</u>$_3$)$_3$), 1.36 (s, 18H, *o*-C(C<u>H</u>$_3$)$_3$); ^{13}C NMR ($CDCl_3$, 100.6 MHz) δ 149.6-125.6 (aromatic), 112.6 (C<u>H</u> (cod)), 103.2 (C<u>H</u> (cod)), 80.1 (C3), 67.9 (C2), 35.8 (*o*-<u>C</u>(CH$_3$)$_3$'), 35.4 (*o*-<u>C</u>(CH$_3$)$_3$), 34.9 (*p*-<u>C</u>(CH$_3$)$_3$'), 34.7 (*p*-<u>C</u>(CH$_3$)$_3$), 32.7 (o-C(<u>C</u>H$_3$)$_3$), 31.4 (p-C(<u>C</u>H$_3$)$_3$'), 31.3 (p-C(<u>C</u>H$_3$)$_3$), 30.5 (C<u>H</u>$_2$ (cod)), 29.5 (C<u>H</u>$_2$ (cod)); ^{31}P NMR ($CDCl_3$, 161.97 MHz) δ 127.85 (d, $J_{P,\ Rh}$ = 253.5 Hz). MS (Maldi) *m/z* 1191.6 $[M]^+$, 1083.6 $[M\text{-}(cod)]^+$; HRMS (Maldi) calcd for $[C_{68}H_{98}O_7P_2Rh]^+$ 1191.5843; found 1191.5837.

[Rh(cod)(76b)]BF_4 (92a)

Beginning with 0.025 g (0.062 mmol) of $[Rh(cod)_2]BF_4$ in the minimum quantity of CH_2Cl_2, 0.061 g (0.068 mmol) of diphosphite **74b** and following the general procedure, 0.054 g (79%) of complex [Rh(cod)(**74b**)]BF_4 **92a** was obtained as a yellow-orange solid. ^{1}H NMR ($CDCl_3$, 400 MHz) δ 7.13 (d, 2H, J= 2.9 Hz, aromatic), 7.01 (d, 2H, J= 2.9 Hz, aromatic), 6.75 (d, 2H, J= 2.9 Hz, aromatic), 6.62 (d, 2H, J= 2.9 Hz, aromatic), 5.64 (s broad, 2H, C<u>H</u> (cod)), 5.43 (s broad, 2H, H3), 4.80 (s broad, 2H, C<u>H</u> (cod)), 4.07 (m, 2H, H2), 3.87 (s, 6H, *p*-OCH$_3$'), 3.83 (s, 6H, *p*-OCH$_3$), 3.66 (t, 2H, H2'), 2.26 (m broad, 4H, C<u>H</u>$_2$ (cod)), 2.15 (m broad, 2H, C<u>H</u>$_2$ (cod)), 1.82 (m broad, 2H, C<u>H</u>$_2$ (cod)), 1.71 (s, 18H, *o*-C(C<u>H</u>$_3$)$_3$'), 1.48 (s, 18H, *o*-C(C<u>H</u>$_3$)$_3$); ^{13}C NMR ($CDCl_3$, 100.6 MHz) δ 157.3 -114.2 (aromatic), 113.6 (C<u>H</u> (cod)), 103.8 (C<u>H</u> (cod)), 80.3 (C3), 68.1 (C2), 56.2 (*p*-O<u>C</u>H$_3$'), 55.3 (*p*-O<u>C</u>H$_3$), 36.1 (*o*-<u>C</u>(CH$_3$)$_3$'), 35.7 (*o*-<u>C</u>(CH$_3$)$_3$), 32.7 (o-C(<u>C</u>H$_3$)$_3$), 31.6 (*o*-C(<u>C</u>H$_3$)$_3$'), 30.8 (C<u>H</u>$_2$ (cod)), 30.1 (C<u>H</u>$_2$ (cod)); ^{31}P NMR ($CDCl_3$, 161.97 MHz) δ 129.36 (d, $J_{P,\ Rh}$ = 256.0 Hz). MS (Maldi) *m/z* 1087.4 $[M]^+$, 979.4 $[M\text{-}(cod)]^+$; HRMS (Maldi) calcd for $[C_{56}H_{74}O_{11}P_2Rh]^+$ 1087.3761; found 1087.3756.

Hydroformylation experiments

In a typical experiment, the autoclave was purged three times with CO. The solution was formed from $[Rh(acac)(CO)_2]$ (0.013 mmol), diphosphite (0.015

mmol) and styrene (13 mmol) in toluene (15 ml). After the desired reaction time, the autoclave was cooled to room temperature and depressurised. The reaction mixture was analysed by gas chromatography. The aldehydes obtained from the hydroformylation were oxidised to carboxylic acids to determine the enantiomeric excess.

In situ HP-NMR hydroformylation experiments

In a typical experiment, a sapphire tube (ø10 mm) was filled under argon with a solution of [Rh(acac)$(CO)_2$] (2.10^{-2} M) and ligand (molar ratio PP/Rh=1.1) in [D_8]toluene (2 ml). The solution was analysed and then the HP-NMR tube was purged three times with CO and pressurized to the appropriate pressure of CO/H_2 . After a reaction time of 15 hours during which the solution was shaken at 80ºC of temperature, the solution was analysed.

[Rh(acac)(74a)]

^{1}H NMR (C_6D_8, 300 MHz) δ 7.72-6.92 (m, 28H, aromatic), 5.61 (broad, 2H, H3), 5.15 (s, 1H, C<u>H</u>), 3.92 (m broad, 2H, H2), 3.61 (d, 2H, H1), 3.28 (d, 2H, H1'), 1.96 (s, 18H, *o*-C(C<u>H</u>$_3$)$_3$'), 1.80 (s, 18H, *p*-C(C<u>H</u>$_3$)$_3$), 1.32 (s, 6H, C<u>H</u>$_3$), 1.32 (s, 18H, *p*-C(C<u>H</u>$_3$)$_3$), 1.20 (s, 18H, *o*-C(C<u>H</u>$_3$)$_3$), 1.09 (s, 18H, C(C<u>H</u>$_3$)$_3$); ^{31}P NMR (C_6D_8, 121.47 MHz) δ 140.77 (d, $J_{Rh,\ P}$= 301.4 Hz.).

[RhH$(CO)_2$(74a)]

^{1}H NMR (C_6D_8, 300 MHz) δ 7.81-6.99 (m, 28H, aromatic), 5.40 (broad, 2H, J= 8.5 Hz, H3), 4.04 (broad, 2H, H2), 3.58 (dd, 2H, H1), 3.58 (dd, 2H, H1'), 1.67 (s, 18H, *o*-C(C<u>H</u>$_3$)$_3$'), 1.63 (s, 18H, *p*-C(C<u>H</u>$_3$)$_3$), 1.29 (s, 18H, *p*-C(C<u>H</u>$_3$)$_3$), 1.21 (s, 18H, *o*-C(C<u>H</u>$_3$)$_3$), 1.16 (s, 18H, C(C<u>H</u>$_3$)$_3$), -9.93 (t, 1H, $J_{H,\ Rh}$ = 2.0 Hz, $J_{H,\ P}$ = 2.0 Hz) ; ^{31}P NMR (C_6D_8, 121.47 MHz) δ 152.70 (d, $J_{Rh,\ P}$= 231.9 Hz.).

[Rh(acac)(74b)]

^{1}H NMR (C_6D_8, 300 MHz) δ 7.73-6.78 (m, 28H, aromatic), 5.61 (s broad, 2H, H3), 5.15 (s, 1H, C<u>H</u>), 4.00 (s broad, 2H, H2), 3.61 (d, 2H, H1), 3.42 (d, 2H, H1'), 3.39 (s, 6H, OC<u>H</u>$_3$'), 3.35 (s, 6H, OC<u>H</u>$_3$), 1.94 (s, 18H, *o*-C(C<u>H</u>$_3$)$_3$'), 1.72 (s, 18H, *o*-C(C<u>H</u>$_3$)$_3$), 1.43 (s, 6H, C<u>H</u>$_3$), 1.11 (s, 18H, C(C<u>H</u>$_3$)$_3$); ^{31}P NMR (C_6D_8, 121.47 MHz) δ 141.29 (d, $J_{Rh,\ P}$= 300.4 Hz.).

[RhH(CO)$_2$(74b)]

^{1}H NMR (C_6D_8, 300 MHz) δ 7.79 - 6.64 (m, 28H, aromatic), 5.38 (m broad, 2H, J= 9.9 Hz, H3), 4.17 (broad, 2H, H2), 3.84 (dd, 2H, H1), 3.67 (dd, 2H, H1'), 3.32 (s, 6H, OC<u>H</u>$_3$'), 3.29 (s, 6H, OC<u>H</u>$_3$), 1.62 (s, 18H, *o*-C(C<u>H</u>$_3$)$_3$'), 1.57 (s, 18H, *o*-C(C<u>H</u>$_3$)$_3$), 1.17 (s, 18H, C(C<u>H</u>$_3$)$_3$), -9.91 (q, 1H, $J_{H,\ Rh}$ = 3.4 Hz, $J_{H,\ P}$ = 3.9 Hz) ; ^{31}P NMR (C_6D_8, 121.47 MHz) δ 155.33 (d, $J_{Rh,\ P}$= 230.0 Hz.).

[Rh(acac)(74'a)]

^{1}H NMR (C_6D_8, 300 MHz) δ 7.58 (m, 4H, aromatic), 7.34 (m, 4H, aromatic), , 5.10 (s, 1H, C<u>H</u>), 4.83 (broad, 2H, H3), 3.88 (m broad, 2H, H2), 1.93 (s, 18H, *o*-C(C<u>H</u>$_3$)$_3$'), 1.77 (s, 18H, *o*-C(C<u>H</u>$_3$)$_3$), 1.56 (s, 6H, C<u>H</u>$_3$), 1.28 (s, 18H, *p*-C(C<u>H</u>$_3$)$_3$), 1.27 (s, 18H, *p*-C(C<u>H</u>$_3$)$_3$), 0.97 (d, 6H, $J_{1,2}$ = 6.2 Hz, H1); ^{31}P NMR (C_6D_8, 121.47 MHz) δ 141.13 (d, $J_{Rh,\ P}$= 299.4 Hz.).

[RhH(CO)$_2$(74'a)]

^{1}H NMR (C_6D_8, 300 MHz) δ 7.60 (m, 4H, aromatic), 7.32 (m, 4H, aromatic), , 4.95 (m, 2H, H3), 4.11 (m, 2H, H2), 1.69 (s, 18H, *o*-C(C<u>H</u>$_3$)$_3$'), 1.63 (s, 18H, *o*-C(C<u>H</u>$_3$)$_3$), 1.26 (s, 36H, *p*-C(C<u>H</u>$_3$)$_3$), 1.16 (d, 6H, $J_{1,2}$ = 6.2 Hz, H1), -10.14 (q broad, 1H, $J_{H,\ Rh}$ = 2.7 Hz, $J_{H,\ P}$ = 3.8 Hz) ; ^{31}P NMR (C_6D_8, 121.47 MHz) δ 155.43 (d, $J_{Rh,\ P}$= 231.6 Hz.).

[RhH(CO)$_2$(75a)]

^{1}H NMR (C_6D_8, 300 MHz) δ 7.81-6.96 (m, 28H, aromatic), 5.59 (dd, 2H, H3), 4.67 (m broad, 2H, H2), 3.95 (dd, 2H, H1), 3.63 (dd, 2H, H1'), 1.64 (s, 18H, *o*-C(C$\underline{H}_3$)$_3$'), 1.60 (s, 18H, *p*-C(C$\underline{H}_3$)$_3$), 1.31 (s, 18H, *p*-C(C$\underline{H}_3$)$_3$), 1.16 (s, 18H, *o*-C(C$\underline{H}_3$)$_3$), 1.13 (s, 18H, C(C$\underline{H}_3$)$_3$), -9.85 (q, 1H, $J_{H, Rh}$ = 2.9 Hz, $J_{H, P}$ = 3.1 Hz) ; ^{31}P NMR (C_6D_8, 121.47 MHz) δ 158.09 (d, $J_{Rh, P}$= 233.6 Hz.).

[Rh(acac)(75'a)]

^{1}H NMR (C_6D_8, 300 MHz) δ 7.61 (m, 4H, aromatic), 7.33 (m, 4H, aromatic), 5.25 (s broad, 2H, H3), 5.13 (s, 1H, C$\underline{H}$), 3.92 (m broad, 2H, $J_{2,1}$ = 6.2 Hz, H2), 1.92 (s, 18H, *o*-C(C$\underline{H}_3$)$_3$'), 1.81 (s, 18H, *o*-C(C$\underline{H}_3$)$_3$), 1.56 (s, 6H, C$\underline{H}_3$), 1.30 (s, 18H, *p*-C(C$\underline{H}_3$)$_3$), 1.27 (s, 18H, *p*-C(C$\underline{H}_3$)$_3$), 0.80 (d, 6H, $J_{1,2}$ = 6.2 Hz, H1); ^{31}P NMR (C_6D_8, 121.47 MHz) δ 141.55 (d, $J_{Rh, P}$= 300.1 Hz.).

[RhH(CO)$_2$(75'a)]

^{1}H NMR (C_6D_8, 300 MHz) δ 7.58 (m, 4H, aromatic), 7.32 (m, 4H, aromatic), 5.18 (m, 2H, H3), 4.16 (m, 2H, H2), 1.69 (s, 18H, *o*-C(C$\underline{H}_3$)$_3$'), 1.62 (s, 18H, *o*-C(C$\underline{H}_3$)$_3$), 1.27 (s, 36H, *p*-C(C$\underline{H}_3$)$_3$), 0.83 (d, 6H, $J_{1,2}$ = 6.5 Hz, H1), -10.05 (q, 1H, $J_{H, Rh}$ = 3.9 Hz, $J_{H, P}$ = 4.3 Hz) ; ^{31}P NMR (C_6D_8, 121.47 MHz) δ 155.27 (d, $J_{Rh, P}$= 234.1 Hz.).

[RhH(CO)$_2$(76a)]

^{1}H NMR (C_6D_8, 300 MHz) δ 7.61 (d, 2H, J = 2.3 Hz, aromatic), 7.59 (d, 2H, J= 2.3 Hz, aromatic), 7.30 (d, 2H, J= 2.3 Hz, aromatic), 7.28 (d, 2H, J= 2.3 Hz, aromatic), 5.35 (m, 2H, H3), 3.86 (dd, 2H, H2), 3.60 (dd, 2H, H1') 1.69 (s, 18H, *o*-C(C$\underline{H}_3$)$_3$'), 1.60 (s, 18H, *o*-C(C$\underline{H}_3$)$_3$), 1.25 (s, 36H, *p*-C(C$\underline{H}_3$)$_3$), -10.24 (q, 1H, $J_{H, Rh}$ = 3.8 Hz, $J_{H, P}$ = 3.9 Hz) ; ^{31}P NMR (C_6D_8, 121.47 MHz) δ 156.40 (d, $J_{Rh, P}$= 232.1 Hz.).

Hydrogenation experiments

The experiments were prepared in a multiple reaction vessel autoclave in a glovebox. After the addition of the substrate to a solution of $[Rh(cod)(L)]BF_4$ ($2.5x10^{-3}$ mmol) in the corresponding solvent (2.5 ml) the autoclave was pressurised to the desired pressure with hydrogen. After the desired reaction time the autoclave was depressurised. The reaction mixture was analysed by gas chromatography.

2.5 References

[1] R. I. Hollingsworth, G. Wang, *Chem. Rev.* **2000**, *100*, 4267.

[2] D. Steinborn, H. Junicke, *Chem. Rev.* **2000**, *100*, 4283.

[3] T. V. RajanBabu, A. L. Casalnuovo, T. A. Ayers, in *Advances in Catalytic Processes, Vol. 2* (Ed.: M. P. Doyle), Ed.; JAI Press: Greenwich, CT, **1998**, pp. 1.

[4] S. Castillón, C. Claver, Y. Díaz, *Chem. Soc. Rev.* **2005**, *34*, 702.

[5] M. Dieguez, O. Pàmies, A. Ruiz, Y. Diaz, S. Castillon, C. Claver, *Coord. Chem. Rev.* **2004**, *248*, 2165.

[6] M. Dieguez, O. Pàmies, C. Claver, *Chem. Rev.* **2004**, *104*, 3189.

[7] G. Descotes, D. Lafont, D. Sinou, *J. Organomet. Chem.* **1978**, *150*, C14.

[8] W. R. Cullen, Y. Sugi, *Tetrahedron Lett.* **1978**, *19*, 1635.

[9] R. Jackson, D. J. Thompson, *J. Organomet. Chem.* **1978**, *159*.

[10] M. Beller, B. Cornils, C. D. Frohning, C. W. Kohlpaintner, *J. Mol. Catal. A: Chem.* **1995**, *104*, 17.

[11] F. Agbossou, J. F. Carpentier, A. Mortreux, *Chem. Rev.* **1995**, *95*, 2485.

[12] S. Gladiali, J. C. Bayon, C. Claver, *Tetrahedron: Asymmetry* **1995**, *6*, 1453.

[13] K. Nozaki, in *Comprehensive Asymmetric Catalysis. Chapter 11, Vol. 1*, Jacobsen, E.N., Pfaltz, A., Yamamoto, H. ed., Springer-Verlag, Berlin, **1999**.

[14] P. W. N. M. van Leeuwen, Claver, C., *Rhodium Catalyzed Hydroformylation, Vol. 22*, Kluwer Academic Press., Dordrecht, **2000**.

[15] P. W. N. M. van Leeuwen, in *Homogeneous Catalysis: Understanding the art, Vol. 8*, Kluwer Academic Publishers, Dordrecht, **2004**, p. 139.

[16] M. Dieguez, O. Pàmies, C. Claver, *Tetrahedron: Asymmetry* **2004**, *15*, 2113.

[17] A. J. Chalk, in *Flavors and Fragances: A World Perspective* (Ed.: B. M. Lawrence, Mookherjee, B. D. and Willis, B. J.), Elsevier Science, Amsterdam, **1988**.

[18] C. Botteghi, M. Marchetti, S. Paganelli, in *Transition Metal for Organic Synthesis. Building Blocks and Fine Chemicals, Vol. 1* (Eds.: M. Beller, C. Bolm), Wiley-WCH, Weinheim, **1998**.

[19] R. F. Heck, D. S. Breslow, *J. Am. Chem. Soc.* **1961**, *83*, 4023.

[20] R. F. Heck, D. S. Breslow, *J. Am. Chem. Soc.* **1962**, *84*, 2499.

[21] R. F. Heck, *Acc. Chem. Res.* **1969**, *2*, 10.

[22] D. Evans, G. Yagupsky, Wilkinso.G, *J. Chem. Soc. A* **1968**, 2660.

[23] D. Evans, J. A. Osborn, Wilkinso.G, *J. Chem. Soc. A* **1968**, 3133.

[24] C. K. Brown, Wilkinso.G, *J. Chem. Soc. A* **1970**, 2753.

[25] P. W. N. M. van Leeuwen, C. P. Casey, G. T. Whiteker, in *Chapter 4. Rhodium Catalyzed Hydroformylation, Vol. 22* (Ed.: P. W. N. M. van Leeuwen, Claver, C.), Kluwer Academic Press., Dordrecht, **2000**, p. 296.

[26] A. Castellanos-Paez, S. Castillón, C. Claver, P. W. N. M. van Leeuwen, W. G. J. de Lange, *Organometallics* **1998**, *17*, 2543.

[27] O. Roelen, *US 2327066* **1943**.

[28] B. Cornils, in *New Syntheses with Carbon Monoxide* (Ed.: J. Falbe), Springer-Verlag, Berlin, **1980**, pp. 1.

[29] J. K. Stille, H. Su, P. Brechot, G. Parrinello, L. S. Hegedus, *Organometallics* **1991**, *10*, 1183.

[30] G. Consiglio, S. C. A. Nefkens, A. Borer, *Organometallics* **1991**, *10*, 2046.

[31] M. Diéguez, M. M. Pereira, A. M. Masdeu Bultó, C. Claver, J. C. Bayón, *J Mol. Catal. A: Chem.* **1999**, *143*.

[32] J. E. Babin, G. T. Whiteker, [Chem. Abs. 1993, 119, P159 872 h], (Union Carbide Chem. Plastics Techn. Co.)WO 93/03839, **1993**.

[33] G. J. H. Buisman, L. A. van Der Veen, A. Klootwijk, W. G. J. De Lange, P. C. J. Kamer, P. W. N. M. van Leeuwen, D. Vogt, *Organometallics* **1997**, *16*, 2929.

[34] M. Diéguez, O. Pàmies, A. Ruiz, S. Castillón, C. Claver, *Chem. Commun.* **2000**, 1607.

[35] M. Diéguez, O. Pàmies, A. Ruiz, C. Claver, *New J. Chem.* **2002**, *26*, 827.

[36] M. Diéguez, O. Pàmies, A. Ruiz, C. Claver, S. Castillón, *Chem. Eur. J.* **2001**, *7*, 3086.

[37] C. J. Cobley, K. Gardner, J. Klosin, C. Praquin, C. Hill, G. T. Whiteker, A. Zanotti-Gerosa, J. L. Petersen, K. A. Abboud, *J. Org. Chem.* **2004**, *69*, 4031.

[38] C. J. Cobley, J. Klosin, C. Qin, G. T. Whiteker, *Org. Lett.* **2004**, *6*, 3277.

[39] K. Nozaki, N. Sakai, T. Nanno, T. Higashijima, S. Mano, T. Horiuchi, H. Takaya, *J. Am. Chem. Soc.* **1997**, *119*, 4413.

[40] G. Franciò, W. Leitner, *Chem. Commun.* **1999**, 1663.

[41] G. J. Clarkson, J. R. Ansell, D. J. Cole-Hamilton, P. J. Pogorzelec, J. Whittell, M. Wills, *Tetrahedron: Asymmetry* **2004**, *15*, 1787.

[42] S. Breeden, M. Wills, *J. Org. Chem.* **1999**, *64*, 9735.

[43] A. T. Axtell, C. J. Cobley, J. Klosin, G. T. Whiteker, A. Zanotti-Gerosa, K. A. Abboud, *Angew. Chem. Int. Ed.* **2005**, *44*, 5834.

[44] D. J. Wink, T. J. Kwok, A. Yee, *Inorg. Chem.* **1990**, *29*, 5006.

[45] N. Sakai, K. Nozaki, K. Mashima, H. Takaya, *Tetrahedron: Asymmetry* **1992**, *3*, 581.

[46] G. J. H. Buisman, P. C. J. Kamer, P. W. N. M. van Leeuwen, *Tetrahedron: Asymmetry* **1993**, *4*, 1625.

[47] G. J. H. Buisman, E. J. Vos, P. C. J. Kamer, P. W. N. M. van Leeuwen, *J. Chem. Soc., Dalton Trans.* **1995**, 409.

[48] G. J. H. Buisman, L. A. van der Veen, P. C. J. Kamer, P. van Leeuwen, *Organometallics* **1997**, *16*, 5681.

[49] S. Cserépi-Szucs, I. Tóth, J. Bakos, L. Párkanyi, *Tetrahedron: Asymmetry* **1998**, *9*, 3135.

[50] S. Cserépi-Szucs, G. Huttner, L. Zsolnai, J. Bakos, *J. Organomet. Chem.* **1999**, *586*, 70.

[51] S. Cserépi-Szucs, G. Huttner, L. Zsolnai, A. Szölosy, C. Hegedüs, J. Bakos, *Inorg. Chim. Acta* **1999**, *296*, 222.

[52] Y. Jiang, S. Xue, Z. Li, J. Deng, A. Mi, A. S. C. Chan, *Tetrahedron: Asymmetry* **1998**, *9*, 3185.

[53] Z. Freixa, J. C. Bayón, *J. Chem. Soc., Dalton Trans.* **2001**, 2067.

[54] G. J. H. Buisman, M. E. Martin, E. J. Vos, A. Klootwijk, P. C. J. Kamer, P. W. N. M. van Leeuwen, *Tetrahedron: Asymmetry* **1995**, *6*, 719.

[55] R. Kadyrov, D. Heller, R. Selke, *Tetrahedron: Asymmetry* **1998**, *9*, 329.

[56] O. Pàmies, G. Net, A. Ruiz, C. Claver, *Tetrahedron: Asymmetry* **2000**, *11*, 1097.

[57] M. Dieguez, O. Pàmies, C. Claver, *Chem. Commun.* **2005**, 1221.

[58] N. Sakai, S. Mano, K. Nozaki, H. Takaya, *J. Am. Chem. Soc.* **1993**, *115*, 7033.

[59] K. Nozaki, T. Matsuo, F. Shibahara, T. Hiyama, *Adv. Syn. Catal.* **2001**, *343*, 61.

[60] K. Nozaki, Y. Itoi, F. Shibahara, E. Shirakawa, T. Ohta, H. Takaya, T. Hiyama, *J. Am. Chem. Soc.* **1998**, *120*, 4051.

[61] K. Nozaki, F. Shibahara, Y. Itoi, E. Shirakawa, T. Ohta, H. Takaya, T. Hiyama, *Bull. Chem. Soc. Jpn.* **1999**, *72*, 1911.

[62] A. Kless, J. Holz, D. Heller, R. Kadyrov, R. Selke, C. Fischer, A. Börner, *Tetrahedron: Asymmetry* **1996**, *7*, 33.

[63] S. Deerenberg, P. C. J. Kamer, P. W. N. M. van Leeuwen, *Organometallics* **2000**, *19*, 2065.

[64] M. Diéguez, O. Pàmies, G. Net, A. Ruiz, C. Claver, *Tetrahedron: Asymmetry* **2001**, *12*, 3441.

[65] P. Meakin, J. P. Jesson, F. N. Tebbe, M. El., *J. Am. Chem. Soc.* **1971**, *93*, 1797.

[66] P. Meakin, J. P. Jesson, Muettert.El, *J. Am. Chem. Soc.* **1972**, *94*, 5271.
[67] K. Nozaki, T. Matsuo, F. Shibahara, T. Hiyama, *Organometallics* **2003**, *22*, 594.
[68] R. Noyori, in *Asymmetric Catalysis in Organic Synthesis*, Wiley, New York, **1994**.
[69] I. Ojima, in *Catalytic Asymmetric Synthesis*, Wiley, New York, **1993**.
[70] C. R. Landis, J. Halpern, *J. Am. Chem. Soc.* **1987**, *109*, 1746.
[71] W. J. Tang, X. M. Zhang, *Chem. Rev.* **2003**, *103*, 3029.
[72] W. S. Knowles, M. J. Sabacky, *Chem. Commun.* **1968**, 1445.
[73] L. Horner, H. Siegel, H. Buthe, *Angew. Chem. Int. Ed.* **1968**, *7*, 942.
[74] J. A. Osborn, F. H. Jardine, J. F. Young, Wilkinso.G, *J. Chem. Soc. A* **1966**, 1711.
[75] H. B. Kagan, T. P. Dang, *J. Am. Chem. Soc.* **1972**, *94*, 6429.
[76] W. S. Knowles, B. D. Vineyard, M. J. Sabacky, *J. Chem. Soc. Chem. Commun.* **1972**, 10.
[77] W. S. Knowles, *J. Chem. Educ.* **1986**, *63*, 222.
[78] W. S. Knowles, *Angew. Chem. Int. Ed.* **2002**, *41*, 1999.
[79] A. Miyashita, A. Yasuda, H. Takaya, K. Toriumi, T. Ito, T. Souchi, R. Noyori, *J. Am. Chem. Soc.* **1980**, *102*, 7932.
[80] R. Noyori, *Science* **1990**, *248*, 1194.
[81] W. A. Nugent, T. V. Rajanbabu, M. J. Burk, *Science* **1993**, *259*, 479.
[82] M. J. Burk, *Acc. Chem. Res.* **2000**, *33*, 363.
[83] Y. Y. Yan, T. V. RajanBabu, *Org. Lett.* **2000**, *2*, 4137.
[84] W. Li, X. Zhang, *J. Org. Chem.* **2000**, *65*, 5871.
[85] X. Zhang, *U.S. Patent WO 01/34612 A2* **2001**.
[86] W. Li, J. P. Waldkirch, X. Zhang, *J. Org. Chem.* **2002**, *67*, 7618.
[87] J. Holz, M. Quirmbach, U. Schmidt, D. Heller, R. Stürmer, A. Börner, *J. Org. Chem.* **1998**, *63*, 8031.
[88] W. Li, Z. Zhang, D. Xiao, X. Zhang, *J. Org. Chem.* **2000**, *65*, 3489.
[89] D. Liu, W. Li, X. Zhang, *Org. Lett.* **2002**, *4*, 4471.
[90] X. Zhang, *WO Patent 03/040149 A2* **2003**.
[91] A. Bayer, P. Murszat, U. Thewalt, B. Rieger, *Eur. J. Inorg. Chem.* **2002**, 2614.
[92] J. Holz, U. Schmidt, H.-J. Drexler, D. Heller, A. Börner, R. Stürmer, H.-P. Krimmer, *Eur. J. Org. Chem.* **2001**, 4615.
[93] D. Carmichael, H. Doucet, J. M. Brown, *Chem. Commun.* **1999**, 261.
[94] M. Diéguez, O. Pàmies, A. Ruiz, S. Castillón, C. Claver, *Tetrahedron: Asymmetry* **2000**, *11*, 4701.
[95] R. Selke, *React. Kinet. Catal. Lett.* **1979**, *10*, 135.
[96] D. Sinou, G. Descotes, *React. Kinet. Catal. Lett.* **1980**, *14*, 463.
[97] R. Selke, H. Pracejus, *J. Mol. Catal.* **1986**, *37*, 213.
[98] R. Selke, *J. Organomet. Chem.* **1989**, *370*, 249.

[99] R. Selke, M. Schwarze, H. Baudisch, I. Grassert, M. Michalik, G. Oehme, N. Stoll, B. Costisella, *J. Mol. Catal.* **1993**, *84*, 223.

[100] T. V. RajanBabu, T. A. Ayers, A. L. Casalnuovo, *J. Am. Chem. Soc.* **1994**, *116*, 4101.

[101] T. A. Ayers, T. V. RajanBabu, *U.S. Patent 5510507* **1996**.

[102] T. V. RajanBabu, T. A. Ayers, G. A. Halliday, K. K. You, J. C. Calabrese, *J. Org. Chem.* **1997**, *62*, 6012.

[103] E. Guimet, M. Diéguez, A. Ruiz, C. Claver, *Tetrahedron: Asymmetry* **2004**, *15*, 2247.

[104] E. Guimet, J. Parada, M. Diéguez, A. Ruiz, C. Claver, *Appl. Catal. A* **2005**, *282*, 215.

[105] E. Guimet, M. Diéguez, A. Ruiz, C. Claver, *Tetrahedron: Asymmetry* **2005**, *16*, 2161.

[106] E. Guimet, M. Diéguez, A. Ruiz, C. Claver, *Inorg. Chim. Acta* **2005**, *358*, 3824.

[107] M. Aghmiz, A. Aghmiz, Y. Diaz, A. Masdeu-Bulto, C. Claver, S. Castillón, *J. Org. Chem.* **2004**, *69*, 7502.

[108] M. T. Reetz, T. Neugebauer, *Angew. Chem. Int. Ed.* **1999**, *38*, 179.

[109] M. Diéguez, A. Ruiz, C. Claver, *J. Org. Chem.* **2002**, *67*, 3796.

[110] D. Horton, K. D. Philips, *Methods Carbohydr. Chem* **1976**, *7*, 68.

[111] D. A. Otero, R. Simpson, *Carbohydr. Res.* **1984**, *128*, 79.

[112] S. Claustre, F. Bringaud, L. Azema, R. Baron, J. Perie, M. Willson, *Carbohydr. Res.* **1999**, *315*, 339.

[113] R. D. Guthrie, I. D. Jenkins, J. J. Watters, M. W. Wright, R. Yamasaki, *Aust. J. Chem.* **1982**, *35*, 2169.

[114] T. Jongsma, M. Fossen, G. Challa, P. W. N. M. van Leeuwen, *J. Mol. Catal.* **1993**, *83*, 17.

[115] R. J. Rafka, B. J. Morton, *Carbohydr. Res.* **1994**, *260*, 155.

[116] S. Cassel, C. Debaig, T. Benvegnu, P. Chaimbault, M. Lafosse, D. Plusquellec, P. Rollin, *Eur. J. Org. Chem.* **2001**, 875.

[117] A. Terfort, *Synthesis-Stuttgart* **1992**, 951.

[118] P. Uriz, E. Fernandez, N. Ruiz, C. Claver, *Inorg. Chem. Commun.* **2000**, *3*, 515.

[119] M. Dieguez, O. Pàmies, G. Net, A. Ruiz, C. Claver, *Tetrahedron: Asymmetry* **2001**, *12*, 651.

[120] C. Claver, P. W. N. M. van Leeuwen, in *Chapter 5. Rhodium Catalyzed Hydroformylation, Vol. 22* (Ed.: P. W. N. M. van Leeuwen, Claver, C.), Kluwer Academic Press., Dordrecht, **2000**, p. 296.

[121] O. Pamies, G. Net, A. Ruiz, C. Claver, *Tetrahedron: Asymmetry* **2000**, *11*, 1097.

Chapter 3

Rhodium-diphosphite catalysed hydroformylation of allylbenzene and propenylbenzene derivatives

Abstract. *The asymmetric hydroformylation of allylbenzenes and propenylbenzenes is an important tool for obtaining high value intermediates for the pharmaceutical and perfume industry. We have studied these reactions with rhodium-chiral diphosphite systems. The diphosphite ligands* ***6*** *and* ***7*** *with carbohydrate backbone have high regioselectivities in trans-anethole hydroformylation and moderate ones in estragole hydroformylation. Only low enantioselectivities have been observed in the trans-anethole hydroformylation with the rhodium-diphosphite* ***6*** *based system.*

3.1 Introduction

The asymmetric hydroformylation reaction is an important tool for synthesizing enantiomerically pure aldehydes. These are important precursors of biologically pure compounds, biodegradable polymers and liquid crystals.[1-3] On the other hand, the hydroformylation of terpenes makes it possible to produce aldehydes of interest to the perfume industry (Scheme 3.1).[4-8]

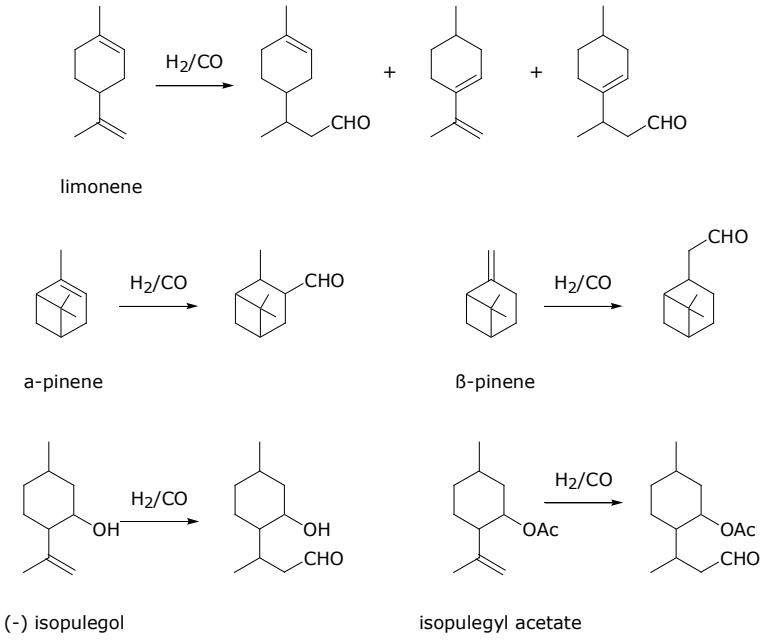

Scheme 3.1. Hydroformylation of some terpenes

The hydroformylation of terpenes such as eugenol, safrole and estragol, which are allylbenzenes, and their isomers isoeugenol, isosafrole and *trans*-anethole, which are propenylbenzenes (Figure 3.1) is interesting for the formation of aldehyde derivatives for the flavour industry.[8] Although asymmetric hydroformylation of vinylaromatic compounds has been widely studied[1-3, 9] there are very few studies on the hydroformylation of allylbenzenes and propenylbenzenes.[10-13]

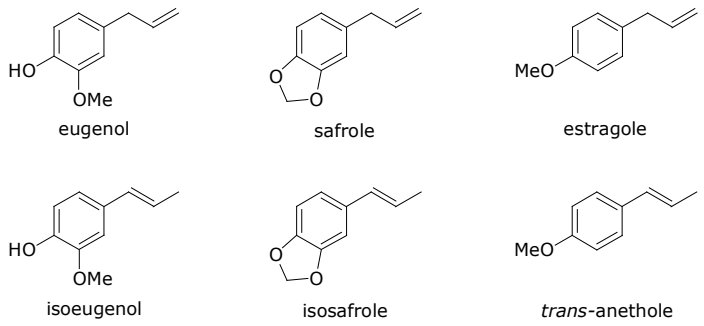

Figure 3.1. Allylbenzenes and propenylbenzenes

The hydroformylation of propenylbenzenes **1** (Scheme 3.2) makes it possible to synthesize two branched aldehydes **3** and **4**, but the isomerisation of these olefins to the terminal alkenes **2**, allylbenzenes, also leads to the formation of the branched and linear aldehydes **4** and **5**, respectively.

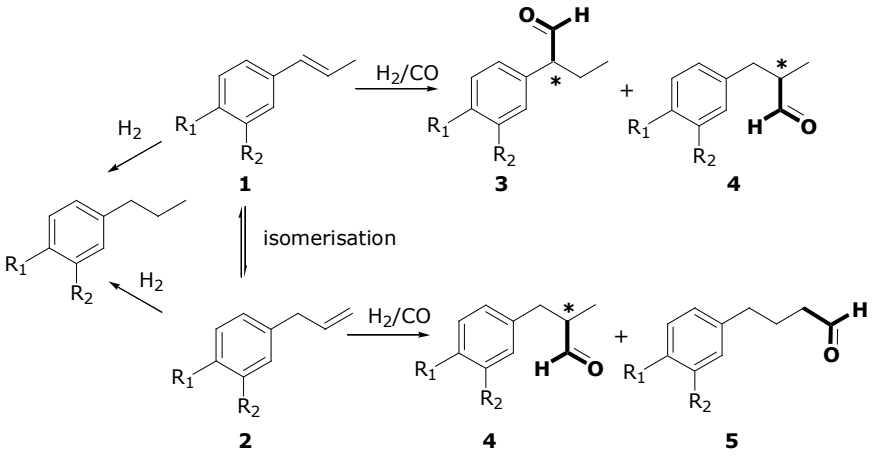

R_1	R_2		compound		compound
OCH_3	H	**1a**	*trans*-anethol	**2a**	estragole
OH	OCH_3	**1b**	isoeugenol	**2b**	eugenol
-OCH_2O-		**1c**	isosafrol	**2c**	safrole

Scheme 3.2. Hydroformylation of allylbenzene and propenylbenzene

The hydroformylation of eugenol **2b** and isoeugenol **1b** with unmodified rhodium catalysts at very high pressures was studied 25 years ago.[10] A mixture of aldehydes **3**, **4** and **5** was obtained (Scheme 3.2). Temperature was observed to have a strong influence on the regioselectivity. At low temperature (70ºC), the ratio of aldehydes obtained from **1b** and from **2b** was very different, while at 130ºC the ratios were closer. This indicates that an isomerization process takes place when the temperature increases, so the process is less selective (Table 3.1).

Kalck et al.[11] reported high selectivities for linear aldehydes **5** when they used the catalytic system $[Rh_2(\mu\text{-}SR)_2(CO)_2L_2]$ (L: PPh_3, $P(OMe)_3$ and $P(OPh)_3$) in the hydroformylation of allylbenzenes (estragole **1c**, eugenol **2b**, eugenol methyl ether and safrole **3c**)

Table 3.1. Hydroformylation of isoeugenol **1b** and eugenol **2b** by $[Rh(Cl)(COD)]_2$[a] [10]

Substrate	**1b**			**2b**		
Temperature	**3 b (α)**	**4 b (β)**	**5 b (γ)**	**3 b (α)**	**4 b (β)**	**5 b (γ)**
70	95	5	0	0	48	52
80	90	10	0	3	45	52
100	50	45	5	11	37	52
130	40	50	10	41	24	35

[a] Reaction conditions: 20 ppm $[Rh(Cl)(COD)]_2$, 600 bar *(*CO/H_2=1/1*)*

The asymmetric hydroformylation of *trans*-anethole **1a** and estragole **2a** was studied by Kollár[12] using $PtCl_2$(bdpp)+$SnCl_2$ (bdpp=(2,4-bis-diphenylphosphino) pentane) and $[Rh(nbd)Cl]_2$+L (nbd= norbornadiene, L: PPh_3 or DIOP) catalytic systems. The regioselectivities with the platinum system were low and were improved when rhodium systems were used. The enantioselectivity observed was low in the hydroformylation of *trans*-anethol **1a** and estragole **2a** with both systems. With $PtCl_2$(bdpp)+$SnCl_2$ and DIOP as the ligand, the regioselectivity to the branched aldehdyde **3a** was a 53% and with an enantioselectivity of 27.5%.

Dos Santos et al.[13] reported the hydroformylation of various allylbenzenes and propenylbenzenes with rhodium-based systems. They studied the electronic and steric effects of the ligands on the final distribution of the aldehydes and they found that, when monodentate ligands were used, the regioselectivity depended on the

basicity of the ligand. Thus, in the hydroformylation of eugenol **2b** with the $Rh/P(OPh)_3$ catalytic system, isomerisation to the internal olefin was observed, but when the reaction was driven in the presence of PPh_3 it was not. However, the use of more basic phosphines, such as $P(Cy)_3$ and $P(n\text{-}Bu)_3$, decreased the activity and the regioselectivity to the linear aldehyde. The activity of the less basic ligands is higher because the electron-withdrawing ligands decreased the back-donation to carbon monoxide and thus weakened the binding of the carbonyls. This favours the dissociation of carbon monoxide because it increases the reaction rate.[3] The effect of the basicity of the monodentate ligand on the regioselectivity could be explained by the basicity of the hydride. A basic phosphine leads to an increase in the nucleophilicty of the hydride. Therefore the interaction of the hydride with the terminal carbon (which bears a more positive fractional charge than the β-carbon) is favoured leading to amounts of branched aldehyde **4a**.[13]

Table 3.2. Hydroformylation of eugenol **2b** by $[Rh(COD)(OAc)]_2$/diphosphine system.[a][13]

Diphosphine[b]	Bite angle (º)	Time (h)	Conv.[c] (%)	4 (β)	5 (γ)	5/4 (γ/β)
dppe	85	24	55	62	38	0.6
dppp	91	24	74	69	31	0.5
dppb	98	24	99	34	66	1.9
BISBI	123	7	81	2	98	49.0
NAPHOS	120	7	90	2	98	49.0

[a] Reaction conditions: substrate (10.0 mmol), $[Rh(COD)(OAc)]_2$ (0.005 mmol), diphosphine (0.20 mmol), benzene (40 ml), 2Mpa *(*CO/H_2*=1/1)*, 80ºC. [b] dppe:1,2-bis(diphenylphosphino)ethane; dppp:1,3-bis(diphenylphosphino)propane; dppb: 1,4-bis(diphenylphosphino)butane, NAPHOS: 2,2'-bis[(diphenylphosphino)methyl]-1,1'-binaphthyl; BISBI: 2,2'-bis[(diphenylphosphino)methyl]-1,1'-biphenyl.[c] Determined by GC; hydrogenated substrate is detected in trace amounts.

When diphosphine-based systems (dppe, dppb, BISBI and NAPHOS) were used, the bite angle of the diphosphine and the regioselectivity were related (Table 3.2). Thus, it can be observed that ligands with big bite angles (BISBI and NAPHOS) afforded the linear aldehyde almost exclusively, while for ligands with small bite angles (dppe, dppp) the regioselectivity for the linear aldehyde decreased dramatically (<40%). This behaviour has been attributed to the coordination mode of these ligands. In the trigonal-bipyramidal rhodium-hydride species, the ligands

with small bite angles coordinate in apical-equatorial positions giving more basicity to the hydride (*trans* to a P ligand) than the diphosphines with major bite angle (around 120º) that coordinates in equatorial-equatorial mode. The greater basicity of the hydride makes it possible to obtain greater amounts of the branched aldehyde because the favoured interaction of the hydride with the terminal carbon. This effect has already been studied in the hydroformylation of 1-alkenes.[14] Although it is usually accepted that the influence of the bite angle on the regioselectivity is related to electronic effects, steric factors cannot be ignored. In spite of the numerous studies on the correlation between the bite angle and the regioselectivity, this relationship has yet to be clarified.[15-19]

It is known that the hydroformylation rate of propenylbenzes is lower than that of allylbenzenes. The rate determining step in the hydroformylation reaction is usually the coordination of the alkene, and because the internal alkenes are more hindered their coordination is more disfavoured than the terminal alkenes. With unmodified rhodium systems, the regioselectivities depend on temperature and pressure. At high temperature, isomerisation increases because β-elimination is favoured.[3] The increase in the partial pressure of carbon monoxide (CO/H_2=2/1) led to a slight decrease in the activity and did not affect the regioselectivity. As in the case of allylbenzenes, when diphosphine ligands were studied, the nature of the ligand was also seen to depend on the regioselectivity. Thus, NAPHOS with a larger bite angle provided regioselectivities over 90% to the α-aldehyde (**3**), while dppp showed regioselectivities around 70% in this isomer.

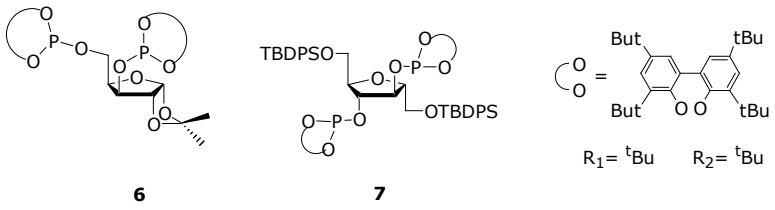

6 **7**

Figure 3.2. Diphosphite chiral ligands with a carbohydrate backbone

Chiral diphosphite ligands have been widely used in asymmetric hydroformylation and they have shown good activities, regioselectivities and enantioselectivities.[9]

However, they have not been used in the hydroformylation of allylbenzenes and propenylbenzenes. In this context, we decided to study the hydroformylation of *trans*-anethole **1a** and estragole **2a** with a rhodium catalyst modified with diphosphite chiral ligands **6**[20] and **7**[21] (Figure 3.2). Diphosphite ligand **6** has C_1-symmetry and three carbons between the phosphorus moieties, which forms an eight-member chelate ring. However, ligand **7** has C_2-symmetry with two carbons in the bridge between the phosphorus atoms, which forms a seven-member chelate ring. These ligands have been previously used in the rhodium-catalysed hydroformylation of styrene and have shown high regioselectivities to branched aldehyde and moderate enantioselectivities (95% and 40%(*S*), respectively, for ligand **6**, and 97% and 46%(*S*), respectively, for ligand **7**). It is to be expected that the higher substitution of the double bond in *trans*-anethole will produce a change in the regioselectivity and stereoselectivity of the process.

3.2 Results and discussion

3.2.1 Asymmetric hydroformylation of *trans*-anethol 1a (propenybenzene)

We studied the hydroformylation of *trans*-anethole **1a** with a rhodium-based system (Scheme 3.2). Unlike styrene, the model substrate in asymmetric hydroformylation, this substrate is an internal olefin. The *trans*-anethole **1a** needs more drastic conditions of reaction than the styrene, and two branched aldehydes **3a** and **4a** could be obtained with the formyl group in α- or β-positions, respectively. If **1a** isomerises to estragole **2a**, the hydroformylation of **2a** will lead to the formation of two aldehydes: the branched β-isomer **4a** and the linear aldehyde **5a**.

The *trans*-anethole was hydroformylated by an *in situ* formed catalyst, by adding diphosphite ligands **6** or **7** to a solution of the rhodium precursor ([Rh(acac)$(CO)_2$]). The results are summarised in Table 3.3.

The Rh/**6** catalytic system gives a higher conversion than when no ligand or PPh_3 were used, while the selectivity in isomer **3a** was lower than in the presence of PPh_3 and higher than in the absence of ligand (Table 3.3, entries 1, 2, 3).

Increasing the reaction temperature from 60 to 80 ºC (Table 3.3, entry 3 *vs*. 4) produces no significant changes in the isomerisation, a small increase in the conversion but a considerable decrease in the selectivity of **3a**. Similar behaviour was observed by Dos Santos et al.[13] in the hydroformylation of propenylbenzenes with an unmodified rhodium catalyst. This effect is general in hydroformylation and has been observed in other substrates. It is a consequence of the increase in the β-elimination rate when the temperature increases.[3]

Table 3.3. Hydroformylation of *trans*-anethole **1a** with the Rh/**6** and Rh/**7** catalytic system.[a]

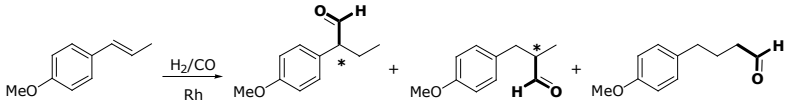

1a **3a** **4a** **5a**

Entry	Rh/L/S	L	T (ºC)	P CO (atm)	P H_2 (atm)	% conv ald.[b]	% isom.[b]	product distribution (%)[b]			%ee 3a (α)[b]	%ee 4a (β)[b]
								3a (α)	4a (β)	5a (γ)		
1	1/-/200	-	60	20	20	56	5	68	30	2	-	-
2	1/4/200	PPh_3	60	20	20	18	6	>99	<1	0	-	-
3	1/1/200	**6**	60	20	20	87	2	81	19	<1	0	0
4	1/1/444	**6**	80	20	20	92	4	66	31	3	0	0
5	1/2/200	**6**	60	20	20	84	<1	84	16	<1	0	0
6	1/1/200	**6**	60	10	20	70	2	68	30	2	0	0
7	1/1/200	**6**	60	20	40	96	<1	86	14	<1	8	15
8	1/1/200	**7**	60	20	20	79	8	65	33	3	0	0
9	1/2/200	**7**	60	20	20	39	5	75	22	3	0	0

[a] *trans*- anethole 1.8 mmol, [Rh(acac)$(CO)_2$] 0.009mmol, 10 ml. toluene, reaction time: 24h.

[b] % determined by G.C. hydrogenated substrate is detected in trace amounts.

The comparison of the results of the Rh/**6** system and the unmodified rhodium system, at the same conditions, revealed that only one equivalent of the ligand was required to maintain the active species coordinated to the ligand. When the

rhodium/diphosphite ratio was 1 or 2 (Table 3.3, entries 3 and 5) the regioselectivity to branched aldehyde **3a** was similar (81 and 84 %), while with unmodified rhodium system the regioselectivity is 68% to branched aldehyde **3a** (Table 3, entry 1).

A decrease in CO partial pressure led to a decrease in the activity and regioselectivity in α-isomer **3a** (Table 3.3, entry 6 *vs*. entry 3). At lower pressures, the CO insertion rate decreases and the β-elimination is favoured, which leads to a higher isomerization.[3]

The increase in the hydrogen partial pressure significantly affected the conversion but did not affect the regioselectivity of the reaction (Table 3, entry 7). This suggests that hydrogenolysis is the rate determining step.

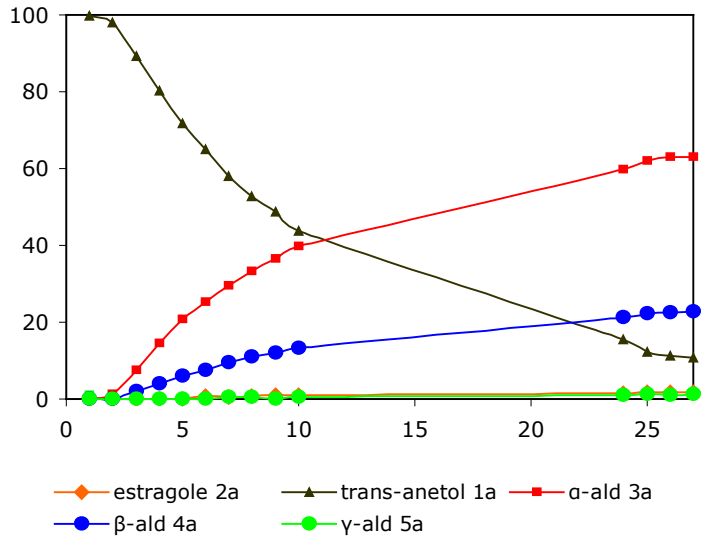

Figure 3.3. Product distribution versus reaction time diagram of the hydroformylation of trans-anethole **1a** with diphosphite **6**-rhodium catalyst (T: 60ºC, pressure 35 atm. CO/H_2 1:1)

Figure 3.3 shows the composition of the reaction mixture during the hydroformylation with the rhodium-diphosphite **6** system. After an induction period of one hour, the formation of aldehydes increases rapidly with a TOF= 17.2h^{-1}

(60ºC). This TOF is lower than for the same system in styrene hydroformylation TOF=53 h^{-1} (40ºC) P=25 bar.[22] The isomerisation is very low (<1%) , and the estragole formed is rapidly hydroformylated.

We also studied the hydroformylation of *trans*-anethole **1a** using the Rh/**7** catalytic system (Table 3.3, entries 8 and 9). In this case, unlike the rhodium-diphosphite ligand **6** system described above, two equivalents of the diphosphite ligand were necessary to maintain the active species coordinated to ligand. When the rhodium/ligand ratio is 1/1 (Table 3.3, entry 8) the regioselectivity is the same as for the unmodified rhodium system (Table 3.3, entry 1). In fact when the rhodium/ligand ratio is 1/2 (Table 3.3, entry 9), the regioselectivity to the α–isomer **3a** increases and the activity is lower than when it is 1/1. This indicates that intermediate rhodium-diphosphite ligand **7** species are less stable than with ligand **6** and require more equivalents of ligands to maintain these species with the ligand coordinated.

The results of the two diphosphite ligands, obtained in the same conditions, show that the catalyst based on ligand **6** is more selective in α–aldehyde **3a** than diphosphite **7** (Table 3.3, entry 5 *vs*.9). This could be attributed to the nature of ligand **6**, which forms an eight-member chelate ring. Ligand **7**, on the other hand, forms a seven-member chelate ring. This correlation has also been observed in the hydroformylation of **1a** with diphosphine ligands[13] and it has been explained above.

3.2.2 Asymmetric hydroformylation of estragol 2a (allylbenzene)

Next we carried out the asymmetric hydroformylation of estragole **2a**. The results are summarised in Table 3.4. The conditions are the same as the employed for the hydroformylation of *trans*-anethole **1a**.

In this case, at least four equivalents of ligand were required to prevent the formation of unmodified rhodium species, which are more active but less regioselective. When the rhodium/ligand ratio increases from Rh/L 1/1 to 1/4

(Table 3.4, entries 2-4) the regioselectivity to the β-aldehyde **4a** and γ-aldehyde **5a** increases.

Table 3.4. Hydroformylation of estragole **2a** with the catalytic system Rh/**6**.[a]

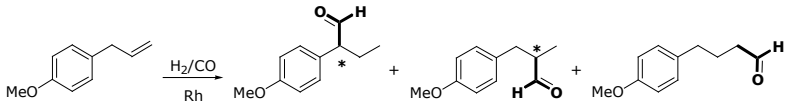

2a **3a** **4a** **5a**

Entry	Rh/L/S	L	T (ºC)	P CO (atm)	P H_2 (atm)	% conv ald.[b]	% isom.[b]	product distribution (%)[b]			%ee 3a (α)[b]	%ee 4a (β)[b]
								3a (α)	4a (β)	5a (γ)		
1	1/4/200	PPh_3	60	20	20	53	24	<1	50	50	-	-
2	1/1/200	**6**	60	20	20	83	6.6	45	31	24	0	0
3	1/2/200	**6**	60	20	20	94	1.5	25	36	39	0	0
4	1/4/200	**6**	60	20	20	86	6.1	0.0	47	53	0	0
5	1/2/1000	**6**	60	20	20	87	9.2	47	28	25	0	0

[a]estragole 1.8 mmol, [Rh(acac)$(CO)_2$] 0.009 mmol, 10 ml. toluene, reaction time: 24h.
[b] % determined by G.C. hydrogenated substrate is detected in trace amounts.

The comparison between the catalytic systems Rh/PPh_3 and Rh/**6** showed that with ligand PPh_3 the activity was lower and the regioselectivities were very similar (Table 3.4, entries 1 and 4). The lower activity of the PPh_3 ligand is attributed to the fact that the basicity of this ligand is greater than that of the diphosphite ligands. Greater basicity disfavours the dissociation of carbon monoxide and leads to a less active catalyst. The similar regioselectivities shown by these two different systems, Rh/PPh_3 and Rh/**6**, is unexpected if we consider the results reported in the literature. The Rh/PPh_3 system showed high regioselectivities for linear aldehydes in the hydroformylation of propenylbenzenes.[13] One explanation for this could be the excess of ligand used. Whereas we used a Rh/L ratio of 1/4 in the study mentioned above, the other results were obtained after using an Rh/L ratio of 1/20 and the regioselectivity to the linear aldehyde **5a** was nearly 70%. We also observed that when the rhodium/substrate ratio increased from 1:200 to 1:1000 (Table 3.4, entry

3 and 5), the regioselectivity to the γ–isomer **5a** was lower, indicating that the presence of more substrate led to more isomerisation.

3.3 Conclusions

The use of rhodium-diphosphite based systems in the hydroformylation of *trans*-anethole **1a** and estragole **2a** has not been reported before. In this study, rhodium-diphosphite system **6** was used in the hydroformylation of *trans*-anethole **1a** and led to high selectivities to aldehyde **3a** (as high as 86%) under mild conditions (60ºC, 40 bar). This is not so different from the diphosphine ligands used before which afforded up to 93% of aldehyde **3a** with BISBI ligand. We also observed that our diphosphite **6** based system is more active in this reaction than phosphine ligands in similar reaction conditions. When rhodium-diphosphite **7** was used in the *trans*-anethole **1a** hydroformylation, the regioselectivity was lower than when diphosphite **6** was used. We attributed this to the formation of a seven-seven member chelate ring of diphosphite **7** when it coordinates to the rhodium. On the other hand, in the hydroformylation of this substrate new chiral centers (in aldehydes **3a** and **4a**) are formed by the introduction of formyl groups. We also studied the asymmetric induction of the two diphosphite chiral ligands **6** and **7** in this reaction. We only observed low enantioselectivities in the case of diphosphite **6** in *trans*-anethole **1a** hydroformylation.

In the hydroformylation of estragole **2a**, we used rhodium-diphosphite **6** ligand. In this case, regioselectivities to the branched aldehyde **4a** were low (47% of **4a** and 53% of **5a**) when excess of ligand was added. We also investigated the enantioselectivity but we did not observe asymmetric induction in the conditions studied.

3.4 Experimental section

General methods

All syntheses were performed by standard Schlenk techniques under a nitrogen or argon atmosphere. Diphosphites **6** and **7** were prepared by previously described

methods.[20][23] Solvents were purified by standard procedures. All the other reagents were used as commercially available. Gas chromatographic analyses were run on a Hewlett-Packard HP 5890A instrument (split/splitless injector, J&W Scientific, HP-5, 25 m column, internal diameter 0.25 mm, film thickness 0.33 mm, carrier gas: 150 kPa Ar, F.I.D. detector) equipped with a Hewlett-Packard HP3396 series II integrator. Hydroformylation reactions were carried out in a Parr 450 ml. multiple reaction vessel autoclave. Enantiomeric excesses were measured after oxidation of the aldehydes to the corresponding carboxylic acids on a Hewlett-Packard HP 5890A gas chromatograph (split/splitless injector, J&W Scientific, Supelco β-DEX 110 (30 m. column, internal diameter 0.25 mm., carrier gas: 100 kPa He, F.I.D. detector).

Hydroformylation experiments

The catalytic precursors were prepared in a multiple reaction vessel autoclave in a glovebox, by adding the ligands to a solution of $[Rh(acac)(CO)_2]$ (0.009 mmol) in toluene (10 ml). Then the substrate was added. After pressurising to the desired pressure with syngas and heating the autoclave to the reaction temperature, the reaction mixture was stirred for 24 h. Then the autoclave was cooled to room temperature and depressurised. The reaction mixture was analysed by gas chromatography. The aldehydes obtained from the hydroformylation were oxidised to carboxylic acids to determine the enantiomeric excess.

3.5 References

[1] F. Agbossou, J. F. Carpentier, A. Mortreaux, *Chem. Rev.* **1995**, *95*, 2485.

[2] M. Beller, B. Cornils, C. D. Frohning, C. W. Kohlpaintner, *J. Mol. Catal. A: Chem.* **1995**, *104*, 17.

[3] P. W. N. M. van Leeuwen, C. Claver, *Rhodium Catalyzed Hydroformylation, Vol. 22*, Kluwer Academic, **2000**.

[4] J. L. F. Monteiro, C. O. Veloso, *Top. Catal.* **2004**, *27*, 169.

[5] C. M. Foca, H. J. V. Barros, E. N. dos Santos, E. V. Gusevskaya, J. C. Bayon, *New J. Chem.* **2003**, *27*, 533.

[6] I. Cipres, P. Kalck, D. C. Park, F. Serein-Spirau, *J. Mol. Catal.* **1991**, *66*, 399.

[7] L. Kollar, G. Bodi, *Chirality* **1995**, *7*, 121.

[8] A. J. Chalk, in *Flavors and Fragances: A World Perspective* (Ed.: B. M. Lawrence, Mookherjee, B. D. and Willis, B. J.), Elsevier Science, Amsterdam, **1988**.

[9] M. Dieguez, O. Pamies, C. Claver, *Tetrahedron: Asymmetry* **2004**, *15*, 2113.

[10] H. Siegel, W. Himmele, *Angew. Chem. Int. Ed.* **1980**, *19*, 178.

[11] P. Kalck, D. C. Park, F. Serein, *J. Mol. Catal.* **1986**, *36*, 349.

[12] L. Kollar, E. Farkas, J. Batiu, *J. Mol. Catal. A: Chem.* **1997**, *115*, 283.

[13] A. C. da Silva, K. C. B. de Oliveira, E. V. Gusevskaya, E. N. dos Santos, *J. Mol. Catal. A: Chem.* **2002**, *179*, 133.

[14] P. W. N. M. van Leeuwen, C. P. Casey, G. T. Whiteker, in *Chapter 4. Rhodium Catalyzed Hydroformylation, Vol. 22* (Ed.: P. W. N. M. van Leeuwen, Claver, C.), Kluwer Academic Press., Dordrecht, **2000**, p. 296.

[15] C. P. Casey, G. T. Whiteker, M. G. Melville, L. M. Petrovich, J. A. Gavney, D. R. Powell, *J. Am. Chem. Soc.* **1992**, *114*, 5535.

[16] M. Kranenburg, Y. E. M. Vanderburgt, P. C. J. Kamer, P. W. N. M. van Leeuwen, K. Goubitz, J. Fraanje, *Organometallics* **1995**, *14*, 3081.

[17] C. P. Casey, L. M. Petrovich, *J. Am. Chem. Soc.* **1995**, *117*, 6007.

[18] C. P. Casey, E. L. Paulsen, E. W. Beuttenmueller, B. R. Proft, L. M. Petrovich, B. A. Matter, D. R. Powell, *J. Am. Chem. Soc.* **1997**, *119*, 11817.

[19] P. Dierkes, P. W. N. M. van Leeuwen, *J. Chem. Soc., Dalton Trans.* **1999**, 1519.

[20] G. J. H. Buisman, M. E. Martin, E. J. Vos, A. Klootwijk, P. C. J. Kamer, P. W. N. M. Van Leeuwen, *Tetrahedron: Asymmetry* **1995**, *6*, 719.

[21] To be published. See Chapter 2.

[22] O. Pamies, G. Net, A. Ruiz, C. Claver, *Tetrahedron-Asymmetry* **2000**, *11*, 1097.

[23] To be published. See Chapter 2.

[24] G. J. H. Buisman, P. C. J. Kamer, P. W. N. M. van Leeuwen, *Tetrahedron: Asymmetry* **1993**, *4*, 1625.

[25] T. Jongsma, M. Fossen, G. Challa, P. W. N. M. van Leeuwen, *J. Mol. Catal.* **1993**, *83*, 17.

[26] M. Aghmiz, A. Aghmiz, Y. Diaz, A. Masdeu-Bulto, C. Claver, S. Castillon, *J. Org. Chem.* **2004**, *69*, 7502.

Chapter 4

Metal nanoparticles stabilized by chiral ligands with carbohydrate backbone

Abstract. *The synthesis of new metal nanoparticles is reported. Palladium, ruthenium and rhodium nanoparticles have been synthesised following the organometallic approach in the presence of chiral carbohydrate derivative ligands. The shape, size and agglomeration of the nanoparticles depend strongly on the metal precursor and the stabiliser used. We also report the use of rhodium nanoparticles in the styrene hydroformylation reaction that provides low conversions, high regioselectivities and enantioselectivities that are slightly higher than those obtained with an equivalent molecular system.*

4.1 Introduction

4.1.1 Background information on metal nanoparticles

Recently, interest in chemical species of nanometric size has been growing.[1-17] Inorganic particles in solution, or colloids, as Graham described in 1861 as very slow sedimentation and noncrystalline state[18], have been known for ages. The first rational synthesis of gold colloids was described by Faraday in 1857.[19] Since then, many methods to produce particles in solution have been reported.[1-17]

These species have attracted renewed interest because they have unique properties, somewhere between those of bulk and single-particle species.[10] For example, if a metal particle with bulk properties is reduced to the size of a few dozen or a few hundred atoms, the density of states in the valence band and the conductivity band, respectively, decreases to such an extent that the electronic properties change dramatically. In fact, the separation between the bands increases when the size of the material decreases.

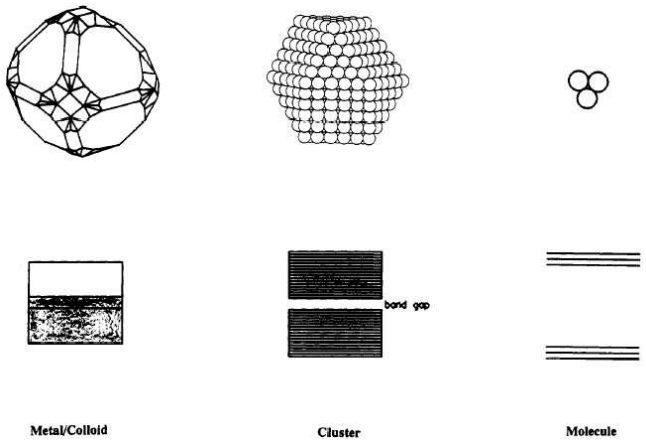

Figure 4.1. Illustration of the electronic states in (a) a metal particle with bulk properties and its typical band structure, (b) a large cluster of cubic close-packed atoms with a small band gap, and (c) a simple triatomic cluster with completely separated bonding and antibonding molecular orbitals[1]

Three metal atoms, for instance, form energetically well-defined bonding and antibonding molecular orbitals (Figure 4.1c). However, the main point of interest is to be seen in the transition from Figure 4.1a to Figure 4.1b or vice versa. If the number of electronic dimensions in a bulk system is reduced considerably a "quantum dot" (dimension zero) is formed, which corresponds to the nanoparticles or nanoclusters. In the nanoparticles, the quasi-continuous density of states is replaced by a discrete energy level.[1]

This renewed interest in the intermediate physical and chemical properties of these objects has evidenced that there is a need to control the particles' monodispersity, size, shape, organization and the nature of the chemical species on surface. *Modern* transition-metal nanoclusters differ from *classical* colloids in several important aspects. They are generally: a) smaller (1-10 nm in diameter) than *classical* colloids (>10 nm), b) isolable and redissolvable, unlike *classical* colloids c) soluble in organic solvents (*classical* colloid chemistry is typically aqueous) and d) have a well defined composition. In addition *modern* transition-metal nanoclusters have: e) narrower size dispersions, f) clean surfaces, g) reproducible synthesis and h) reproducible catalytic activities.[10, 15]

Full-shell ("magic number") metal clusters

Metal clusters which have a complete, regular outer geometry are known as full-shell, or "magic number", clusters (Figure 4.2). Full-shell clusters are constructed by successively packing layers, or shells, of metal atoms around a single metal atom. The total number of metal atoms, per υth shell is given by the equation: $10\ \upsilon^2+2$ ($\upsilon>0$).

Thus, the full-shell metal clusters contain a total number of atoms of 13 (1+12), 55 (13+42), 147 (55+92), 309, 561, etc.[20] Figure 4.2 shows the idealised representation of cubeoctahedron structure full-shell "magic number" clusters. Note that as the number of atoms increases, the percentage of surface atoms decreases.

	Number of shells	Atoms present before actual shell	Number of atoms in actual shell ($10\ v^2+2$)	Total number of atoms in cluster (magic numbers)	Relative amount of surface atoms
	1	1	12	13	92%
	2	13	42	55	76%
	3	55	92	147	63%
	4	147	162	309	52%
	5	309	252	561	45%

Figure 4.2. Idealised representation of the cubeoctahedron structure of full-shell "magic number" clusters. Each atom has the maximum number of nearest neighbours, which impart some degree of extra stability to full-shell clusters.[4]

Mechanistic studies of nanocluster formation and growth

Turkevich et al.[21-23] proposed the first reproducible standard protocols for preparing metal colloids (e.g. the reduction of $[AuCl_4]_2$ with sodium citrate). They also proposed the mechanism for the formation of nanoclusters that consist of nucleation, growth and agglomeration. This proposed mechanism, refined by more recent thermodynamic and kinetic results,[24-27] is presented in Scheme 4.1.

First, the metal salt is reduced to give zerovalent metal atoms, which can collide in solution with metal ions, metal atoms or clusters, to form an irreversible stable nuclei. The diameter of the nuclei depends on the strength of the metal-metal bonds and the difference between the redox potentials of the metal salt and the reducing agent applied.[12]

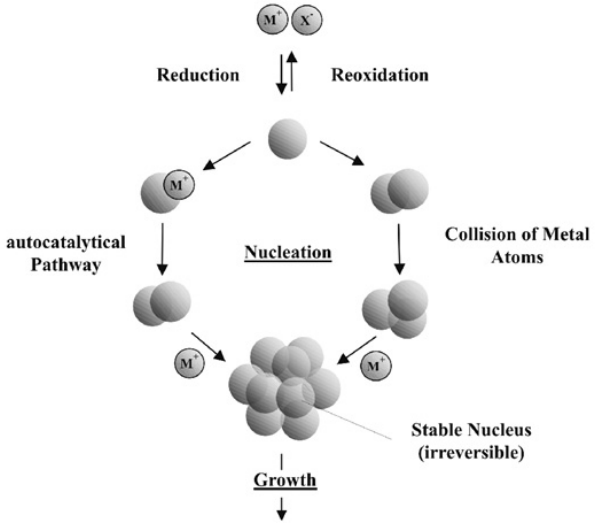

Scheme 4.1. Formation of nanostructured metal colloids by reduction of metal salts[12]

Finke et al. proposed a new mechanism for the formation of transition metal nanoclusters.[28-32] They used hydrogen as reducing agent to study iridium(0) clusters, and proposed a three-step mechanism consisting of a slow and continuous nucleation step, followed by a fast autocatalytic surface growth and then a bimolecular agglomeration step. The autocatalytic growth of the surface begins after the formation of $Ir(0)_n$ nuclei with a small size but critique (n). When the cluster reaches a size of the "magic number" gains a thermodynamic stability associated to a full-shell metal cluster. The nanocluster increases its stability because the surface atoms have the maximum metal-metal bonds. Recently, Finke et al.[33, 34] proposed a more general four-step mechanism involving double autocatalysis (Scheme 4.2). These studies were performed with platinum(0) clusters and hydrogen as reducing agent. The mechanism consists of: 1) a slow continuous nucleation, 2) fast autocatalytic surface growth, 3) bimolecular agglomeration and 4) an autocatalytic agglomeration step between small and large, bulk-metal-like particles.

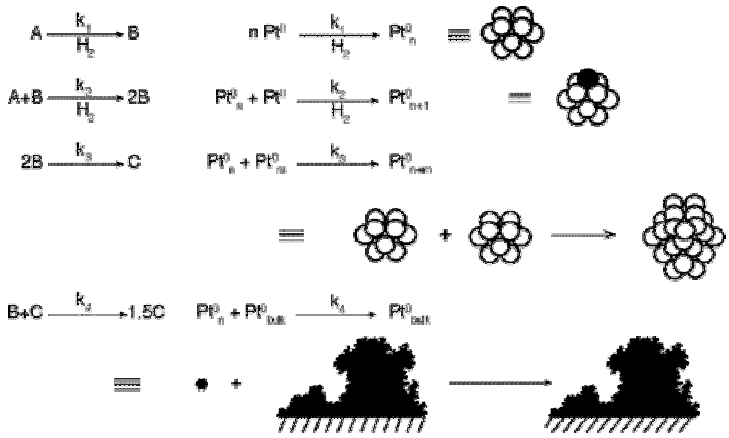

Scheme 4.2. Proposed four-step, double autocatalytic mechanism in graphic form[33]

4.1.2 Formation of transition-metal nanoparticles

4.1.2.1 Stabilisation of transition-metal nanoparticles

The metal particles are unstable with respect to the agglomeration to the bulk. The agglomeration is an undesired process because it leads to the loss of the properties associated with the colloidal state of the metal particles. The stability of these particles results from the equilibrium of the van der Waals attractive forces and the electrostatic repulsive forces. In the absence of repulsive forces opposed to van der Waals forces the colloidal metal particles will aggregate. Thus a stabilising agent is needed to provide stable nanoparticles. There are two general kinds of stabilisation procedures: 1) electrostatic stabilisation by the surface adsorbed anions and 2) steric stabilisation by the presence of bulky groups. The combination of these two kinds of stabilisation lead to 3) electrosteric stabilisation.[14]

Electrostatic stabilisation

The electrical double-layer around the particle consisting of adsorbed ions on the surface (dissolved halides, carboxylates or polyoxianions, generally aqueous) and their respective counterions (Figure 4.3) generates a Coulombic repulsion between

the particles. If the associated electrical potential is high enough, then the electrostatic repulsion prevents the aggregation. However, the electrostatic stabilisation can be strongly influenced by various factors, such as a thermal or ionic strength change, which can modify the electrical double-layer.[10, 14, 35-37]

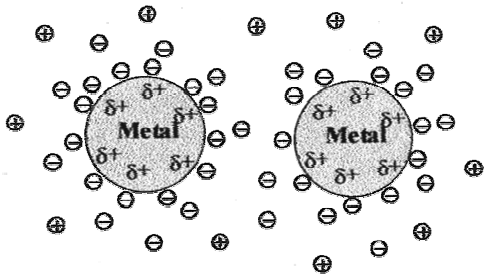

Figure 4.3. Schematic representation of electrostatic stabilisation of metal colloid particles[14]

Steric stabilisation

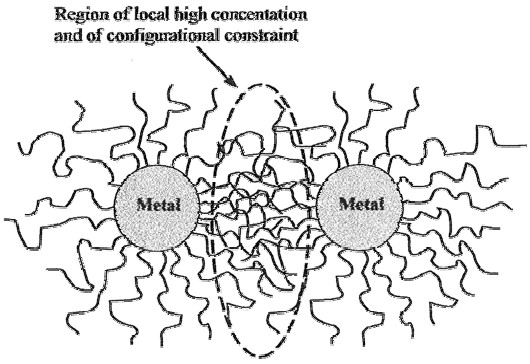

Figure 4.4. Schematic representation of steric stabilisation of metal colloid particles[14]

The adsorption of molecules, such polymers or oligomers, at the surface of the particle provides a protective layer. This layer prevents aggregation in two ways: 1) in the interparticle space (Figure 4.4), movement is restricted which decreases the entropy and, thus, increases the free energy; and 2) the concentration of these molecules in the interparticle space is high and the solvent re-establishes the

equilibrium by diluting the macromolecules and thus separating the particles. Steric stabilisation is used in both organic and aqueous media, while electrostatic stabilisation is mainly used in aqueous media. However, the properties of the macromolecules, length or composition, can have a strong influence on the stability of the particles.[14, 36, 38]

Electrosteric stabilisation

Ionic surfactants provide a stabilisation which combines electrostatic and steric stabilisation. These compounds have a polar group that can generate an electrostatic stabilisation, and a lypophilic side chain that can provide steric repulsion.[39-42] Compounds such as $(Bu_4N^+)/(P_2W_{15}Nb_3O_{62}^{-9})$, which combines bulky ammonium counteranions with a highly charged polyoxoanion, provide an efficient electrosterical stability toward the agglomeration (Figure 4.5).[10, 40]

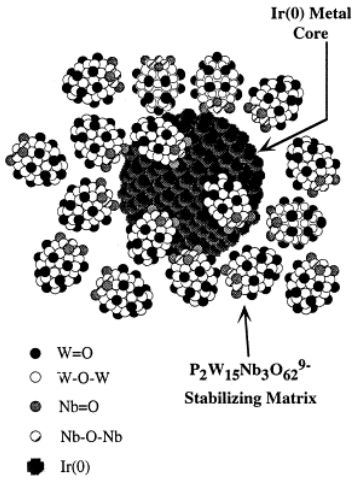

Figure 4.5. Idealized, roughly-to-scale representation of a $P_2W_{15}Nb_3O_{62}^{9-}$ polyoxoanion and Bu_4N^+ stabilized 20±3Å $Ir(0)\sim_{300}$ nanocluster, $[Ir(0)\sim_{300}(P_4W_{30}Nb_6O_{123}^{16-})\sim_{33}]$ $(Bu_4N)\sim_{300}Na\sim_{228}$. For the sake of clarity, only 17 of the polyoxoanions are shown, and the polyoxoanion is shown in its monomeric, $P_2W_{15}Nb_3O_{62}^{9-}$ form (and not as its Nb–O–Nb bridged, anhydride, $P_4W_{30}Nb_6O_{123}^{16-}$ form). The ~330 Bu_4N^+ and ~228 Na^+ cations have also been omitted, again for the sake of clarity.[39]

4.1.2.2 Synthesis of transition-metal nanoparticles

Dispersions of metallic nanoparticles can be obtained by two main methods: mechanic subdivision of metallic aggregates (physical method) or nucleation and growth of metallic atoms (chemical method) (Scheme 4.3). The chemical methods provides metal nanoparticles with greater control of shape, size, surface, composition and reproducibility than physical methods.

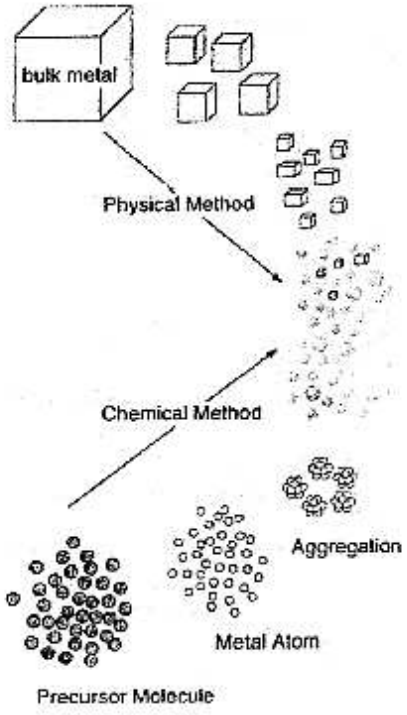

Scheme 4.3. Schematic illustration of preparative methods of metal nanoparticles[15]

The colloids synthesised by chemical methods can be dispersed in liquid media or immobilised on a solid support. The literature describes five main general methods for synthesizing transition-metal colloids (Scheme 4.4): 1) chemical reduction of metal salts, 2) thermal, photochemical or sonochemical decomposition, 3)

electrochemical reduction, 4) metal vapor synthesis and 5) ligand reduction and displacement from organometallic complexes.

The chemical reduction of metal salts

This is the most widely used method for synthesizing metal colloids. Several reducing agents have been used: for example molecular hydrogen or carbon monoxide, hydrides or salts such as sodium borohydride, or oxidable agents such as alcohols. The most commonly used stabilising agents are polymers such as PVP (polyvinylpyrrolidone), PVA (polyvinilyc alcohol) or PVE (polyvinylic ether) and dendrimers such as PAMAM (polyamidoamine).[14]

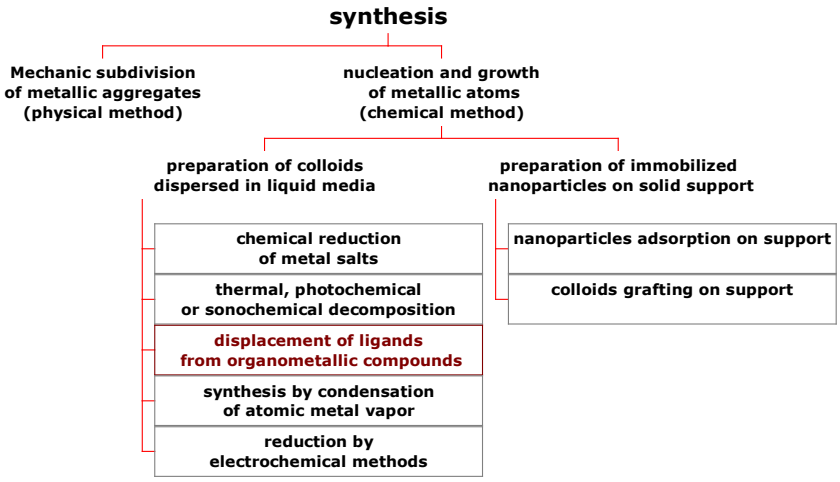

Scheme 4.4. Methods for synthesizing metal nanoparticles

Thermal, photochemical or sonochemical decomposition

This method consists in the decomposition of transition metal salts or organometallic complexes to their respective zerovalent element by thermolysis (by application of heat),[14, 43, 44] photolysis (by ionisation radiations or UV-Visible irradiation)[14, 26, 45-48] or sonochemical reduction (by application of ultrasounds).[49-51]

Metal vapour synthesis

Metal vapour synthesis consists of evaporating relatively volatile metals at reduced pressure and subsequently co-condensating them at low temperatures with the vapours of organic solvents. The colloidal particles nucleate and grow as the frozen mixture warms to melting.[14, 52, 53]

Electrochemical reduction

Recently Reetz et al.[14, 54-56] developed the electrochemical method which consists in the dissolution of the anode to form metal atoms. These are then reduced on the cathode to form particles after the aggregation, in the presence of ammonium salts which are both electrolyte and stabilising agent.

Ligand reduction and displacement from organometallics

The synthesis procedure consists of decomposing an organometallic precursor, mainly zerovalent organometallic complexes, in an organic solvent. This method makes it possible to synthesize nanoparticles with clean surface, because not reductive chemical agents are used. In other methods of synthesis, the impurities generated, such as salts or water, are in contact with the surface and are difficult to remove, so they modify the properties of the nanoparticles.

The rhodium precursor $[Rh_2(\mu\text{-}Cl)_2(CO)_4]$ was decomposed under hydrogen to form small rhodium nanoparticles (1.5-2.5 nm).[57] Finke et al.[39, 58] used iridium and rhodium organometallic complexes to synthesise, under hydrogen, stable and monodisperse nanoparticles. $Fe(CO)_5$ was used to synthesise nanoparticles in anisol in the presence of PPO (poly(dimethylphenylene oxide)) as stabilisers by sonolysis.[59]

Bradley and co-workers synthesised platinum nanoparticles that were stabilised with PVP by using molecular hydrogen to reduce $[Pt(dba)_2]$[60] and $[Pt_2(dba)_3]$.[61] (dba: dibenzylidene acetone) Palladium and platinum nanoparticles were also

synthesised from $[Pd(dba)_2]$ and $[Pt(dba)_2]$ using CO in the presence of cellulose acetate or cellulose nitrate in THF.[62, 63]

The organometallic approach to nanoparticles synthesis developed by Chaudret and co-workers[14, 16, 17] make it possible to synthesise metal nanoparticles in mild conditions and control the size, shape and surface environment. This procedure consists in the decomposition of an organometallic precursor able to decompose in mild conditions, generally using a reducing gas, hydrogen or carbon monoxide (Scheme 4.5). The ideal precursor is a zerovalent olefinic complex, which leads to the production of an alkane unable to form strong bonds with the growing metal surface in these conditions. Precursors of this type are $[Ni(C_8H_{12})]$[64] and $[Ru(C_8H_{10})(C_8H_{12})]$,[65, 66] which both decompose under hydrogen in mild conditions. Such metal precursors as $[Co(C_8H_{13})(C_8H_{12})]$[67, 68] or $[Rh(\eta^3\text{-}C_3H_5)_3]$,[69, 70] with allylic groups, which decompose easily in these mild conditions, have also been used. However, when olefinic precursors are not available other complexes have been used. $[Pd(dba)_2]$, $[Pt(dba)_2]$[59] or $[Rh(acac)(C_8H_{12})]$,[69, 71] for example, also decompose in mild conditions, but release potential ligands can perturb the surface.

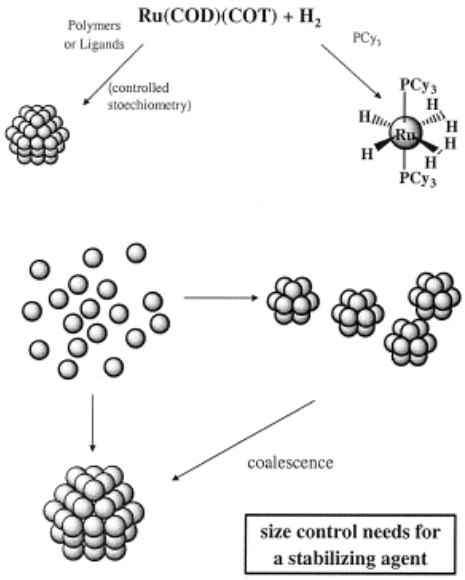

Scheme 4.5. Illustration of the general synthetic method for the synthesis of metal nanoparticles followed by Chaudret and co-workers[16]

The nanoparticles synthesised by the organometallic approach were stabilised with polymers, solvents or ligands. Polymers, such as PVP or cellulose acetate, were used as stabilisers in the synthesis of ruthenium,[62, 65, 72] platinum,[73] nickel,[64] cobalt[74] and bimetallic nanoparticles.[72, 74, 75] However, in this synthesis a polymer is not required to stabilize the particles. This method have been used to synthesise nanoparticles stabilised by solvents. [$Pt(dba)_2$] reacts with carbon monoxide in THF to give a colloid containing fcc (face-centered cubic) particles with a mean size of 1.2 nm and a narrow size distribution.[59] The synthesis of ruthenium nanoparticles from [$Ru(C_8H_{10})(C_8H_{12})$] with H_2 in THF, or non coordinating solvents, leads to the precipitation of ruthenium powder.[66, 76] However, when alcohols were used as solvent, colloidal solutions with ruthenium nanoparticles were obtained. In synthesis carried out in THF/MeOH mixtures, a correlation was found between the size of the particles obtained and the THF/MeOH ratio (Figure 4.6).[76]

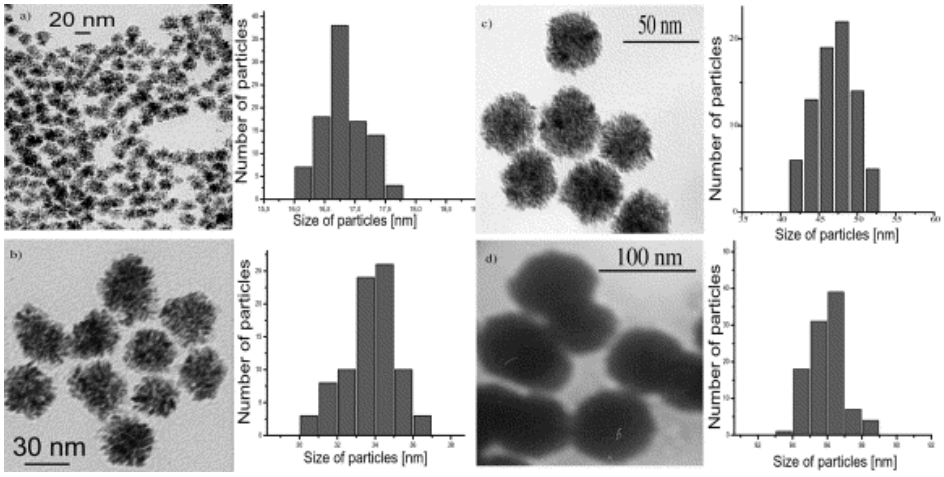

Figure 4.6. TEM Micrographs and histograms of the size of ruthenium nanoparticles synthesized in different MeOH/THF mixtures (a: MeOH/THF = 5/95; b: MeOH/THF = 25/75; c: MeOH/THF = 50/50; d: MeOH/THF = 90/10).[16, 76]

Ligand-protected nanoparticles can also be synthesised by this method, usually the synthesis are carried out in the presence of substoichiometric quantity of ligand. Monodentate ligands, such as PPh_3, thiophenols, long-chain thiols or amines, have been used to synthesise different metal nanoparticles.[16] Bidentate ligands have

also been used to stabilise metal nanoparticles by this method, for instance, a diphosphine ligand such as bis(diphenylphosphino)decane.[77] These makes it possible to use nanoparticles in asymmetric catalysis when the metal nanoparticles are stabilised with chiral ligands. Chiral oxazoline or amino alcohol ligands have been used to stabilize palladium and ruthenium nanoparticles.[78] In both cases, the ligands provide an excellent stabilisation of the particles, which can be handled like molecular species. Diphosphite chiral ligands were also used as stabilisers of palladium nanoparticles.[79] These palladium nanoparticles were active in the asymmetric allylic alkylation, providing excellent enantioselectivities and kinetic resolution of the substrate.

4.1.3 Methods for characterizing metal nanoparticles

The key goal of nanoparticles characterisation is to establish their size, structure and general composition. The techniques that are most often used to characterise nanoparticles are summarised in Figure 4.7. Nanoparticles can be characterised both by techniques that are common in the field of nanomaterials (TEM, SEM, XRD etc.) and by techniques derived from molecular chemistry (spectroscopies:IR, UV, NMR; magnetic measurements).

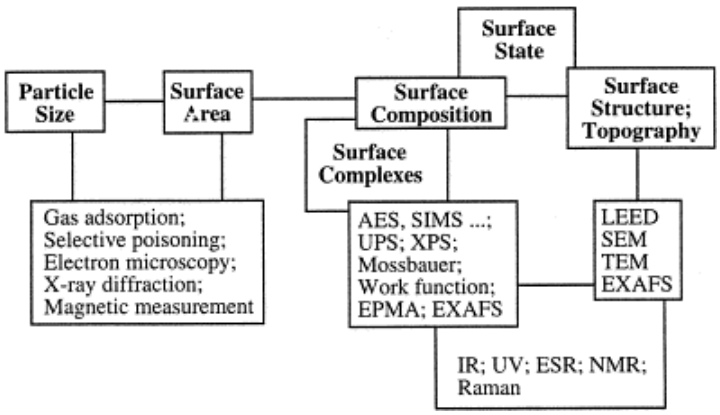

Figure 4.7. Common methods available for the characterisation of nanoparticles[10]

Transmission electron microscopy

Transmission electron microscopy (TEM) or high resolution TEM are the most widely used techniques for characterizing metal nanoparticles. These techniques provide direct visual information about size, shape, dispersity, structure and morphology. TEM has routine magnifications of ≥ 100000 with a resolution of ± 4 Å and HRTEM have a routine magnifications of ≥ 1000000 with a resolution of ± 2 Å. The disadvantages of these techniques are: 1) electron beam induces structural rearrangement, aggregation or decomposition of the nanoparticles, 2) three-dimensional samples must be interpreted from two-dimensional images and 3) the samples are dried and examined under high-vacuum condition, so no direct information of nanoparticles in solution is obtained.[10]

Infrared spectroscopy

Infrared spectroscopy (IR) has been used to study the surface of nanoparticles and the adsorption of molecules on the surface. Carbon monoxide has been widely used as a ligand because it easily adsorbs on metal surfaces and has a characteristic vibrational frequencies around 1800-2100 cm^{-1}.[3, 16, 17]

X-ray diffraction

X-ray diffraction is a non destructive technique which can identify the crystal phase for particles larger than 3 nm. When the nanoparticles are smaller, the acquisition of structural information is more difficult.[61] More sophisticated techniques such as EXAFS (Extended X-ray Absorption Fine Structure), to determine the atomic number, distance and coordination number of the atoms surrounding the element whose absorption edge is being examined, can also be employed.

Wide angle X-Ray Scattering

Wide angle X-Ray Scattering (WAXS) is an X-ray diffraction technique that is often used to determine the crystalline structure. This technique specifically analyses of Bragg Peaks scattered to wide angles, which (by Bragg's law) implies that they are

caused by small structures. The samples are analysed in solid state, sealed in 1mm Lindemann glass capillaries. The diffused corrected intensity is due to: 1) chemical composition of the nanoparticles, 2) structure of the nanoparticles and 3) interactions between the nanoparticles. The radial distribution function is obtained by the Fourier transform of the intensity, and facilitates interpretation. The WAXS provides a distribution of the metal-metal bonds inside a homogeneous assembly of nanoparticles, since well-defined RDF indicates well-crystallised nanoparticles. Using a model is then possible to have an access to the structure of the particle and to its coherence length, assuming that all particles adopt the same size an structure (Figure 4.8 shows an example of a Radial distribution function (RDF) obtained from WAXS analysis).

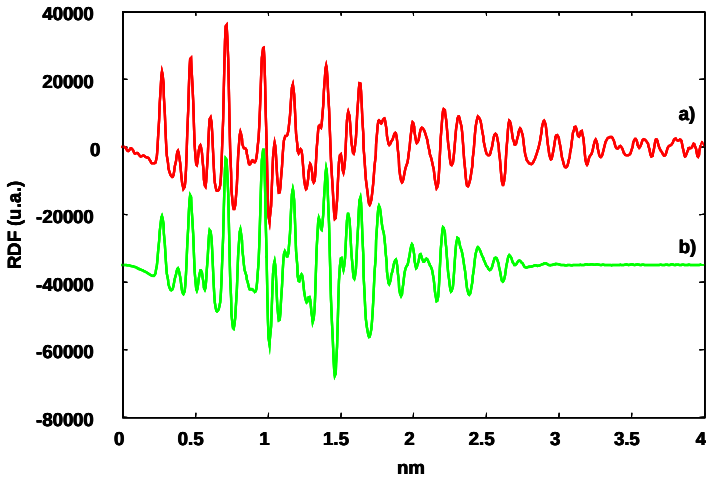

Figure 4.8. Radial distribution function (RDF) obtained from WAXS analysis. Comparison between a) experimental results of rhodium nanoparticles stabilised with diphosphite ligand and b) theoretical RDF of spherical rhodium nanoparticles with fcc structure and 3 nm of diameter.

Nuclear magnetic resonance

The NMR of metal nanoparticles can provide two sorts of information: about the ligands that surround the metal core and about the intra-core metallic atoms. NMR studies of the metal core are typically more difficult because the nuclear-spin lattice

relaxation time, and the nuclear resonance itself, are sensitive to any metallic property the cluster may exhibit. The NMR of ligand-protected nanoparticles is little developed, however, several recent studies demonstrate that it is possible to observe long chain ligands ligated to metal particles by ^{1}H and ^{13}CNMRspectroscopy .In this case, the nuclei close to the metal surface are not visible because of the slow tumbling of the metal particle in solution.[16, 65]

4.1.4 Catalytic applications of metal nanoparticles

Recently, interest in the catalytic properties of transition metal colloids has been growing. This is due to the very large specific surface of the metal nanoparticles, consequently a large number of metal atoms are available to the substrates.[14] Metal nanoparticles have been proven to be efficient and selective catalysts for reactions which are also catalysed by molecular complexes such as olefin hydrogenation or C-C coupling, as well as for reactions which are not or poorly catalysed by molecular species such as aromatic hydrocarbons hydrogenation.[10-12, 14, 15, 80, 81] Recently, metal nanoparticles have been applied to enantioselective catalyst for reactions such as hydrogenation[82-87] or allylic alkylation.[79]

4.1.4.1 Hydrogenation catalysed by metal nanoparticles

Hydrogenation of olefins (terminal, internal or cyclic) and benzene derivatives have been widely studied with transition metal nanoparticles as catalysts. In this kind of reactions, transition metal nanoparticles showed good activities and selectivities.[14, 15]

Cinnamaldehyde was hydrogenated to cinnamic alcohol by Liu et al. High selectivities to the alcohol were obtained using several metal and bimetallic colloids such as Pt, Pt/Co in PVP or Pt immobilised in supports such as polystyrene or alumina.[88] Chloronitrobenzenes (*ortho*-, *para*- or *meta*-) were successfully hydrogenated to the corresponding chloroanilines with Pd/PVP, Pt/PVP and Ru/PVP systems.[89, 90] The hydrogenation of other substrates such as 1,5-cyclooctadiene,[91] citronelal[92] or ketones[93] have also been studied with colloidal systems.

Nevertheless, the most studied reaction is the hydrogenation of arene derivatives. Arene hydrogenation is an important industrial catalytic transformation. Generally heterogeneous catalysts have been used in this reaction but homogeneous systems have also been reported.[10, 14] However, in recent years the application of colloidal systems in arene hydrogenation has increased dramatically. Rhodium is the most frequently used metal, followed by ruthenium. They both showed high activities in heterogeneous catalysis. The most commonly used precursors are [Rh(μ-Cl)(diene)]$_2$, $RhCl_3.H_2O$ and $RuCl_3.H_2O$ and the most commonly used stabilisers are tetraalkylammonium salts. Generally, the catalysis is biphasic (aqueous/organic) and takes place in mild reaction conditions (room temperature and 1 atm H_2).[15] The hydrogenation of arenes with two or more substituents on the benzene ring produces *cis* or *trans* diastereoisomers, and the metal nanoparticles favour the thermodynamically less favourable *cis* diastereoisomer. Enantioselective hydrogenation is possible when multisubstituted arenes are hydrogenated.

Finke et al.[94] reported the use of Rh(0) nanoparticles in arene hydrogenation. The nanoparticles were formed *in situ* by reducing $[Bu_4N]_5Na_3[(1,5\text{-}COD)Rh.P_2W_{15}Nb_3O_{62}]$ with H_2, and they showed high activities and selectivities in anisole hydrogenation.

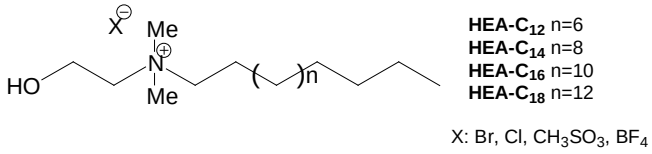

Figure 4.9. N-alkyl-N-(2-hydroxyethyl)ammonium salts, HEA-Cn-X[95, 96]

Roucoux and co-workers have also reported the hydrogenation of arenes with metal nanoparticles. Rhodium nanoparticles were synthesised by reducing $RhCl_3.3H_2O$ with sodium borohydride and stabilised with various surfactants, (N-alkyl$_n$-N-(2-hydroxyethyl)ammonium salts HEA-Cn-X (Figure 4.9), and were successfully used in biphasic arene hydrogenation. The catalytic systems were efficient under mild conditions (room temperature and 1 atm H_2 pressure). The aqueous phase which contains the protected rhodium(0) colloids were reused without a significant loss of

activity.[41, 95, 97] These authors also observed that the nature of the surfactant counteranion has a strong influence on the catalyst results, the best results were obtained when chloride was used as counteranion.[96] Various heterocyclic aromatic compounds were also hydrogenated with rhodium nanoparticles stabilised with this kind of surfactants.[98] Iridium nanoparticles synthesised from $IrCl_3$ by the same method in the presence of HEA-16-Cl showed high activities and selectivities in arene hydrogenation.[99]

Dupont et al. synthesised stable transition-metal nanoparticles of the type $[M^0]_n$ (M: Ir[100, 101], Rh[100, 101], Pt[100] and Ru[101, 102]) by reducing the corresponding metal precursors dissolved in 1–n-butyl-3-methylimidazolium (BMI) hexafluorophosphate ionic liquid (Figure 4.10) by molecular hydrogen. The isolated $[M^0]_n$ nanoparticles were redispersed in the ionic liquid or in various solvents or they were used in solventless conditions for the liquid-liquid biphasic, homogeneous or heterogeneous hydrogenation of arenes under mild reaction conditions (75ºC and 4 atm H_2). The recovered metal nanoparticles were reused several times without any significant loss in catalytic activity.

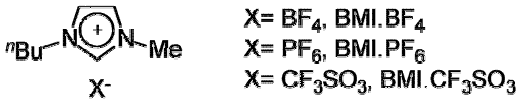

Figure 4.10. Imidazolium room temperature ionic liquids[103]

4.1.4.2 C-C coupling reactions catalysed by metal nanoparticles

C-C coupling reactions, such as Heck or Suzuki couplings, have been catalysed by metal nanoparticles.[14] The most common metal used is palladium. Reetz and co-workers[104] described the use of palladium nanoparticles, synthesised by the electrochemical process (see above), in the Heck coupling reaction. The same authors also used Pd and Pd/Ni nanoparticles in Suzuki coupling reactions, and the bimetallic colloid showed the best activities.[105] Titanium[106] and nickel[107] nanoparticles were also synthesised by the same method and successfully applied to olefin-forming McMurry-type coupling of aldehydes and ketones, and to the 3+2 cycloaddition reactions, respectively.

El-Sayed and co-workers have used palladium[108-113] and platinum[114] nanoparticles, stabilised with various stabilisers such as dendrimers (PAMAM) or polymers (PVP and others), in Suzuki coupling reactions. They have investigated how the characteristics of the nanoparticles (size, shape or stability) affect catalytic activity.[115]

Dupont and co-workers[116] have also used palladium nanoparticles dispersed in ionic liquid BMI.PF_6 (Figure 4.10, see above) to investigate the Heck reaction. These Pd(0) nanoparticles with 2 nm diameter were efficient catalyst precursors for coupling of aryl halides with *n*-butylacrylate. *In situ* TEM analysis of the ionic liquid catalytic solution after the catalytic reaction showed the formation of larger nanoparticles (6 nm). It was also observed significant metal leaching (up 34%) from the ionic phase to the organic phase at low substrate conversions and drops to 5-8% leaching at higher conversions. These results strongly suggest that the Pd(0) nanoparticles serve as a reservoir of "homogeneous" catalytic active species.

4.1.4.3 Enantioselective reactions catalysed by metal nanoparticles

Metal nanoparticles have been proven to be efficient and selective catalysts for reactions such as olefin hydrogenation or C-C coupling reactions. However, despite impressive progress in asymmetric catalysis, the use of metal nanoparticles as enantioselective catalysts is not very widespread. The first example was reported by Lemaire and co-workers.[117] Rhodium nanoparticles stabilised with a chiral amine were used in the hydrogenation of disubstituted arenes but the enantioselectivities were poor.

The most studied enantioselective reaction catalysed by metal colloids is the hydrogenation of ethyl piruvate. Bönnemann[83, 85] studied this reaction with platinum colloids stabilised with dihydrocinchonidine salt. They obtained enantioselectivities of 75-80% in (*R*)-ethyl lactate. Platinum nanoparticles stabilised by PVP and modified with cinchonidine were also tested in this reaction, and showed enantioselectivities of 95-98% (*R*).[82, 84, 118] Recently, Roucoux and co-workers,[119] described the biphasic version of this reaction. The aqueous phase containing the Pt(0) nanocatalysts was used for further runs with a total

conservation of activity and enantioselectivity for (*R*)-ethyl lactate up to 55%. Similar systems based on rhodium[120] and iridium[121] nanoparticles, stabilised with PVP and modified with cinchonidine, have also been described, the enantioselectivities obtained were lower than with palladium- and platinum- based systems.

Recently, palladium nanoparticles synthesised by the organometallic approach[16, 17] have been applied to the asymmetric allylic alkylation of rac-3-acetoxy-1,3-diphenyl-1-propene with dimethyl malonate (Scheme 4.6).[79]

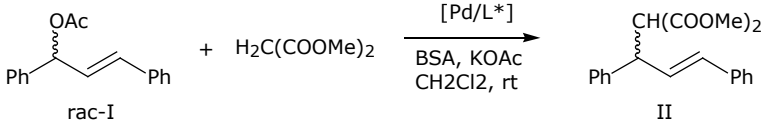

Scheme 4.6. Asymmetric allylic alkylation of rac-3-acetoxy-1,3-diphenyl-1-propene with dimethyl malonate

The palladium nanoparticles, **Colloid.1**, were synthesised by decomposing $[Pd_2(dba)_3]$ by H_2 (3 bar) at room temperature in THF in the presence of diphosphite ligand **1** (Figure 4.11). These palladium nanoparticles behaved as efficient kinetic resolution catalyst giving >95% of enantiomeric excess in II and 89% of enantiomeric excess in the remaining substrate I at 56% of conversion (Scheme 4.6).

One of the problematic point of the application of metal nanoparticles in catalysis is to know the true nature of the catalysis, colloidal or molecular. In this study the authors observed that the reactions using the two different catalytic systems, colloidal system and the respective molecular system, displayed some clear differences, the most notable ones being the absence of completion of the reaction associated to a very high kinetic resolution when using **Coll.1** as a catalyst. In contrast, quasi total conversion but no kinetic resolution of the substrate was observed using the respective molecular system as the catalyst. The authors carried out several experiments, such as kinetic studies, comparison of the colloidal system with diluted molecular systems or poisoning test, among others, to rule out

the possibility of the formation from the particles of a small amount of an active molecular catalyst. With this studies they demonstrated that two different mechanisms operate according to the nature of the catalyst.

Objective

With these previous results we decided to synthesise new palladium nanoparticles from the same palladium precursor, $[Pd_2(dba)_3]$, stabilised with diphosphites **2** and **3**, and with phosphine-phosphite ligand **4** (Figure 4.11), in order to compare the effect of the ligand on the stabilisation and the characteristics of the nanoparticles. We also extended this method to synthesise other metal nanoparticles, ruthenium and rhodium, stabilised with carbohydrate derivative ligands (Figure 4.11) in order to compare the effect of the metal precursor and the stabiliser used, on the nanoparticles synthesised. Palladium nanoparticles synthesised in the presence of chiral ligands **1**, **2**, **3** and **4** were applied in the palladium-catalysed allylic alkylation as catalyst. Rhodium colloids synthesised in the presence of chiral ligands **1** and **3** were used as catalyst in the hydroformylation of styrene.

4.2 Results and discussion

The synthesis of nanoparticles through the organometallic approach was developed by Chaudret and co-workers.[16, 17] It makes it possible to synthesize nanoparticles of uniform small size (1–3 nm) and clean surface, and it consists in the decomposition of an organometallic precursor, preferably a zerovalent olefinic precursor, able to decompose in mild conditions, generally with a reducing gas, such as hydrogen or carbon monoxide, in the presence polymers or ligands in sub-estequiometric amounts.

Among the different ligands used to stabilise nanoparticles, such as oxazolines,[78] phosphines,[77] etc., [16, 17] diphosphite ligands (Figure 4.11) are interesting for stabilising metal nanoparticles because they have phosphorus and oxygen atoms, that can interact, strongly and weakly, respectively, with the surface. As has been mentioned above, palladium nanoparticles synthesised by the organometallic approach and stabilised with chiral xylofuranoside diphosphite **1** (Figure 4.11) have

been previously described.[79] In order to study how of the skeleton and the phosphorus moieties of the ligands influenced the stabilisation and characterisation of the nanoparticles, we have synthesised a new series of palladium nanoparticles stabilised with diphosphite ligands **2** and **3** and with phosphine-phosphite ligand **4** (Figure 4.11). Ruthenium nanoparticles were prepared from $[Ru(C_8H_{10})(C_8H_{12})]$ and rhodium nanoparticles were synthesised from two different rhodium precursor, $[Rh(\eta^3\text{-}C_3H_5)_3]$ and $[Rh(\mu\text{-}OMe)(COD)]_2$ in the presence of diphosphite ligands **1** and **3**. Phosphorus chiral ligands derived from carbohydrates **1**[122], **2**[123], **3**[124] and **4**[125], were prepared by methods described previously.

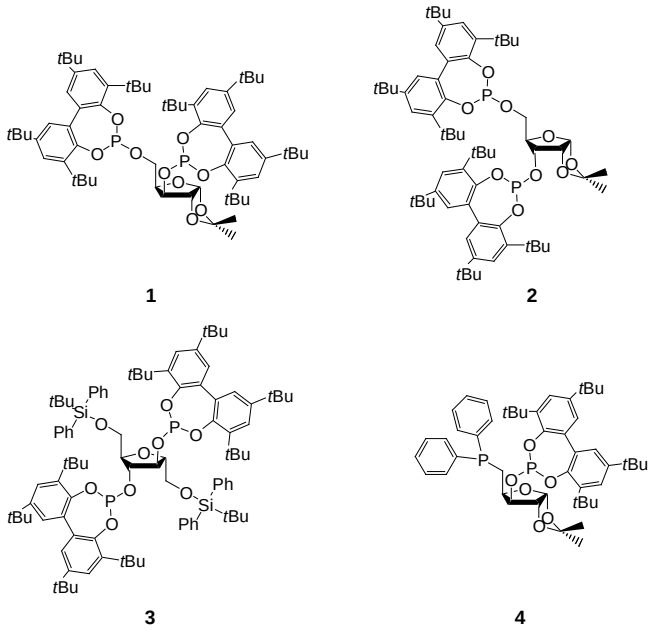

Figure 4.11. Phosphorus chiral ligands derived from carbohydrates

4.2.1 Synthesis of palladium nanoparticles from the precursor $[Pd_2(dba)_3]$

Palladium nanoparticles stabilised with diphosphite ligand **1**, **Colloid.1**, have been previously described.[79] These nanoparticles were synthesised by the organometallic approach from the precursor $[Pd_2(dba)_3]$ following the reaction presented in Scheme 4.7 with a Pd/L ratio of 1/0.2. Transmission electron microscopy revealed the presence of small, elongated, but in some cases

agglomerated, particles with a mean size of *ca*. 4 nm (Figure 4.12), while Wide-angle X-ray scattering analyses showed the fcc structure of bulk palladium.

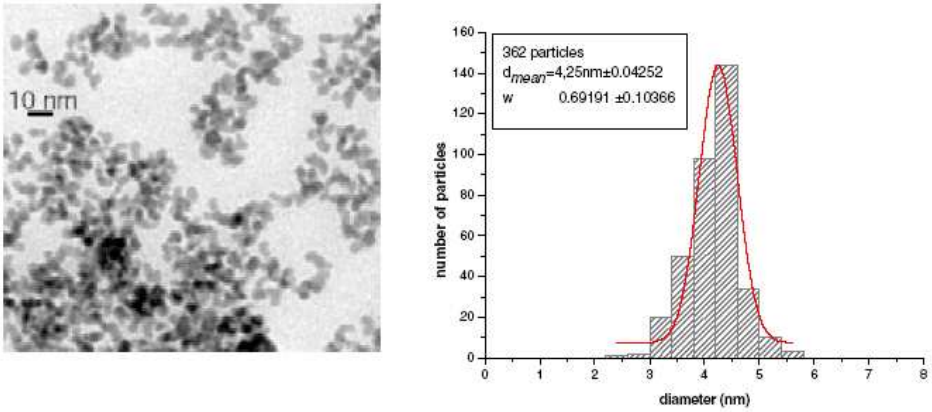

Figure 4.12. Transmission electron micrograph of **Coll.1** and size histogram built from ca. 360 nanoparticles

The synthesis of palladium nanoparticles from the precursor $[Pd_2(dba)_3]$ was carried out following the reaction presented in Scheme 4.7. Diphosphite ligands **2** and **3** and phosphine-phosphite ligand **4** have been used as stabilisers.

$$[Pd_2(dba)_3] \xrightarrow[0.2\ L,\ THF]{3\ bar\ H_2} [Pd_x(dba)_y(THF)_zL_w] + dba\text{-}H_2$$

Coll.1 L: **1** **Coll.2** L: **2**
Coll.3 L: **3** **Coll.4** L: **4**

Scheme 4.7. Synthesis of palladium nanoparticles from $[Pd_2(dba)_3]$ in the presence of chiral ligands **2**, **3** and **4**

The initial THF solution of the palladium precursor in the presence of the ligand was purple red. After pressurization at room temperature under 3 bars of hydrogen for 30 minutes, the solution became black in a few minutes. The nanoparticles were isolated by precipitation with pentane. The nanoparticles synthesised were analysed by TEM (Transmission electron microscopy), WAXS (Wide-angle X-ray scattering) and elemental analysis. The samples for microscopy analysis were prepared from a

drop of the colloidal solution, which was deposited under argon on a holey carbon covered copper grid. The samples for WAXS analysis were prepared from the isolated nanoparticles, which were sealed in 1mm Lindemann glass capillaries.

First, we synthesised palladium nanoparticles with diphosphite chiral ligand **2** as stabiliser, **Colloid.2**. The diphosphite **2**, with C_1-symmetry differs of the previously used diphosphite **1** only in the configuration of C-3 of the sugar backbone (Figure 4.11). Figure 4.13 shows the nanoparticles synthesised with a palladium/diphosphite ratio of 1/0.2, **Colloid.2**. The elemental analysis of the black isolated nanoparticles of **Colloid.2** was 72.97 %Pd, 0.37%P, 13.99%C, 0.38%H, which displays a Pd/P ratio of 57/1. We observed nanoparticles similar to those described for **Colloid.1**, stabilised with diphosphite **1**. The TEM micrograph revealed small nanoparticles with a mean diameter *ca*. 4 nm, which are in some cases agglomerated. The WAXS analyses for **Colloid.2** showed the fcc structure of bulk palladium with a coherence length between 3.5 and 4 nm, which is in good accordance with TEM observations.

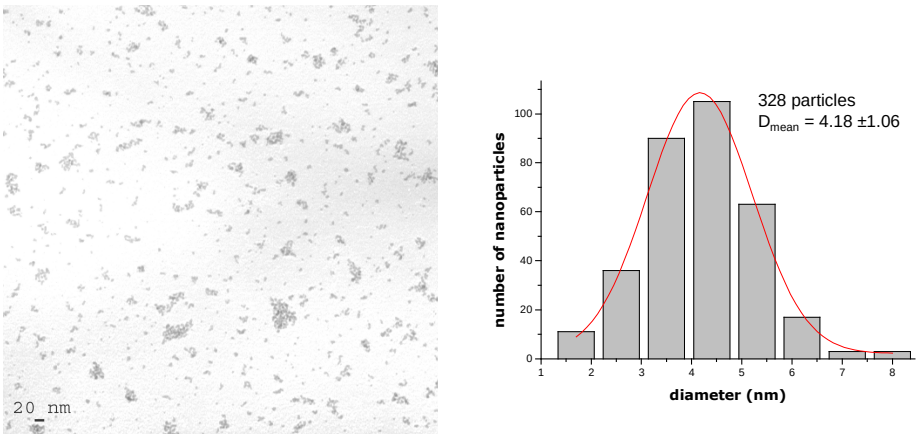

Figure 4.13. Transmission electron micrograph of **Coll.2** and size histogram built from ca. 330 nanoparticles

We also prepared palladium nanoparticles, namely **Colloid.3**, stabilised with diphosphite ligand **3**, which is a new diphosphite ligand with C_2-symmetry previously described in Chapter 2. The elemental analysis of the black isolated

nanoparticles of **Colloid.3** was 68.77 %Pd, 0.33%P, 2.93%Si, 8.82%C, 0.65%H, which displays a Pd/P ratio of 60/1, similar to that in **Colloid.2**. The TEM micrographs, Figure 4.14, show irregularly shaped nanoparticles with a mean diameter *ca*. 6 nm. WAXS analysis revealed fcc structure of bulk palladium with a coherence length of at least 4 nm, which is smaller than the mean diameter determined by TEM. This can be attributed to the nanoparticles' lack of crystallinity. TEM observations indicate that the nanoparticles are irregularly shaped that can be attributed to a coalescence of the nanoparticles that is a lack of stabilising effect.

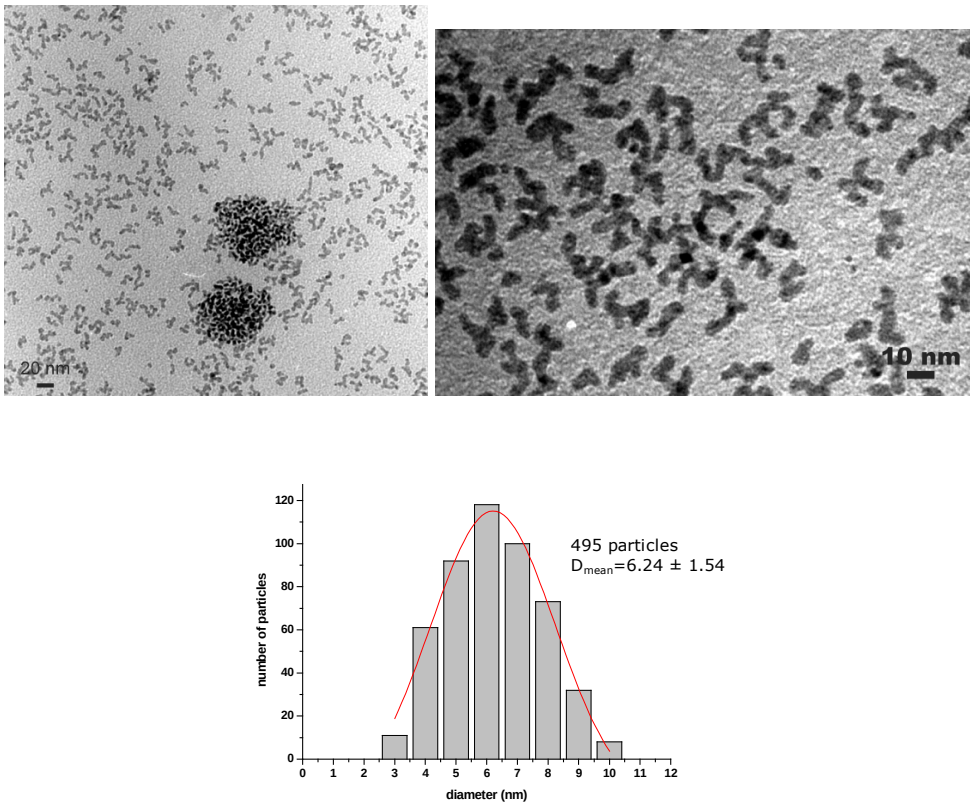

Figure 4.14. Transmission electron micrographs of **Coll.3** and size histogram built from *ca*. 500 nanoparticles

Palladium nanoparticles stabilised with phosphine-phosphite ligand **4**, **Colloid.4**, which has the same carbohydrate backbone than the diphosphite ligand **1**, were synthesised by following the general procedure. The elemental analysis of the black

isolated nanoparticles of **Colloid.4** was 71.59%Pd, 1.97%P, 15.94%C, 1.28%H, which displays a Pd/P ratio of 11/1, much higher than the observed in the colloids **Coll.2** and **Coll.3**.

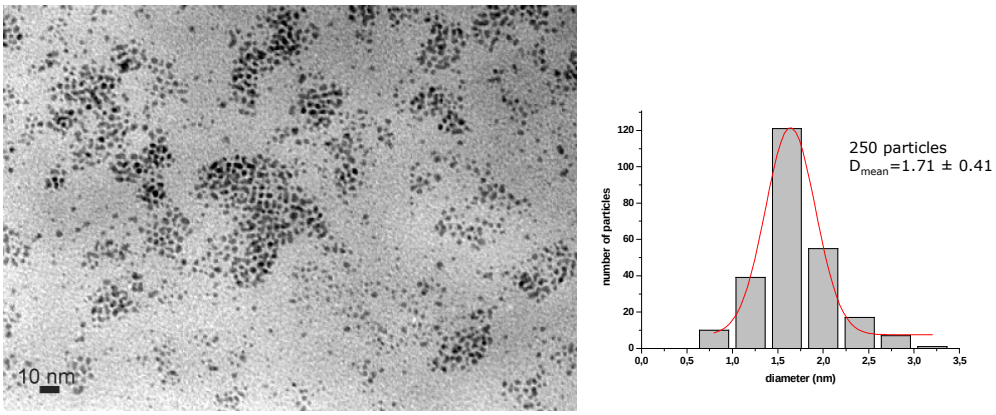

Figure 4.15. Transmission electron micrographs of **Coll.4** and size histogram built from *ca*. 250 nanoparticles

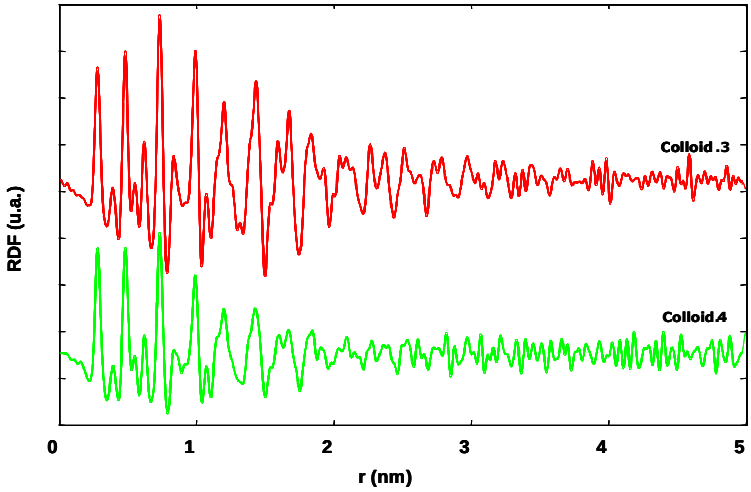

Figure 4.16. RDF of **Coll.3** and **Coll.4** obtained from WAXS analysis

The use of phosphine-phosphite ligand **4** to stabilise palladium nanoparticles, **Colloid.4**, led to the formation of different nanoparticles from those obtained with diphosphite ligands. Thus, the TEM analysis revealed well-dispersed, small,

spherical nanoparticles with a mean diameter, *ca*. 2 nm (Figure 4.15), in contrast to the irregularly shaped palladium nanoparticles stabilised with diphosphite ligands **1** to **3** with a mean diameter of *ca.* 4 nm. The spherical shape may indicate better stabilisation and in addition, the size histogram is very narrow. The WAXS analysis revealed fcc structure of the bulk palladium with a coherence length of *ca*. 2.5-3 nm, which means that the nanoparticles were smaller.

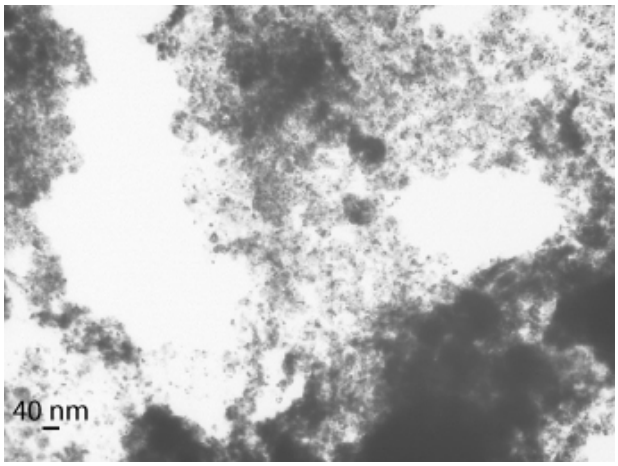

Figure 4.17. Transmission electron micrograph of **Coll.5**

In order to improve the palladium nanoparticles synthesised with ligand **4**, **Colloid.4**, we synthesised new nanoparticles modifying the following reaction conditions: a) at 60ºC, **Colloid.5**, and b) increasing the palladium/ligand ratio to 1/0.4, **Colloid.6**. **Colloid.5** was analysed by TEM, WAXS analysis and elemental analysis, but **Colloid.6** was only analysed by TEM because the nanoparticles did not precipitate. The elemental analysis of the black isolated nanoparticles of **Colloid.5** was 60.67 %Pd, 3.55%P; which displays a Pd/P ratio of 5/1. In both cases the TEM micrographs (Figure 4.17 and 4.19) revealed more agglomerated nanoparticles than when *standard* conditions (room temperature, palladium/ligand ratio 1/0.2) were used, and no isolated nanoparticles were observed.

The WAXS analysis of **Colloid.5** revealed the fcc structure of the bulk palladium with a coherence length of *ca*. 3.5-4 nm. However, the nanoparticles were not

crystallised so well, since the RDF is not well-defined, as for **Colloid.4**, (see Figure 4.18). The TEM analysis showed much more agglomeration than in the case of palladium nanoparticles **Colloid.4**.

We can conclude that palladium nanoparticles stabilised with phosphorus chiral ligands have been successfully synthesised. These colloids are composed of small nanoparticles which display the fcc structure of bulk palladium with a mean diameter of 2-6 nm. TEM analysis of palladium nanoparticles stabilised with diphosphite **1** to **3** revealed small, irregularly-shaped sometimes agglomerated particles with a mean size of *ca*. 4 nm for colloids **Coll.1** and **Coll.2**, and *ca*. 6 nm for colloid **Coll.3**. Ligand **4**, with a phosphine function, made it possible to obtain smaller palladium nanoparticles. **Colloid.4** presents particles with a mean diameter of *ca*. 2 nm, with more regular shape than when diphosphite ligands were used as stabilisers. The palladium nanoparticles **Coll.4** showed more presence of ligand (Pd/P ratio of 11/1 instead of the ratio showed by diphosphite stabilised palladium nanoparticles, 57/1 for **Coll.2** and 60/1 for **Coll.3**, see above) indicating that the ligand interact stronger with the surface than diphosphite ligands.

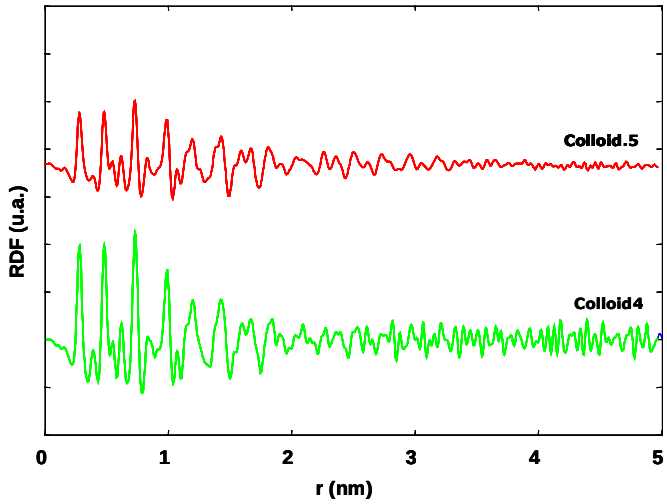

Figure 4.18. RDF of **Coll.4** and **Coll.5** obtained from WAXS analysis

We also studied the effect of the temperature and the palladium/ligand ratio on the nanoparticles stabilised with phosphine-phosphite ligand **4**. We observed that an

increase in the temperature or an increase in the quantity of ligand did not improve the results and led to more agglomeration and no well crystallisation.

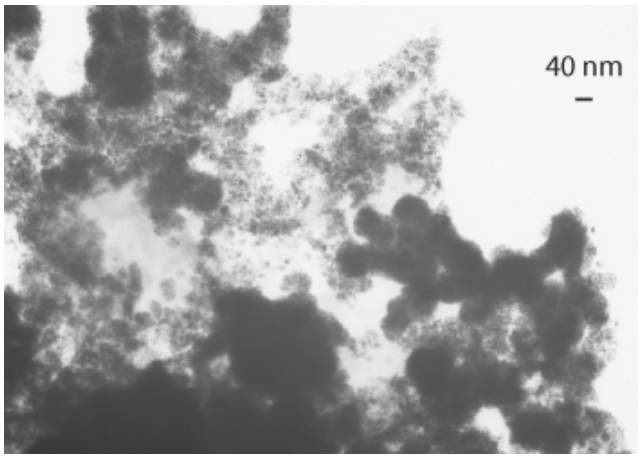

Figure 4.19. Transmission electron micrograph of **Coll.6**

4.2.2 Synthesis of ruthenium nanoparticles from the precursor [Ru(C_8H_{10})(C_8H_{12})]

Ruthenium nanoparticles were synthesised by the organometallic approach using [Ru(C_8H_{10})(C_8H_{12})][126] as metal precursor in the presence of diphosphite ligands **1** and **3**, colloids **Coll.7** and **Coll.8**, respectively, with a Ru/L ratio of 1/0.2.

$$[Ru(C_8H_{10})(C_8H_{12})] \xrightarrow[0.2\ L,\ THF]{3\ bar\ H_2} [Ru_x(THF)_yL_z] + C_8H_{16}$$

Coll.7 L:**1**
Coll.8 L:**3**

Scheme 4.8. Synthesis of ruthenium nanoparticles from [Ru(C_8H_{10})(C_8H_{12})] in the presence of chiral ligands **1** and **3**

The initial solution of the ruthenium precursor and the ligand in THF was yellow. After pressurization at room temperature under 3 bars of hydrogen, the solution became black in a few minutes. The nanoparticles were isolated by precipitation

with pentane and analysed by TEM, WAXS and elemental analysis. The samples for microscopy analysis were prepared from a drop of the colloidal solution, which was deposited under argon on a holey carbon covered copper grid. The samples for WAXS analysis were prepared from the isolated nanoparticles, which were sealed in 1mm Lindemann glass capillaries.

In both cases the TEM analysis revealed small nanoparticles which were well dispersed on the grid with a mean diameter *ca*. 2.5 nm. However, the shape of the nanoparticles depends on the ligand used. **Colloid.7**, stabilised with diphosphite **1**, showed ruthenium nanoparticles of irregular shape (Figure 4.20), which were agglomerated in some cases. The ruthenium nanoparticles stabilised with diphosphite **3**, **Colloid.8**, appeared in TEM micrographs as spherical nanoparticles without agglomeration (Figure 4.21).

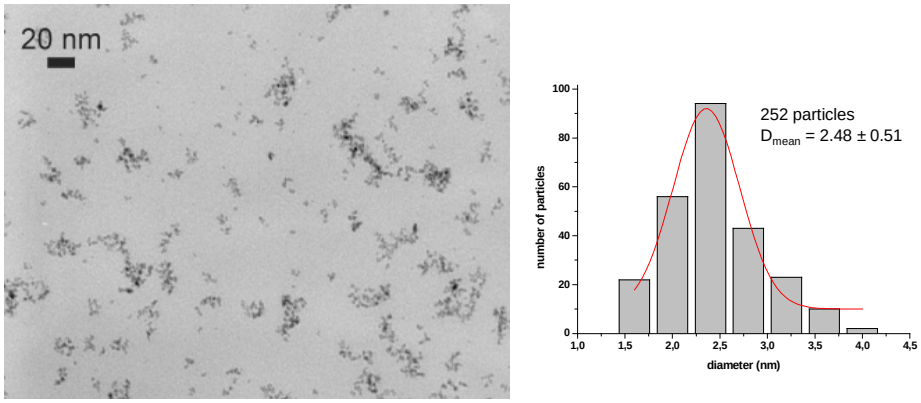

Figure 4.20. Transmission electron micrograph of **Coll.7** and size histogram built from *ca*. 250 nanoparticles

The elemental analysis of the black isolated nanoparticles of **Colloid.7** was 42.19%Ru, 1.86%P, 7.72%C, 1.18%H, which displays a Ru/P ratio of 7/1. The elemental analysis of the black isolated nanoparticles of **Colloid.8** was 44.67%Ru, 1.34%P, 2.40%Si, 24.82%C, 2.99%H, which displays a Ru/P ratio of 10/1. Although **Colloid.7** and **Colloid.8** had similar percentages of ruthenium and phosphorus in the elemental analysis and similar Ru/P ratios, which indicated similar amounts of ligand in both colloids, the amount of carbon and hydrogen is

greater for **Colloid.8**. This suggests the presence of more solvent on the surface of the nanoparticles for **Colloid.8** than for **Colloid.7**.

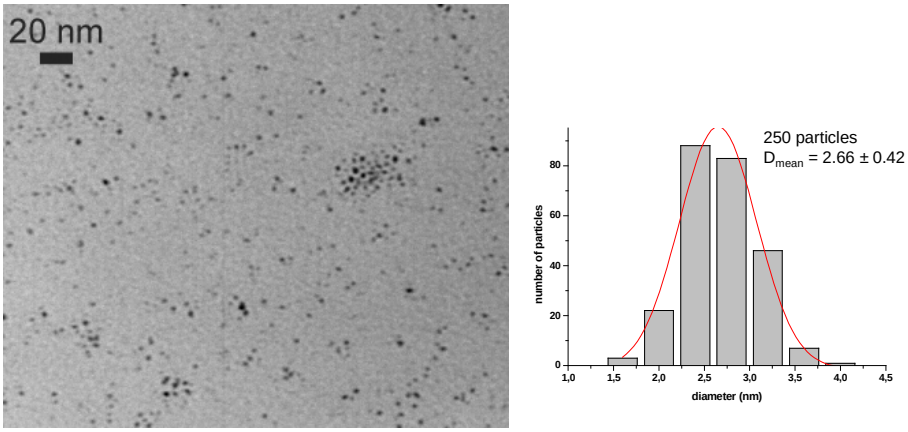

Figure 4.21. Transmission electron micrograph of **Coll.8** and size histogram built from *ca*. 250 nanoparticles

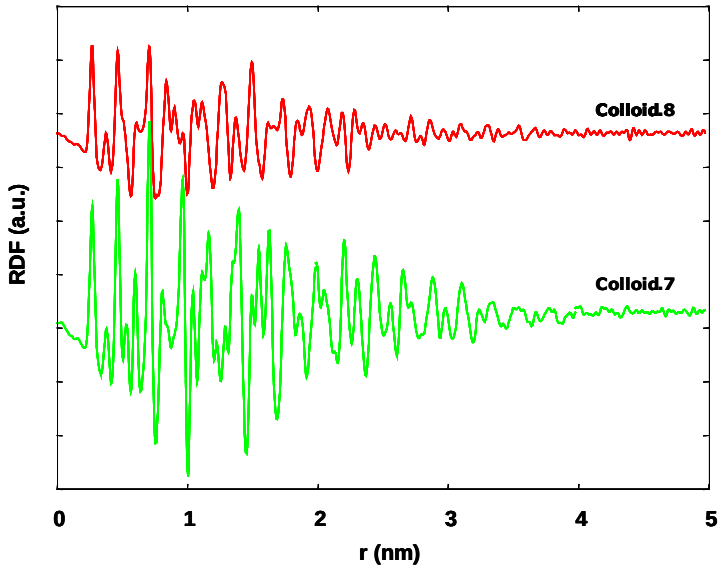

Figure 4.22. RDF of **Coll.7** and **Coll.8** obtained from WAXS analysis

WAXS analysis of **Colloid.7** (Figure 4.22) showed the peaks corresponding to well-crystallised hcp (hexagonal close-packed) ruthenium particles with a coherence length of *ca*. 3 nm, which is in good accordance with the mean diameter determined by TEM analysis. On the other hand, the WAXS analysis of **Colloid.8**, which would expected to be similar to that of **Colloid.7**, revealed a different RDF, perhaps suggesting that the stabiliser behaves differently. We can conclude that ruthenium nanoparticles stabilised with ligand **1**, **Colloid.7**, are well-crystallised nanoparticles, while for **Colloid.8**, the ruthenium nanoparticles stabilised with ligand **3**, displayed a RDF that indicated that the nanoparticles were noy well-crystallised. Further work with **Colloid.8** is required to better understand these difference between the ligand behaviour.

4.2.3 Synthesis of rhodium nanoparticles

Rhodium nanoparticles were obtained by decomposition of two different rhodium precursors, $[Rh(\eta^3\text{-}C_3H_5)_3]$[127, 128] and $[Rh(\mu\text{-}OMe)(COD)]_2$,[129] which were synthesised by previously described methods. The nanoparticles were synthesised in tetrahydrofuran solution in the presence of various stabilisers, at room temperature and under 3 bars of hydrogen. Two different precursors and various stabilisers were used to compare the effect of these variables on the nanoparticles obtained.

The rhodium complex $[Rh(\eta^3\text{-}C_3H_5)_3]$ has been successfully used before as the metal precursor in the synthesis of rhodium nanoparticles.[69, 70] Small, mean diameter of 5 nm , and well dispersed rhodium nanoparticles were synthesised from this precursor in the presence of HDA (hexadecylamine), but when the surfactant HEA-16-Cl (N,N-dimethyl-N-cetyl-N-(2-hydroxyethyl) ammonium chloride)[41, 95] was used as stabiliser sponge-like agglomerates with 34 nm of mean diameter were obtained.[69] Recently, rhodium nanoparticles were synthesised from this precursor by an original method, namely the solid-state decomposition under dihydrogen of an organometallic precursor dispersed in polymer films or directly as nanocrystals.[70] The decomposition of $[Rh(\eta^3\text{-}C_3H_5)_3]$ in a standard PMMA film (poly(methylmethacrylate)) led to small nanoparticles of about 2 nm of diameter.

4.2.3.1 Synthesis of rhodium nanoparticles from the precursor $[Rh(\eta^3\text{-}C_3H_5)_3]$

Rhodium nanoparticles have been synthesised from the precursor $[Rh(\eta^3\text{-}C_3H_5)_3]$, in the presence of diphosphite ligands **1** or **3** as stabilisers, following the reaction presented in Scheme 4.9.

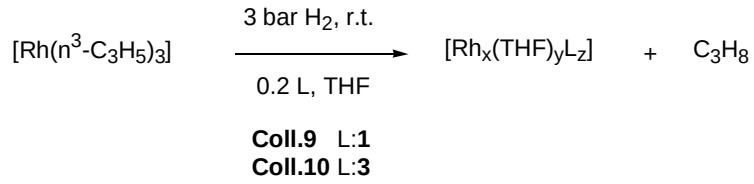

Scheme 4.9. Synthesis of rhodium nanoparticles from $[Rh(\eta^3\text{-}C_3H_5)_3]$ in the presence of chiral ligands **1** and **3**

The initial solution of the rhodium precursor in the presence of diphosphite ligand, **1** or **3**, was pale yellow, and became black in a few minutes, which confirmed the decomposition of the rhodium precursor. After 18 hours of vigorous stirring under 3 bars of hydrogen, the evaporation of the solvent gave a black precipitate which was washed several times with pentane to afford **Colloid.9** and **Colloid.10**, respectively. The nanoparticles synthesised were analysed by TEM, WAXS and elemental analysis.

The elemental analysis of the black isolated nanoparticles of **Colloid.9** was 34.23%Rh, 0.61%P, 4.70%C, 0.47%H, which displays a Rh/P ratio of 17/1. The elemental analysis of the black isolated nanoparticles of **Colloid.10** was 37.74%Rh, 2.48%P, 3.88 %Si, 6.79%C, 0.59%H, which displays a Rh/P ratio of 5/1.

Figures 4.23 and 4.24 present the transmission electron micrographs of **Colloid.9** and **Colloid.10**, respectively obtained from $[Rh(\eta^3\text{-}C_3H_5)_3]$ and diphosphite ligands **1** and **3**. In both cases the TEM micrographs revealed similar nanoparticles which were well dispersed, small and with a spherical shape. Small agglomerates consisting of a few nanoparticles were observed. Size histograms were built of at

least 150-250 particles and mean diameters of *ca*. 3 nm and *ca.* 2 nm were found for **Colloid.9** and **Colloid.10**, respectively.

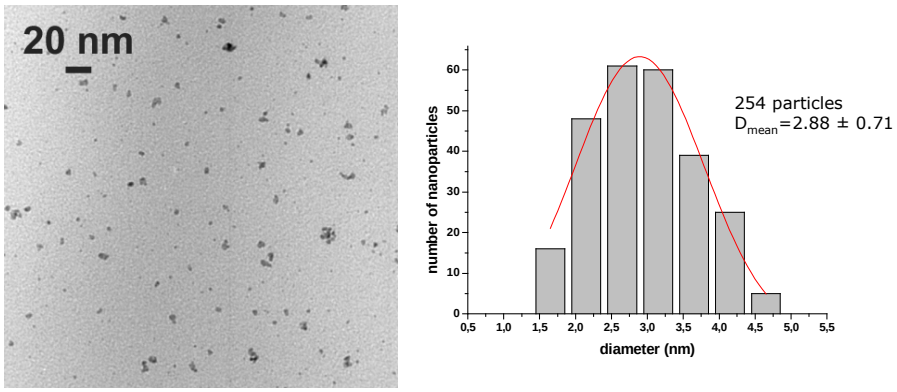

Figure 4.23. Transmission electron micrograph of **Coll.9** and size histogram built from *ca*. 250 nanoparticles

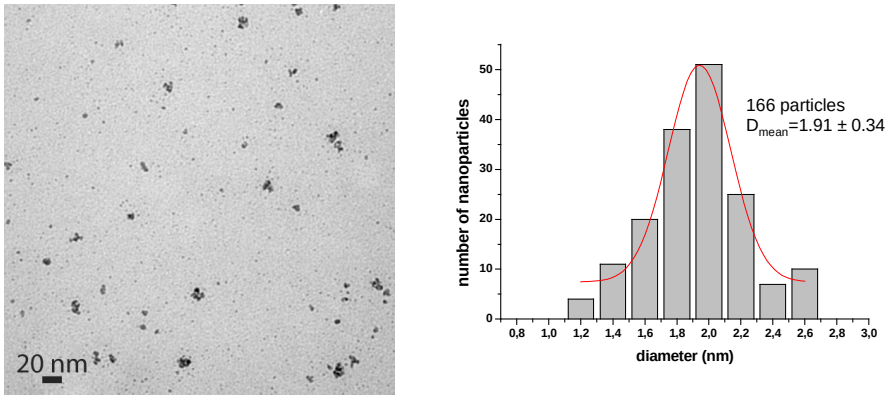

Figure 4.24. Transmission electron micrograph of **Coll.10** and size histogram built from *ca*. 170 nanoparticles

In **Colloid.9** and in **Colloid.10**, the WAXS measurement (Figure 4.25) revealed, identical well-crystallised rhodium nanoparticles displaying a fcc structure and a coherence length near 3.5-4 nm. However, **Colloid.9** showed particles with a slightly shorter coherence length than **Colloid.10**, which is in agreement with the size determined by TEM micrographs. Nevertheless, in both cases the coherence length determined by WAXS measurement was higher than the mean diameter

resulting from TEM observations. This phenomena is unusual and probably comes from the fact that larger particles can strongly influence the measurement even if they are not very numerous. The difference between the mean diameter determined by TEM and the coherence length is higher for **Colloid.10**.

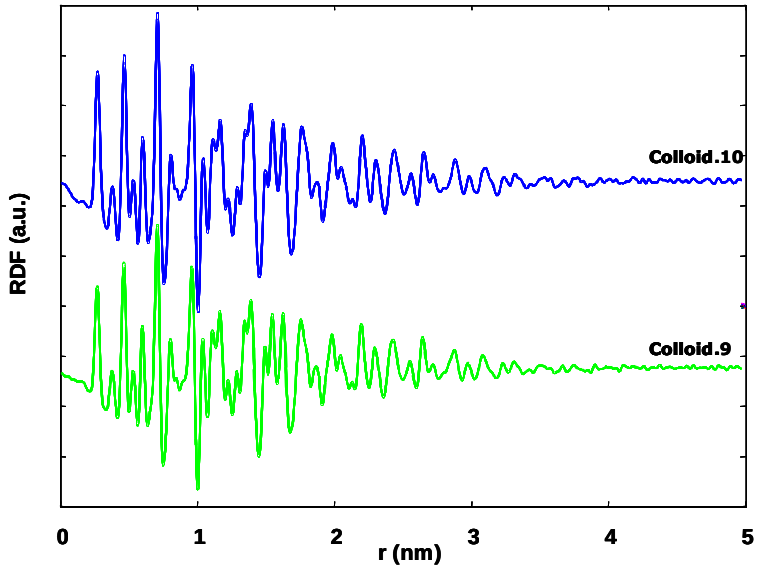

Figure 4.25. RDF of **Coll.9** and **Coll.10** obtained from WAXS analysis

4.2.3.2 Synthesis of rhodium nanoparticles from the precursor $[Rh(\mu\text{-}OMe)(COD)]_2$

To our knowledge the $[Rh(\mu\text{-}OMe)(COD)]_2$ complex had not been previously used as a metal precursor to synthesise rhodium nanoparticles. The advantage of this precursor is that is easier to prepare than $[Rh(\eta^3\text{-}C_3H_5)_3]$ and other rhodium complexes. However, methanol is produced during the decomposition. So, first of all, we tested the decomposition of this precursor in the presence of a *classical* stabiliser like PVP (polyvinylpirrolidone MW= 40000), a well-known organic polymer in the nanoparticles domain.

Rhodium nanoparticles were synthesised from the precursor $[Rh(\mu\text{-}OMe)(COD)]_2$ in the presence of PVP, namely **Colloid.11**, according to the synthesis presented in Scheme 4.10.

The initial THF solution of the rhodium precursor and PVP (Rh/PVP 2.5%) was pale yellow and became brown-black under 3 bar of hydrogen pressure due to the decomposition of the precursor. After one hour, the solution was completely black. We maintained the vigorous magnetic stirring for 18 hours. The evaporation of the solvent gave a grey precipitate which was washed several times with pentane. The nanoparticles synthesised were analysed by TEM, WAXS and elemental analysis.

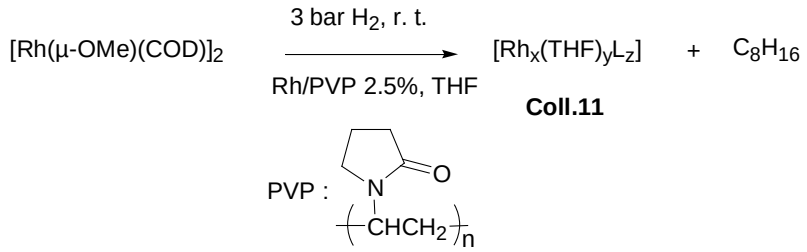

Scheme 4.10. Synthesis of rhodium nanoparticles from $[Rh(\mu\text{-}OMe)(COD)]_2$ in the presence of PVP

The elemental analysis of the grey isolated nanoparticles of **Colloid.11** was 9.31%Rh, 53.71%C, 7.46%H, 9.95%N. The TEM micrograph of **Colloid.11** (Figure 4.26) shows well dispersed, small nanoparticles.

The TEM micrograph of **Colloid.11** at higher magnification (Figure 4.26) showed small aggregates of a few nanoparticles with an irregular shape with a mean diameter of *ca.* 3 nm. This agrees with the WAXS measurement (Figure 4.27) that revealed well-crystallised rhodium nanoparticles displaying a fcc structure and a coherence length of 3.5 nm.

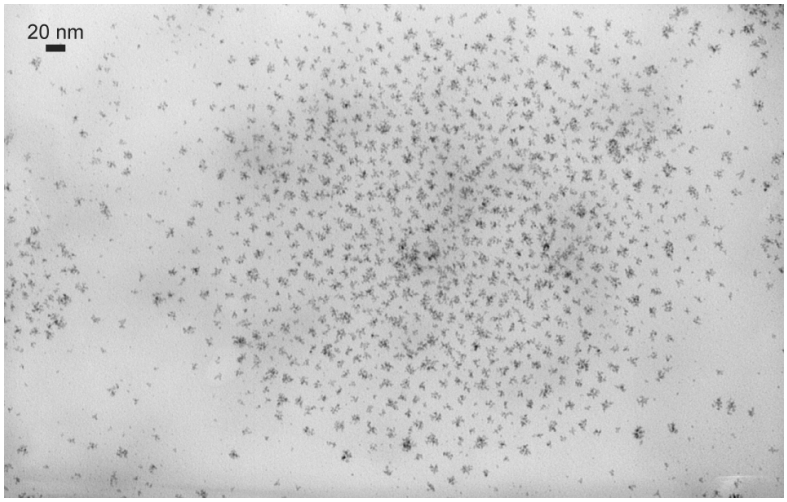

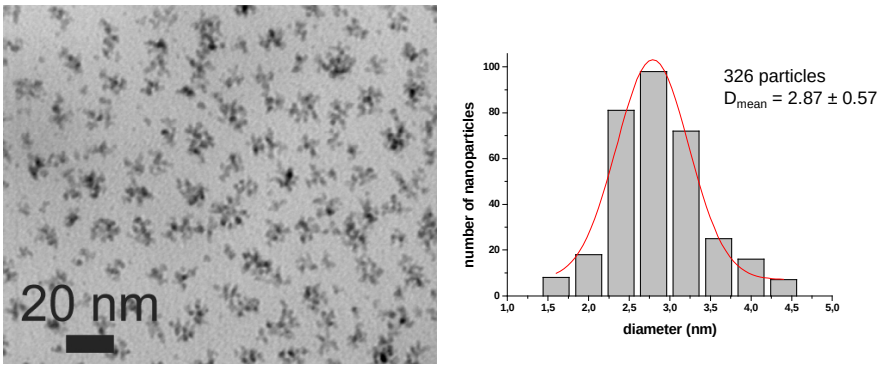

Figure 4.26. Transmission electron micrographs of **Coll.11** and size histogram built from ca. 325 nanoparticles

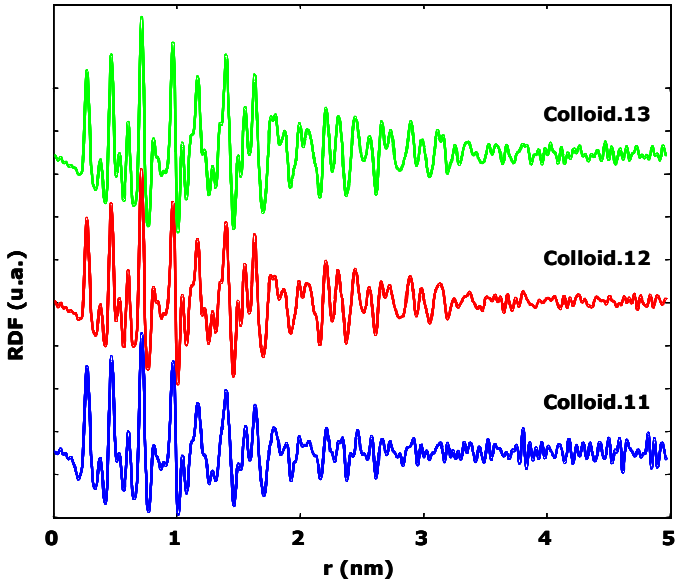

Figure 4.27. RDF of **Coll.11**, **Coll.12** and **Coll.13** obtained from WAXS analysis

Rhodium nanoparticles from the precursor $[Rh(\mu\text{-}OMe)(COD)]_2$ were also synthesised using diphosphite chiral ligands **1** and **3** (Scheme 4.11) as stabilisers. The decomposition takes place in a similar way to when PVP was used as stabiliser (Scheme 4.10). The rhodium nanoparticles stabilised with diphosphite ligand **1**, **Colloid.12**, and with diphosphite ligand **3**, **Colloid.13**, were analysed by TEM, WAXS and elemental analysis.

$$[Rh(\mu\text{-}OMe)(COD)]_2 \xrightarrow[0.2\ L,\ THF]{3\ bar\ H_2,\ r.t.} [Rh_x(THF)_yL_z] + C_8H_{16}$$

Coll.12 L:**1**
Coll.13 L:**3**

Scheme 4.11. Synthesis of rhodium nanoparticles from $[Rh(\mu\text{-}OMe)(COD)]_2$ in the presence of chiral ligands **1** and **3**

The elemental analysis of the black isolated nanoparticles of **Colloid.12** was 73.69%Rh, 0.10%P, 2.84%C, 0.10%H, which displays a Rh/P ratio of 222/1. The

elemental analysis of the black isolated nanoparticles of **Colloid.13** was 16.71%Rh, 0.11%P, 5.24%Si, 4.59%C, 0.11%H, which displays a Rh/P ratio of 45/1.

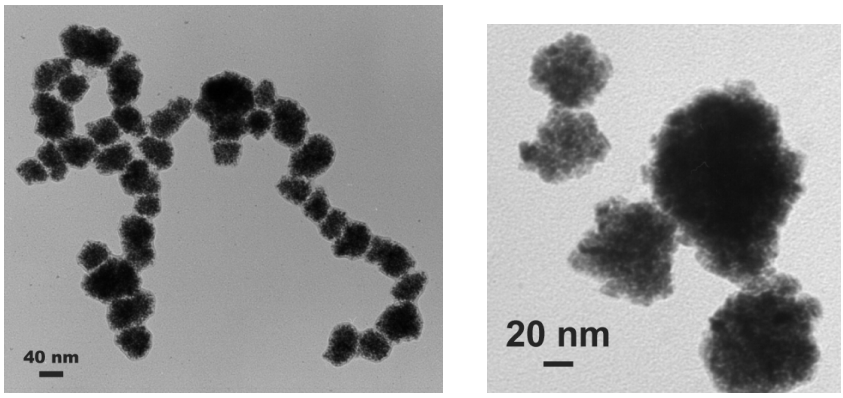

Figure 4.28. Transmission electron micrographs of **Coll.12**

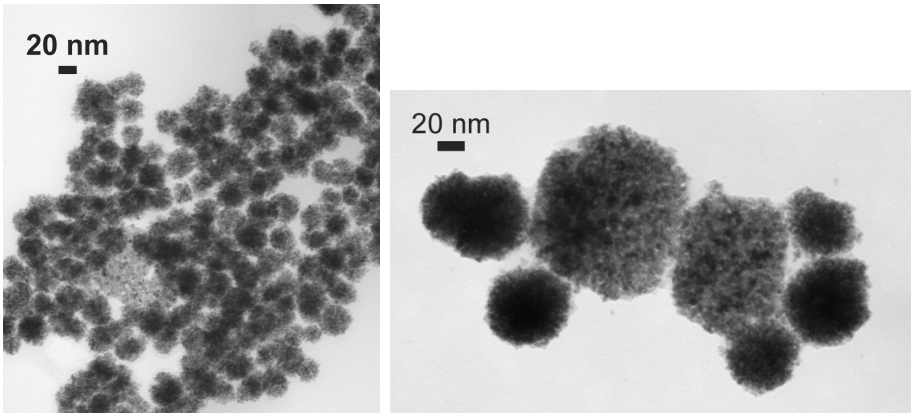

Figure 4.29. Transmission electron micrographs of **Coll.13**

TEM micrographs of **Colloid.12** and **Colloid.13** (Figure 4.28 and 4.29, respectively) showed similar large, sponge-like spherical superstructures which in some cases were aggregated among them. For **Colloid.12** these superstructures have a mean diameter of *ca*. 50 nm and for **Colloid.13**. of *ca*. 35 nm. At highest magnification we observed that these large structures in fact seem to be composed of small individual nanoparticles with a diameter of about 4 nm in both colloids. The WAXS measurement (Figure 4.27) revealed that in both colloids, **Colloid.12** and **Colloid.13**, had identical, well-crystallised, rhodium nanoparticles displaying a fcc

structure and a coherence length of 4 nm. Although the TEM and WAXS analysis indicate that these superstructures are agglomerates of small nanoparticles, we can not exclude the possibility that they are large, porous and polycrystalline particles. However, further analysis are necessaries to distinguish between these two possibilities.

Similar sponge-like structures have been previously described with rhodium nanoparticles[69, 130] and with such metal nanoparticles as ruthenium[66, 76], nickel[64] and platinum[131-133]. These studies have observed that the reaction parameters (metal precursor, method of synthesis, temperature, solvent, etc.) played an important role in the final properties of the nanoparticles (size, shape, etc.). We also observed that when PVP is used as stabiliser, nanoparticles were small but changing of the PVP for diphosphite ligands led to the formation of large structures. This may mean that the diphosphite ligands have a lower stabilising effect than the PVP. On the other hand, we have observed that if another rhodium precursor, $[Rh(\eta^3\text{-}C_3H_5)_3]$ is used, in the same reaction conditions with the same diphosphite ligands **1** and **3** as stabilisers, the resulting nanoparticles are small (see Figures 4.23 and 4.24). The characteristics of the nanoparticles synthesised depend on the rhodium precursor used and can be attributed to the products obtained by the decomposition of the precursor. The decomposition of the olefinic precursor $[Rh(\eta^3\text{-}C_3H_5)_3]$ leads to the production of propane which cannot produce strong bonds with the growing metal surface in these conditions.[17] This is not the case with the rhodium precursor $[Rh(\mu\text{-}OMe)(COD)]_2$. Indeed the decomposition of this precursor produces cyclooctane and methanol which remain in the solution. Methanol can interact with the surface atoms of the nanoparticles. Previous studies demonstrated that the concentration of different alcohols in the reaction media affects the characteristics of the nanoparticles synthesised. [66, 69, 76] In our case, the presence of methanol can enhance the solubility of the PVP leading to better stabilised nanoparticles (small and well dispersed, see Figure 4.26) than diphosphite ligands. However, when diphosphite ligands are used as stabilisers the presence of cyclooctane and methanol can lead to the formation of droplets segregated of the rest of the solvent in which agglomerates may be form. This behaviour was observed in the synthesis of ruthenium nanoparticles from $[Ru(C_8H_{10})(C_8H_{12})]$ in the presence of alcohols.[16, 76]

4.2.4 Application in catalysis of metal nanoparticles

Allylic alkylation

In the frame of a collaboration with the Universitat de Barcelona and Laboratoire de Chimie de Coordination CNRS (Toulouse) we have studied the application of palladium nanoparticles stabilised with diphosphite ligands **2** and **3**, **Coll.2** and **Coll.3**, respectively, in palladium-catalysed allylic alkylation of rac-3-acetoxy-1,3-diphenyl-1-propene with dimethyl malonate (Scheme 4.12).

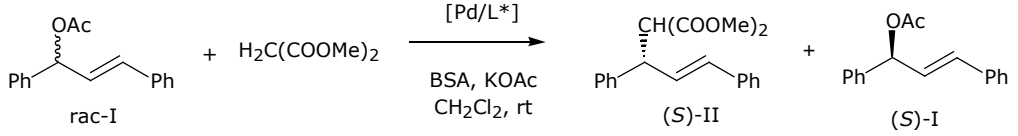

Scheme 4.12. Asymmetric allylic alkylation of rac-3-acetoxy-1,3-diphenyl-1-propene with dimethyl malonate

The aim is to compare the influence of configuration of the stereocenter at position 3 (**2**), the presence of phosphine-phosphite moieties (**4**) instead of diphosphite, and the existence of C_2-symmetry ligands (**3**), with colloids stabilised by ligand **1**, **Coll.1**. The application of **Colloid.1** system in this reaction lead to an enantiomeric excess of >95%(*S*) in II with high kinetic resolution in the substrate (rac-I) (89% (*S*) in the remaining substrate) at 56% of conversion.[79] **Colloid.2** system was not stable under catalytic conditions showing not reproducible results. **Colloid.3** system led also to an enantiomeric excess of >98%(*S*) in II with high kinetic resolution in the substrate (rac-I) (98% (*S*) in the remaining substrate). This behaviour is similar to that of C**olloid.1**, although in this case the system slowly evolves until a 73% of conversion, while for **Colloid.1** the reaction stops at 56% of conversion and does not evolve even after 7 days of reaction. This result proves that the excellent kinetic resolution in the reaction of allylic alylation is not an singular case for **Colloid.1**, but a more general behaviour of palladium-diphosphite nanoparticles.

Hydroformylation of styrene

Colloid.12 and **Colloid.13**, which contain rhodium nanoparticles synthesised from the precursor $[Rh(\mu\text{-}OMe)(COD)]_2$ in the presence diphosphite ligands **1** and **3**, respectively, have been used as catalyst in the rhodium-catalysed asymmetric hydroformylation of styrene (Scheme 4.13). The results are given in Tables 4.1 and 4.2. We used these colloids in order to optimise the conditions of this reaction and then apply them to other rhodium colloids.

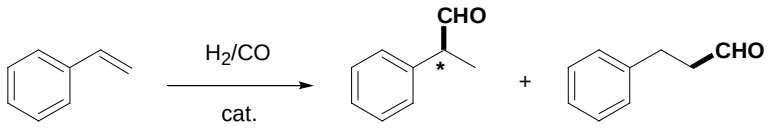

Scheme 4.13. Hydroformylation reaction

Table 4.1. Styrene hydroformylation with **Colloid.12** and **Colloid.13**[a]

Entry	Catalyst	Rh/L/S[b]	t(h)	% conv.[c]	% ald.[d]	% regio.[e]	% ee
1	**Coll.12**	1/-/200	24	28	92	57	0
2	**Coll.12**	1/0.2/200	24	11	97	>99	40 (*S*)
3	**Coll.13**	1/-/200	24	95	97	54	13 (*S*)
4	**Coll.13**	1/0.2/200	24	80	97	90	24 (*S*)

[a]3 mg. nanoparticle, temp.: 80ºC, P=20 bar Pco/H_2=1, Rh/S 1:200 styrene 5.8 mmol, 10 ml. toluene [b]Molar ratio between rhodium, excess ligand added to the catalysis and substrate [c]% conversion styrene G.C.[d] %2-phenylpropanal + 3-phenylpropanal [e]% 2-phenylpropanal

The reaction was carried out at 80ºC and 20 bar of pressure (Pco/H_2=1) with and without the addition of an excess of the respective ligand in the catalytic media. For the **Colloid.12** catalytic system, conversions were in both cases (Table 4.1, entry 1 and 2). The **Colloid.13** catalytic system was more active in the same conditions (Table 4.1, entry 3 and 4). In all cases we observed a high selectivity to the aldehydes (upper 90%). The addition of the respective free ligand to the catalysis led to a less active but more regioselective catalyst system. The enantioselectivity of the catalytic system was also affected by the addition of ligand. For **Colloid.12** the addition of free ligand **1** increased the enantioselectivity from 0% to 40% (*S*)

(Table 4.1, entries 1 and 2) and for **Colloid.13** the addition of the free ligand **3** increased the enantioselectivity from 13% to 24% (*S*) (Table 4.1, entries 3 and 4).

The comparison of TEM micrographs before and after catalysis (Figure 4.30 and 4.31) did not show any significant change in the size and shape of the particles, indicating that they were stable under the catalytic reaction conditions.

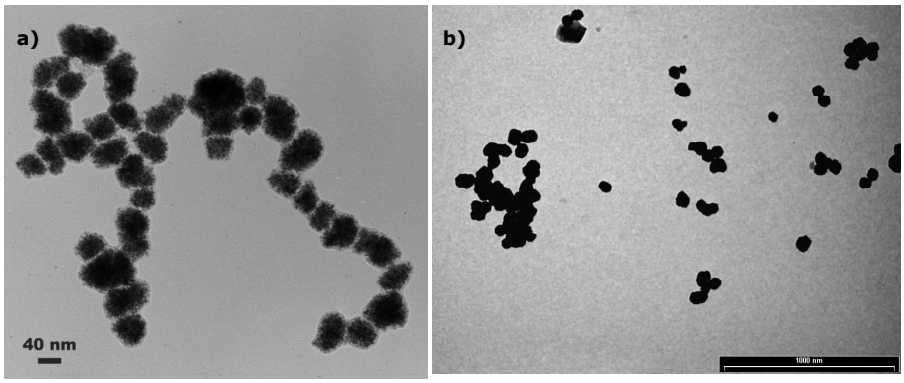

Figure 4.30. Transmission electron micrographs of **Coll.12** a) before and b) after catalysis

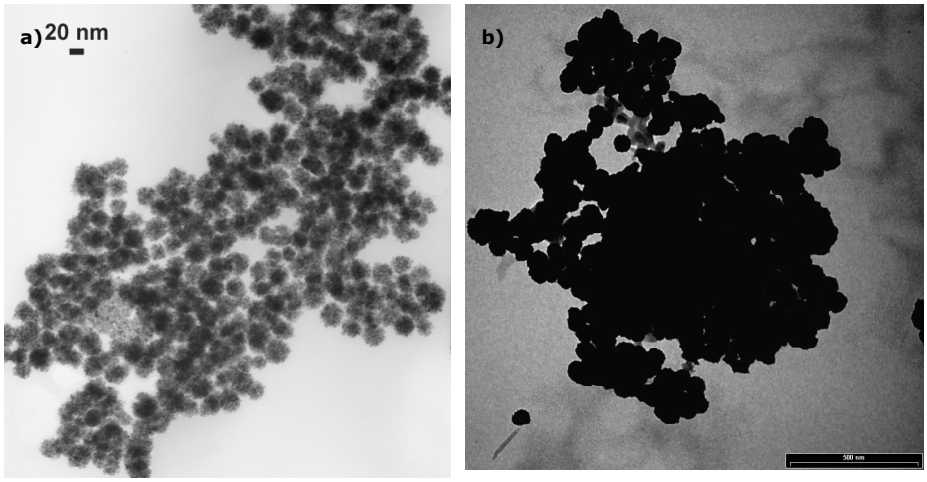

Figure 4.31. Transmission electron micrograph of **Coll.13** a) before and b) after catalysis

In an attempt to obtain more information about colloidal catalysis, the colloids were compared to molecular equivalent systems. Table 4.2 gives the results obtained

with the colloidal systems, **Colloid.12** and **Colloid.13**, and with the respective molecular systems, **Molecular.12** and **Molecular.13**. In both cases, we studied the effect of the substrate concentration on the colloidal systems. In addition, the effect of the excess of ligand has been studied for **Colloid.13** catalytic system.

Table 4.2. Styrene hydroformylation with **Colloid.12** and **Colloid.13**[a]

Entry	Catalyst	Rh/L/S[b]	t (h)	% conv.[c]	TOF (h^{-1})	% ald.[d]	% regio.[e]	% ee
1	**Mol.12**[f]	1/1/200	15	92	-	98	95	36 (*S*)
2	**Coll.12**	1/0.2/200	15	3	0.7	41	>99	-
3			30	10	0.9	98	>99	-
4			45	35	2.2	98	95	45 (*S*)
5	**Coll.12**	1/0.2/400	15	2	0.8	71	>99	-
6			30	8	1.4	97	>99	-
7			45	33	3.9	98	97	47 (*S*)
8	**Coll.12**	1/0.1/200	15	2	0.4	90	>99	-
9			30	11	0.9	98	>99	-
10			45	37	2.3	98	96	43 (*S*)
11	**Mol.13**[g]	1/1/200	15	99	-	>99	78	20 (*S*)
12	**Coll.13**	1/0.2/200	15	31	24.5	92	97	-
13			30	70	27.5	98	95	-
14			45	90	23.9	98	95	31 (*S*)
15	**Coll.13**	1/0.2/400	15	35	55.1	93	97	-
16			30	76	60.4	99	95	-
17			45	94	50.3	99	95	32 (*S*)

[a]3 mg. nanoparticle, temp.: 70ºC, P=40 bar Pco/H_2=1, Rh/S 1:200 styrene 5.8 mmol, 10 ml. toluene [b]Molar ratio between rhodium, excess ligand added to the catalysis and substrate [c]% conversion styrene G.C.[d] %2-phenylpropanal + 3-phenylpropanal [e]% 2-phenylpropanal[f] [Rh]= $9.04x10^{-4}$M temp.: 70ºC, P=40 bar Pco/H_2=1, Rh/S 1:200 styrene 1.8 mmol, 10 ml. toluene[g] Substrate/Rh=200, styrene 2.7 mmol, $[Rh(acac)(CO)_2]$ 0.0135mmol temp: 60ºC P=20 bar, 15 ml toluene Pco/H_2=1

If we compare the results of the molecular systems with the ones of the colloidal systems we can observe that the molecular system is highly active, with total conversion at 15 hours of reaction (Table 4.2, entries 1 and 11). The colloidal

systems, **Colloid.12** and **Colloid.13**, on the other hand, are not very active: the TOF's of **Colloid.12** were less than 4 h^{-1}, while for **Colloid.13** they were around 50 h^{-1}. Although the regioselectivity with the molecular and the colloidal systems is similar, the enatioselectivity is higher with the colloidal systems than with the molecular ones.

The addition of a high quantity of substrate led to more active catalysts in both cases, **Colloid.12** and **Colloid.13**, (Table 4.2, entries 5-7 and 15-17) which indicated that the rate is proportional to the concentration of the substrate. An increase in the free ligand added (Table 4.2, entries 2 to 4 vs. 8 to 10) does not affect the activity and the selectivity.

In order to better compare between the colloidal and molecular catalytic systems, which display very different reaction rates, a series of experiments was carried out. The catalyst concentration of the homogenous molecular system was decreased, so that the reaction rates were comparable to those of the colloidal ones. The results are summarised in Table 4.3.

Table 4.3. Styrene hydroformylation with diluted **Molecular.12** catalyst[a]

Entry	Rh/L/S[b]	t (h)	% conv.[c]	TOF (h^{-1})	% ald.[d]	% regioselec.[e]	% ee
1	1/1/200[f]	15	92	12.2	98	95	36(*S*)
2	1/1/2000[g]	15	84	111.9	96	87	0
3	1/1/20000[h]	15	35	466.7	99	84	-
4		30	91	608.0	97	79	0
5	1/1/100000[i]	15	7	433.3	>99	>99	-
6		30	59	1963.3	93	85	0
8	1/1/200000[j]	15	0	-	-	-	-
9		30	<1	-	>99	>99	-

[a]temp.: 70ºC, P=40 bar Pco/H_2=1, styrene 1.8 mmol, 10 ml. toluene [b]Molar ratio between rhodium, excess ligand added in the catalysis and substrate [c]% conversion styrene G.C.[d] %2-phenylpropanal + 3-phenylpropanal [e]% 2-phenylpropanal [f][Rh]= $9.04x10^{-4}$M, [g][Rh]= $9.04x10^{-5}$M,[h][Rh]= $9.04x10^{-4}$M, [i][Rh]= $1.81x10^{-6}$M, [j][Rh]= $9.04x10^{-7}$M

Table 4.4. Styrene hydroformylation with diluted **Molecular.12** catalyst and excess of ligand **1**[a]

Entry	Rh/L/S[b]	t (h)	% conv.[b]	TOF (h^{-1})	% ald.	% regioselec.[c]	% ee
1	1/1/200	15	89	11.9	96	96	37(*S*)
2	1/1/2000	15	35	46.7	94	91	-
3		30	86	57.1	94.1	95	36 (*S*)
4	1/1/20000	15	5	60.0	80	>99	-
5		30	16	109.3	90	>99	-
6		45	85	373.3	94	92	19 (*S*)
7	1/1/100000	15	1	-	-	>99	-
8		30	7	236.7	82	>99	-
9		45	15	342.2	87	>99	-
10		60	30	506.7	89	>99	29 (*S*)
10	1/1/200000	15	<1	-	-	>99	-
11		30	8	513.3	84	>99	-
12		45	18	795.6	88	>99	-
13		60	31	1013.3	89	>99	29 (*S*)

[a]temp.: 70ºC, P=40 bar Pco/H_2=1, styrene 1.8 mmol, ligand **1** 5.8 mmol, 10 ml. toluene [b]Molar ratio between rhodium, excess ligand added to the catalysis and substrate [c]% conversion styrene G.C.[d] %2-phenylpropanal + 3-phenylpropanal [e]% 2-phenylpropanal [f][Rh]= $9.04x10^{-4}$M, [g][Rh]= $9.04x10^{-5}$M,[h][Rh]= $9.04x10^{-4}$M, [i][Rh]= $1.81x10^{-6}$M,[j][Rh]= $9.04x10^{-7}$M

It appears that a decrease in the catalyst concentration decreases the conversion. This is in agreement with the reaction kinetics of the hydroformylation reaction, which is proportional to the rhodium concentration.[134] With dilutions higher than 1/1/2000 (Table 4.3, entries 2, 4 and 6) no enantioselectivity was observed. This may be due to the formation of $[RhH(CO)_4]$ which is a highly active achiral hydroformylation catalyst.[134] The formation of this species is favoured for small concentration of rhodium respect to the CO quantity in the medium, which displaces the coordinated ligand. So we decided to make a new series of essays with diluted molecular systems (see Table 4.4), in which we added the same concentration of ligand as in the colloidal systems (Table 4.1 and 4.2). We observed that the presence of added ligand led to lower activity (e. g., Table 4.3, entry 3 and 4 *vs.* Table 4.4 entries 4 and 5) but catalysts that were more enantioselective. This

indicates that the excess of ligand is enough to maintain the active species with ligand coordinated.

The results of the experiments carried out with the diluted molecular and the colloidal catalytic systems could suggest the formation of molecular system. Nevertheless, while the molecular system, diluted or not, displayed enantioselectivities in the range 19-37% (*S*), the colloidal ones showed enantioselectivities as high as 45% (*S*) (Table 4.2, entries 4, 7 and 10).

Table 4.5. Poison Test.
Styrene hydroformylation with **Colloid.12** and **Molecular.12** catalyst[a]

Entry	Catalyst	Rh/L/S/poison[c]	t (h)	% conv[d]	TOF (h^{-1})	% ald.[e]	% regio.[f]	% ee
1	**Mol.12**[b]	1/1/200/-	15	92	-	98	95	36 (*S*)
2	**Mol.12**[b]	1/1/200/4 (CS_2)	15	96	-	>99	93	15 *(S)*
3	**Mol.12**[b]	1/1/200/100 (Hg)	15	96	-	>99	92	15 *(S)*
4	**Coll.12**	1/0.2/200/-	15	3	0.7	41	>99	-
5			30	10	0.9	98	>99	-
6			45	35	2.2	98	95	45 (*S*)
7	**Coll.12**	1/0.2/200/4	15	14	2.6	>99	>99	-
8		(CS_2)	30	47	4.2	>99	96	40 *(S)*
9			45	64	3.8	>99	96	36 *(S)*
10	**Coll.12**	1/0.2/200/100	15	3	0.5	>99	>99	-
11		(Hg)	30	18	1.6	>99	95	33 *(S)*
12			45	38	2.3	>99	95	30 *(S)*

[a]3 mg. nanoparticle, temp.: 70ºC, P=40 bar Pco/H_2=1, Rh/S 1:200 styrene 5.8 mmol, 10 ml. toluene [b][Rh]= $9.04x10^{-4}$M temp.: 70ºC, P=40 bar Pco/H_2=1, Rh/S 1:200 styrene 1.8 mmol, 10 ml. toluene [c]Molar ratio between rhodium, excess ligand added to the catalysis, substrate and poison [d]% conversion styrene G.C.[e] %2-phenylpropanal + 3-phenylpropanal [f]% 2-phenylpropanal

However, the fact that the asymmetric induction between **Colloid.12** and **Molecular.12** systems is different suggests that the catalytic system is different. In order to rule out the possibility of a small amount of molecular catalyst to be formed from the particles a series of experiments were carried out in the presence

of *classical* poisons (CS_2 and Hg). The results of these test are summarised in Table 4.5.

The molecular system tested in the presence of CS_2 or Hg (Table 4.5, entries 2 and 3) gave similar results. The activity and regioselectivity of the poisoned and unpoisoned molecular systems are almost identical (Table 4.5, entry 1). However, in the presence of CS_2 or Hg the enantioselectivity decreases from 36% to 15%ee.

In the colloidal system the presence of CS_2 (Table 4.5, entries 7 to 9) led to an increase of the activity but a slightly decrease on the enantioselectivity, than in the colloidal catalyst system without poison. When Hg was used as poison (Table 4.5, entries 10 to 12) the activity of the system was quite similar to that of the system without poison (Table 4.5, entries 4 to 6), but the enantioselectivity was clearly smaller. It is expected that the addition of poison to the active surfaces (colloidal or heterogeneous) led to a decrease in the activity.

Nevertheless, it is also necessary to consider that rhodium does not amalgamate with Hg(0)[135] and CS_2 begins to dissociate from the heterogeneous catalyst at higher temperatures than 50ºC, [135] and the experiments were carried out at 70ºC, these results are not conclusive. The results obtained with colloidal and molecular catalytic systems, and the poisoning tests suggest the formation of small amounts of molecular system form the colloidal one, however, these are difficult to analyse and further analysis are needed to be able to clearly conclude.

4.3 Conclusions

New palladium, ruthenium and rhodium nanoparticles have been successfully synthesised in the presence of carbohydrate derivative ligands (**1-4**)**.** We observed that the shape, size and dispersion of the nanoparticles depend strongly on the metal precursor and the stabiliser used.

Palladium nanoparticles were synthesised from $[Pd_2(dba)_3]$ with phosphite ligands **2** and **3** and phosphine-phosphite ligand **4** as stabilisers. The synthesis was done following the organometallic approach, at room temperature and under 3 bars of

hydrogen pressure. In the presence of diphosphite ligands, small nanoparticles (diameter *ca*. 3.5-4 nm) well-crystallised and contain a few agglomerates were obtained. When phosphine-phosphite ligand **4** was used as stabiliser, smaller nanoparticles could be prepared. This indicates that the nature of the ligand has a strong influence on the morphology of the nanoparticles synthesised. We also studied the effect of the temperature and the palladium/ligand ratio on the nanoparticles stabilised with phosphine-phosphite ligand **4**. We observed that an increase in the temperature or the quantity of ligand did not improve the results and led to more agglomeration and no well crystallisation.

Ruthenium nanoparticles have also been synthesised by the organometallic approach using $[Ru(C_8H_{10})(C_8H_{12})]$ as metal precursor and diphosphite ligands **1** and **3** as stabilisers, at room temperature under 3 bars of hydrogen pressure. When diphosphite ligand **1** was used as stabiliser, nanoparticles were well-crystallised with a mean diameter *ca*. 3 nm. However, when diphosphite ligand **3** was used not well-crystallised nanoparticles were obtained.

Rhodium nanoparticles were obtained by decomposition of two different rhodium precursors, $[Rh(\eta^3\text{-}C_3H_5)_3]$ and $[Rh(\mu\text{-}OMe)(COD)]_2$, following the organometallic approach. The rhodium nanoparticles produced from $[Rh(\eta^3\text{-}C_3H_5)_3]$ were synthesised in tetrahydrofuran in the presence of diphosphite ligands **1** and **3** as stabilisers at room temperature and under 3 bars of hydrogen pressure. In these conditions small and well-crystallised nanoparticles were obtained. The rhodium nanoparticles synthesised from the precursor $[Rh(\mu\text{-}OMe)(COD)]_2$ were stabilised with PVP (polyvinylpyrrolidone MW= 40000) and diphosphite ligands **1** and **3**, giving rise, respectively, to small and well-crystallised nanoparticles with PVP and large particles with diphosphite ligands. Although further study is required if it is to be determined whether these particles are really large, porous and pollycrystalline or whether they consist of small individual nanoparticles, we can conclude that the nature of the metal precursor affects the particles synthesised.

The palladium nanoparticles **Coll.2** and **Coll.3** were used as catalyst in palladium-catalysed allylic alkylation of rac-3-acetoxy-1,3-diphenyl-1-propene with dimethyl malonate. **Colloid.2** system was not stable under catalytic conditions showing not

reproducible results. However, **Colloid.3** system led to an enantiomeric excess of >98%(*S*) in II with high kinetic resolution in the substrate (rac-I) (98% (*S*) in the remaining substrate). This behaviour is similar to that of the previously reported for **Colloid.1**.[79]

Finally, we studied the use of rhodium nanoparticles, synthesised from [Rh(μ-OMe)(COD)]$_2$ in the presence of diphosphite ligands **1** and **3** (**Colloid.12** and **Colloid.13**, respectively), as catalyst in the styrene hydroformylation reaction. In both cases the activities were very low. The introduction of an excess of ligand increased the regioselectivity and enantioselectivity. The respective molecular system of **Colloid.12**, **Molecular.12**, and the poisoning test were studied in order to exclude the possible formation of homogeneous catalyst in the colloidal system. The results are difficult to analyse and further analysis are needed to be able to clearly conclude.

4.4 Experimental section

General methods

All syntheses were performed by using standard Schlenk techniques and Fisher-Porter bottle techniques under argon atmosphere. Solvents were purified by standard procedures. Ligands **1**,[122] **2**,[123] **3**,[124] and **4**[125] were prepared by methods described previously. All other reagents were used as commercially available. ^{1}H, ^{13}C{^{1}H} and ^{31}P{^{1}H} NMR spectra were recorded on a Varian Gemini 400 MHz spectrometer. Chemical shifts are relative to $SiMe_4$ (^{1}H and ^{13}C) as internal standard or H_3PO_4 (^{31}P) as external standard. All NMR spectral assignments were determined by COSY and HSQC spectra. TEM analysis were prepared by slow evaporation of a drop of each colloidal solution deposited under argon onto a holey carbon-covered copper grid. The TEM experiments were performed at the "Service Commun de Microscopie Electronique de l'Université Paul Sabatier" on a JEOL 200 CX-T electron microscope operating at 200kV and a Philips CM12 electron microscope operating at 120 kV with respective resolutions of 4.5 and 5 Å. The TEM analyses of the nanoparticles after catalysis were performed in the "Servei de Recursos Científics" on a Zeiss 10 CA electron microscope at 100 kV with a

resolution of 3Å. The size distribution of the particles was determined by a manual analysis of enlarged images. At least 150 particles on a given grid were measured in order to obtain a statistical size distribution and a mean diameter. WAXS experiments were mainly performed at CEMES "Centre d'Elaboration des Matériaux et d'Etudes Structurales, CNRS, Toulouse". All samples were sealed in Lindemann glass capillaries. Measurements of the X-ray intensity scattered by the sample irradiated with graphite-monochromatized molybdenum Ka (0.071069 nm) radiation were performed using a dedicated two-axis diffractometer. In order to extract the structure-related component of WAXS, the so-called reduced intensity function(s), then Fourier transformed to allow for radial distribution function (RDF) analysis. Gas chromatographic analyses were run on a Hewlett-Packard HP 5890A instrument (split/splitless injector, J&W Scientific, HP-5, 25 m column, internal diameter 0.25 mm, film thickness 0.33 mm, carrier gas: 150 kPa Ar, F.I.D. detector) equipped with a Hewlett-Packard HP3396 series II integrator. Hydroformylation reactions were carried out in a Parr 450 ml. multiple reaction vessel autoclave. Enantiomeric excesses were measured after oxidation of the aldehydes to the corresponding carboxylic acids on a Hewlett-Packard HP 5890A gas chromatograph (split/splitless injector, J&W Scientific, Supelco β-DEX 110 (30 m. column, internal diameter 0.25 mm., carrier gas: 100 kPa He, F.I.D. detector).

Synthesis of metal precursors

$[Ru(C_8H_{10})(C_8H_{12})]$[126]

0.34 g (1.3 mmol) of hydrated $RuCl_3$ was completely dissolved in absolute ethanol (10 ml) under nitrogen. 1,5 cyclooctadiene, previously deoxygenated and filtered through alumina, and zinc dust (3.0 g, 46 mmol) were added and the solution was heated at 80ºC for 3 hours. The resulting solution was filtered and the residue was washed with pentane (50 ml). The filtrate was evaporated to dryness under reduced pressure at room temperature and the solid residue obtained was extracted with pentane (2 x 60 ml). The solution was concentrated and passed through alumina using pentane. The yellow pentane solution was concentrated to 5

ml and cooled to −78ºC giving 0.20 g of yellow crystals. The resulting highly sensitive yellow crystals were stored under argon at −30ºC.

$[Rh(\mu\text{-}OMe)(COD)]_2$[127, 128]

To a solution of $[Rh(\mu\text{-}Cl)(COD)]_2$ (175 mg., 0.36 mmol) in dichloromethane (15 ml.) a solution of KOH (40 mg., 0.71 mmol) in methanol (5 ml) was added. Immediately a yellow solid precipitated. After being stirred for 30 minutes at room temperature, the solvent was removed under reduced pressure. Then 10 ml of methanol and subsequently 15 ml of water were added to the residue after which the solid was collected by filtration, and cleaned with water (3 x 5 ml). The solid was dried under reduced pressure over phosphorus (V) oxide and used without further purification.

$[Rh(\eta^3\text{-}C_3H_5)_3]$[129]

To a cold (-10ºC) stirred suspension of $RhCL_3.H_2O$ (1.1 g, 5.3 mmol) in THF (93 ml) allylmagnesium chloride (17.5 ml, 2M, 35 mmol) was added dropwise over a period of 10 minutes. The solution slowly lost its yellow-brown color as the $RhCL_3.H_2O$ disappeared over a period of about 1 hour. The solution was then allowed to warm to 10ºC and stirred for an additional 16 hours. The THF wass removed under reduced pressure and the residue extracted with pentane (3 x 150 ml). The yellow pentane extracted was filtered through celite and the pentane was removed under reduced pressure. The bright yellow residue was transferred to a sublimator and sublimed onto a water-cooled prove over a period of 2 hours using static vacuum (50-60ºC/10^{-4}torr). Yield: 0.8 g (82%)

Synthesis of metal nanoparticles

Synthesis of palladium nanoparticles from the precursor $[Pd_2(dba)_3]$

In the standard procedure, 160 mg. of palladium precursor $[Pd_2(dba)_3]$ (0.175 mmol) were dissolved under argon at −110ºC (ethanol/N_2 bath) in a solution of 160

ml of tetrahydrofuran containing 0.2 equivalents of ligand in a closed pressure bottle. After pressurization at room temperature under 3 bars of hydrogen for 30 minutes, the initial red solution became black in a few minutes. The vigorous magnetic stirring and the hydrogen pressure were maintained for 18 hours. After that period of time, the hydrogen pressure was eliminated, and a drop of the colloidal solution was deposited under argon on a holey carbon covered copper grid for electron microscopy analysis. Precipitation with a tetrahydrofuran/pentane mixture at low temperature gave a black precipitate which was washed with pentane (2x 40 ml) and dried under vacuum. The colloids were characterized by TEM analysis, elemental analysis and WAXS.

Colloid.2 was synthesised according to the standard procedure from 160 mg of $[Pd_2(dba)_3]$ (0.175 mmol) and 74.7 mg of diphosphite **2** (0.070 mmol) in 160 ml of tetrahydrofuran. The nanoparticles synthesised were analysed by TEM (Transmission electron microscopy), WAXS (Wide-angle X-ray scattering) and elemental analysis. The elemental analysis of the black isolated nanoparticles of **Colloid.2** was 72.97 %Pd, 0.37%P, 13.99%C, 0.38%H.

Colloid.3 was synthesised according to the standard procedure from 160 mg of $[Pd_2(dba)_3]$ (0.175 mmol) and 106.2 mg of diphosphite **3** (0.070 mmol) in 160 ml of tetrahydrofuran. The nanoparticles synthesised were analysed by TEM (Transmission electron microscopy), WAXS (Wide-angle X-ray scattering) and elemental analysis. The elemental analysis of the black isolated nanoparticles of **Colloid.3** was 68.77 %Pd, 0.33%P, 2.93%Si, 8.82%C, 0.65%H;

Colloid.4 was synthesised according to the standard procedure from 160 mg of $[Pd_2(dba)_3]$ (0.175 mmol) and 55.7 mg of diphosphite **4** (0.070 mmol) in 160 ml of tetrahydrofuran. The nanoparticles synthesised were analysed by TEM (Transmission electron microscopy), WAXS (Wide-angle X-ray scattering) and elemental analysis. The elemental analysis of the black isolated nanoparticles of **Colloid.4** was 71.59%Pd, 1.97%P, 15.94%C, 1.28%H.

Colloid.5 was synthesised according to the standard procedure from 80 mg of $[Pd_2(dba)_3]$ (0.088 mmol) and 27.9 mg of diphosphite **4** (0.035 mmol) in 80 ml of

tetrahydrofuran at 60ºC. The nanoparticles synthesised were analysed by TEM (Transmission electron microscopy), WAXS (Wide-angle X-ray scattering) and elemental analysis. The elemental analysis of the black isolated nanoparticles of **Colloid.5** was 60.67%Pd, 3.55%P.

Colloid.6 was synthesised according to the standard procedure from 80 mg of $[Pd_2(dba)_3]$ (0.088 mmol) and 55.7 mg of diphosphite **4** (0.070 mmol) in 80 ml of tetrahydrofuran. The black nanoparticles synthesised did not precipitate and were only analysed by TEM (Transmission electron microscopy).

Synthesis of ruthenium nanoparticles from the precursor $[Ru(C_8H_{10})(C_8H_{12})]$

In the standard procedure 160 mg. of ruthenium precursor $[Ru(C_8H_{10})(C_8H_{12})]$ (0.508 mmol) were dissolved under argon at –110ºC (ethanol/N_2 bath) in a solution of 160 ml of tetrahydrofuran containing 0.1 equivalents of ligand in a closed pressure bottle. After pressurization at room temperature under 3 bars of hydrogen for 30 minutes, the initial yellow solution became black in a few minutes. The vigorous magnetic stirring and the hydrogen pressure were maintained for 18 hours. After that period of time, the hydrogen pressure was eliminated, and a drop of the colloidal solution was deposited under argon on a holey carbon covered copper grid for electron microscopy analysis. Precipitation with a tetrahydrofuran/pentane mixture at low temperature gave a black precipitate which was washed with pentane (2x 40 ml) and dried under vacuum. The colloids were characterized by TEM analysis, elemental analysis and WAXS.

Colloid.7 was synthesised according to the standard procedure from 160 mg of $[Ru(C_8H_{10})(C_8H_{12})]$ (0.508 mmol) and 54.2 mg of diphosphite **1** (0.051 mmol) in 160 ml of tetrahydrofuran. The nanoparticles synthesised were analysed by TEM (Transmission electron microscopy), WAXS (Wide-angle X-ray scattering) and elemental analysis. The elemental analysis of the black isolated nanoparticles of **Colloid.7** was 42.19%Ru, 1.86%P, 7.72%C, 1.18%H.

Colloid.8 was synthesised according to the standard procedure from 160 mg of $[Ru(C_8H_{10})(C_8H_{12})]$ (0.508 mmol) and 77.1 mg of diphosphite **3** (0.051 mmol) in 160 ml of tetrahydrofuran. The elemental analysis of the black isolated nanoparticles of **Colloid.8** was 44.67%Ru, 1.34%P, 2.40%Si, 24.82%C, 2.99%H.

Synthesis of rhodium nanoparticles from the precursor $[Rh(\eta^3\text{-}C_3H_5)_3]$

In the standard procedure 80 mg of rhodium precursor $[Rh(\eta^3\text{-}C_3H_5)_3]$ (0.354 mmol) were dissolved under argon at –110ºC (ethanol/N_2 bath) in a solution of 80 ml of tetrahydrofuran containing 0.2 equivalents of ligand in a closed pressure bottle. After pressurization at room temperature under 3 bars of hydrogen for 30 minutes, the initial yellow solution became black in one hour. The vigorous magnetic stirring and the hydrogen pressure were maintained for 18 hours. After that period of time, the hydrogen pressure was eliminated, and a drop of the colloidal solution was deposited under argon on a holey carbon covered copper grid for electron microscopy analysis. Precipitation with a tetrahydrofuran/pentane mixture at low temperature gave a black precipitate which was washed with pentane (2x 40 ml.) and dried under vacuum. The colloids were characterized by TEM analysis, elemental analysis and WAXS.

Colloid.9 was synthesised according to the standard procedure from 80 mg of $[Rh(\eta^3\text{-}C_3H_5)_3]$ (0.354 mmol) was 75.5 mg of diphosphite **1** (0.071 mmol) in 80 ml of tetrahydrofuran. The nanoparticles synthesised were analysed by TEM (Transmission electron microscopy), WAXS (Wide-angle X-ray scattering) and elemental analysis. The elemental analysis of the black isolated nanoparticles of **Colloid.9** was 34.23%Rh, 0.61%P, 4.70%C, 0.47%H.

Colloid.10 was synthesised according to the standard procedure from 80 mg of $[Rh(\eta^3\text{-}C_3H_5)_3]$ (0.354 mmol) and 107.4 mg of diphosphite **3** (0.071 mmol) in 80 ml of tetrahydrofuran. The nanoparticles synthesised were analysed by TEM (Transmission electron microscopy), WAXS (Wide-angle X-ray scattering) and elemental analysis. The elemental analysis of the black isolated nanoparticles of **Colloid.10** was 37.74%Rh, 2.48%P, 3.88 %Si, 6.79%C, 0.59%H.

Synthesis of rhodium nanoparticles from the precursor $[Rh(\mu\text{-}OMe)(COD)]_2$

In the standard procedure 160 mg. of rhodium precursor $[Rh(\mu\text{-}OMe)(COD)]_2$ (0.330 mmol) were dissolved under argon at –110ºC (ethanol/N_2 bath) in a solution of 160 ml of tetrahydrofuran containing 0.2 equivalents of ligand in a closed pressure bottle. After pressurization at room temperature under 3 bars of hydrogen for 30 minutes, the initial yellow solution became black in a few minutes. The vigorous magnetic stirring and the hydrogen pressure were maintained for 18 hours. After that period of time, the hydrogen pressure was eliminated, and a drop of the colloidal solution was deposited under argon on a holey carbon covered copper grid for electron microscopy analysis. Precipitation with a tetrahydrofuran/pentane mixture at low temperature gave a black precipitate which is washed with pentane (2x 40 ml.) and dried under vacuum. The colloids were characterized by TEM analysis, elemental analysis and WAXS.

Colloid.11. was synthesised according to the standard procedure from 80 mg of $[Rh(\mu\text{-}OMe)(COD)]_2$ (0.165 mmol) and 330.4 mg of PVP (polyvinylpyrrolidone MW= 40000, Rh/PVP 2.5% weight) in 80 ml of tetrahydrofuran. The nanoparticles synthesised were analysed by TEM (Transmission electron microscopy), WAXS (Wide-angle X-ray scattering) and elemental analysis. The elemental analysis of the grey isolated nanoparticles of **Colloid.11** was 9.31%Rh, 53.71%C, 7.46%H, 9.95%N.

Colloid.12 was synthesised according to the standard procedure from 160 mg of $[Rh(\mu\text{-}OMe)(COD)]_2$ (0.331 mmol) and 141.2 mg of diphosphite **1** (0.132 mmol) in 160 ml of tetrahydrofuran. The nanoparticles synthesised were analysed by TEM (Transmission electron microscopy), WAXS (Wide-angle X-ray scattering) and elemental analysis. The elemental analysis of the black isolated nanoparticles of **Colloid.12** was 73.69%Rh, 0.10%P, 2.84%C, 0.10%H.

Colloid.13 was synthesised according to the standard procedure from 160 mg of $[Rh(\mu\text{-}OMe)(COD)]_2$ (0.331 mmol) and 200.6 mg of diphosphite **3** (0.132 mmol) in

160 ml of tetrahydrofuran. The nanoparticles synthesised were analysed by TEM (Transmission electron microscopy), WAXS (Wide-angle X-ray scattering) and elemental analysis. The elemental analysis of the black isolated nanoparticles of **Colloid.13** was 16.71%Rh, 0.11%P, 5.24%Si, 4.59%C, 0.38%H.

Hydroformylation experiments

The catalytic precursors were prepared in a multiple reaction vessel autoclave in a glovebox. The experiments with colloidal systems were carried out with 3 mg. nanoparticle, $5.8x10^{-3}$ mmol of ligand and 5.8 mmol of styrene in 10 ml of toluene. The experiments with molecular systems were carried out from 0.009 mmol of $[Rh(acac)(CO)_2]$, 0.018 mmol of ligand and 1.8 mmol of styrene in 10 ml of toluene. After pressurising to the desired pressure with syngas and heating the autoclave to the reaction temperature, the reaction mixture was stirred for 24 h. Then the autoclave was cooled to room temperature and depressurised. The reaction mixture was analysed by gas chromatography. The aldehydes obtained from the hydroformylation were oxidised to carboxylic acids to determine the enantiomeric excess.

4.5 References

[1] G. Schmid, *Chem. Rev.* **1992**, *92*, 1709.

[2] L. N. Lewis, *Chem. Rev.* **1993**, *93*, 2693.

[3] G. Schmid, *Clusters and Colloids: From Theory to Applications* **1994**.

[4] L. J. De Jongh, *Physics and Chemistry of Metal Cluster Compounds*, Kluwer Academic Publisher, Dordrecht, **1994**.

[5] K. J. Klabunde, G. Cardenas-Trivino, *Active Metals: Preparation, Characterization, Applications* **1996**, 237.

[6] N. Toshima, T. Yonezawa, *New J. Chem.* **1998**, *22*, 1179.

[7] L. N. Lewis, *Catalysis by Di- and Polynuclear Metal Cluster Complexes* **1998**, 373.

[8] K. S. Weddle, J. D. Aiken III, R. G. Finke, *J. Am. Chem. Soc.* **1998**, *120*, 5653.

[9] G. Schmid, M. Bäumle, M. Geerkens, I. Heim, C. Osemann, T. Sawitowski, *Chem. Soc. Rev.* **1999**, *28*, 179.

[10] J. D. Aiken III, R. G. Finke, *J. Mol. Catal. A: Chem.* **1999**, *145*, 1.

[11] M. A. El-Sayed, *Acc. Chem. Res.* **2001**, *34*, 257.

[12] H. Bönnemann, R. M. Richards, *Eur. J. Inorg. Chem.* **2001**, 2455.
[13] D. L. Feldheim, C. A. Foss Jr., *Metal Nanoparticles* **2002**.
[14] A. Roucoux, J. Schulz, H. Patin, *Chem. Rev.* **2002**, *102*, 3757.
[15] J. A. Widegren, R. G. Finke, *J. Mol. Catal. A: Chem.* **2003**, *191*, 187.
[16] K. Philippot, B. Chaudret, *C. R. Chimie* **2003**, *6*, 1019.
[17] B. Chaudret, *C. R. Physique* **2005**, *6*, 117.
[18] T. Graham, *Phil. Trans. Roy. Soc.* **1861**, *151*, 183.
[19] M. Faraday, *Philos. Trans. R. Soc. London* **1857**, *147*, 145.
[20] G. Schmid, *Endeavour* **1990**, *14*, 172.
[21] J. Turkevich, G. Kim, *Science* **1970**, *169*, 873.
[22] J. Turkevich, P. C. Stevenson, J. Hillier, *Discussions of the Faraday Society* **1951**, 55.
[23] J. Turkevich, *Gold Bulletin* **1985**, *18*, 86.
[24] T. Leisner, C. Rosche, S. Wolf, F. Granzer, L. Woste, *Surface Review and Letters* **1996**, *3*, 1105.
[25] R. Tausch-Treml, A. Henglein, J. Lilie, *Ber. Bunsen-Ges. Phys. Chem.* **1978**, *82*, 1335.
[26] M. Michaelis, A. Henglein, *J. Phys. Chem.* **1992**, *96*, 4719.
[27] J. Rothe, J. Hormes, H. Bonnemann, W. Brijoux, K. Siepen, *J. Am. Chem. Soc.* **1998**, *120*, 6019.
[28] M. A. Watzky, R. G. Finke, *J. Am. Chem. Soc.* **1997**, *119*, 10382.
[29] J. A. Widegren, J. D. Aiken, S. Ozkar, R. G. Finke, *Chem. Mater.* **2001**, *13*, 312.
[30] M. A. Watzky, R. G. Finke, *Chem. Mater.* **1997**, *9*, 3083.
[31] B. J. Hornstein, R. G. Finke, *Chem. Mater.* **2004**, *16*, 139.
[32] B. J. Hornstein, R. G. Finke, *Chem. Mater.* **2004**, *16*, 3972.
[33] C. Besson, E. E. Finney, R. G. Finke, *Chem. Mater.* **2005**, *17*, 4925.
[34] C. Besson, E. E. Finney, R. G. Finke, *J. Am. Chem. Soc.* **2005**, *127*, 8179.
[35] R. G. Finke, *Metal Nanoparticles: Synthesis, Characterization and Applications*, Marcel Dekkers, New York, **2002**.
[36] R. J. Hunter, *Foundations of Colloid Science, Vol. 1*, Oxford University Press, New York, **1987**.
[37] M. E. Labib, *Colloids and Surfaces* **1988**, *29*, 293.
[38] D. H. Napper, *Polymeric Stabilization of Colloidal Dispersions*, Academic Press, London, **1983**.
[39] J. D. Aiken III, Y. Lin, R. G. Finke, *J. Mol. Catal. A: Chem.* **1996**, *114*, 29.
[40] Y. Lin, R. G. Finke, *J. Am. Chem. Soc.* **1994**, *116*, 8335.
[41] J. Schulz, A. Roucoux, H. Patin, *Chem. Eur. J.* **2000**, *6*, 618.
[42] V. Mevellec, B. Leger, M. Mauduit, A. Roucoux, *Chem. Commun.* **2005**, 2838.
[43] K. Esumi, T. Tano, K. Meguro, *Langmuir* **1989**, *5*, 268.

[44] T. Tano, K. Esumi, K. Meguro, *J. Colloid Interface Sci.* **1989**, *133*, 530.

[45] J. L. Marignier, J. Belloni, M. O. Delcourt, J. P. Chevalier, *Nature* **1985**, *317*, 344.

[46] K. Kurihara, J. Kizling, P. Stenius, J. H. Fendler, *J. Am. Chem. Soc.* **1983**, *105*, 2574.

[47] K. Torigoe, K. Esumi, *Langmuir* **1992**, *8*, 59.

[48] K. Esumi, A. Suzuki, N. Aihara, K. Usui, K. Torigoe, *Langmuir* **1998**, *14*, 3157.

[49] K. S. Suslick, M. W. Grinstaff, S.-B. Choe, A. A. Cichowlas, *Nature* **1991**, *353*, 414.

[50] K. S. Suslick, T. Hyeon, M. Fang, *Chem. Mater.* **1996**, *8*, 2172.

[51] Y. Koltypin, G. Katabi, X. Cao, R. Prozorov, A. Gedanken, *Journal of Non-Crystalline Solids* **1996**, *201*, 159.

[52] M. Andrews, G. A. Ozin, C. G. Francis, *Inorg. Synth.* **1981**, *22*, 116.

[53] K. J. Klabunde, P. L. Timms, P. S. Skell, S. Ittel, *Inorg. Synth.* **1979**, *19*, 59.

[54] M. T. Reetz, W. Helbig, *J. Am. Chem. Soc.* **1994**, *116*, 7401.

[55] M. T. Reetz, S. A. Quaiser, *Angew. Chem. Int. Ed.* **1995**, *34*, 2240.

[56] M. T. Reetz, W. Helbig, S. A. Quaiser, *Active Metals: Preparation, Characterization, Applications* **1996**, 279.

[57] P. S. Roberto Giordano, Philippe Kalck, Yolande Kihn, Joachim Schreiber, Christiane Marhic, Jean-Luc Duvail,, *European Journal of Inorganic Chemistry* **2003**, *2003*, 610.

[58] S. Ozkar, R. G. Finke, *J. Am. Chem. Soc.* **2002**, *124*, 5796.

[59] D. deCaro, T. O. Ely, A. Mari, B. Chaudret, E. Snoeck, M. Respaud, J. M. Broto, A. Fert, *Chem. Mater.* **1996**, *8*, 1987.

[60] J. S. Bradley, E. W. Hill, S. Behal, C. Klein, B. Chaudret, A. Duteil, *Chem. Mater.* **1992**, *4*, 1234.

[61] D. De Caro, J. S. Bradley, *New J. Chem.* **1998**, *22*, 1267.

[62] A. Duteil, R. Quéau, B. Chaudret, R. Mazel, C. Roucau, J. S. Bradley, *Chem. Mater.* **1993**, *5*, 341.

[63] J. S. Bradley, J. M. Millar, E. W. Hill, S. Behal, B. Chaudret, A. Duteil, *Faraday Discuss.* **1991**, *92*, 255.

[64] T. O. Ely, C. Amiens, B. Chaudret, E. Snoeck, M. Verelst, M. Respaud, J.-M. Broto, *Chem. Mater.* **1999**, *11*, 526.

[65] C. Pan, K. Pelzer, K. Philippot, Chaudret, F. Dassenoy, P. Lecante, M.-J. Casanove, *J. Am. Chem. Soc.* **2001**, *123*, 7584.

[66] O. Vidoni, K. Philippot, C. Amiens, B. Chaudret, O. Balmes, J. Malm, J. Bovin, F. Senocq, M. J. Casanove, *Angew. Chem. Int. Ed.* **1999**, *38*, 3736.

[67] M. Respaud, J. M. Broto, H. Rakoto, A. R. Fert, L. Thomas, B. Barbara, M. Verelst, E. Snoeck, P. Lecante, A. Mosset, J. Osuna, T. O. Ely, C. Amiens, B. Chaudret, *Phys. Rev. B* **1998**, *57*, 2925.

[68] M. Respaud, J. M. Broto, H. Rakoto, J. C. Ousset, J. Osuna, T. Ould Ely, C. Amiens, B. Chaudret, S. Askenazy, *Physica B* **1998**, *246-247*, 532.

[69] E. Ramírez-Meneses, *Synthèse et caractérisation de nanoparticules métalliques à base de Rhodium, Platine et Palladium, stabilisées par des ligands.* **2004**, Laboratoire de Chimie de Coordination du CNRS. (Toulouse).

[70] D. Wostek-Wojciechowska, J. K. Jeszka, C. Amiens, B. Chaudret, P. Lecante, *J. Colloid Interface Sci.* **2005**, *287*, 107.

[71] D. Zitoun, M. Respaud, M. C. Fromen, M. J. Casanove, P. Lecante, C. Amiens, B. Chaudret, *Phys. Rev. Lett.* **2002**, *89*.

[72] F. Dassenoy, M. J. Casanove, P. Lecante, C. Pan, K. Philippot, C. Amiens, B. Chaudret, *Phys. Rev. B* **2001**, *63*.

[73] F. Dassenoy, K. Philippot, T. Ould-Ely, C. Amiens, P. Lecante, E. Snoeck, A. Mosset, M. J. Casanove, B. Chaudret, *New J. Chem.* **1998**, *22*, 703.

[74] T. O. Ely, C. Pan, C. Amiens, B. Chaudret, F. Dassenoy, P. Lecante, M. J. Casanove, A. Mosset, M. Respaud, J. M. Broto, *J. Phys. Chem. B* **2000**, *104*, 695.

[75] C. Pan, F. Dassenoy, M. J. Casanove, K. Philippot, C. Amiens, P. Lecante, A. Mosset, B. Chaudret, *J. Phys. Chem. B* **1999**, *103*, 10098.

[76] K. Pelzer, O. Vidoni, K. Philippot, B. Chaudret, V. Collière, *Adv. Funct. Mater.* **2003**, *13*, 118.

[77] E. Ramirez, S. Jansat, K. Philippot, P. Lecante, M. Gomez, A. M. Masdeu-Bulto, B. Chaudret, *J. Organomet. Chem.* **2004**, *689*, 4601.

[78] M. Gomez, K. Philippot, V. Colliere, P. Lecante, G. Muller, B. Chaudret, *New J. Chem.* **2003**, *27*, 114.

[79] S. Jansat, M. Gomez, K. Philippot, G. Muller, E. Guiu, C. Claver, S. Castillon, B. Chaudret, *J. Am. Chem. Soc.* **2004**, *126*, 1592.

[80] J. D. Aiken, R. G. Finke, *J. Am. Chem. Soc.* **1999**, *121*, 8803.

[81] J. Dupont, G. S. Fonseca, A. P. Umpierre, P. F. P. Fichtner, S. R. Teixeira, *J. Am. Chem. Soc.* **2002**, *124*, 4228.

[82] J. U. Kohler, J. S. Bradley, *Langmuir* **1998**, *14*, 2730.

[83] H. Bönnemann, G. A. Braun, *Chem. Eur. J.* **1997**, *3*, 1200.

[84] J. U. Kohler, J. S. Bradley, *Catal. Lett.* **1997**, *45*, 203.

[85] H. Bönnemann, G. A. Braun, *Angew. Chem. Int. Ed.* **1996**, *35*, 1992.

[86] M. Studer, H. U. Blaser, C. Exner, *Adv. Synth. Catal.* **2003**, *345*, 45.

[87] X. B. Zuo, H. F. Liu, D. W. Guo, X. Z. Yang, *Tetrahedron* **1999**, *55*, 7787.

[88] W. Y. Yu, H. F. Liu, Q. Tao, *Chem. Commun.* **1996**, 1773.

[89] X. L. Yang, Z. L. Deng, H. F. Liu, *J. Mol. Catal. A: Chem.* **1999**, *144*, 123.

[90] M. H. Liu, W. Y. Yu, H. F. Liu, *J. Mol. Catal. A: Chem.* **1999**, *138*, 295.

[91] H. Hirai, H. Chawanya, N. Toshima, *Bull. Chem. Soc. Jpn.* **1985**, *58*, 682.

[92] W. Y. Yu, H. F. Liu, M. H. Liu, Z. J. Liu, *React. Funct. Polym.* **2000**, *44*, 21.

[93] G. S. Fonseca, J. D. Scholten, J. Dupont, *Synlett* **2004**, 1525.

[94] J. A. Widegren, R. G. Finke, *Inorg. Chem.* **2002**, *41*, 1558.
[95] J. Schulz, A. Roucoux, H. Patin, *Chem. Commun.* **1999**, 535.
[96] A. Roucoux, J. Schulz, H. Patin, *Adv. Synth. Catal.* **2003**, *345*, 222.
[97] E. Schulz, S. Levigne, A. Roucoux, H. Patin, *Adv. Synth. Catal.* **2002**, *344*, 266.
[98] V. Mevellec, A. Roucoux, *Inorg. Chim. Acta* **2004**, *357*, 3099.
[99] V. Mevellec, A. Roucoux, E. Ramirez, K. Philippot, B. Chaudret, *Adv. Synth. Catal.* **2004**, *346*, 72.
[100] C. W. Scheeren, G. Machado, J. Dupont, P. F. P. Fichtner, S. R. Texeira, *Inorg. Chem.* **2003**, *42*, 4738.
[101] C. S. Consorti, F. R. Flores, J. Dupont, *J. Am. Chem. Soc.* **2005**, *127*, 12054.
[102] E. T. Silveira, A. P. Umpierre, L. M. Rossi, G. Machado, J. Morais, G. V. Soares, I. L. R. Baumvol, S. R. Teixeira, P. F. P. Fichtner, J. Dupont, *Chem. Eur. J.* **2004**, *10*, 3734.
[103] G. S. Fonseca, A. P. Umpierre, P. F. P. Fichtner, S. R. Teixeira, J. Dupont, *Chem. Eur. J.* **2003**, *9*, 3263.
[104] M. T. Reetz, G. Lohmer, *Chem. Commun.* **1996**, 1921.
[105] M. T. Reetz, R. Breinbauer, K. Wanninger, *Tetrahedron Lett.* **1996**, *37*, 4499.
[106] M. T. Reetz, S. A. Quaiser, C. Merk, *Chem. Ber.* **1996**, *129*, 741.
[107] M. T. Reetz, R. Breinbauer, P. Wedemann, P. Binger, *Tetrahedron* **1998**, *54*, 1233.
[108] Y. Li, X. M. Hong, D. M. Collard, M. A. El-Sayed, *Org. Lett.* **2000**, *2*, 2385.
[109] Y. Li, M. A. El-Sayed, *J. Phys. Chem. B* **2001**, *105*, 8938.
[110] Y. Li, E. Boone, M. A. El-Sayed, *Langmuir* **2002**, *18*, 4921.
[111] R. Narayanan, M. A. El-Sayed, *J. Am. Chem. Soc.* **2003**, *125*, 8340.
[112] R. Narayanan, M. A. El-Sayed, *J. Phys. Chem. B* **2004**, *108*, 8572.
[113] R. Narayanan, M. A. El-Sayed, *J. Catal.* **2005**, *234*, 348.
[114] R. Narayanan, M. A. El-Sayed, *Langmuir* **2005**, *21*, 2027.
[115] R. Narayanan, M. A. El-Sayed, *J. Phys. Chem. B* **2005**, *109*, 12663.
[116] C. C. Cassol, A. P. Umpierre, G. Machado, S. I. Wolke, J. Dupont, *J. Am. Chem. Soc.* **2005**, *127*, 3298.
[117] K. Nasar, F. Fache, M. Lemaire, J. C. Beziat, M. Besson, P. Gallezot, *J. Mol. Catal.* **1994**, *87*, 107.
[118] X. B. Zuo, H. F. Liu, M. H. Liu, *Tetrahedron Lett.* **1998**, *39*, 1941.
[119] V. Mevellec, C. Mattioda, J. Schulz, J. P. Rolland, A. Roucoux, *J. Catal.* **2004**, *225*, 1.
[120] Y. L. Huang, J. R. Chen, H. Chen, R. X. Li, Y. Z. Li, L. E. Min, X. J. Li, *J. Mol. Catal. A* **2001**, *170*, 143.
[121] X. B. Zuo, H. F. Liu, C. Yue, *J. Mol. Catal. A* **1999**, *147*, 63.
[122] G. J. H. Buisman, M. E. Martin, E. J. Vos, A. Klootwijk, P. C. J. Kamer, P. W. N. M. Van Leeuwen, *Tetrahedron: Asymmetry* **1995**, *6*, 719.

[123] O. Pamies, G. Net, A. Ruiz, C. Claver, *Tetrahedron; Asymmetry* **1999**, *10*, 2007.

[124] To be published. See Chapter 2.

[125] O. Pamies, M. Dieguez, G. Net, A. Ruiz, C. Claver, *Chem. Commun.* **2000**, 2383.

[126] P. Pertici, G. Vitulli, *Inorg. Synth.* **1983**, *22*, 178.

[127] M. D. Fryzuk, W. E. Piers, in *Organomet. Synth., Vol. 3* (Eds.: R. B. King, J. J. Eisch), Elsevier, Amsterdam, **1986**, p. 128.

[128] W. A. Herrmann, in *Synthetic Methods of Organometallic and Inorganic Chemistry* (Ed.: W. A. Herrmann), Stuttgart, **1996**, p. 38.

[129] R. Uson, L. A. Oro, J. A. Cabeza, *Inorg. Synth.* **1985**, *23*, 126.

[130] T. D. Ewers, A. K. Sra, B. C. Norris, R. E. Cable, C.-H. Cheng, D. F. Shantz, R. E. Schaak, *Chem. Mater.* **2005**, *17*, 514.

[131] H. P. Liang, H. M. Zhang, J. S. Hu, Y. G. Guo, L. J. Wan, C. L. Bai, *Angew. Chem. Int. Ed.* **2004**, *43*, 1540.

[132] G. Schmid, A. Lehnert, J. Malm, J. Bovin, *Angew. Chem. Int. Ed.* **1991**, *30*, 874.

[133] Y. J. Song, Y. Yang, C. J. Medforth, E. Pereira, A. K. Singh, H. F. Xu, Y. B. Jiang, C. J. Brinker, F. van Swol, J. A. Shelnutt, *J. Am. Chem. Soc.* **2004**, *126*, 635.

[134] P. W. N. M. van Leeuwen, C. Claver, *Rhodium Catalyzed Hydroformylation, Vol. 22*, Kluwer Academic, **2000**.

[135] J. A. Widegren, R. G. Finke, *J. Mol. Catal. A: Chem.* **2003**, *198*, 317.

Conclusions

The conclusions of Chapter 2, *Carbohydrate derivative diphosphite ligands in asymmetric catalysis*, can be summarised as follows:

- New diphosphite ligands (**74-76**) with C_2-symmetry and a tetrahydrofuran backbone have been synthesised in moderate to good yields starting from D-glucosamine, D-glucitol and (2*S*,3*S*)-diethyl tartrate. The structure of diphosphite ligands **74**-**76** was determined by one-dimensional ^{1}H, ^{13}C and ^{31}P NMR. Monocrystals of **74a** suitable for X-ray diffraction were obtained and the structure of **74a** could be proved unambiguously by single crystal X-ray diffraction. The tetrahydrofuran backbone showed a twisted conformation.

- The Rhodium cationic complexes of diphosphite ligands of general formula [Rh(cod)(L)]BF_4, (L= **74a**-**c**, **74'a**,**b**, **75a**, **75'a** and **76a**-**b**) were prepared by reacting [Rh(cod)$_2$]BF_4 with the respective ligands. The structure of the rhodium complexes **90-92** was elucidated by NMR spectroscopic techniques. Monocrystals of the complexes [Rh(cod)(**74a**)]BF_4 (**90a**) and [Rh(cod)(**75'a**)]BF_4 (**91'a**), suitable for X-ray diffraction, were obtained by slow diffusion of hexane into a CH_2Cl_2 solution of the complex. The rhodium atom is coordinated in both molecules in a slightly distorted square planar geometry.

- This new family of diphosphite ligands has been applied to the rhodium-catalysed asymmetric hydroformylation of styrene and related substituted vinyl arenes. High regioselectivities to the branched aldehyde (up to 90%) and moderate enantioselectivities (up to 46%ee) were obtained in the asymmetric hydroformylation of styrene. In the hydroformylation of *p*-methoxystyrene was obtained 60% of enantioselectivity. The configuration and substitution of the remote stereocenters at positions 2 and 5 of the tetrahydrofuran ring were observed to have a considerable influence on the enantioselectivity. The most significant result is that the configuration of

the major isomer obtained in the hydroformylation reaction can be controlled by changing the configuration of these stereocenters.

- The intermediate species in hydroformylation with diphosphite ligands **74a**, **74b**, **74'a**, **75a**, **75'a** and **76a** were studied by high pressure-NMR spectroscopy. These species were prepared *in situ* under hydroformylation conditions, observing that the formation of the hydridorhodiumcarbonyl specie was very slow. The small $^{2}J_{P\text{-}H}$ coupling constants (2.0 to 9.0 Hz) and the large $^{1}J_{Rh\text{-}P}$ coupling constants (230.0 to 234.1 Hz) indicate that the ligands coordinate in an equatorial-equatorial fashion in the trigonal-bipyramidal hydridorhodiumcarbonyl species. The low temperature study of the hydridorhodiumcarbonyl species under hydroformylation conditions detected that the phosphorous atoms were non equivalent, which proved the C_1-symmetry of these complexes.

- Rhodium complexes were tested in the asymmetric hydrogenation of methyl acetamidoacrylate. The conversions and the enantioselectivities were low and were mainly influenced by the substitution in the biphenyl moiety and by the configuration of the remote centres at positions 2 and 5 of the tetrahydrofuran ring.

The conclusions of Chapter 3, *Rhodium-diphosphite catalysed hydroformylation of allylbenzene and propenylbenzene derivatives*, can be summarised as follows:

- The use of rhodium-diphosphite based systems in the hydroformylation of *trans*-anethole **1a** and estragole **2a** has not been previously reported. In this study, rhodium-diphosphite system **6** was used in the hydroformylation of *trans*-anethole **1a** and led to high selectivities on aldehyde **3a** (as high as 86%) under mild conditions (60ºC, 40 bar). This is not so different from the diphosphine ligands used before which afforded up to 93% of aldehyde **3a** with BISBI ligand. We also observed that our diphosphite **6** based system is more active in this reaction than phosphine ligands in similar reaction conditions. When rhodium-diphosphite **7** was used in the *trans*-anethole **1a** hydroformylation, the regioselectivity was lower than when

diphosphite **6** was used. We attributed this to the formation of a seven-seven member chelate ring of diphosphite **7** when it coordinates to the rhodium. On the other hand, in the hydroformylation of this substrate new chiral centers (in aldehydes **3a** and **4a**) are formed by the introduction of formyl groups. We also studied the asymmetric induction of the two diphosphite chiral ligands **6** and **7** in this reaction. We only observed low enantioselectivities in the case of diphosphite **6** in *trans*-anhetole **1a** hydroformylation.

- In the hydroformylation of estragole **2a**, we used rhodium-diphosphite **6** ligand. In this case, regioselectivities on the branched aldehyde **4a** were low (47% of **4a** and 53% of **5a**) when excess of ligand was added. We also investigated the enantioselectivity but we did not observe asymmetric induction in the conditions studied.

The conclusions of Chapter 4, *Metal nanoparticles stabilized by chiral ligands with carbohydrate backbone*, can be summarised as follows:

- New palladium, ruthenium and rhodium nanoparticles have been successfully synthesised in the presence of carbohydrate derivative ligands (**1-4**)**.** We observed that the shape, size and dispersion of the nanoparticles depend strongly on the metal precursor and the stabiliser used.

- Palladium nanoparticles were synthesised from $[Pd_2(dba)_3]$ with phosphite ligands **2** and **3** and phosphine-phosphite ligand **4** as stabilisers. The synthesis was done following the organometallic approach, at room temperature and under 3 bars of hydrogen pressure. In the presence of diphosphite ligands, small nanoparticles (diameter *ca*. 3.5-4 nm) well-crystallised and contain a few agglomerates were obtained. When phosphine-phosphite ligand **4** was used as stabiliser, smaller nanoparticles could be prepared. This indicates that the nature of the ligand has a strong influence on the morphology of the nanoparticles synthesised. We also studied the effect of the temperature and the palladium/ligand ratio on the nanoparticles stabilised with phosphine-phosphite ligand **4**. We observed

that an increase in the temperature or the quantity of ligand did not improve the results and led to more agglomeration and no well crystallisation.

- Ruthenium nanoparticles have also been synthesised by the organometallic approach using $[Ru(C_8H_{10})(C_8H_{12})]$ as metal precursor and diphosphite ligands **1** and **3** as stabilisers, at room temperature under 3 bars of hydrogen pressure. When diphosphite ligand **1** was used as stabiliser, nanoparticles were well-crystallised with a mean diameter *ca*. 3 nm. However, when diphosphite ligand **3** was used not well-crystallised nanoparticles were obtained.

- Rhodium nanoparticles were obtained by decomposition of two different rhodium precursors, $[Rh(\eta^3\text{-}C_3H_5)_3]$ and $[Rh(\mu\text{-}OMe)(COD)]_2$, following the organometallic approach. The rhodium nanoparticles produced from $[Rh(\eta^3\text{-}C_3H_5)_3]$ were synthesised in tetrahydrofuran in the presence of diphosphite ligands **1** and **3** as stabilisers at room temperature and under 3 bars of hydrogen pressure. In these conditions small and well-crystallised nanoparticles were obtained. The rhodium nanoparticles synthesised from the precursor $[Rh(\mu\text{-}OMe)(COD)]_2$ were stabilised with PVP (polyvinylpyrrolidone MW= 40000) and diphosphite ligands **1** and **3**, giving rise, respectively, to small and well-crystallised nanoparticles with PVP and large particles with diphosphite ligands. Although further study is required if it is to be determined whether these particles are really large, porous and pollycrystalline or whether they consist of small individual nanoparticles, we can conclude that the nature of the metal precursor affects the particles synthesised.

- In collaboration with the Universitat de Barcelona and Laboratoire de Chimie de Coordination CNRS (Toulouse), we have studied the application of palladium nanoparticles stabilised with diphosphite ligands **2** and **3**, **Coll.2** and **Coll.3**, respectively, in palladium-catalysed allylic alkylation of rac-3-acetoxy-1,3-diphenyl-1-propene with dimethyl malonate. **Colloid.2** system was not stable under catalytic conditions showing not reproducible results.

Colloid.3 system led to an enantiomeric excess of >98%(*S*) in II with high kinetic resolution in the substrate (rac-I) (98% (*S*) in the remaining substrate) at 73% of conversion after 9 hours of reaction. This behaviour is similar to that of the previously reported for **Colloid.1**.

- We studied the use of rhodium nanoparticles, synthesised from [Rh(μ-OMe)(COD)]$_2$ in the presence of diphosphite ligands **1** and **3** (**Colloid.12** and **Colloid.13**, respectively), as catalyst in the styrene hydroformylation reaction. In both cases the activities were very low. The introduction of an excess of ligand increased the regioselectivity and enantioselectivity. The respective molecular system of **Colloid.12**, **Molecular.12**, and the poisoning test were studied in order to exclude the possible formation of homogeneous catalyst in the colloidal system. The results are difficult to analyse and further analysis are needed to be able to clearly conclude.

Resum

En els darrers anys, la creixent demanda de compostos enantiomèricament purs, ja sigui en el camp dels fàrmacs, agroquímics, additius o fragàncies entre d'altres, ha suposat un gran desafiament per la comunitat científica. Dels diferents mètodes per produir compostos enantiomèricament purs, la catàlisi homogènia asimètrica és cada cop una estratègia més emprada, com es reflecteix en les nombroses publicacions en aquest camp. Habitualment aquesta mètode consisteix en la transformació d'un substrat proquiral en presencia d'un metall de transició modificat amb un lligand quiral que actua com a catalitzador. En el camp de la catàlisi asimètrica el desenvolupament de nous lligands quirals és, doncs, essencial.

El carbohidrats han estat molt utilitzats en síntesi orgànica tan com a material de partida com a auxiliars quirals degut a què aquests compostos es presenten de forma natural com a compostos enantiomèricament purs i presenten una gran riquesa tan d'estructures carbonades com de grups funcionals, i molt important també el fet de que són compostos accessibles econòmicament. Tot i els avantatges exposats fins ara, fins fa poc es trobaven pocs exemples en la seva utilització com a precursors de lligands en catàlisi asimètrica. A finals dels anys 70 és quan es troben els primers exemples de lligands derivats de carbohidrats. A partir d'aquests primers exemples s'obre un nou ventall de possibilitats per a la síntesi de lligands quirals. Habitualment aquests tipus de lligands tenen una estructura bàsica de piranosa (anell de sis baules) o furanosa (anell de cinc baules) i es funcionalitzen fàcilment com a fosfits, fosfonits o fosfinits degut a la presencia de funcions hidroxíliques en l'esquelet. En la literatura científica es troben nombrosos exemples d'aplicació de lligands derivats de carbohidrats amb els quals s'han obtingut excel·lents resultats en diferents reaccions catalítiques.

La major part de lligands derivats de carbohidrats presenten simetria C_1. En els últims temps s'han sintetitzat lligands amb simetria C_2 derivats de carbohidrats, aquests tenen l'avantatge respecte els anteriors de que es redueixen el número d'espècies catalítiques, fet que fa que es formin menys espècies isòmeres i així fan augmentar la selectivitat del procés. Recentment, s'han sintetitzat nous lligands difosfinit amb simetria C_2 que presenten estructura de tetrahidrofurà amb quatre substituents en l'anell. Aquests lligands s'obtenen fàcilment a partir de la D-

glucosamina i del D-glucitol. La seva utilització en la hidrogenació asimètrica de substrats proquirals ha donat excel·lents resultats.

Així doncs, una part de la tesi que es presenta s'ha centrat en la síntesi de nous difosfits derivats de carbohidrats, del D-glucitol i de la D-glucosamina, i de la seva aplicació com a lligands de catalitzadors homogenis quirals en diferents reaccions.

En el capítol 2 es discuteix la síntesi i caracterització de nous lligands difosfit. Aquesta nova sèrie de lligands modulables es caracteritza per tenir estructura de furanòsid amb simetria C_2, on es poden introduir diferents substituents en l'anell i en els àtoms de fòsfor i canviar la configuració dels estereocentres de les posicions 2 i 5 de l'anell tetrahidrofurà. També s'estudien els respectius compostos de coordinació de rodi. Els lligands difosfit s'han utilitzat en la reacció d'hidroformilació asimètrica de l'estirè i d'altres substrats relacionats catalitzada per rodi. Els complexes de rodi s'han emprat com a catalitzadors en la reacció de hidrogenació asimètrica de l' α-acetamidoacrilat de metil.

Els lligands difosfit s'han sintetitzat a partir del corresponent diol en presència d'excés del corresponent fosforoclorhidrit i piridina obtenint de moderats a bons rendiments. Els compostos intermedis diol s'han sintetitzat d'acord a rutes de sintesi prèviement descrites a la bibliografia a partir de la D-glucosamina, del D-glucitol i del (2*S*,3*S*)-tartrat de dietil. Els compostos s'han caracteritzat per espectroscòpia de ressonància magnètica nuclear monodimensional ^{1}H, ^{13}C i ^{31}P i les senyals s'han assignat inequívocament per tècniques bidimensionals COSY i HSQC. Els complexes de rodi $[Rh(cod)(L)]BF_4$, on L és un lligand difosfit prèviament descrit, s'han sintetitzat per reacció del complex de rodi $[Rh(cod)_2]BF_4$ en diclorometà en presència del corresponent lligand. Els complexes s'han caracteritzat per espectroscòpia de ressonància magnètica nuclear monodimensional ^{1}H, ^{13}C i ^{31}P i les senyals s'han assignat inequívocament per tècniques bidimensionals COSY i HSQC. La mononuclearitat del complexes es va confirmar per espectroscòpia MALDI-Tof.

Els lligands difosfit derivats de carbohidrats s'han emprat en la reacció de hidroformilació asimètrica d'estirè catalitzada per rodi. Els sistemes Rh/difosfit han

proporcionat moderades activitats i altes regioselectivitats en l'aldehid 2-fenilpropanal. Les enantioselectivitats observades en aquests sistemes van ser moderades (fins un ee del 46 % (*S*)) i fortament influïdes per la natura del lligand. Es va observar que eren necessaris grups voluminosos *terc*-butil en posició *orto* dels anells bifenil units als fòsfor per obtenir un sistema enantioselectiu. En general els lligands que contenen grups metoxi en posició *para* en els grups bifenil units al fòsfor mostren millors excessos enantiomèrics que els corresponents lligands que tenen un grup *terc*-butil en dita posició. Els substituents de l'anell i la seva configuració influeixen en el sentit de la inducció asimètrica; amb els lligands D-manitol amb substituents *terc*-butildifenilsilil s'obté majoritàriament el producte hidroformilat (*S*) mentre que el conté grups metil en les mateixes posició obté majoritàriament el producte (*R*), en canvi el lligands derivats del L-iditol es va observar la tendència contraria; amb substituents *terc*-butildifenilsilil s'obté majoritàriament el producte hidroformilat (*R*) mentre que el conté grups metil en les mateixes posició obté majoritariament el producte (*S*). Així doncs, s'observen efectes enfrontats entre la configuració dels esterocentres 2 i 5 de l'anell tetrahidrofurà i dels substituents en aquestes posicions, mostrant-se millors amb els lligands que contenen el grup voluminós *terc*-butildifenilsilil. S'ha estudiat també la hidroformilació de diversos vinilarens, 4-metoxiestirè, 4-flúorestirè i del 2-vinilnaftalè, amb el lligand que mostra millors enantioselectivitats en la hidoformilació d'estirè, derivat del D-manitol amb substituents *terc*-butildifenilsilil. S'han obtingut fins una del 60% (*S*) d'excés enantiomèric en la hidroformilació del 4-metoxiestirè.

També s'han estudiat les espècies intermèdies de la reacció de hidroformilació amb els lligands difosfit mitjançant RMN d'alta pressió. En tots el casos estudiats s'ha observat la formació del complex $[RhH(CO)_2(L)]$ (L: difosfit), que és la espècie considerada generalment com el *resting state* en la reacció d'hidroformilació i que s'assumeix que té una estructura de bipiràmide trigonal on l'hidrur es coordina en posició axial. En el RMN $^{31}P\{^1H\}$ s'ha observat un doblet al voltant dels 155 ppm amb una constant d'acoblament rodi-fòsfor d'uns 230 Hz, i en el RMN ^1H un multiplet, corresponent a l'hidrur, a uns –10 ppm mostrant una $^1J_{Rh-H}$ entre 2 i 4 Hz i una $^2J_{P-H}$ entre 2 i 9 Hz. Aquest valors indiquen que en aquest complex tots els lligands difosfit estudiats es coordinen en posició bisequatorial. Encara que els

lligands tinguin simetria C_2, aquesta es perd quant es forma el complex $[RhH(CO)_2(L)]$ (L: difosfit). En tots el casos es van detectar doblets amples a temperatura ambient, que indiquen o bé que hi ha un equilibri fluxional o bé que els desplaçaments químics d'ambdós àtoms de fòsfor coincideixen accidentalment. Es per això que es va realitzar l'estudi a baixa temperatura de les espècies$[RhH(CO)_2(L)]$ (L: difosfit). En tots els casos es va observar un eixamplament de les senyals i en alguns casos es van arribar a resoldre les senyals de RMN $^{31}P\{^1H\}$ al voltant dels –100ºC. En aquests casos es van observar dos doble doblets que indicaven que l'equilibri fluxional s'aturava i es distingien els dos fòsfors, indicant les diferents constants d'acoblament que la coordinació bisequatorial es mantenia.

Els complexes de rodi $[Rh(cod)(L)]BF_4$ (L: difosfit) s'han emprat com a catalitzadors en la reacció d'hidrogenació asimètrica de l' α-acetamidoacrilat de metil. En general s'han observat baixes activitats i enantioselectivitats. La estructura del lligand va afectar considerablement a l'enantioselectivitat; mentre que els lligands amb estructura del D-manitol obtenien majoritàriament el producte hidrogenat (*R*), els lligands amb esructura de L-iditol obtenien majoritàriament el producte hidrogenat (*S*).

La reacció d'hidroformilació alilbenzens i propenilbenzens es una eina important per a obtenir intermedis d'alt valor afegit de la indústria farmacèutica i cosmètica. En el capítol 3 s'ha estudiat la hidroformilació asimètrica de alilbenzens i propenilbenzens catalitzada per rodi modificat amb lligands difosfit derivats de carbohidrats, ja que fins ara només s'havien estudiat amb sistemes basats amb difosfines. En la hidroformilació de l'anetol (propenilbenzè), amb el sistema Rh/difosfit, es van obtenir elevades regioselectivitats en el producte α-hidroformilat, fins a un 86%, observant-se millors activitats que les obtingudes per sistemes basats difosfines en condicions semblats, prèviament publicats. Només en algun cas es va observar enantioselectivitat. En la hidroformilació de l'estragol (alilbenzè), es van obtenir regioselectivitats moderades, 47% en l'isòmer β i 53% en l'isòmer γ, i en cap cas es van observar excessos enantiomèrics.

Recentment, l'interès per les propietats catalítiques dels col·loides de metalls de transició ha crescut. Aquest fet es degut a la gran superfície específica de les nanopartícules metàl·liques, que fa que un gran nombre d'àtoms metàl·lics estiguin disponibles per als substrats. S'ha demostrat que aquest tipus de compost és eficient com a catalitzador en diferents reaccions catalítiques. Generalment s'ha aplicat a reaccions que no són, o bé que ho són poc, catalitzades per espècies moleculars, com per exemple la hidrogenació d'hidrocarburs aromàtics. Encara que també s'han utilitzat en reaccions d'hidrogenació d'altres substrats i en reaccions d'acoblament carboni-carboni, entre d'altres. Més recentment, les nanopartícules metàl·liques s'han aplicat a reaccions catalítiques enantioselectives. Ha destacar els resultats obtinguts en la reacció de alquilació alílica catalitzada per nanopartícules de pal·ladi, on es van obtenir enantioselectivitats de més d'un 95% amb resolució cinètica en el substrat. Aquestes nanopartícules van ser sintetitzades a través de l'aproximació organometàl·lica, desenvolupada per Chaudret i colaboradors, en presència d'un difosfit quiral derivat de la D-xylosa.

Degut a aquests bons resultats, un dels objectius de la tesi que es presenta és la síntesi de nanopartícules metàl·liques de pal·ladi estabilitzades per lligands derivats de carbohidrats mitjançant l'aproximació organometàl·lica, i per extensió la síntesi de naopartícules metàl·liques de rodi i ruteni en presència d'aquest tipus de lligand pel mateix mètode. Així com l'aplicació d'aquestes nanopartícules com a catalitzadors en reaccions catalítiques enantioselectives.

S'han sintetizat nanopartícules de pal·ladi a partir del precursor metàl·lic $[Pd_2(dba)_3]$ en presència de tres lligand, dos difosfits i un lligand fosfina-fosfit, derivats de carbohidrats i amb similar estructura de furanòsid, sota 3 bars de pressió d'hidrogen. Les nanopartícules van ésser caracteritzades per TEM (Microscòpia electrònica de transmissió), WAXS (Dispersió de raigs X a grans angles) i anàlisi elemental. En tots el casos es van obtenir estructures ben cristal·litzades, estructura ccc del pal·ladi metàl·lic, amb diàmetre mitjà de uns 4 nm per les nanopartícules estabilitzades per els lligands difosfit i d'aproximadament 2 nm per les nanopartícules de pal·ladi estabilitzades amb el lligands fosfina-fosfit.

La síntesi de nanopartícules de ruteni es va realitzar emprant la mateixa metodologia utilitzant com a precursor metàl·lic el complex $[Ru(C_8H_{10})(C_8H_{12})]$. La síntesi es va dur a terme en presencia de diferents lligands difosfit. Les nanopartícules obtingudes es van caracteritzar per TEM, WAXS i anàlisi elemental. En un cas, amb el lligand derivat de la D-xylosa, es van obtenir nanoparícules ben cristal·litzades amb un diàmetre mitjà d'aproximadament 3 nm, en canvi quan es va emprar l'altre difosfit, derivat del D-glucitol, les nanopartícules obtingudes no estaven ben cristal·litzades.

Les nanopartícules de rodi es van sintetitzar a partir de dos precursors metàl·lics diferents, $[Rh(\eta^3\text{-}C_3H_5)_3]$ and $[Rh(\mu\text{-}OMe)(COD)]_2$, en presencia de dos lligands difosfit, seguint el mateix procediment que amb els altres metalls. Les nanopartícules es van caracteritzar per TEM, WAXS i anàlisi elemental. Quan es va utilitzar $[Rh(\eta^3\text{-}C_3H_5)_3]$ com a precursor metàl·lic, es van obtenir petites nanopartícules ben cristal·litzades mentre que amb $[Rh(\mu\text{-}OMe)(COD)]_2$ es van obtenir partícules grans, què o bé estan formades per petites nanopartiícules o bé són partícules grans poroses i policristal·lines.

Les nanopartícules de rodi es van utilitzar com a catalitzadors de la reacció asimètrica d'hidroformilació d'estirè. Es van obtenir baixes conversions i la regio- i enantioselectivitat van augmentar quan es va afegir excés del corresponent lligand. Es va estudiar del corresponent sistema molecular, diluït o no, i es van realitzar test d'enverinament del catalitzador amb mercuri i disulfur de carboni per tal de excloure la possibilitat de la formació de sistema homogeni quan s'utilitza el sistema co·loïdal. Els resultats van ser difícils d'analitzar i més anàlisis són necessaris per tal de distingir quina espècies és la responsable de l'activitat catalítica.

Appendix

Table 1. Bond lengths [Å] and angles [°] for **74a**

Si(1)-O(2)	1.6440(14)
Si(1)-C(6)	1.8797(19)
Si(1)-C(12)	1.8825(17)
Si(1)-C(18)	1.892(2)
O(1)-C(1)	1.435(3)
O(1)-C(4)	1.442(3)
C(1)-C(5)	1.519(2)
C(1)-C(2)	1.525(2)
Si(2)-O(3)	1.6456(14)
Si(2)-C(29)	1.878(2)
Si(2)-C(23)	1.8809(18)
Si(2)-C(93)	1.897(2)
C(2)-O(13)	1.429(2)
C(2)-C(3)	1.506(2)
O(2)-C(5)	1.422(2)
P(1)-O(13)	1.6180(15)
P(1)-O(4)	1.6294(15)
P(1)-O(5)	1.6474(16)
C(3)-O(12)	1.428(2)
C(3)-C(4)	1.525(2)
O(3)-C(22)	1.420(3)
P(2)-O(12)	1.6217(14)
P(2)-O(7)	1.6245(17)
P(2)-O(6)	1.6479(16)
C(4)-C(22)	1.510(2)
O(4)-C(36)	1.394(2)
O(5)-C(50)	1.392(2)
O(6)-C(65)	1.397(2)
C(6)-C(7)	1.400(3)
C(6)-C(11)	1.409(3)
C(7)-C(8)	1.398(3)
O(7)-C(76)	1.399(2)
C(8)-C(9)	1.392(4)
C(9)-C(10)	1.394(4)
C(10)-C(11)	1.391(3)
C(12)-C(13)	1.393(2)
C(12)-C(17)	1.410(3)
C(13)-C(14)	1.400(3)
C(14)-C(15)	1.385(3)
C(15)-C(16)	1.396(3)
C(16)-C(17)	1.393(3)
C(18)-C(20)	1.535(3)
C(18)-C(19)	1.536(3)
C(18)-C(21)	1.540(3)
C(23)-C(24)	1.405(2)
C(23)-C(28)	1.410(3)
C(24)-C(25)	1.396(3)
C(25)-C(26)	1.389(3)
C(26)-C(27)	1.401(3)
C(27)-C(28)	1.396(3)
C(29)-C(34)	1.398(3)
C(29)-C(30)	1.401(3)
C(30)-C(31)	1.397(3)
C(31)-C(32)	1.401(3)
C(32)-C(33)	1.386(4)
C(33)-C(34)	1.394(3)
C(36)-C(37)	1.397(2)
C(36)-C(41)	1.416(2)
C(37)-C(38)	1.410(2)
C(37)-C(51)	1.486(2)
C(38)-C(39)	1.390(2)
C(39)-C(40)	1.402(2)
C(39)-C(42)	1.535(2)
C(40)-C(41)	1.405(3)
C(41)-C(46)	1.547(2)
C(42)-C(44)	1.522(3)
C(42)-C(43)	1.535(3)
C(42)-C(45)	1.536(3)
C(46)-C(48)	1.522(4)
C(46)-C(47)	1.542(3)
C(46)-C(49)	1.546(3)
C(50)-C(51)	1.399(2)
C(50)-C(55)	1.408(2)
C(51)-C(52)	1.396(2)
C(52)-C(53)	1.399(2)
C(53)-C(54)	1.408(3)
C(53)-C(56)	1.535(3)
C(54)-C(55)	1.401(3)
C(55)-C(60)	1.539(3)
C(56)-C(57)	1.531(4)
C(56)-C(58)	1.531(3)
C(56)-C(59)	1.547(4)
C(60)-C(63)	1.530(4)
C(60)-C(61)	1.548(3)
C(60)-C(62)	1.556(3)
C(65)-C(70)	1.399(3)
C(65)-C(66)	1.402(3)
C(66)-C(67)	1.399(2)
C(66)-C(75)	1.488(3)
C(67)-C(68)	1.395(3)
C(68)-C(69)	1.398(3)
C(68)-C(89)	1.540(3)
C(69)-C(70)	1.413(3)
C(70)-C(71)	1.541(3)
C(71)-C(72)	1.532(3)
C(71)-C(74)	1.547(3)
C(71)-C(73)	1.548(3)
C(75)-C(76)	1.396(3)
C(75)-C(80)	1.405(2)
C(76)-C(77)	1.400(3)
C(77)-C(78)	1.395(3)
C(77)-C(81)	1.556(3)
C(78)-C(79)	1.407(3)
C(79)-C(80)	1.385(3)
C(79)-C(85)	1.534(3)
C(81)-C(82)	1.495(4)
C(81)-C(84)	1.517(4)
C(81)-C(83)	1.538(5)
C(85)-C(88)	1.526(4)
C(85)-C(86)	1.537(4)
C(85)-C(87)	1.540(4)
C(89)-C(90)	1.532(4)
C(89)-C(92)	1.535(3)
C(89)-C(91)	1.545(3)
C(93)-C(94)	1.529(3)
C(93)-C(95)	1.535(4)
C(93)-C(96)	1.536(4)
C(1TA)-C(2TA)	1.473(16)
C(2TA)-C(3TA)	1.25(3)
C(3TA)-C(4TA)	1.51(2)
C(4TA)-C(5TA)	1.40(2)
C(5TA)-C(6TA)	1.23(3)
C(1LA)-C(2LA)	1.568(16)
C(2LA)-C(3LA)	1.70(2)
C(3LA)-C(4LA)	1.468(16)
C(4LA)-C(5LA)	1.536(13)
C(5LA)-C(6LA)	1.50(3)

O(2)-Si(1)-C(6)	107.03(8)	C(28)-C(23)-Si(2)	125.11(14)
O(2)-Si(1)-C(12)	108.82(8)	C(25)-C(24)-C(23)	121.36(18)
C(6)-Si(1)-C(12)	113.41(8)	C(26)-C(25)-C(24)	120.64(19)
O(2)-Si(1)-C(18)	105.77(9)	C(25)-C(26)-C(27)	119.14(18)
C(6)-Si(1)-C(18)	109.07(9)	C(28)-C(27)-C(26)	120.12(19)
C(12)-Si(1)-C(18)	112.33(8)	C(27)-C(28)-C(23)	121.46(18)
C(1)-O(1)-C(4)	110.46(13)	C(34)-C(29)-C(30)	117.15(19)
O(1)-C(1)-C(5)	109.41(15)	C(34)-C(29)-Si(2)	123.19(15)
O(1)-C(1)-C(2)	105.20(15)	C(30)-C(29)-Si(2)	119.60(14)
C(5)-C(1)-C(2)	114.51(15)	C(31)-C(30)-C(29)	122.0(2)
O(3)-Si(2)-C(29)	108.61(9)	C(30)-C(31)-C(32)	119.3(2)
O(3)-Si(2)-C(23)	107.24(8)	C(33)-C(32)-C(31)	119.6(2)
C(29)-Si(2)-C(23)	113.37(8)	C(32)-C(33)-C(34)	120.2(2)
O(3)-Si(2)-C(93)	105.92(9)	C(33)-C(34)-C(29)	121.7(2)
C(29)-Si(2)-C(93)	112.34(9)	O(4)-C(36)-C(37)	117.65(14)
C(23)-Si(2)-C(93)	108.97(10)	O(4)-C(36)-C(41)	120.31(14)
O(13)-C(2)-C(3)	110.86(14)	C(37)-C(36)-C(41)	121.85(14)
O(13)-C(2)-C(1)	112.52(16)	C(36)-C(37)-C(38)	118.69(14)
C(3)-C(2)-C(1)	102.35(13)	C(36)-C(37)-C(51)	123.68(14)
C(5)-O(2)-Si(1)	126.79(12)	C(38)-C(37)-C(51)	117.62(14)
O(13)-P(1)-O(4)	102.55(8)	C(39)-C(38)-C(37)	121.77(14)
O(13)-P(1)-O(5)	95.89(7)	C(38)-C(39)-C(40)	117.36(15)
O(4)-P(1)-O(5)	102.56(7)	C(38)-C(39)-C(42)	120.95(15)
O(12)-C(3)-C(2)	111.49(14)	C(40)-C(39)-C(42)	121.64(15)
O(12)-C(3)-C(4)	111.23(16)	C(39)-C(40)-C(41)	123.82(15)
C(2)-C(3)-C(4)	101.44(13)	C(40)-C(41)-C(36)	116.18(14)
C(22)-O(3)-Si(2)	127.02(13)	C(40)-C(41)-C(46)	120.75(16)
O(12)-P(2)-O(7)	101.02(8)	C(36)-C(41)-C(46)	122.93(16)
O(12)-P(2)-O(6)	95.98(7)	C(44)-C(42)-C(43)	109.4(2)
O(7)-P(2)-O(6)	102.76(8)	C(44)-C(42)-C(39)	111.35(16)
O(1)-C(4)-C(22)	110.21(15)	C(43)-C(42)-C(39)	112.21(16)
O(1)-C(4)-C(3)	103.88(16)	C(44)-C(42)-C(45)	108.7(2)
C(22)-C(4)-C(3)	114.85(15)	C(43)-C(42)-C(45)	107.4(2)
C(36)-O(4)-P(1)	123.90(11)	C(39)-C(42)-C(45)	107.67(16)
O(2)-C(5)-C(1)	108.20(15)	C(48)-C(46)-C(47)	110.1(2)
C(50)-O(5)-P(1)	120.79(12)	C(48)-C(46)-C(49)	107.1(2)
C(65)-O(6)-P(2)	119.57(12)	C(47)-C(46)-C(49)	106.1(2)
C(7)-C(6)-C(11)	117.29(18)	C(48)-C(46)-C(41)	112.63(17)
C(7)-C(6)-Si(1)	117.10(15)	C(47)-C(46)-C(41)	109.23(15)
C(11)-C(6)-Si(1)	125.53(15)	C(49)-C(46)-C(41)	111.38(18)
C(8)-C(7)-C(6)	121.5(2)	O(5)-C(50)-C(51)	116.70(14)
C(76)-O(7)-P(2)	122.80(12)	O(5)-C(50)-C(55)	120.67(16)
C(9)-C(8)-C(7)	120.1(2)	C(51)-C(50)-C(55)	122.40(16)
C(8)-C(9)-C(10)	119.4(2)	C(52)-C(51)-C(50)	118.97(15)
C(11)-C(10)-C(9)	120.3(2)	C(52)-C(51)-C(37)	118.92(15)
C(10)-C(11)-C(6)	121.4(2)	C(50)-C(51)-C(37)	121.82(14)
C(13)-C(12)-C(17)	117.46(16)	C(51)-C(52)-C(53)	121.39(16)
C(13)-C(12)-Si(1)	124.28(14)	C(52)-C(53)-C(54)	117.35(16)
C(17)-C(12)-Si(1)	118.21(13)	C(52)-C(53)-C(56)	122.68(17)
C(3)-O(12)-P(2)	127.01(13)	C(54)-C(53)-C(56)	119.94(16)
C(12)-C(13)-C(14)	121.43(19)	C(55)-C(54)-C(53)	123.82(16)
C(2)-O(13)-P(1)	128.68(13)	C(54)-C(55)-C(50)	115.99(16)
C(15)-C(14)-C(13)	120.19(19)	C(54)-C(55)-C(60)	121.93(17)
C(14)-C(15)-C(16)	119.62(18)	C(50)-C(55)-C(60)	122.01(17)
C(17)-C(16)-C(15)	119.87(19)	C(57)-C(56)-C(58)	109.1(2)
C(16)-C(17)-C(12)	121.39(18)	C(57)-C(56)-C(53)	112.22(17)
C(20)-C(18)-C(19)	109.39(19)	C(58)-C(56)-C(53)	109.7(2)
C(20)-C(18)-C(21)	108.42(19)	C(57)-C(56)-C(59)	107.7(2)
C(19)-C(18)-C(21)	109.50(19)	C(58)-C(56)-C(59)	109.4(2)
C(20)-C(18)-Si(1)	111.58(16)	C(53)-C(56)-C(59)	108.60(18)
C(19)-C(18)-Si(1)	108.83(14)	C(63)-C(60)-C(55)	111.3(2)
C(21)-C(18)-Si(1)	109.11(15)	C(63)-C(60)-C(61)	110.4(2)
O(3)-C(22)-C(4)	109.06(17)	C(55)-C(60)-C(61)	109.82(18)
C(24)-C(23)-C(28)	117.26(17)	C(63)-C(60)-C(62)	107.4(2)
C(24)-C(23)-Si(2)	117.52(13)	C(55)-C(60)-C(62)	111.30(19)

C(61)-C(60)-C(62)	106.5(2)
O(6)-C(65)-C(70)	121.18(17)
O(6)-C(65)-C(66)	116.14(16)
C(70)-C(65)-C(66)	122.56(16)
C(67)-C(66)-C(65)	118.96(18)
C(67)-C(66)-C(75)	119.28(17)
C(65)-C(66)-C(75)	121.64(15)
C(68)-C(67)-C(66)	120.93(18)
C(67)-C(68)-C(69)	118.13(16)
C(67)-C(68)-C(89)	118.55(19)
C(69)-C(68)-C(89)	123.3(2)
C(68)-C(69)-C(70)	123.37(19)
C(65)-C(70)-C(69)	115.93(18)
C(65)-C(70)-C(71)	122.38(16)
C(69)-C(70)-C(71)	121.61(18)
C(72)-C(71)-C(70)	111.90(18)
C(72)-C(71)-C(74)	107.05(18)
C(70)-C(71)-C(74)	111.47(19)
C(72)-C(71)-C(73)	108.2(2)
C(70)-C(71)-C(73)	108.87(16)
C(74)-C(71)-C(73)	109.24(19)
C(76)-C(75)-C(80)	118.97(18)
C(76)-C(75)-C(66)	122.47(15)
C(80)-C(75)-C(66)	118.55(17)
C(75)-C(76)-O(7)	117.32(18)
C(75)-C(76)-C(77)	121.77(17)
O(7)-C(76)-C(77)	120.80(18)
C(78)-C(77)-C(76)	116.44(19)
C(78)-C(77)-C(81)	119.5(2)
C(76)-C(77)-C(81)	124.03(18)
C(77)-C(78)-C(79)	123.6(2)
C(80)-C(79)-C(78)	117.40(17)
C(80)-C(79)-C(85)	122.4(2)
C(78)-C(79)-C(85)	120.2(2)
C(79)-C(80)-C(75)	121.23(19)
C(82)-C(81)-C(84)	111.8(5)
C(82)-C(81)-C(83)	106.5(4)
C(84)-C(81)-C(83)	104.4(4)
C(82)-C(81)-C(77)	110.5(2)
C(84)-C(81)-C(77)	111.4(2)
C(83)-C(81)-C(77)	112.0(2)
C(88)-C(85)-C(79)	112.1(2)
C(88)-C(85)-C(86)	108.1(2)
C(79)-C(85)-C(86)	108.1(2)
C(88)-C(85)-C(87)	108.8(3)
C(79)-C(85)-C(87)	110.31(19)
C(86)-C(85)-C(87)	109.4(2)
C(90)-C(89)-C(92)	108.8(2)
C(90)-C(89)-C(68)	111.8(2)
C(92)-C(89)-C(68)	109.50(17)
C(90)-C(89)-C(91)	108.75(18)
C(92)-C(89)-C(91)	109.0(2)
C(68)-C(89)-C(91)	108.98(18)
C(94)-C(93)-C(95)	109.0(2)
C(94)-C(93)-C(96)	108.6(2)
C(95)-C(93)-C(96)	110.1(2)
C(94)-C(93)-Si(2)	111.12(18)
C(95)-C(93)-Si(2)	109.43(17)
C(96)-C(93)-Si(2)	108.47(16)
C(3TA)-C(2TA)-C(1TA)	135.1(16)
C(2TA)-C(3TA)-C(4TA)	124.4(12)
C(5TA)-C(4TA)-C(3TA)	132.4(14)
C(6TA)-C(5TA)-C(4TA)	132.5(15)
C(1LA)-C(2LA)-C(3LA)	120.4(7)
C(4LA)-C(3LA)-C(2LA)	108.0(9)
C(3LA)-C(4LA)-C(5LA)	101.6(12)
C(6LA)-C(5LA)-C(4LA)	101.5(12)

Table 2. Torsion angles [°] for **74a**.

C(4)-O(1)-C(1)-C(5)	129.32(17)
C(4)-O(1)-C(1)-C(2)	5.9(2)
O(1)-C(1)-C(2)-O(13)	-147.96(15)
C(5)-C(1)-C(2)-O(13)	91.89(19)
O(1)-C(1)-C(2)-C(3)	-28.91(19)
C(5)-C(1)-C(2)-C(3)	-149.06(17)
C(6)-Si(1)-O(2)-C(5)	91.96(16)
C(12)-Si(1)-O(2)-C(5)	-30.96(18)
C(18)-Si(1)-O(2)-C(5)	-151.84(15)
O(13)-C(2)-C(3)-O(12)	-81.63(19)
C(1)-C(2)-C(3)-O(12)	158.16(15)
O(13)-C(2)-C(3)-C(4)	159.89(15)
C(1)-C(2)-C(3)-C(4)	39.68(18)
C(29)-Si(2)-O(3)-C(22)	-25.33(19)
C(23)-Si(2)-O(3)-C(22)	97.53(17)
C(93)-Si(2)-O(3)-C(22)	-146.20(16)
C(1)-O(1)-C(4)-C(22)	142.91(17)
C(1)-O(1)-C(4)-C(3)	19.4(2)
O(12)-C(3)-C(4)-O(1)	-155.36(14)
C(2)-C(3)-C(4)-O(1)	-36.69(18)
O(12)-C(3)-C(4)-C(22)	84.2(2)
C(2)-C(3)-C(4)-C(22)	-157.13(17)
O(13)-P(1)-O(4)-C(36)	-60.79(15)
O(5)-P(1)-O(4)-C(36)	38.26(14)
Si(1)-O(2)-C(5)-C(1)	142.14(14)
O(1)-C(1)-C(5)-O(2)	-55.72(19)
C(2)-C(1)-C(5)-O(2)	62.1(2)
O(13)-P(1)-O(5)-C(50)	156.91(13)
O(4)-P(1)-O(5)-C(50)	52.63(14)
O(12)-P(2)-O(6)-C(65)	154.28(14)
O(7)-P(2)-O(6)-C(65)	51.52(15)
O(2)-Si(1)-C(6)-C(7)	17.62(17)
C(12)-Si(1)-C(6)-C(7)	137.64(15)
C(18)-Si(1)-C(6)-C(7)	-96.37(16)
O(2)-Si(1)-C(6)-C(11)	-165.72(16)
C(12)-Si(1)-C(6)-C(11)	-45.70(19)
C(18)-Si(1)-C(6)-C(11)	80.29(18)
C(11)-C(6)-C(7)-C(8)	0.5(3)
Si(1)-C(6)-C(7)-C(8)	177.42(17)
O(12)-P(2)-O(7)-C(76)	-58.03(17)
O(6)-P(2)-O(7)-C(76)	40.77(17)
C(6)-C(7)-C(8)-C(9)	1.1(3)
C(7)-C(8)-C(9)-C(10)	-1.6(4)
C(8)-C(9)-C(10)-C(11)	0.5(4)
C(9)-C(10)-C(11)-C(6)	1.1(3)
C(7)-C(6)-C(11)-C(10)	-1.6(3)
Si(1)-C(6)-C(11)-C(10)	-178.25(16)
O(2)-Si(1)-C(12)-C(13)	134.13(17)
C(6)-Si(1)-C(12)-C(13)	15.1(2)
C(18)-Si(1)-C(12)-C(13)	-109.10(18)
O(2)-Si(1)-C(12)-C(17)	-43.14(18)
C(6)-Si(1)-C(12)-C(17)	-162.14(16)
C(18)-Si(1)-C(12)-C(17)	73.62(18)
C(2)-C(3)-O(12)-P(2)	114.54(17)
C(4)-C(3)-O(12)-P(2)	-133.02(15)
O(7)-P(2)-O(12)-C(3)	134.54(15)
O(6)-P(2)-O(12)-C(3)	30.27(16)
C(17)-C(12)-C(13)-C(14)	-2.1(3)
Si(1)-C(12)-C(13)-C(14)	-179.39(18)

C(3)-C(2)-O(13)-P(1)	120.41(16)
C(1)-C(2)-O(13)-P(1)	-125.64(16)
O(4)-P(1)-O(13)-C(2)	123.69(16)
O(5)-P(1)-O(13)-C(2)	19.39(17)
C(12)-C(13)-C(14)-C(15)	1.3(4)
C(13)-C(14)-C(15)-C(16)	0.6(4)
C(14)-C(15)-C(16)-C(17)	-1.6(4)
C(15)-C(16)-C(17)-C(12)	0.7(4)
C(13)-C(12)-C(17)-C(16)	1.1(3)
Si(1)-C(12)-C(17)-C(16)	178.55(19)
O(2)-Si(1)-C(18)-C(20)	70.06(17)
C(6)-Si(1)-C(18)-C(20)	-175.13(16)
C(12)-Si(1)-C(18)-C(20)	-48.52(18)
O(2)-Si(1)-C(18)-C(19)	-169.14(15)
C(6)-Si(1)-C(18)-C(19)	-54.33(17)
C(12)-Si(1)-C(18)-C(19)	72.28(17)
O(2)-Si(1)-C(18)-C(21)	-49.71(17)
C(6)-Si(1)-C(18)-C(21)	65.10(17)
C(12)-Si(1)-C(18)-C(21)	-168.29(15)
Si(2)-O(3)-C(22)-C(4)	139.59(14)
O(1)-C(4)-C(22)-O(3)	-52.4(2)
C(3)-C(4)-C(22)-O(3)	64.5(2)
O(3)-Si(2)-C(23)-C(24)	13.79(19)
C(29)-Si(2)-C(23)-C(24)	133.66(16)
C(93)-Si(2)-C(23)-C(24)	-100.44(17)
O(3)-Si(2)-C(23)-C(28)	-170.05(18)
C(29)-Si(2)-C(23)-C(28)	-50.2(2)
C(93)-Si(2)-C(23)-C(28)	75.7(2)
C(28)-C(23)-C(24)-C(25)	0.8(3)
Si(2)-C(23)-C(24)-C(25)	177.25(17)
C(23)-C(24)-C(25)-C(26)	0.4(3)
C(24)-C(25)-C(26)-C(27)	-0.9(3)
C(25)-C(26)-C(27)-C(28)	0.3(4)
C(26)-C(27)-C(28)-C(23)	0.9(4)
C(24)-C(23)-C(28)-C(27)	-1.4(3)
Si(2)-C(23)-C(28)-C(27)	-177.58(18)
O(3)-Si(2)-C(29)-C(34)	130.54(18)
C(23)-Si(2)-C(29)-C(34)	11.5(2)
C(93)-Si(2)-C(29)-C(34)	-112.63(19)
O(3)-Si(2)-C(29)-C(30)	-46.5(2)
C(23)-Si(2)-C(29)-C(30)	-165.6(2)
C(93)-Si(2)-C(29)-C(30)	70.3(2)
C(34)-C(29)-C(30)-C(31)	-1.5(4)
Si(2)-C(29)-C(30)-C(31)	175.8(3)
C(29)-C(30)-C(31)-C(32)	2.9(5)
C(30)-C(31)-C(32)-C(33)	-2.2(5)
C(31)-C(32)-C(33)-C(34)	0.3(4)
C(32)-C(33)-C(34)-C(29)	1.2(4)
C(30)-C(29)-C(34)-C(33)	-0.6(3)
Si(2)-C(29)-C(34)-C(33)	-177.68(18)
P(1)-O(4)-C(36)-C(37)	-66.35(18)
P(1)-O(4)-C(36)-C(41)	118.43(15)
O(4)-C(36)-C(37)-C(38)	179.31(15)
C(41)-C(36)-C(37)-C(38)	-5.5(2)
O(4)-C(36)-C(37)-C(51)	-2.0(2)
C(41)-C(36)-C(37)-C(51)	173.15(15)
C(36)-C(37)-C(38)-C(39)	0.6(2)
C(51)-C(37)-C(38)-C(39)	-178.16(15)
C(37)-C(38)-C(39)-C(40)	3.1(2)
C(37)-C(38)-C(39)-C(42)	-174.49(16)
C(38)-C(39)-C(40)-C(41)	-2.1(3)
C(42)-C(39)-C(40)-C(41)	175.45(17)
C(39)-C(40)-C(41)-C(36)	-2.5(3)
C(39)-C(40)-C(41)-C(46)	173.30(16)
O(4)-C(36)-C(41)-C(40)	-178.63(15)
C(37)-C(36)-C(41)-C(40)	6.3(2)
O(4)-C(36)-C(41)-C(46)	5.7(2)
C(37)-C(36)-C(41)-C(46)	-169.32(16)
C(38)-C(39)-C(42)-C(44)	-146.3(2)
C(40)-C(39)-C(42)-C(44)	36.2(3)
C(38)-C(39)-C(42)-C(43)	-23.4(3)
C(40)-C(39)-C(42)-C(43)	159.2(2)
C(38)-C(39)-C(42)-C(45)	94.6(2)
C(40)-C(39)-C(42)-C(45)	-82.8(2)
C(40)-C(41)-C(46)-C(48)	117.2(2)
C(36)-C(41)-C(46)-C(48)	-67.3(2)
C(40)-C(41)-C(46)-C(47)	-120.1(2)
C(36)-C(41)-C(46)-C(47)	55.4(3)
C(40)-C(41)-C(46)-C(49)	-3.2(3)
C(36)-C(41)-C(46)-C(49)	172.32(19)
P(1)-O(5)-C(50)-C(51)	-71.67(19)
P(1)-O(5)-C(50)-C(55)	113.83(18)
O(5)-C(50)-C(51)-C(52)	-178.08(16)
C(55)-C(50)-C(51)-C(52)	-3.7(3)
O(5)-C(50)-C(51)-C(37)	-4.3(3)
C(55)-C(50)-C(51)-C(37)	170.05(17)
C(36)-C(37)-C(51)-C(52)	-133.59(18)
C(38)-C(37)-C(51)-C(52)	45.1(2)
C(36)-C(37)-C(51)-C(50)	52.7(2)
C(38)-C(37)-C(51)-C(50)	-128.63(18)
C(50)-C(51)-C(52)-C(53)	2.1(3)
C(37)-C(51)-C(52)-C(53)	-171.86(17)
C(51)-C(52)-C(53)-C(54)	0.4(3)
C(51)-C(52)-C(53)-C(56)	178.29(19)
C(52)-C(53)-C(54)-C(55)	-1.4(3)
C(56)-C(53)-C(54)-C(55)	-179.4(2)
C(53)-C(54)-C(55)-C(50)	-0.1(3)
C(53)-C(54)-C(55)-C(60)	176.9(2)
O(5)-C(50)-C(55)-C(54)	176.84(18)
C(51)-C(50)-C(55)-C(54)	2.7(3)
O(5)-C(50)-C(55)-C(60)	-0.1(3)
C(51)-C(50)-C(55)-C(60)	-174.3(2)
C(52)-C(53)-C(56)-C(57)	4.6(3)
C(54)-C(53)-C(56)-C(57)	-177.6(2)
C(52)-C(53)-C(56)-C(58)	126.0(2)
C(54)-C(53)-C(56)-C(58)	-56.1(3)
C(52)-C(53)-C(56)-C(59)	-114.4(2)
C(54)-C(53)-C(56)-C(59)	63.5(3)
C(54)-C(55)-C(60)-C(63)	119.3(2)
C(50)-C(55)-C(60)-C(63)	-63.9(3)
C(54)-C(55)-C(60)-C(61)	-118.1(2)
C(50)-C(55)-C(60)-C(61)	58.7(3)
C(54)-C(55)-C(60)-C(62)	-0.4(3)
C(50)-C(55)-C(60)-C(62)	176.3(2)
P(2)-O(6)-C(65)-C(70)	111.28(18)
P(2)-O(6)-C(65)-C(66)	-72.59(18)
O(6)-C(65)-C(66)-C(67)	-179.98(15)
C(70)-C(65)-C(66)-C(67)	-3.9(3)
O(6)-C(65)-C(66)-C(75)	-4.0(2)
C(70)-C(65)-C(66)-C(75)	172.05(16)
C(65)-C(66)-C(67)-C(68)	1.1(3)
C(75)-C(66)-C(67)-C(68)	-174.92(16)
C(66)-C(67)-C(68)-C(69)	1.6(3)
C(66)-C(67)-C(68)-C(89)	-177.86(16)
C(67)-C(68)-C(69)-C(70)	-1.9(3)
C(89)-C(68)-C(69)-C(70)	177.60(17)
O(6)-C(65)-C(70)-C(69)	179.50(15)
C(66)-C(65)-C(70)-C(69)	3.6(3)
O(6)-C(65)-C(70)-C(71)	2.8(3)
C(66)-C(65)-C(70)-C(71)	-173.06(17)

C(68)-C(69)-C(70)-C(65)	-0.7(3)
C(68)-C(69)-C(70)-C(71)	176.02(17)
C(65)-C(70)-C(71)-C(72)	179.76(18)
C(69)-C(70)-C(71)-C(72)	3.3(3)
C(65)-C(70)-C(71)-C(74)	-60.4(2)
C(69)-C(70)-C(71)-C(74)	123.1(2)
C(65)-C(70)-C(71)-C(73)	60.2(2)
C(69)-C(70)-C(71)-C(73)	-116.3(2)
C(67)-C(66)-C(75)-C(76)	-128.89(18)
C(65)-C(66)-C(75)-C(76)	55.2(2)
C(67)-C(66)-C(75)-C(80)	50.3(2)
C(65)-C(66)-C(75)-C(80)	-125.65(18)
C(80)-C(75)-C(76)-O(7)	176.81(15)
C(66)-C(75)-C(76)-O(7)	-4.0(2)
C(80)-C(75)-C(76)-C(77)	-6.8(3)
C(66)-C(75)-C(76)-C(77)	172.39(17)
P(2)-O(7)-C(76)-C(75)	-67.5(2)
P(2)-O(7)-C(76)-C(77)	116.04(18)
C(75)-C(76)-C(77)-C(78)	8.4(3)
O(7)-C(76)-C(77)-C(78)	-175.35(17)
C(75)-C(76)-C(77)-C(81)	-169.63(18)
O(7)-C(76)-C(77)-C(81)	6.7(3)
C(76)-C(77)-C(78)-C(79)	-3.5(3)
C(81)-C(77)-C(78)-C(79)	174.60(19)
C(77)-C(78)-C(79)-C(80)	-2.9(3)
C(77)-C(78)-C(79)-C(85)	175.75(19)
C(78)-C(79)-C(80)-C(75)	4.7(3)
C(85)-C(79)-C(80)-C(75)	-173.92(18)
C(76)-C(75)-C(80)-C(79)	-0.1(3)
C(66)-C(75)-C(80)-C(79)	-179.27(17)
C(78)-C(77)-C(81)-C(82)	99.3(4)
C(76)-C(77)-C(81)-C(82)	-82.7(4)
C(78)-C(77)-C(81)-C(84)	-135.8(5)
C(76)-C(77)-C(81)-C(84)	42.2(5)
C(78)-C(77)-C(81)-C(83)	-19.2(4)
C(76)-C(77)-C(81)-C(83)	158.7(3)
C(80)-C(79)-C(85)-C(88)	-7.0(3)
C(78)-C(79)-C(85)-C(88)	174.4(2)
C(80)-C(79)-C(85)-C(86)	112.0(3)
C(78)-C(79)-C(85)-C(86)	-66.6(3)
C(80)-C(79)-C(85)-C(87)	-128.4(3)
C(78)-C(79)-C(85)-C(87)	53.0(3)
C(67)-C(68)-C(89)-C(90)	-176.89(18)
C(69)-C(68)-C(89)-C(90)	3.6(3)
C(67)-C(68)-C(89)-C(92)	-56.3(3)
C(69)-C(68)-C(89)-C(92)	124.3(3)
C(67)-C(68)-C(89)-C(91)	62.9(2)
C(69)-C(68)-C(89)-C(91)	-116.6(2)
O(3)-Si(2)-C(93)-C(94)	67.09(19)
C(29)-Si(2)-C(93)-C(94)	-51.3(2)
C(23)-Si(2)-C(93)-C(94)	-177.83(17)
O(3)-Si(2)-C(93)-C(95)	-172.43(18)
C(29)-Si(2)-C(93)-C(95)	69.14(19)
C(23)-Si(2)-C(93)-C(95)	-57.35(19)
O(3)-Si(2)-C(93)-C(96)	-52.2(2)
C(29)-Si(2)-C(93)-C(96)	-170.66(18)
C(23)-Si(2)-C(93)-C(96)	62.8(2)
C(1TA)-C(2TA)-C(3TA)-C(4TA)	21(6)
C(2TA)-C(3TA)-C(4TA)-C(5TA)	-169(4)
C(3TA)-C(4TA)-C(5TA)-C(6TA)	175(3)
C(1LA)-C(2LA)-C(3LA)-C(4LA)	-56.3(14)
C(2LA)-C(3LA)-C(4LA)-C(5LA)	178.5(8)
C(3LA)-C(4LA)-C(5LA)-C(6LA)	175.3(10)

Table 3. Bond lengths [Å] and angles [°] for [Rh(cod)(**74a**)]BF_4 (**90a**)

Rh(1)-P(1)	2.2539(8)
Rh(1)-P(2)	2.2560(8)
Rh(1)-C(100)	2.271(3)
Rh(1)-C(104)	2.273(3)
Rh(1)-C(99)	2.275(3)
Rh(1)-C(103)	2.305(3)
P(1)-O(3X)	1.583(2)
P(1)-O(1)	1.596(2)
P(1)-O(4X)	1.606(2)
O(1)-C(1)	1.439(3)
C(1)-C(4)	1.497(4)
C(1)-C(2)	1.523(4)
Si(1)-O(4)	1.645(2)
Si(1)-C(16)	1.867(4)
Si(1)-C(6)	1.871(4)
Si(1)-C(9')	1.878(4)
P(2)-O(2)	1.595(2)
P(2)-O(2X)	1.607(2)
P(2)-O(1X)	1.610(2)
O(2)-C(4)	1.437(3)
C(2)-O(3)	1.430(4)
C(2)-C(5)	1.508(4)
Si(2)-O(5)	1.648(2)
Si(2)-C(27)	1.879(3)
Si(2)-C(23)	1.880(3)
Si(2)-C(33)	1.884(3)
O(3)-C(3)	1.445(4)
C(3)-C(22)	1.503(4)
C(3)-C(4)	1.538(4)
O(4)-C(5)	1.422(4)
O(5)-C(22)	1.416(4)
C(6)-C(7)	1.312(19)
C(6)-C(11)	1.388(10)
C(6)-C(7')	1.508(13)
C(6)-C(6')	1.541(16)
C(6)-C(8')	1.678(8)
C(7)-C(8)	1.48(2)
C(8)-C(9)	1.351(13)
C(9)-C(10)	1.343(12)
C(10)-C(11)	1.356(14)
C(12)-C(9')	1.542(10)
C(13)-C(9')	1.511(18)
C(14)-C(9')	1.605(9)
C(9')-C(10')	1.368(8)
C(9')-C(14')	1.40(2)
C(10')-C(11')	1.383(11)
C(11')-C(12')	1.407(12)
C(12')-C(13')	1.380(12)
C(13')-C(14')	1.42(3)
C(16)-C(17)	1.396(5)
C(16)-C(21)	1.405(5)
C(17)-C(18)	1.405(6)
C(18)-C(19)	1.369(7)
C(19)-C(20)	1.392(7)
C(20)-C(21)	1.410(6)
C(23)-C(24)	1.510(5)
C(23)-C(26)	1.511(5)
C(23)-C(25)	1.566(5)

C(27)-C(32)	1.392(4)	C(80)-C(91)	1.530(5)
C(27)-C(28)	1.412(4)	C(81)-C(82)	1.388(4)
C(28)-C(29)	1.387(4)	C(82)-C(95)	1.536(5)
C(29)-C(30)	1.368(6)	C(83)-C(86)	1.40(5)
C(30)-C(31)	1.401(5)	C(83)-C(84)	1.42(3)
C(31)-C(32)	1.389(5)	C(83)-C(85')	1.501(6)
C(33)-C(38)	1.393(4)	C(83)-C(86')	1.531(6)
C(33)-C(34)	1.398(4)	C(83)-C(84')	1.554(6)
C(34)-C(35)	1.400(5)	C(83)-C(85)	1.67(2)
C(35)-C(36)	1.371(6)	C(87)-C(89)	1.520(5)
C(36)-C(37)	1.390(6)	C(87)-C(90)	1.531(5)
C(37)-C(38)	1.391(5)	C(87)-C(88)	1.555(5)
O(4X)-C(40)	1.411(4)	C(91)-C(93)	1.282(18)
C(40)-C(41)	1.391(4)	C(91)-C(92')	1.414(8)
C(40)-C(45)	1.411(4)	C(91)-C(94')	1.533(7)
C(41)-C(48)	1.394(5)	C(91)-C(93')	1.601(7)
C(41)-C(42)	1.496(4)	C(91)-C(92)	1.735(19)
C(42)-C(43)	1.372(4)	C(91)-C(94)	1.77(2)
C(42)-C(49)	1.406(4)	C(95)-C(98)	1.529(5)
C(43)-C(52)	1.405(4)	C(95)-C(96)	1.547(5)
C(43)-O(3X)	1.427(4)	C(95)-C(97)	1.552(4)
C(45)-C(46)	1.397(5)	C(99)-C(100)	1.360(5)
C(45)-C(53)	1.521(5)	C(99)-C(106)	1.521(4)
C(46)-C(47)	1.400(5)	C(104)-C(103)	1.375(5)
C(47)-C(48)	1.399(5)	C(104)-C(105)	1.501(5)
C(47)-C(57)	1.515(6)	C(100)-C(101)	1.508(5)
C(49)-C(50)	1.388(4)	C(101)-C(102)	1.531(5)
C(50)-C(51)	1.394(5)	C(102)-C(103)	1.514(4)
C(50)-C(61)	1.541(5)	C(105)-C(106)	1.537(5)
C(51)-C(52)	1.396(5)	C(1S)-Cl(2)	1.713(10)
C(52)-C(65)	1.550(4)	C(1S)-Cl(1)	1.719(10)
C(53)-C(56)	1.395(9)	C(1S')-Cl(1')	1.75(2)
C(53)-C(56')	1.404(10)	C(1S')-Cl(2')	1.82(2)
C(53)-C(55)	1.434(13)	B(1S)-F(1S)	1.283(10)
C(53)-C(54')	1.462(14)	B(1S)-F(2S')	1.284(14)
C(53)-C(55')	1.835(10)	B(1S)-F(2S)	1.343(8)
C(53)-C(54)	1.867(9)	B(1S)-F(3S)	1.364(7)
C(57)-C(59)	1.520(8)	B(1S)-F(4S')	1.42(2)
C(57)-C(58)	1.526(7)	B(1S)-F(4S)	1.457(8)
C(57)-C(60)	1.534(8)	B(1S)-F(1S')	1.64(2)
C(61)-C(63)	1.526(5)	P(1)-Rh(1)-P(2)	95.00(3)
C(61)-C(64)	1.527(5)	P(1)-Rh(1)-C(100)	156.78(9)
C(61)-C(62)	1.528(5)	P(2)-Rh(1)-C(100)	91.46(8)
C(65)-C(67)	1.45(3)	P(1)-Rh(1)-C(104)	90.62(9)
C(65)-C(68)	1.51(3)	P(2)-Rh(1)-C(104)	154.64(9)
C(65)-C(66')	1.523(5)	C(100)-Rh(1)-C(104)	93.03(12)
C(65)-C(67')	1.530(6)	P(1)-Rh(1)-C(99)	166.35(8)
C(65)-C(68')	1.542(6)	P(2)-Rh(1)-C(99)	90.55(9)
C(65)-C(66)	1.72(4)	C(100)-Rh(1)-C(99)	34.82(12)
O(2X)-C(70)	1.423(3)	C(104)-Rh(1)-C(99)	79.23(12)
C(70)-C(71)	1.384(4)	P(1)-Rh(1)-C(103)	91.53(8)
C(70)-C(75)	1.400(4)	P(2)-Rh(1)-C(103)	167.91(8)
C(71)-C(78)	1.401(4)	C(100)-Rh(1)-C(103)	78.71(11)
C(71)-C(72)	1.498(4)	C(104)-Rh(1)-C(103)	34.95(11)
C(72)-C(79)	1.394(4)	C(99)-Rh(1)-C(103)	85.37(12)
C(72)-C(73)	1.397(4)	O(3X)-P(1)-O(1)	99.30(11)
C(73)-C(82)	1.395(4)	O(3X)-P(1)-O(4X)	104.71(11)
C(73)-O(1X)	1.409(3)	O(1)-P(1)-O(4X)	100.73(11)
C(75)-C(76)	1.392(4)	O(3X)-P(1)-Rh(1)	113.00(8)
C(75)-C(83)	1.545(4)	O(1)-P(1)-Rh(1)	121.50(8)
C(76)-C(77)	1.392(4)	O(4X)-P(1)-Rh(1)	115.17(8)
C(77)-C(78)	1.390(4)	C(1)-O(1)-P(1)	122.02(17)
C(77)-C(87)	1.531(4)	O(1)-C(1)-C(4)	112.1(2)
C(79)-C(80)	1.402(4)	O(1)-C(1)-C(2)	112.0(2)
C(80)-C(81)	1.393(5)	C(4)-C(1)-C(2)	101.4(2)

O(4)-Si(1)-C(16)	109.20(14)	C(12)-C(9')-Si(1)	106.3(4)
O(4)-Si(1)-C(6)	102.61(15)	C(14)-C(9')-Si(1)	104.5(4)
C(16)-Si(1)-C(6)	111.57(17)	C(9')-C(10')-C(11')	124.8(7)
O(4)-Si(1)-C(9')	108.71(15)	C(10')-C(11')-C(12')	119.3(8)
C(16)-Si(1)-C(9')	113.94(17)	C(13')-C(12')-C(11')	118.6(7)
C(6)-Si(1)-C(9')	110.16(17)	C(12')-C(13')-C(14')	118.8(11)
O(2)-P(2)-O(2X)	98.54(10)	C(9')-C(14')-C(13')	122.5(16)
O(2)-P(2)-O(1X)	100.50(11)	C(17)-C(16)-C(21)	117.0(4)
O(2X)-P(2)-O(1X)	105.66(11)	C(17)-C(16)-Si(1)	124.4(3)
O(2)-P(2)-Rh(1)	122.96(8)	C(21)-C(16)-Si(1)	118.6(3)
O(2X)-P(2)-Rh(1)	112.77(8)	C(16)-C(17)-C(18)	121.5(4)
O(1X)-P(2)-Rh(1)	114.06(8)	C(19)-C(18)-C(17)	120.8(5)
C(4)-O(2)-P(2)	123.57(17)	C(18)-C(19)-C(20)	119.3(4)
O(3)-C(2)-C(5)	111.0(2)	C(19)-C(20)-C(21)	120.0(4)
O(3)-C(2)-C(1)	102.2(2)	C(16)-C(21)-C(20)	121.3(4)
C(5)-C(2)-C(1)	114.7(3)	O(5)-C(22)-C(3)	109.2(3)
O(5)-Si(2)-C(27)	109.41(13)	C(24)-C(23)-C(26)	109.8(3)
O(5)-Si(2)-C(23)	105.03(14)	C(24)-C(23)-C(25)	107.7(3)
C(27)-Si(2)-C(23)	108.88(14)	C(26)-C(23)-C(25)	107.5(3)
O(5)-Si(2)-C(33)	107.68(13)	C(24)-C(23)-Si(2)	111.8(2)
C(27)-Si(2)-C(33)	114.73(14)	C(26)-C(23)-Si(2)	111.2(2)
C(23)-Si(2)-C(33)	110.65(15)	C(25)-C(23)-Si(2)	108.7(2)
C(2)-O(3)-C(3)	110.6(2)	C(32)-C(27)-C(28)	116.9(3)
O(3)-C(3)-C(22)	110.3(2)	C(32)-C(27)-Si(2)	124.6(2)
O(3)-C(3)-C(4)	104.4(2)	C(28)-C(27)-Si(2)	117.8(2)
C(22)-C(3)-C(4)	113.9(2)	C(29)-C(28)-C(27)	121.4(3)
O(2)-C(4)-C(1)	112.3(2)	C(30)-C(29)-C(28)	120.4(3)
O(2)-C(4)-C(3)	110.3(2)	C(29)-C(30)-C(31)	119.8(3)
C(1)-C(4)-C(3)	102.4(2)	C(32)-C(31)-C(30)	119.5(3)
C(5)-O(4)-Si(1)	128.4(2)	C(31)-C(32)-C(27)	122.0(3)
O(4)-C(5)-C(2)	109.6(3)	C(38)-C(33)-C(34)	117.1(3)
C(22)-O(5)-Si(2)	126.2(2)	C(38)-C(33)-Si(2)	118.2(2)
C(7)-C(6)-C(11)	119.9(9)	C(34)-C(33)-Si(2)	124.7(2)
C(7)-C(6)-C(7')	108.9(11)	C(33)-C(34)-C(35)	121.6(3)
C(11)-C(6)-C(7')	25.4(6)	C(36)-C(35)-C(34)	119.6(4)
C(7)-C(6)-C(6')	5.3(14)	C(35)-C(36)-C(37)	120.3(3)
C(11)-C(6)-C(6')	124.0(10)	C(36)-C(37)-C(38)	119.5(4)
C(7')-C(6)-C(6')	114.0(10)	C(37)-C(38)-C(33)	121.9(4)
C(7)-C(6)-C(8')	100.0(10)	C(40)-O(4X)-P(1)	126.47(19)
C(11)-C(6)-C(8')	78.9(6)	C(41)-C(40)-C(45)	122.8(3)
C(7')-C(6)-C(8')	103.5(7)	C(41)-C(40)-O(4X)	119.0(3)
C(6')-C(6)-C(8')	97.3(7)	C(45)-C(40)-O(4X)	117.8(3)
C(7)-C(6)-Si(1)	119.0(8)	C(40)-C(41)-C(48)	118.2(3)
C(11)-C(6)-Si(1)	118.8(5)	C(40)-C(41)-C(42)	124.7(3)
C(7')-C(6)-Si(1)	116.9(6)	C(48)-C(41)-C(42)	117.1(3)
C(6')-C(6)-Si(1)	115.9(8)	C(43)-C(42)-C(49)	118.2(3)
C(8')-C(6)-Si(1)	105.8(3)	C(43)-C(42)-C(41)	123.7(3)
C(6)-C(7)-C(8)	118.2(13)	C(49)-C(42)-C(41)	118.0(3)
C(9)-C(8)-C(7)	118.6(9)	C(42)-C(43)-C(52)	123.9(3)
C(10)-C(9)-C(8)	119.5(8)	C(42)-C(43)-O(3X)	116.5(3)
C(9)-C(10)-C(11)	122.3(8)	C(52)-C(43)-O(3X)	119.5(3)
C(10)-C(11)-C(6)	119.6(8)	C(43)-O(3X)-P(1)	118.47(18)
C(10')-C(9')-C(14')	113.9(11)	C(46)-C(45)-C(40)	115.4(3)
C(10')-C(9')-C(13)	115.7(9)	C(46)-C(45)-C(53)	118.7(3)
C(14')-C(9')-C(13)	7(2)	C(40)-C(45)-C(53)	125.8(3)
C(10')-C(9')-C(12)	37.0(5)	C(45)-C(46)-C(47)	124.8(3)
C(14')-C(9')-C(12)	110.4(13)	C(48)-C(47)-C(46)	116.1(3)
C(13)-C(9')-C(12)	116.2(11)	C(48)-C(47)-C(57)	123.7(3)
C(10')-C(9')-C(14)	69.4(5)	C(46)-C(47)-C(57)	120.2(3)
C(14')-C(9')-C(14)	110.1(13)	C(41)-C(48)-C(47)	122.6(3)
C(13)-C(9')-C(14)	104.2(12)	C(50)-C(49)-C(42)	121.3(3)
C(12)-C(9')-C(14)	105.1(6)	C(49)-C(50)-C(51)	117.4(3)
C(10')-C(9')-Si(1)	124.4(4)	C(49)-C(50)-C(61)	122.5(3)
C(14')-C(9')-Si(1)	119.4(10)	C(51)-C(50)-C(61)	120.0(3)
C(13)-C(9')-Si(1)	119.1(9)	C(50)-C(51)-C(52)	124.4(3)

C(51)-C(52)-C(43)	114.8(3)	C(79)-C(72)-C(71)	116.6(3)
C(51)-C(52)-C(65)	117.8(3)	C(73)-C(72)-C(71)	124.4(3)
C(43)-C(52)-C(65)	127.3(3)	C(82)-C(73)-C(72)	122.5(3)
C(56)-C(53)-C(56')	27.2(4)	C(82)-C(73)-O(1X)	118.5(3)
C(56)-C(53)-C(55)	125.0(9)	C(72)-C(73)-O(1X)	118.7(2)
C(56')-C(53)-C(55)	128.5(8)	C(73)-O(1X)-P(2)	129.12(18)
C(56)-C(53)-C(54')	121.6(8)	C(76)-C(75)-C(70)	115.1(3)
C(56')-C(53)-C(54')	114.6(7)	C(76)-C(75)-C(83)	120.4(2)
C(55)-C(53)-C(54')	21.0(5)	C(70)-C(75)-C(83)	124.4(3)
C(56)-C(53)-C(45)	120.7(5)	C(77)-C(76)-C(75)	124.6(3)
C(56')-C(53)-C(45)	119.3(5)	C(78)-C(77)-C(76)	117.1(3)
C(55)-C(53)-C(45)	111.0(7)	C(78)-C(77)-C(87)	121.3(3)
C(54')-C(53)-C(45)	117.7(7)	C(76)-C(77)-C(87)	121.6(3)
C(56)-C(53)-C(55')	73.7(5)	C(77)-C(78)-C(71)	121.3(3)
C(56')-C(53)-C(55')	100.5(5)	C(72)-C(79)-C(80)	120.7(3)
C(55)-C(53)-C(55')	78.2(6)	C(81)-C(80)-C(79)	117.5(3)
C(54')-C(53)-C(55')	96.2(7)	C(81)-C(80)-C(91)	121.0(3)
C(45)-C(53)-C(55')	102.5(4)	C(79)-C(80)-C(91)	121.4(3)
C(56)-C(53)-C(54)	96.5(5)	C(82)-C(81)-C(80)	124.1(3)
C(56')-C(53)-C(54)	69.4(5)	C(81)-C(82)-C(73)	116.2(3)
C(55)-C(53)-C(54)	94.8(6)	C(81)-C(82)-C(95)	119.9(3)
C(54')-C(53)-C(54)	74.4(6)	C(73)-C(82)-C(95)	123.7(3)
C(45)-C(53)-C(54)	97.0(5)	C(86)-C(83)-C(84)	118(3)
C(55')-C(53)-C(54)	160.5(4)	C(86)-C(83)-C(85')	125.2(19)
C(47)-C(57)-C(59)	109.7(4)	C(84)-C(83)-C(85')	74(2)
C(47)-C(57)-C(58)	112.2(3)	C(86)-C(83)-C(86')	16(2)
C(59)-C(57)-C(58)	112.4(5)	C(84)-C(83)-C(86')	119.6(16)
C(47)-C(57)-C(60)	109.1(4)	C(85')-C(83)-C(86')	109.7(4)
C(59)-C(57)-C(60)	106.0(5)	C(86)-C(83)-C(75)	105.0(15)
C(58)-C(57)-C(60)	107.1(5)	C(84)-C(83)-C(75)	120.5(10)
C(63)-C(61)-C(64)	110.0(3)	C(85')-C(83)-C(75)	112.6(3)
C(63)-C(61)-C(62)	107.9(3)	C(86')-C(83)-C(75)	113.0(4)
C(64)-C(61)-C(62)	108.8(4)	C(86)-C(83)-C(84')	96(3)
C(63)-C(61)-C(50)	108.4(3)	C(84)-C(83)-C(84')	34(2)
C(64)-C(61)-C(50)	109.2(3)	C(85')-C(83)-C(84')	107.8(4)
C(62)-C(61)-C(50)	112.4(3)	C(86')-C(83)-C(84')	105.5(4)
C(67)-C(65)-C(68)	118(3)	C(75)-C(83)-C(84')	107.9(3)
C(67)-C(65)-C(66')	131.8(13)	C(86)-C(83)-C(85)	102(2)
C(68)-C(65)-C(66')	53(3)	C(84)-C(83)-C(85)	103.9(19)
C(67)-C(65)-C(67')	49.3(16)	C(85')-C(83)-C(85)	31.2(13)
C(68)-C(65)-C(67')	146.0(15)	C(86')-C(83)-C(85)	86.8(12)
C(66')-C(65)-C(67')	108.3(4)	C(75)-C(83)-C(85)	105.0(9)
C(67)-C(65)-C(68')	60.4(15)	C(84')-C(83)-C(85)	136.3(13)
C(68)-C(65)-C(68')	61(3)	C(89)-C(87)-C(90)	109.7(3)
C(66')-C(65)-C(68')	106.5(3)	C(89)-C(87)-C(77)	111.1(3)
C(67')-C(65)-C(68')	108.0(4)	C(90)-C(87)-C(77)	112.2(3)
C(67)-C(65)-C(52)	117.5(12)	C(89)-C(87)-C(88)	108.7(3)
C(68)-C(65)-C(52)	105.1(16)	C(90)-C(87)-C(88)	107.4(3)
C(66')-C(65)-C(52)	109.9(3)	C(77)-C(87)-C(88)	107.6(3)
C(67')-C(65)-C(52)	108.3(3)	C(93)-C(91)-C(92')	117.6(11)
C(68')-C(65)-C(52)	115.6(3)	C(93)-C(91)-C(80)	127.3(11)
C(67)-C(65)-C(66)	98(3)	C(92')-C(91)-C(80)	113.8(4)
C(68)-C(65)-C(66)	108(4)	C(93)-C(91)-C(94')	62.5(15)
C(66')-C(65)-C(66)	57(2)	C(92')-C(91)-C(94')	113.4(6)
C(67')-C(65)-C(66)	54(2)	C(80)-C(91)-C(94')	106.5(3)
C(68')-C(65)-C(66)	135.1(13)	C(93)-C(91)-C(93')	44.5(14)
C(52)-C(65)-C(66)	109.3(13)	C(92')-C(91)-C(93')	109.0(5)
C(70)-O(2X)-P(2)	117.76(17)	C(80)-C(91)-C(93')	107.5(4)
C(71)-C(70)-C(75)	123.2(3)	C(94')-C(91)-C(93')	106.1(5)
C(71)-C(70)-O(2X)	116.7(2)	C(93)-C(91)-C(92)	111.2(13)
C(75)-C(70)-O(2X)	120.0(2)	C(92')-C(91)-C(92)	32.9(8)
C(70)-C(71)-C(78)	118.3(3)	C(80)-C(91)-C(92)	105.2(6)
C(70)-C(71)-C(72)	123.9(3)	C(94')-C(91)-C(92)	142.4(8)
C(78)-C(71)-C(72)	117.6(3)	C(93')-C(91)-C(92)	82.8(8)
C(79)-C(72)-C(73)	118.8(3)	C(93)-C(91)-C(94)	107.9(17)

C(92')-C(91)-C(94)	56.9(10)
C(80)-C(91)-C(94)	109.0(6)
C(94')-C(91)-C(94)	61.0(10)
C(93')-C(91)-C(94)	143.4(7)
C(92)-C(91)-C(94)	89.8(12)
C(98)-C(95)-C(82)	109.7(3)
C(98)-C(95)-C(96)	111.0(3)
C(82)-C(95)-C(96)	111.0(3)
C(98)-C(95)-C(97)	107.5(3)
C(82)-C(95)-C(97)	111.8(3)
C(96)-C(95)-C(97)	105.7(3)
C(100)-C(99)-C(106)	124.2(3)
C(100)-C(99)-Rh(1)	72.41(17)
C(106)-C(99)-Rh(1)	111.8(2)
C(103)-C(104)-C(105)	125.1(3)
C(103)-C(104)-Rh(1)	73.82(18)
C(105)-C(104)-Rh(1)	107.8(2)
C(99)-C(100)-C(101)	125.8(3)
C(99)-C(100)-Rh(1)	72.76(17)
C(101)-C(100)-Rh(1)	107.9(2)
C(100)-C(101)-C(102)	115.4(3)
C(103)-C(102)-C(101)	113.5(3)
C(104)-C(103)-C(102)	124.0(3)
C(104)-C(103)-Rh(1)	71.23(18)
C(102)-C(103)-Rh(1)	111.8(2)
C(104)-C(105)-C(106)	115.3(3)
C(99)-C(106)-C(105)	113.9(3)
Cl(2)-C(1S)-Cl(1)	116.7(6)
Cl(1')-C(1S')-Cl(2')	106.0(10)
F(1S)-B(1S)-F(2S')	110.5(10)
F(1S)-B(1S)-F(2S)	117.3(8)
F(2S')-B(1S)-F(2S)	38.1(10)
F(1S)-B(1S)-F(3S)	114.3(7)
F(2S')-B(1S)-F(3S)	133.5(9)
F(2S)-B(1S)-F(3S)	106.5(5)
F(1S)-B(1S)-F(4S')	26.0(14)
F(2S')-B(1S)-F(4S')	110.9(13)
F(2S)-B(1S)-F(4S')	134.3(12)
F(3S)-B(1S)-F(4S')	114.8(9)
F(1S)-B(1S)-F(4S)	107.4(6)
F(2S')-B(1S)-F(4S)	75.7(11)
F(2S)-B(1S)-F(4S)	108.2(6)
F(3S)-B(1S)-F(4S)	101.9(6)
F(4S')-B(1S)-F(4S)	82.3(14)
F(1S)-B(1S)-F(1S')	61.4(13)
F(2S')-B(1S)-F(1S')	88.6(15)
F(2S)-B(1S)-F(1S')	65.4(14)
F(3S)-B(1S)-F(1S')	101.8(8)
F(4S')-B(1S)-F(1S')	87.2(17)
F(4S)-B(1S)-F(1S')	156.3(8)

Table 4. Torsion angles [°] for [Rh(cod)(**74a**)]BF_4 (**90a**).

P(2)-Rh(1)-P(1)-O(3X)	140.90(9)
C(100)-Rh(1)-P(1)-O(3X)	-113.5(2)
C(104)-Rh(1)-P(1)-O(3X)	-14.34(12)
C(99)-Rh(1)-P(1)-O(3X)	27.3(4)
C(103)-Rh(1)-P(1)-O(3X)	-49.29(12)
P(2)-Rh(1)-P(1)-O(1)	23.13(9)
C(100)-Rh(1)-P(1)-O(1)	128.7(2)
C(104)-Rh(1)-P(1)-O(1)	-132.11(12)
C(99)-Rh(1)-P(1)-O(1)	-90.5(4)
C(103)-Rh(1)-P(1)-O(1)	-167.06(12)
P(2)-Rh(1)-P(1)-O(4X)	-98.82(10)
C(100)-Rh(1)-P(1)-O(4X)	6.8(2)
C(104)-Rh(1)-P(1)-O(4X)	105.94(13)
C(99)-Rh(1)-P(1)-O(4X)	147.6(4)
C(103)-Rh(1)-P(1)-O(4X)	70.99(12)
O(3X)-P(1)-O(1)-C(1)	160.0(2)
O(4X)-P(1)-O(1)-C(1)	53.0(2)
Rh(1)-P(1)-O(1)-C(1)	-75.6(2)
P(1)-O(1)-C(1)-C(4)	93.0(3)
P(1)-O(1)-C(1)-C(2)	-153.9(2)
P(1)-Rh(1)-P(2)-O(2)	25.09(10)
C(100)-Rh(1)-P(2)-O(2)	-132.58(12)
C(104)-Rh(1)-P(2)-O(2)	127.2(2)
C(99)-Rh(1)-P(2)-O(2)	-167.40(12)
C(103)-Rh(1)-P(2)-O(2)	-97.3(4)
P(1)-Rh(1)-P(2)-O(2X)	142.74(8)
C(100)-Rh(1)-P(2)-O(2X)	-14.93(11)
C(104)-Rh(1)-P(2)-O(2X)	-115.1(2)
C(99)-Rh(1)-P(2)-O(2X)	-49.75(12)
C(103)-Rh(1)-P(2)-O(2X)	20.3(4)
P(1)-Rh(1)-P(2)-O(1X)	-96.73(9)
C(100)-Rh(1)-P(2)-O(1X)	105.60(11)
C(104)-Rh(1)-P(2)-O(1X)	5.4(2)
C(99)-Rh(1)-P(2)-O(1X)	70.78(12)
C(103)-Rh(1)-P(2)-O(1X)	140.9(4)
O(2X)-P(2)-O(2)-C(4)	162.4(2)
O(1X)-P(2)-O(2)-C(4)	54.6(2)
Rh(1)-P(2)-O(2)-C(4)	-73.3(2)
O(1)-C(1)-C(2)-O(3)	-161.8(2)
C(4)-C(1)-C(2)-O(3)	-42.2(3)
O(1)-C(1)-C(2)-C(5)	78.0(3)
C(4)-C(1)-C(2)-C(5)	-162.4(3)
C(5)-C(2)-O(3)-C(3)	150.6(3)
C(1)-C(2)-O(3)-C(3)	27.9(3)
C(2)-O(3)-C(3)-C(22)	120.2(3)
C(2)-O(3)-C(3)-C(4)	-2.6(3)
P(2)-O(2)-C(4)-C(1)	86.9(3)
P(2)-O(2)-C(4)-C(3)	-159.52(19)
O(1)-C(1)-C(4)-O(2)	-81.8(3)
C(2)-C(1)-C(4)-O(2)	158.7(2)
O(1)-C(1)-C(4)-C(3)	159.9(2)
C(2)-C(1)-C(4)-C(3)	40.4(3)
O(3)-C(3)-C(4)-O(2)	-144.0(2)
C(22)-C(3)-C(4)-O(2)	95.6(3)
O(3)-C(3)-C(4)-C(1)	-24.3(3)
C(22)-C(3)-C(4)-C(1)	-144.6(3)
C(16)-Si(1)-O(4)-C(5)	-33.1(3)
C(6)-Si(1)-O(4)-C(5)	-151.5(3)
C(9')-Si(1)-O(4)-C(5)	91.8(3)
Si(1)-O(4)-C(5)-C(2)	135.9(3)
O(3)-C(2)-C(5)-O(4)	-66.6(3)
C(1)-C(2)-C(5)-O(4)	48.6(4)
C(27)-Si(2)-O(5)-C(22)	-51.2(3)
C(23)-Si(2)-O(5)-C(22)	-168.0(2)
C(33)-Si(2)-O(5)-C(22)	74.1(3)
O(4)-Si(1)-C(6)-C(7)	-164.4(10)
C(16)-Si(1)-C(6)-C(7)	78.8(11)
C(9')-Si(1)-C(6)-C(7)	-48.8(11)
O(4)-Si(1)-C(6)-C(11)	32.8(6)
C(16)-Si(1)-C(6)-C(11)	-84.0(6)
C(9')-Si(1)-C(6)-C(11)	148.4(5)
O(4)-Si(1)-C(6)-C(7')	61.6(8)
C(16)-Si(1)-C(6)-C(7')	-55.2(8)
C(9')-Si(1)-C(6)-C(7')	177.2(8)
O(4)-Si(1)-C(6)-C(6')	-159.6(7)
C(16)-Si(1)-C(6)-C(6')	83.6(7)
C(9')-Si(1)-C(6)-C(6')	-44.0(7)

O(4)-Si(1)-C(6)-C(8')	-53.1(4)
C(16)-Si(1)-C(6)-C(8')	-169.9(3)
C(9')-Si(1)-C(6)-C(8')	62.5(4)
C(11)-C(6)-C(7)-C(8)	-17(2)
C(7')-C(6)-C(7)-C(8)	-42.7(18)
C(6')-C(6)-C(7)-C(8)	125(17)
C(8')-C(6)-C(7)-C(8)	65.5(15)
Si(1)-C(6)-C(7)-C(8)	-180.0(9)
C(6)-C(7)-C(8)-C(9)	13(2)
C(7)-C(8)-C(9)-C(10)	-3.3(15)
C(8)-C(9)-C(10)-C(11)	-1.3(15)
C(9)-C(10)-C(11)-C(6)	-3.0(15)
C(7)-C(6)-C(11)-C(10)	13.0(16)
C(7')-C(6)-C(11)-C(10)	83(2)
C(6')-C(6)-C(11)-C(10)	9.1(14)
C(8')-C(6)-C(11)-C(10)	-82.3(10)
Si(1)-C(6)-C(11)-C(10)	175.6(7)
O(4)-Si(1)-C(9')-C(10')	17.3(6)
C(16)-Si(1)-C(9')-C(10')	139.4(5)
C(6)-Si(1)-C(9')-C(10')	-94.4(6)
O(4)-Si(1)-C(9')-C(14')	179.1(16)
C(16)-Si(1)-C(9')-C(14')	-58.9(16)
C(6)-Si(1)-C(9')-C(14')	67.4(16)
O(4)-Si(1)-C(9')-C(13)	-173.0(13)
C(16)-Si(1)-C(9')-C(13)	-51.0(13)
C(6)-Si(1)-C(9')-C(13)	75.3(13)
O(4)-Si(1)-C(9')-C(12)	53.4(6)
C(16)-Si(1)-C(9')-C(12)	175.5(6)
C(6)-Si(1)-C(9')-C(12)	-58.3(6)
O(4)-Si(1)-C(9')-C(14)	-57.4(4)
C(16)-Si(1)-C(9')-C(14)	64.7(4)
C(6)-Si(1)-C(9')-C(14)	-169.1(4)
C(14')-C(9')-C(10')-C(11')	11.3(18)
C(13)-C(9')-C(10')-C(11')	3.9(17)
C(12)-C(9')-C(10')-C(11')	104.0(12)
C(14)-C(9')-C(10')-C(11')	-92.3(10)
Si(1)-C(9')-C(10')-C(11')	173.9(7)
C(9')-C(10')-C(11')-C(12')	-1.6(14)
C(10')-C(11')-C(12')-C(13')	-2.4(13)
C(11')-C(12')-C(13')-C(14')	-3.8(19)
C(10')-C(9')-C(14')-C(13')	-18(3)
C(13)-C(9')-C(14')-C(13')	90(15)
C(12)-C(9')-C(14')-C(13')	-58(3)
C(14)-C(9')-C(14')-C(13')	58(3)
Si(1)-C(9')-C(14')-C(13')	178.7(17)
C(12')-C(13')-C(14')-C(9')	15(3)
O(4)-Si(1)-C(16)-C(17)	121.8(3)
C(6)-Si(1)-C(16)-C(17)	-125.4(3)
C(9')-Si(1)-C(16)-C(17)	0.1(4)
O(4)-Si(1)-C(16)-C(21)	-58.8(3)
C(6)-Si(1)-C(16)-C(21)	53.9(3)
C(9')-Si(1)-C(16)-C(21)	179.4(3)
C(21)-C(16)-C(17)-C(18)	0.0(6)
Si(1)-C(16)-C(17)-C(18)	179.3(3)
C(16)-C(17)-C(18)-C(19)	-1.2(7)
C(17)-C(18)-C(19)-C(20)	1.3(7)
C(18)-C(19)-C(20)-C(21)	-0.2(6)
C(17)-C(16)-C(21)-C(20)	1.2(5)
Si(1)-C(16)-C(21)-C(20)	-178.2(3)
C(19)-C(20)-C(21)-C(16)	-1.1(6)
Si(2)-O(5)-C(22)-C(3)	158.7(2)
O(3)-C(3)-C(22)-O(5)	-61.6(3)
C(4)-C(3)-C(22)-O(5)	55.4(3)
O(5)-Si(2)-C(23)-C(24)	64.3(3)
C(27)-Si(2)-C(23)-C(24)	-52.8(3)
C(33)-Si(2)-C(23)-C(24)	-179.8(3)
O(5)-Si(2)-C(23)-C(26)	-58.9(3)
C(27)-Si(2)-C(23)-C(26)	-176.0(2)
C(33)-Si(2)-C(23)-C(26)	57.1(3)
O(5)-Si(2)-C(23)-C(25)	-177.0(2)
C(27)-Si(2)-C(23)-C(25)	65.9(2)
C(33)-Si(2)-C(23)-C(25)	-61.0(3)
O(5)-Si(2)-C(27)-C(32)	157.7(3)
C(23)-Si(2)-C(27)-C(32)	-88.0(3)
C(33)-Si(2)-C(27)-C(32)	36.6(4)
O(5)-Si(2)-C(27)-C(28)	-32.2(3)
C(23)-Si(2)-C(27)-C(28)	82.1(3)
C(33)-Si(2)-C(27)-C(28)	-153.3(3)
C(32)-C(27)-C(28)-C(29)	-0.6(5)
Si(2)-C(27)-C(28)-C(29)	-171.4(3)
C(27)-C(28)-C(29)-C(30)	-0.3(6)
C(28)-C(29)-C(30)-C(31)	0.5(6)
C(29)-C(30)-C(31)-C(32)	0.2(6)
C(30)-C(31)-C(32)-C(27)	-1.1(6)
C(28)-C(27)-C(32)-C(31)	1.3(6)
Si(2)-C(27)-C(32)-C(31)	171.4(3)
O(5)-Si(2)-C(33)-C(38)	14.8(3)
C(27)-Si(2)-C(33)-C(38)	136.9(3)
C(23)-Si(2)-C(33)-C(38)	-99.5(3)
O(5)-Si(2)-C(33)-C(34)	-168.0(3)
C(27)-Si(2)-C(33)-C(34)	-45.9(4)
C(23)-Si(2)-C(33)-C(34)	77.8(3)
C(38)-C(33)-C(34)-C(35)	-1.8(5)
Si(2)-C(33)-C(34)-C(35)	-179.0(3)
C(33)-C(34)-C(35)-C(36)	1.2(6)
C(34)-C(35)-C(36)-C(37)	0.2(6)
C(35)-C(36)-C(37)-C(38)	-1.0(6)
C(36)-C(37)-C(38)-C(33)	0.4(6)
C(34)-C(33)-C(38)-C(37)	1.0(6)
Si(2)-C(33)-C(38)-C(37)	178.4(3)
O(3X)-P(1)-O(4X)-C(40)	25.1(3)
O(1)-P(1)-O(4X)-C(40)	127.8(2)
Rh(1)-P(1)-O(4X)-C(40)	-99.6(2)
P(1)-O(4X)-C(40)-C(41)	-58.2(4)
P(1)-O(4X)-C(40)-C(45)	127.7(3)
C(45)-C(40)-C(41)-C(48)	-2.3(5)
O(4X)-C(40)-C(41)-C(48)	-176.1(3)
C(45)-C(40)-C(41)-C(42)	175.2(3)
O(4X)-C(40)-C(41)-C(42)	1.4(5)
C(40)-C(41)-C(42)-C(43)	45.8(5)
C(48)-C(41)-C(42)-C(43)	-136.6(3)
C(40)-C(41)-C(42)-C(49)	-137.4(3)
C(48)-C(41)-C(42)-C(49)	40.2(4)
C(49)-C(42)-C(43)-C(52)	-1.6(5)
C(41)-C(42)-C(43)-C(52)	175.2(3)
C(49)-C(42)-C(43)-O(3X)	-178.8(3)
C(41)-C(42)-C(43)-O(3X)	-2.0(4)
C(42)-C(43)-O(3X)-P(1)	-74.3(3)
C(52)-C(43)-O(3X)-P(1)	108.4(3)
O(1)-P(1)-O(3X)-C(43)	-43.1(2)
O(4X)-P(1)-O(3X)-C(43)	60.7(2)
Rh(1)-P(1)-O(3X)-C(43)	-173.26(17)
C(41)-C(40)-C(45)-C(46)	1.7(5)
O(4X)-C(40)-C(45)-C(46)	175.6(3)
C(41)-C(40)-C(45)-C(53)	-176.0(4)
O(4X)-C(40)-C(45)-C(53)	-2.2(6)
C(40)-C(45)-C(46)-C(47)	-0.6(7)
C(53)-C(45)-C(46)-C(47)	177.3(5)
C(45)-C(46)-C(47)-C(48)	0.1(7)
C(45)-C(46)-C(47)-C(57)	-178.6(5)

C(40)-C(41)-C(48)-C(47)	1.8(6)
C(42)-C(41)-C(48)-C(47)	-175.9(4)
C(46)-C(47)-C(48)-C(41)	-0.8(7)
C(57)-C(47)-C(48)-C(41)	178.0(4)
C(43)-C(42)-C(49)-C(50)	1.5(5)
C(41)-C(42)-C(49)-C(50)	-175.5(3)
C(42)-C(49)-C(50)-C(51)	-0.5(5)
C(42)-C(49)-C(50)-C(61)	176.5(3)
C(49)-C(50)-C(51)-C(52)	-0.5(5)
C(61)-C(50)-C(51)-C(52)	-177.5(3)
C(50)-C(51)-C(52)-C(43)	0.4(5)
C(50)-C(51)-C(52)-C(65)	179.0(3)
C(42)-C(43)-C(52)-C(51)	0.7(5)
O(3X)-C(43)-C(52)-C(51)	177.8(3)
C(42)-C(43)-C(52)-C(65)	-177.7(3)
O(3X)-C(43)-C(52)-C(65)	-0.6(5)
C(46)-C(45)-C(53)-C(56)	163.8(7)
C(40)-C(45)-C(53)-C(56)	-18.5(10)
C(46)-C(45)-C(53)-C(56')	132.3(6)
C(40)-C(45)-C(53)-C(56')	-50.0(9)
C(46)-C(45)-C(53)-C(55)	-36.0(9)
C(40)-C(45)-C(53)-C(55)	141.7(7)
C(46)-C(45)-C(53)-C(54')	-14.0(10)
C(40)-C(45)-C(53)-C(54')	163.6(7)
C(46)-C(45)-C(53)-C(55')	-117.9(4)
C(40)-C(45)-C(53)-C(55')	59.8(5)
C(46)-C(45)-C(53)-C(54)	62.0(5)
C(40)-C(45)-C(53)-C(54)	-120.4(4)
C(48)-C(47)-C(57)-C(59)	127.4(5)
C(46)-C(47)-C(57)-C(59)	-53.9(7)
C(48)-C(47)-C(57)-C(58)	1.7(7)
C(46)-C(47)-C(57)-C(58)	-179.6(5)
C(48)-C(47)-C(57)-C(60)	-116.8(6)
C(46)-C(47)-C(57)-C(60)	61.9(7)
C(49)-C(50)-C(61)-C(63)	-115.7(4)
C(51)-C(50)-C(61)-C(63)	61.3(4)
C(49)-C(50)-C(61)-C(64)	124.4(4)
C(51)-C(50)-C(61)-C(64)	-58.7(4)
C(49)-C(50)-C(61)-C(62)	3.5(5)
C(51)-C(50)-C(61)-C(62)	-179.6(3)
C(51)-C(52)-C(65)-C(67)	126.4(18)
C(43)-C(52)-C(65)-C(67)	-55.2(19)
C(51)-C(52)-C(65)-C(68)	-100(4)
C(43)-C(52)-C(65)-C(68)	78(4)
C(51)-C(52)-C(65)-C(66')	-44.7(5)
C(43)-C(52)-C(65)-C(66')	133.7(4)
C(51)-C(52)-C(65)-C(67')	73.5(4)
C(43)-C(52)-C(65)-C(67')	-108.1(4)
C(51)-C(52)-C(65)-C(68')	-165.2(3)
C(43)-C(52)-C(65)-C(68')	13.2(5)
C(51)-C(52)-C(65)-C(66)	16(3)
C(43)-C(52)-C(65)-C(66)	-166(2)
O(2)-P(2)-O(2X)-C(70)	-41.1(2)
O(1X)-P(2)-O(2X)-C(70)	62.4(2)
Rh(1)-P(2)-O(2X)-C(70)	-172.38(16)
P(2)-O(2X)-C(70)-C(71)	-69.3(3)
P(2)-O(2X)-C(70)-C(75)	112.2(3)
C(75)-C(70)-C(71)-C(78)	-5.2(4)
O(2X)-C(70)-C(71)-C(78)	176.4(2)
C(75)-C(70)-C(71)-C(72)	170.0(3)
O(2X)-C(70)-C(71)-C(72)	-8.5(4)
C(70)-C(71)-C(72)-C(79)	-132.2(3)
C(78)-C(71)-C(72)-C(79)	42.9(4)
C(70)-C(71)-C(72)-C(73)	52.7(4)
C(78)-C(71)-C(72)-C(73)	-132.1(3)
C(79)-C(72)-C(73)-C(82)	-5.1(4)
C(71)-C(72)-C(73)-C(82)	169.9(3)
C(79)-C(72)-C(73)-O(1X)	-178.7(2)
C(71)-C(72)-C(73)-O(1X)	-3.7(4)
C(82)-C(73)-O(1X)-P(2)	134.9(2)
C(72)-C(73)-O(1X)-P(2)	-51.2(3)
O(2)-P(2)-O(1X)-C(73)	121.3(2)
O(2X)-P(2)-O(1X)-C(73)	19.3(3)
Rh(1)-P(2)-O(1X)-C(73)	-105.1(2)
C(71)-C(70)-C(75)-C(76)	5.0(4)
O(2X)-C(70)-C(75)-C(76)	-176.7(2)
C(71)-C(70)-C(75)-C(83)	-172.3(3)
O(2X)-C(70)-C(75)-C(83)	6.0(4)
C(70)-C(75)-C(76)-C(77)	-1.3(5)
C(83)-C(75)-C(76)-C(77)	176.1(3)
C(75)-C(76)-C(77)-C(78)	-1.9(5)
C(75)-C(76)-C(77)-C(87)	176.4(3)
C(76)-C(77)-C(78)-C(71)	1.8(4)
C(87)-C(77)-C(78)-C(71)	-176.5(3)
C(70)-C(71)-C(78)-C(77)	1.6(4)
C(72)-C(71)-C(78)-C(77)	-173.9(3)
C(73)-C(72)-C(79)-C(80)	2.8(4)
C(71)-C(72)-C(79)-C(80)	-172.6(3)
C(72)-C(79)-C(80)-C(81)	0.9(4)
C(72)-C(79)-C(80)-C(91)	177.2(3)
C(79)-C(80)-C(81)-C(82)	-2.8(5)
C(91)-C(80)-C(81)-C(82)	-179.1(3)
C(80)-C(81)-C(82)-C(73)	0.7(4)
C(80)-C(81)-C(82)-C(95)	176.3(3)
C(72)-C(73)-C(82)-C(81)	3.3(4)
O(1X)-C(73)-C(82)-C(81)	177.0(2)
C(72)-C(73)-C(82)-C(95)	-172.1(3)
O(1X)-C(73)-C(82)-C(95)	1.6(4)
C(76)-C(75)-C(83)-C(86)	-17(3)
C(70)-C(75)-C(83)-C(86)	160(3)
C(76)-C(75)-C(83)-C(84)	-153(3)
C(70)-C(75)-C(83)-C(84)	24(3)
C(76)-C(75)-C(83)-C(85')	122.1(5)
C(70)-C(75)-C(83)-C(85')	-60.7(5)
C(76)-C(75)-C(83)-C(86')	-2.8(5)
C(70)-C(75)-C(83)-C(86')	174.4(4)
C(76)-C(75)-C(83)-C(84')	-119.0(4)
C(70)-C(75)-C(83)-C(84')	58.2(4)
C(76)-C(75)-C(83)-C(85)	90.1(15)
C(70)-C(75)-C(83)-C(85)	-92.7(15)
C(78)-C(77)-C(87)-C(89)	-145.1(3)
C(76)-C(77)-C(87)-C(89)	36.7(4)
C(78)-C(77)-C(87)-C(90)	-21.9(5)
C(76)-C(77)-C(87)-C(90)	159.9(3)
C(78)-C(77)-C(87)-C(88)	96.1(4)
C(76)-C(77)-C(87)-C(88)	-82.2(4)
C(81)-C(80)-C(91)-C(93)	0.5(19)
C(79)-C(80)-C(91)-C(93)	-175.7(19)
C(81)-C(80)-C(91)-C(92')	-166.0(5)
C(79)-C(80)-C(91)-C(92')	17.8(6)
C(81)-C(80)-C(91)-C(94')	68.2(5)
C(79)-C(80)-C(91)-C(94')	-107.9(4)
C(81)-C(80)-C(91)-C(93')	-45.2(5)
C(79)-C(80)-C(91)-C(93')	138.7(4)
C(81)-C(80)-C(91)-C(92)	-132.3(9)
C(79)-C(80)-C(91)-C(92)	51.6(10)
C(81)-C(80)-C(91)-C(94)	132.7(10)
C(79)-C(80)-C(91)-C(94)	-43.5(11)
C(81)-C(82)-C(95)-C(98)	-114.8(3)
C(73)-C(82)-C(95)-C(98)	60.4(4)

C(81)-C(82)-C(95)-C(96)	122.1(3)
C(73)-C(82)-C(95)-C(96)	-62.7(4)
C(81)-C(82)-C(95)-C(97)	4.3(4)
C(73)-C(82)-C(95)-C(97)	179.6(3)
P(1)-Rh(1)-C(99)-C(100)	-154.1(3)
P(2)-Rh(1)-C(99)-C(100)	91.77(19)
C(104)-Rh(1)-C(99)-C(100)	-111.6(2)
C(103)-Rh(1)-C(99)-C(100)	-76.8(2)
P(1)-Rh(1)-C(99)-C(106)	-33.6(6)
P(2)-Rh(1)-C(99)-C(106)	-147.7(2)
C(100)-Rh(1)-C(99)-C(106)	120.5(3)
C(104)-Rh(1)-C(99)-C(106)	8.9(2)
C(103)-Rh(1)-C(99)-C(106)	43.7(3)
P(1)-Rh(1)-C(104)-C(103)	-91.78(19)
P(2)-Rh(1)-C(104)-C(103)	165.14(16)
C(100)-Rh(1)-C(104)-C(103)	65.3(2)
C(99)-Rh(1)-C(104)-C(103)	97.4(2)
P(1)-Rh(1)-C(104)-C(105)	145.8(2)
P(2)-Rh(1)-C(104)-C(105)	42.7(4)
C(100)-Rh(1)-C(104)-C(105)	-57.2(2)
C(99)-Rh(1)-C(104)-C(105)	-25.0(2)
C(103)-Rh(1)-C(104)-C(105)	-122.4(3)
C(106)-C(99)-C(100)-C(101)	-4.9(5)
Rh(1)-C(99)-C(100)-C(101)	99.9(3)
C(106)-C(99)-C(100)-Rh(1)	-104.9(3)
P(1)-Rh(1)-C(100)-C(99)	164.86(18)
P(2)-Rh(1)-C(100)-C(99)	-88.86(19)
C(104)-Rh(1)-C(100)-C(99)	66.2(2)
C(103)-Rh(1)-C(100)-C(99)	98.2(2)
P(1)-Rh(1)-C(100)-C(101)	41.9(3)
P(2)-Rh(1)-C(100)-C(101)	148.2(2)
C(104)-Rh(1)-C(100)-C(101)	-56.8(2)
C(99)-Rh(1)-C(100)-C(101)	-122.9(3)
C(103)-Rh(1)-C(100)-C(101)	-24.7(2)
C(99)-C(100)-C(101)-C(102)	-41.2(5)
Rh(1)-C(100)-C(101)-C(102)	40.1(3)
C(100)-C(101)-C(102)-C(103)	-35.1(4)
C(105)-C(104)-C(103)-C(102)	-3.4(5)
Rh(1)-C(104)-C(103)-C(102)	-104.1(3)
C(105)-C(104)-C(103)-Rh(1)	100.7(3)
C(101)-C(102)-C(103)-C(104)	92.6(4)
C(101)-C(102)-C(103)-Rh(1)	11.2(4)
P(1)-Rh(1)-C(103)-C(104)	88.90(19)
P(2)-Rh(1)-C(103)-C(104)	-148.4(3)
C(100)-Rh(1)-C(103)-C(104)	-112.3(2)
C(99)-Rh(1)-C(103)-C(104)	-77.8(2)
P(1)-Rh(1)-C(103)-C(102)	-151.1(2)
P(2)-Rh(1)-C(103)-C(102)	-28.4(6)
C(100)-Rh(1)-C(103)-C(102)	7.6(2)
C(104)-Rh(1)-C(103)-C(102)	120.0(3)
C(99)-Rh(1)-C(103)-C(102)	42.2(2)
C(103)-C(104)-C(105)-C(106)	-43.6(5)
Rh(1)-C(104)-C(105)-C(106)	38.9(3)
C(100)-C(99)-C(106)-C(105)	92.0(4)
Rh(1)-C(99)-C(106)-C(105)	9.0(4)
C(104)-C(105)-C(106)-C(99)	-32.9(4)

Table 5. Bond lengths [Å] and angles [°] for [Rh(cod)(**75'a**)]BF_4 (**91'a**).

Rh(1)-P(1)	2.2536(11)
Rh(1)-P(2)	2.2588(10)
Rh(1)-C(64)	2.276(5)
Rh(1)-C(68)	2.307(5)
Rh(1)-C(65)	2.316(4)
Rh(1)-C(69)	2.325(5)
P(1)-O(3)	1.596(3)
P(1)-O(2)	1.606(3)
P(1)-O(4)	1.615(3)
C(1)-O(2)	1.420(5)
C(1)-C(4)	1.524(5)
C(1)-C(2)	1.545(6)
O(1)-C(2)	1.418(6)
O(1)-C(3)	1.428(6)
P(2)-O(6)	1.587(3)
P(2)-O(5)	1.608(3)
P(2)-O(7)	1.609(3)
C(2)-C(5)	1.468(10)
C(3)-C(6)	1.462(9)
C(3)-C(4)	1.537(6)
O(3)-C(7)	1.408(5)
C(4)-O(5)	1.430(5)
O(4)-C(18)	1.413(5)
O(6)-C(36)	1.396(4)
C(7)-C(8)	1.390(6)
C(7)-C(12)	1.409(6)
O(7)-C(47)	1.403(5)
C(8)-C(9)	1.395(8)
C(8)-C(19)	1.555(8)
C(9)-C(10)	1.384(9)
C(10)-C(11)	1.385(8)
C(10)-C(23)	1.535(7)
C(11)-C(12)	1.399(6)

C(12)-C(13)	1.479(6)	C(69)-C(70)	1.504(8)
C(13)-C(18)	1.400(5)	C(70)-C(71)	1.522(9)
C(13)-C(14)	1.403(6)	C(1B)-O(2B)	1.419(5)
C(14)-C(15)	1.381(7)	C(1B)-C(4B)	1.526(6)
C(15)-C(16)	1.407(6)	C(1B)-C(2B)	1.534(6)
C(15)-C(27)	1.521(6)	O(1B)-C(3B)	1.423(5)
C(16)-C(17)	1.404(6)	O(1B)-C(2B)	1.445(6)
C(17)-C(18)	1.395(6)	P(1B)-O(2B)	1.584(3)
C(17)-C(31)	1.536(5)	P(1B)-O(4B)	1.598(4)
C(19)-C(20)	1.512(8)	P(1B)-O(3B)	1.610(3)
C(19)-C(22)	1.530(8)	P(1B)-Rh(2)	2.2597(11)
C(19)-C(21)	1.565(10)	Rh(2)-P(2B)	2.2550(10)
C(23)-C(26)	1.488(8)	Rh(2)-C(68B)	2.273(4)
C(23)-C(24)	1.531(9)	Rh(2)-C(64B)	2.274(4)
C(23)-C(25)	1.569(13)	Rh(2)-C(67B)	2.295(4)
C(27)-C(28')	1.44(2)	Rh(2)-C(63B)	2.295(4)
C(27)-C(30)	1.463(8)	C(2B)-C(5B)	1.516(7)
C(27)-C(29')	1.525(18)	C(3B)-C(6B)	1.509(8)
C(27)-C(28)	1.551(9)	C(3B)-C(4B)	1.523(6)
C(27)-C(29)	1.560(8)	O(3B)-C(7B)	1.423(5)
C(27)-C(30')	1.695(13)	C(4B)-O(5B)	1.444(5)
C(31)-C(34)	1.532(6)	O(4B)-C(18B)	1.403(6)
C(31)-C(33)	1.535(6)	P(2B)-O(5B)	1.594(3)
C(31)-C(32)	1.536(7)	P(2B)-O(6B)	1.603(3)
C(36)-C(41)	1.397(5)	P(2B)-O(7B)	1.609(3)
C(36)-C(37)	1.404(5)	O(6B)-C(35B)	1.421(4)
C(37)-C(38)	1.405(6)	C(7B)-C(8B)	1.392(8)
C(37)-C(48)	1.544(5)	C(7B)-C(12B)	1.392(9)
C(38)-C(39)	1.399(6)	O(7B)-C(46B)	1.403(5)
C(39)-C(40)	1.382(6)	C(8B)-C(9B)	1.414(7)
C(39)-C(52)	1.531(6)	C(8B)-C(19B)	1.554(9)
C(40)-C(41)	1.397(5)	C(9B)-C(10B)	1.398(10)
C(41)-C(42)	1.496(5)	C(10B)-C(11B)	1.371(11)
C(42)-C(47)	1.390(6)	C(10B)-C(23B)	1.544(7)
C(42)-C(43)	1.390(5)	C(11B)-C(12B)	1.394(7)
C(43)-C(44)	1.390(5)	C(12B)-C(13B)	1.464(10)
C(44)-C(45)	1.386(6)	C(13B)-C(14B)	1.386(9)
C(44)-C(56)	1.534(6)	C(13B)-C(18B)	1.418(7)
C(45)-C(46)	1.394(6)	C(14B)-C(15B)	1.369(12)
C(46)-C(47)	1.405(6)	C(15B)-C(16B)	1.423(9)
C(46)-C(60)	1.547(6)	C(15B)-C(27B)	1.559(10)
C(48)-C(51)	1.521(6)	C(16B)-C(17B)	1.390(8)
C(48)-C(49)	1.540(6)	C(17B)-C(18B)	1.392(10)
C(48)-C(50)	1.542(7)	C(17B)-C(31B)	1.539(8)
C(52)-C(53)	1.496(7)	C(19B)-C(22B)	1.494(8)
C(52)-C(54)	1.557(8)	C(19B)-C(21B)	1.529(7)
C(52)-C(55)	1.559(7)	C(19B)-C(20B)	1.543(6)
C(56)-C(59')	1.398(19)	C(23B)-C(25B)	1.496(15)
C(56)-C(57)	1.482(9)	C(23B)-C(26B)	1.520(8)
C(56)-C(59)	1.501(9)	C(23B)-C(24B)	1.597(15)
C(56)-C(58')	1.533(16)	C(27B)-C(30B)	1.498(15)
C(56)-C(58)	1.606(9)	C(27B)-C(29B)	1.526(12)
C(56)-C(57')	1.690(18)	C(27B)-C(28B)	1.564(13)
C(60)-C(61')	1.443(19)	C(31B)-C(32B)	1.527(9)
C(60)-C(62)	1.479(10)	C(31B)-C(34B)	1.558(8)
C(60)-C(63)	1.556(10)	C(31B)-C(33B)	1.566(7)
C(60)-C(62')	1.58(2)	C(35B)-C(36B)	1.390(6)
C(60)-C(61)	1.599(9)	C(35B)-C(40B)	1.392(6)
C(60)-C(63')	1.618(14)	C(36B)-C(37B)	1.401(5)
C(64)-C(65)	1.336(9)	C(36B)-C(47B)	1.526(6)
C(64)-C(71)	1.528(9)	C(37B)-C(38B)	1.394(5)
C(65)-C(66)	1.510(7)	C(38B)-C(39B)	1.399(6)
C(66)-C(67)	1.516(8)	C(38B)-C(51B)	1.529(5)
C(67)-C(68)	1.533(8)	C(39B)-C(40B)	1.395(5)
C(68)-C(69)	1.312(8)	C(40B)-C(41B)	1.488(6)

C(41B)-C(46B)	1.385(5)	O(4)-P(1)-Rh(1)	121.65(12)
C(41B)-C(42B)	1.406(6)	O(2)-C(1)-C(4)	113.0(3)
C(42B)-C(43B)	1.371(7)	O(2)-C(1)-C(2)	113.0(4)
C(43B)-C(44B)	1.419(7)	C(4)-C(1)-C(2)	102.2(3)
C(43B)-C(55B)	1.525(7)	C(2)-O(1)-C(3)	112.7(3)
C(44B)-C(45B)	1.367(7)	O(6)-P(2)-O(5)	101.26(15)
C(45B)-C(46B)	1.409(6)	O(6)-P(2)-O(7)	105.00(15)
C(45B)-C(59B)	1.558(7)	O(5)-P(2)-O(7)	96.99(16)
C(47B)-C(50B)	1.539(6)	O(6)-P(2)-Rh(1)	107.99(11)
C(47B)-C(49B)	1.540(6)	O(5)-P(2)-Rh(1)	121.78(11)
C(47B)-C(48B)	1.544(6)	O(7)-P(2)-Rh(1)	121.14(12)
C(51B)-C(52B)	1.522(7)	O(1)-C(2)-C(5)	110.6(6)
C(51B)-C(54B)	1.531(6)	O(1)-C(2)-C(1)	103.6(4)
C(51B)-C(53B)	1.535(6)	C(5)-C(2)-C(1)	114.6(4)
C(55B)-C(57B)	1.461(13)	C(1)-O(2)-P(1)	121.8(3)
C(55B)-C(58B)	1.486(10)	O(1)-C(3)-C(6)	111.1(6)
C(55B)-C(56B)	1.503(9)	O(1)-C(3)-C(4)	105.2(4)
C(59B)-C(62B)	1.527(7)	C(6)-C(3)-C(4)	114.8(4)
C(59B)-C(60B)	1.547(8)	C(7)-O(3)-P(1)	128.4(3)
C(59B)-C(61B)	1.567(8)	O(5)-C(4)-C(1)	113.1(3)
C(63B)-C(64B)	1.385(7)	O(5)-C(4)-C(3)	112.5(4)
C(63B)-C(70B)	1.508(6)	C(1)-C(4)-C(3)	102.0(3)
C(64B)-C(65B)	1.497(6)	C(18)-O(4)-P(1)	120.5(2)
C(65B)-C(66B)	1.549(7)	C(4)-O(5)-P(2)	120.8(3)
C(66B)-C(67B)	1.519(7)	C(36)-O(6)-P(2)	129.6(3)
C(67B)-C(68B)	1.354(8)	C(8)-C(7)-O(3)	118.9(4)
C(68B)-C(69B)	1.491(8)	C(8)-C(7)-C(12)	122.1(4)
C(69B)-C(70B)	1.563(7)	O(3)-C(7)-C(12)	118.4(4)
C(1LD)-Cl(1D)	1.50(3)	C(47)-O(7)-P(2)	119.2(3)
C(1LD)-Cl(2D)	1.71(3)	C(7)-C(8)-C(9)	116.1(5)
B(1)-F(1)	1.340(8)	C(7)-C(8)-C(19)	123.1(5)
B(1)-F(4)	1.356(8)	C(9)-C(8)-C(19)	120.8(5)
B(1)-F(2)	1.361(10)	C(10)-C(9)-C(8)	124.6(5)
B(1)-F(3)	1.370(10)	C(9)-C(10)-C(11)	117.1(4)
B(1B)-F(4B)	1.354(15)	C(9)-C(10)-C(23)	121.0(5)
B(1B)-F(2B)	1.373(15)	C(11)-C(10)-C(23)	121.9(6)
B(1B)-F(3B)	1.382(14)	C(10)-C(11)-C(12)	122.0(5)
B(1B)-F(1B)	1.428(12)	C(11)-C(12)-C(7)	118.0(4)
Cl(1C)-C(1LC)	1.781(2)	C(11)-C(12)-C(13)	116.5(4)
C(1LC)-Cl(2C)	17.287	C(7)-C(12)-C(13)	125.5(4)
C(1LC)-Cl(2E)	18.428	C(18)-C(13)-C(14)	116.9(4)
Cl(1B)-C(1LB)	17.134	C(18)-C(13)-C(12)	123.2(4)
C(1LB)-Cl(2B)	1.730(3)	C(14)-C(13)-C(12)	119.6(4)
Cl(1A)-C(1LA)	1.619(19)	C(15)-C(14)-C(13)	122.2(4)
C(1LA)-Cl(2A)	1.91(2)	C(14)-C(15)-C(16)	118.2(4)
P(1)-Rh(1)-P(2)	94.82(4)	C(14)-C(15)-C(27)	122.2(4)
P(1)-Rh(1)-C(64)	90.18(14)	C(16)-C(15)-C(27)	119.5(4)
P(2)-Rh(1)-C(64)	159.54(17)	C(17)-C(16)-C(15)	121.9(4)
P(1)-Rh(1)-C(68)	160.89(15)	C(18)-C(17)-C(16)	116.7(4)
P(2)-Rh(1)-C(68)	90.43(12)	C(18)-C(17)-C(31)	122.7(4)
C(64)-Rh(1)-C(68)	91.27(17)	C(16)-C(17)-C(31)	120.6(4)
P(1)-Rh(1)-C(65)	93.41(13)	C(17)-C(18)-C(13)	122.9(4)
P(2)-Rh(1)-C(65)	163.92(15)	C(17)-C(18)-O(4)	120.1(3)
C(64)-Rh(1)-C(65)	33.8(2)	C(13)-C(18)-O(4)	116.8(4)
C(68)-Rh(1)-C(65)	77.52(18)	C(20)-C(19)-C(22)	107.2(5)
P(1)-Rh(1)-C(69)	163.49(17)	C(20)-C(19)-C(8)	109.8(5)
P(2)-Rh(1)-C(69)	93.25(13)	C(22)-C(19)-C(8)	112.0(6)
C(64)-Rh(1)-C(69)	77.5(2)	C(20)-C(19)-C(21)	111.2(6)
C(68)-Rh(1)-C(69)	32.9(2)	C(22)-C(19)-C(21)	106.5(5)
C(65)-Rh(1)-C(69)	82.46(18)	C(8)-C(19)-C(21)	110.0(4)
O(3)-P(1)-O(2)	102.37(17)	C(26)-C(23)-C(24)	114.9(7)
O(3)-P(1)-O(4)	104.96(16)	C(26)-C(23)-C(10)	111.4(5)
O(2)-P(1)-O(4)	95.79(16)	C(24)-C(23)-C(10)	107.3(5)
O(3)-P(1)-Rh(1)	107.86(12)	C(26)-C(23)-C(25)	102.3(8)
O(2)-P(1)-Rh(1)	121.64(12)	C(24)-C(23)-C(25)	109.3(6)

C(10)-C(23)-C(25)	111.7(5)	C(53)-C(52)-C(55)	109.9(4)
C(28')-C(27)-C(30)	132.2(10)	C(39)-C(52)-C(55)	113.0(4)
C(28')-C(27)-C(15)	114.8(9)	C(54)-C(52)-C(55)	105.0(5)
C(30)-C(27)-C(15)	110.2(4)	C(59')-C(56)-C(57)	135.2(9)
C(28')-C(27)-C(29')	110.2(11)	C(59')-C(56)-C(59)	42.2(9)
C(30)-C(27)-C(29')	59.9(8)	C(57)-C(56)-C(59)	115.2(7)
C(15)-C(27)-C(29')	116.4(8)	C(59')-C(56)-C(58')	113.2(11)
C(28')-C(27)-C(28)	32.7(9)	C(57)-C(56)-C(58')	46.4(7)
C(30)-C(27)-C(28)	114.5(6)	C(59)-C(56)-C(58')	132.7(8)
C(15)-C(27)-C(28)	111.3(5)	C(59')-C(56)-C(44)	114.5(9)
C(29')-C(27)-C(28)	130.5(8)	C(57)-C(56)-C(44)	110.3(4)
C(28')-C(27)-C(29)	72.0(10)	C(59)-C(56)-C(44)	113.3(5)
C(30)-C(27)-C(29)	110.1(6)	C(58')-C(56)-C(44)	114.0(7)
C(15)-C(27)-C(29)	106.2(4)	C(59')-C(56)-C(58)	62.8(9)
C(29')-C(27)-C(29)	50.6(7)	C(57)-C(56)-C(58)	106.0(6)
C(28)-C(27)-C(29)	104.1(6)	C(59)-C(56)-C(58)	103.6(6)
C(28')-C(27)-C(30')	103.6(10)	C(58')-C(56)-C(58)	60.6(7)
C(30)-C(27)-C(30')	45.8(6)	C(44)-C(56)-C(58)	107.6(4)
C(15)-C(27)-C(30')	108.0(5)	C(59')-C(56)-C(57')	108.3(11)
C(29')-C(27)-C(30')	102.2(8)	C(57)-C(56)-C(57')	55.5(8)
C(28)-C(27)-C(30')	74.2(6)	C(59)-C(56)-C(57')	68.2(8)
C(29)-C(27)-C(30')	143.7(6)	C(58')-C(56)-C(57')	100.0(9)
C(34)-C(31)-C(33)	110.7(4)	C(44)-C(56)-C(57')	105.4(7)
C(34)-C(31)-C(32)	107.8(4)	C(58)-C(56)-C(57')	146.4(7)
C(33)-C(31)-C(32)	107.4(4)	C(61')-C(60)-C(62)	141.8(9)
C(34)-C(31)-C(17)	110.4(3)	C(61')-C(60)-C(46)	108.3(9)
C(33)-C(31)-C(17)	109.3(4)	C(62)-C(60)-C(46)	109.8(5)
C(32)-C(31)-C(17)	111.2(4)	C(61')-C(60)-C(63)	51.8(8)
O(6)-C(36)-C(41)	118.7(3)	C(62)-C(60)-C(63)	111.1(6)
O(6)-C(36)-C(37)	118.8(3)	C(46)-C(60)-C(63)	116.4(5)
C(41)-C(36)-C(37)	122.1(4)	C(61')-C(60)-C(62')	108.3(12)
C(36)-C(37)-C(38)	116.4(4)	C(62)-C(60)-C(62')	51.0(10)
C(36)-C(37)-C(48)	123.7(3)	C(46)-C(60)-C(62')	115.6(10)
C(38)-C(37)-C(48)	119.9(3)	C(63)-C(60)-C(62')	127.9(10)
C(39)-C(38)-C(37)	123.4(4)	C(61')-C(60)-C(61)	57.0(9)
C(40)-C(39)-C(38)	117.2(4)	C(62)-C(60)-C(61)	109.0(6)
C(40)-C(39)-C(52)	121.0(4)	C(46)-C(60)-C(61)	105.4(4)
C(38)-C(39)-C(52)	121.8(4)	C(63)-C(60)-C(61)	104.7(6)
C(39)-C(40)-C(41)	122.6(4)	C(62')-C(60)-C(61)	58.4(10)
C(40)-C(41)-C(36)	118.1(4)	C(61')-C(60)-C(63')	109.2(10)
C(40)-C(41)-C(42)	116.9(3)	C(62)-C(60)-C(63')	58.5(6)
C(36)-C(41)-C(42)	124.7(3)	C(46)-C(60)-C(63')	111.3(6)
C(47)-C(42)-C(43)	118.3(4)	C(63)-C(60)-C(63')	58.4(6)
C(47)-C(42)-C(41)	122.7(3)	C(62')-C(60)-C(63')	103.9(11)
C(43)-C(42)-C(41)	118.9(3)	C(61)-C(60)-C(63')	143.2(6)
C(44)-C(43)-C(42)	121.5(4)	C(65)-C(64)-C(71)	128.2(5)
C(45)-C(44)-C(43)	117.9(4)	C(65)-C(64)-Rh(1)	74.7(3)
C(45)-C(44)-C(56)	121.2(4)	C(71)-C(64)-Rh(1)	105.3(4)
C(43)-C(44)-C(56)	120.8(4)	C(64)-C(65)-C(66)	124.7(5)
C(44)-C(45)-C(46)	123.1(4)	C(64)-C(65)-Rh(1)	71.4(3)
C(45)-C(46)-C(47)	116.4(4)	C(66)-C(65)-Rh(1)	112.5(3)
C(45)-C(46)-C(60)	118.1(4)	C(65)-C(66)-C(67)	112.9(4)
C(47)-C(46)-C(60)	125.4(4)	C(66)-C(67)-C(68)	114.2(4)
C(42)-C(47)-O(7)	117.1(3)	C(69)-C(68)-C(67)	125.5(5)
C(42)-C(47)-C(46)	122.1(4)	C(69)-C(68)-Rh(1)	74.3(3)
O(7)-C(47)-C(46)	120.8(3)	C(67)-C(68)-Rh(1)	106.1(3)
C(51)-C(48)-C(49)	106.6(4)	C(68)-C(69)-C(70)	127.3(5)
C(51)-C(48)-C(50)	107.6(4)	C(68)-C(69)-Rh(1)	72.8(3)
C(49)-C(48)-C(50)	110.3(4)	C(70)-C(69)-Rh(1)	111.8(4)
C(51)-C(48)-C(37)	112.0(3)	C(69)-C(70)-C(71)	112.2(4)
C(49)-C(48)-C(37)	110.6(3)	C(70)-C(71)-C(64)	113.6(4)
C(50)-C(48)-C(37)	109.6(4)	O(2B)-C(1B)-C(4B)	114.0(4)
C(53)-C(52)-C(39)	110.4(4)	O(2B)-C(1B)-C(2B)	110.0(3)
C(53)-C(52)-C(54)	109.0(5)	C(4B)-C(1B)-C(2B)	103.2(3)
C(39)-C(52)-C(54)	109.3(4)	C(3B)-O(1B)-C(2B)	108.0(3)

O(2B)-P(1B)-O(4B)	100.5(2)	C(16B)-C(17B)-C(31B)	119.6(6)
O(2B)-P(1B)-O(3B)	99.47(17)	C(18B)-C(17B)-C(31B)	123.5(5)
O(4B)-P(1B)-O(3B)	104.04(19)	C(17B)-C(18B)-O(4B)	117.3(4)
O(2B)-P(1B)-Rh(2)	124.01(14)	C(17B)-C(18B)-C(13B)	123.3(5)
O(4B)-P(1B)-Rh(2)	112.43(13)	O(4B)-C(18B)-C(13B)	119.0(6)
O(3B)-P(1B)-Rh(2)	113.78(13)	C(22B)-C(19B)-C(21B)	109.5(5)
P(2B)-Rh(2)-P(1B)	94.71(4)	C(22B)-C(19B)-C(20B)	107.3(4)
P(2B)-Rh(2)-C(68B)	159.10(16)	C(21B)-C(19B)-C(20B)	110.1(4)
P(1B)-Rh(2)-C(68B)	90.64(13)	C(22B)-C(19B)-C(8B)	111.8(5)
P(2B)-Rh(2)-C(64B)	90.54(11)	C(21B)-C(19B)-C(8B)	110.3(4)
P(1B)-Rh(2)-C(64B)	155.27(12)	C(20B)-C(19B)-C(8B)	107.8(5)
C(68B)-Rh(2)-C(64B)	93.01(16)	C(25B)-C(23B)-C(26B)	108.8(7)
P(2B)-Rh(2)-C(67B)	164.87(16)	C(25B)-C(23B)-C(10B)	111.2(8)
P(1B)-Rh(2)-C(67B)	90.41(12)	C(26B)-C(23B)-C(10B)	108.6(4)
C(68B)-Rh(2)-C(67B)	34.5(2)	C(25B)-C(23B)-C(24B)	110.9(7)
C(64B)-Rh(2)-C(67B)	79.10(16)	C(26B)-C(23B)-C(24B)	106.6(8)
P(2B)-Rh(2)-C(63B)	92.19(10)	C(10B)-C(23B)-C(24B)	110.6(6)
P(1B)-Rh(2)-C(63B)	166.97(12)	C(30B)-C(27B)-C(29B)	113.7(10)
C(68B)-Rh(2)-C(63B)	79.14(16)	C(30B)-C(27B)-C(15B)	109.9(7)
C(64B)-Rh(2)-C(63B)	35.28(16)	C(29B)-C(27B)-C(15B)	109.1(7)
C(67B)-Rh(2)-C(63B)	85.71(16)	C(30B)-C(27B)-C(28B)	107.9(8)
O(1B)-C(2B)-C(5B)	108.0(4)	C(29B)-C(27B)-C(28B)	107.0(9)
O(1B)-C(2B)-C(1B)	105.8(4)	C(15B)-C(27B)-C(28B)	109.0(8)
C(5B)-C(2B)-C(1B)	115.0(4)	C(32B)-C(31B)-C(17B)	112.7(5)
C(1B)-O(2B)-P(1B)	126.5(3)	C(32B)-C(31B)-C(34B)	107.7(5)
O(1B)-C(3B)-C(6B)	113.4(5)	C(17B)-C(31B)-C(34B)	111.1(5)
O(1B)-C(3B)-C(4B)	101.3(3)	C(32B)-C(31B)-C(33B)	106.8(5)
C(6B)-C(3B)-C(4B)	113.2(4)	C(17B)-C(31B)-C(33B)	108.8(5)
C(7B)-O(3B)-P(1B)	117.2(3)	C(34B)-C(31B)-C(33B)	109.6(4)
O(5B)-C(4B)-C(3B)	112.2(3)	C(36B)-C(35B)-C(40B)	123.7(3)
O(5B)-C(4B)-C(1B)	116.4(4)	C(36B)-C(35B)-O(6B)	119.8(3)
C(3B)-C(4B)-C(1B)	103.0(4)	C(40B)-C(35B)-O(6B)	116.3(3)
C(18B)-O(4B)-P(1B)	129.9(3)	C(35B)-C(36B)-C(37B)	115.6(3)
O(5B)-P(2B)-O(6B)	99.46(15)	C(35B)-C(36B)-C(47B)	123.7(3)
O(5B)-P(2B)-O(7B)	101.66(16)	C(37B)-C(36B)-C(47B)	120.7(4)
O(6B)-P(2B)-O(7B)	104.28(15)	C(38B)-C(37B)-C(36B)	123.2(4)
O(5B)-P(2B)-Rh(2)	121.33(12)	C(37B)-C(38B)-C(39B)	117.6(3)
O(6B)-P(2B)-Rh(2)	112.70(11)	C(37B)-C(38B)-C(51B)	122.2(4)
O(7B)-P(2B)-Rh(2)	115.03(12)	C(39B)-C(38B)-C(51B)	120.3(3)
C(4B)-O(5B)-P(2B)	127.1(3)	C(40B)-C(39B)-C(38B)	121.6(4)
C(35B)-O(6B)-P(2B)	118.5(2)	C(35B)-C(40B)-C(39B)	117.3(4)
C(8B)-C(7B)-C(12B)	123.7(4)	C(35B)-C(40B)-C(41B)	123.8(3)
C(8B)-C(7B)-O(3B)	120.6(5)	C(39B)-C(40B)-C(41B)	118.8(4)
C(12B)-C(7B)-O(3B)	115.6(5)	C(46B)-C(41B)-C(42B)	118.9(4)
C(46B)-O(7B)-P(2B)	128.5(3)	C(46B)-C(41B)-C(40B)	124.0(4)
C(7B)-C(8B)-C(9B)	115.7(6)	C(42B)-C(41B)-C(40B)	117.1(4)
C(7B)-C(8B)-C(19B)	124.9(4)	C(43B)-C(42B)-C(41B)	121.8(4)
C(9B)-C(8B)-C(19B)	119.4(5)	C(42B)-C(43B)-C(44B)	116.8(4)
C(10B)-C(9B)-C(8B)	122.0(6)	C(42B)-C(43B)-C(55B)	123.1(5)
C(11B)-C(10B)-C(9B)	118.7(5)	C(44B)-C(43B)-C(55B)	120.1(5)
C(11B)-C(10B)-C(23B)	120.0(7)	C(45B)-C(44B)-C(43B)	123.7(5)
C(9B)-C(10B)-C(23B)	121.3(7)	C(44B)-C(45B)-C(46B)	117.2(4)
C(10B)-C(11B)-C(12B)	122.1(6)	C(44B)-C(45B)-C(59B)	121.0(4)
C(7B)-C(12B)-C(11B)	117.3(6)	C(46B)-C(45B)-C(59B)	121.8(4)
C(7B)-C(12B)-C(13B)	123.3(5)	C(41B)-C(46B)-O(7B)	119.7(4)
C(11B)-C(12B)-C(13B)	119.2(6)	C(41B)-C(46B)-C(45B)	121.3(4)
C(14B)-C(13B)-C(18B)	116.3(7)	O(7B)-C(46B)-C(45B)	118.8(4)
C(14B)-C(13B)-C(12B)	117.2(5)	C(36B)-C(47B)-C(50B)	112.3(3)
C(18B)-C(13B)-C(12B)	126.5(5)	C(36B)-C(47B)-C(49B)	112.4(3)
C(15B)-C(14B)-C(13B)	123.4(6)	C(50B)-C(47B)-C(49B)	107.0(4)
C(14B)-C(15B)-C(16B)	118.0(6)	C(36B)-C(47B)-C(48B)	109.1(3)
C(14B)-C(15B)-C(27B)	124.7(7)	C(50B)-C(47B)-C(48B)	106.5(4)
C(16B)-C(15B)-C(27B)	117.3(8)	C(49B)-C(47B)-C(48B)	109.4(3)
C(17B)-C(16B)-C(15B)	121.9(7)	C(52B)-C(51B)-C(38B)	112.0(3)
C(16B)-C(17B)-C(18B)	116.8(5)	C(52B)-C(51B)-C(54B)	108.2(4)

C(38B)-C(51B)-C(54B)	108.0(3)
C(52B)-C(51B)-C(53B)	108.8(4)
C(38B)-C(51B)-C(53B)	110.6(4)
C(54B)-C(51B)-C(53B)	109.2(4)
C(57B)-C(55B)-C(58B)	100.0(11)
C(57B)-C(55B)-C(56B)	110.5(10)
C(58B)-C(55B)-C(56B)	110.4(9)
C(57B)-C(55B)-C(43B)	112.1(6)
C(58B)-C(55B)-C(43B)	111.6(5)
C(56B)-C(55B)-C(43B)	111.7(5)
C(62B)-C(59B)-C(60B)	112.9(5)
C(62B)-C(59B)-C(45B)	110.6(4)
C(60B)-C(59B)-C(45B)	109.6(4)
C(62B)-C(59B)-C(61B)	106.7(4)
C(60B)-C(59B)-C(61B)	107.4(5)
C(45B)-C(59B)-C(61B)	109.5(5)
C(64B)-C(63B)-C(70B)	123.6(4)
C(64B)-C(63B)-Rh(2)	71.5(2)
C(70B)-C(63B)-Rh(2)	111.5(3)
C(63B)-C(64B)-C(65B)	127.0(4)
C(63B)-C(64B)-Rh(2)	73.2(2)
C(65B)-C(64B)-Rh(2)	107.5(3)
C(64B)-C(65B)-C(66B)	114.5(4)
C(67B)-C(66B)-C(65B)	113.7(4)
C(68B)-C(67B)-C(66B)	124.0(5)
C(68B)-C(67B)-Rh(2)	71.9(3)
C(66B)-C(67B)-Rh(2)	111.2(3)
C(67B)-C(68B)-C(69B)	127.6(4)
C(67B)-C(68B)-Rh(2)	73.6(3)
C(69B)-C(68B)-Rh(2)	107.1(3)
C(68B)-C(69B)-C(70B)	114.7(4)
C(63B)-C(70B)-C(69B)	113.1(4)
Cl(1D)-C(1LD)-Cl(2D)	129(2)
F(1)-B(1)-F(4)	109.4(6)
F(1)-B(1)-F(2)	111.4(8)
F(4)-B(1)-F(2)	106.3(7)
F(1)-B(1)-F(3)	112.6(7)
F(4)-B(1)-F(3)	107.6(7)
F(2)-B(1)-F(3)	109.3(6)
F(4B)-B(1B)-F(2B)	107.3(8)
F(4B)-B(1B)-F(3B)	115.4(12)
F(2B)-B(1B)-F(3B)	106.5(13)
F(4B)-B(1B)-F(1B)	105.9(12)
F(2B)-B(1B)-F(1B)	111.8(10)
F(3B)-B(1B)-F(1B)	109.9(8)
Cl(2C)-C(1LC)-Cl(1C)	107.93(8)
Cl(2C)-C(1LC)-Cl(2E)	83.2
Cl(1C)-C(1LC)-Cl(2E)	105.31(9)
Cl(1B)-C(1LB)-Cl(2B)	118.10(13)
Cl(1A)-C(1LA)-Cl(2A)	106.0(11)

Table 6. Torsion angles [°] for [Rh(cod)(**75'a**)]BF_4 (**91'a**).

P(2)-Rh(1)-P(1)-O(3)	143.55(13)
C(64)-Rh(1)-P(1)-O(3)	-56.3(2)
C(68)-Rh(1)-P(1)-O(3)	38.1(4)
C(65)-Rh(1)-P(1)-O(3)	-22.6(2)
C(69)-Rh(1)-P(1)-O(3)	-97.5(4)
P(2)-Rh(1)-P(1)-O(2)	25.97(14)
C(64)-Rh(1)-P(1)-O(2)	-173.9(2)
C(68)-Rh(1)-P(1)-O(2)	-79.5(4)
C(65)-Rh(1)-P(1)-O(2)	-140.2(2)
C(69)-Rh(1)-P(1)-O(2)	144.9(4)
P(2)-Rh(1)-P(1)-O(4)	-95.29(13)
C(64)-Rh(1)-P(1)-O(4)	64.8(2)
C(68)-Rh(1)-P(1)-O(4)	159.2(4)
C(65)-Rh(1)-P(1)-O(4)	98.5(2)
C(69)-Rh(1)-P(1)-O(4)	23.7(5)
P(1)-Rh(1)-P(2)-O(6)	142.02(11)
C(64)-Rh(1)-P(2)-O(6)	38.4(4)
C(68)-Rh(1)-P(2)-O(6)	-56.37(18)
C(65)-Rh(1)-P(2)-O(6)	-97.4(5)
C(69)-Rh(1)-P(2)-O(6)	-23.55(19)
P(1)-Rh(1)-P(2)-O(5)	25.75(15)
C(64)-Rh(1)-P(2)-O(5)	-77.9(4)
C(68)-Rh(1)-P(2)-O(5)	-172.6(2)
C(65)-Rh(1)-P(2)-O(5)	146.3(5)
C(69)-Rh(1)-P(2)-O(5)	-139.8(2)
P(1)-Rh(1)-P(2)-O(7)	-97.04(14)
C(64)-Rh(1)-P(2)-O(7)	159.4(4)
C(68)-Rh(1)-P(2)-O(7)	64.6(2)
C(65)-Rh(1)-P(2)-O(7)	23.5(5)
C(69)-Rh(1)-P(2)-O(7)	97.4(2)
C(3)-O(1)-C(2)-C(5)	-105.9(6)
C(3)-O(1)-C(2)-C(1)	17.4(6)
O(2)-C(1)-C(2)-O(1)	-155.5(4)
C(4)-C(1)-C(2)-O(1)	-33.7(5)
O(2)-C(1)-C(2)-C(5)	-34.9(6)
C(4)-C(1)-C(2)-C(5)	86.9(6)
C(4)-C(1)-O(2)-P(1)	89.2(4)
C(2)-C(1)-O(2)-P(1)	-155.3(3)
O(3)-P(1)-O(2)-C(1)	162.4(3)
O(4)-P(1)-O(2)-C(1)	55.7(3)
Rh(1)-P(1)-O(2)-C(1)	-77.3(3)
C(2)-O(1)-C(3)-C(6)	-118.7(6)
C(2)-O(1)-C(3)-C(4)	6.1(6)
O(2)-P(1)-O(3)-C(7)	-79.5(4)
O(4)-P(1)-O(3)-C(7)	20.0(4)
Rh(1)-P(1)-O(3)-C(7)	151.1(3)
O(2)-C(1)-C(4)-O(5)	-80.5(5)
C(2)-C(1)-C(4)-O(5)	157.7(4)
O(2)-C(1)-C(4)-C(3)	158.4(4)
C(2)-C(1)-C(4)-C(3)	36.6(5)
O(1)-C(3)-C(4)-O(5)	-148.6(4)
C(6)-C(3)-C(4)-O(5)	-26.2(7)
O(1)-C(3)-C(4)-C(1)	-27.1(5)
C(6)-C(3)-C(4)-C(1)	95.3(7)
O(3)-P(1)-O(4)-C(18)	62.3(3)
O(2)-P(1)-O(4)-C(18)	166.8(3)
Rh(1)-P(1)-O(4)-C(18)	-60.2(3)
C(1)-C(4)-O(5)-P(2)	89.7(4)
C(3)-C(4)-O(5)-P(2)	-155.4(3)
O(6)-P(2)-O(5)-C(4)	163.1(3)
O(7)-P(2)-O(5)-C(4)	56.3(3)
Rh(1)-P(2)-O(5)-C(4)	-77.3(3)
O(5)-P(2)-O(6)-C(36)	-81.2(3)
O(7)-P(2)-O(6)-C(36)	19.3(3)
Rh(1)-P(2)-O(6)-C(36)	149.8(3)
P(1)-O(3)-C(7)-C(8)	132.9(4)
P(1)-O(3)-C(7)-C(12)	-55.7(5)
O(6)-P(2)-O(7)-C(47)	62.8(3)
O(5)-P(2)-O(7)-C(47)	166.5(3)
Rh(1)-P(2)-O(7)-C(47)	-59.5(3)
O(3)-C(7)-C(8)-C(9)	176.6(4)
C(12)-C(7)-C(8)-C(9)	5.6(6)
O(3)-C(7)-C(8)-C(19)	-2.5(6)
C(12)-C(7)-C(8)-C(19)	-173.5(4)
C(7)-C(8)-C(9)-C(10)	-2.4(7)
C(19)-C(8)-C(9)-C(10)	176.7(5)
C(8)-C(9)-C(10)-C(11)	-1.3(7)

C(8)-C(9)-C(10)-C(23)	179.6(5)	O(6)-C(36)-C(37)-C(48)	-0.6(6)
C(9)-C(10)-C(11)-C(12)	1.9(7)	C(41)-C(36)-C(37)-C(48)	-173.5(4)
C(23)-C(10)-C(11)-C(12)	-178.9(4)	C(36)-C(37)-C(38)-C(39)	-2.4(6)
C(10)-C(11)-C(12)-C(7)	1.1(6)	C(48)-C(37)-C(38)-C(39)	176.0(4)
C(10)-C(11)-C(12)-C(13)	-177.8(4)	C(37)-C(38)-C(39)-C(40)	-0.9(6)
C(8)-C(7)-C(12)-C(11)	-5.0(6)	C(37)-C(38)-C(39)-C(52)	-178.5(4)
O(3)-C(7)-C(12)-C(11)	-176.1(4)	C(38)-C(39)-C(40)-C(41)	2.0(6)
C(8)-C(7)-C(12)-C(13)	173.8(4)	C(52)-C(39)-C(40)-C(41)	179.6(4)
O(3)-C(7)-C(12)-C(13)	2.7(6)	C(39)-C(40)-C(41)-C(36)	0.3(6)
C(11)-C(12)-C(13)-C(18)	-131.1(4)	C(39)-C(40)-C(41)-C(42)	-174.7(4)
C(7)-C(12)-C(13)-C(18)	50.1(6)	O(6)-C(36)-C(41)-C(40)	-176.8(3)
C(11)-C(12)-C(13)-C(14)	43.2(5)	C(37)-C(36)-C(41)-C(40)	-3.9(6)
C(7)-C(12)-C(13)-C(14)	-135.6(4)	O(6)-C(36)-C(41)-C(42)	-2.3(6)
C(18)-C(13)-C(14)-C(15)	2.2(6)	C(37)-C(36)-C(41)-C(42)	170.6(4)
C(12)-C(13)-C(14)-C(15)	-172.4(4)	C(40)-C(41)-C(42)-C(47)	-133.2(4)
C(13)-C(14)-C(15)-C(16)	6.2(6)	C(36)-C(41)-C(42)-C(47)	52.2(6)
C(13)-C(14)-C(15)-C(27)	-175.9(4)	C(40)-C(41)-C(42)-C(43)	44.8(5)
C(14)-C(15)-C(16)-C(17)	-6.5(6)	C(36)-C(41)-C(42)-C(43)	-129.8(4)
C(27)-C(15)-C(16)-C(17)	175.6(4)	C(47)-C(42)-C(43)-C(44)	1.7(6)
C(15)-C(16)-C(17)-C(18)	-1.7(6)	C(41)-C(42)-C(43)-C(44)	-176.4(4)
C(15)-C(16)-C(17)-C(31)	176.1(4)	C(42)-C(43)-C(44)-C(45)	4.3(6)
C(16)-C(17)-C(18)-C(13)	10.9(6)	C(42)-C(43)-C(44)-C(56)	-173.7(4)
C(31)-C(17)-C(18)-C(13)	-166.8(4)	C(43)-C(44)-C(45)-C(46)	-4.9(7)
C(16)-C(17)-C(18)-O(4)	-173.5(3)	C(56)-C(44)-C(45)-C(46)	173.0(4)
C(31)-C(17)-C(18)-O(4)	8.8(5)	C(44)-C(45)-C(46)-C(47)	-0.4(7)
C(14)-C(13)-C(18)-C(17)	-11.2(6)	C(44)-C(45)-C(46)-C(60)	176.8(4)
C(12)-C(13)-C(18)-C(17)	163.2(4)	C(43)-C(42)-C(47)-O(7)	171.5(3)
C(14)-C(13)-C(18)-O(4)	173.0(3)	C(41)-C(42)-C(47)-O(7)	-10.4(6)
C(12)-C(13)-C(18)-O(4)	-12.5(5)	C(43)-C(42)-C(47)-C(46)	-7.4(6)
P(1)-O(4)-C(18)-C(17)	118.5(3)	C(41)-C(42)-C(47)-C(46)	170.6(4)
P(1)-O(4)-C(18)-C(13)	-65.6(4)	P(2)-O(7)-C(47)-C(42)	-67.7(4)
C(7)-C(8)-C(19)-C(20)	-66.4(7)	P(2)-O(7)-C(47)-C(46)	111.3(4)
C(9)-C(8)-C(19)-C(20)	114.5(6)	C(45)-C(46)-C(47)-C(42)	6.8(6)
C(7)-C(8)-C(19)-C(22)	174.6(5)	C(60)-C(46)-C(47)-C(42)	-170.2(4)
C(9)-C(8)-C(19)-C(22)	-4.4(7)	C(45)-C(46)-C(47)-O(7)	-172.2(4)
C(7)-C(8)-C(19)-C(21)	56.4(6)	C(60)-C(46)-C(47)-O(7)	10.9(7)
C(9)-C(8)-C(19)-C(21)	-122.7(5)	C(36)-C(37)-C(48)-C(51)	173.0(4)
C(9)-C(10)-C(23)-C(26)	63.6(9)	C(38)-C(37)-C(48)-C(51)	-5.3(6)
C(11)-C(10)-C(23)-C(26)	-115.5(9)	C(36)-C(37)-C(48)-C(49)	54.3(6)
C(9)-C(10)-C(23)-C(24)	-62.9(7)	C(38)-C(37)-C(48)-C(49)	-124.0(4)
C(11)-C(10)-C(23)-C(24)	117.9(6)	C(36)-C(37)-C(48)-C(50)	-67.6(5)
C(9)-C(10)-C(23)-C(25)	177.3(6)	C(38)-C(37)-C(48)-C(50)	114.1(4)
C(11)-C(10)-C(23)-C(25)	-1.8(7)	C(40)-C(39)-C(52)-C(53)	57.7(6)
C(14)-C(15)-C(27)-C(28')	50.8(12)	C(38)-C(39)-C(52)-C(53)	-124.8(5)
C(16)-C(15)-C(27)-C(28')	-131.4(11)	C(40)-C(39)-C(52)-C(54)	-62.2(6)
C(14)-C(15)-C(27)-C(30)	-112.8(6)	C(38)-C(39)-C(52)-C(54)	115.2(5)
C(16)-C(15)-C(27)-C(30)	65.0(7)	C(40)-C(39)-C(52)-C(55)	-178.8(5)
C(14)-C(15)-C(27)-C(29')	-178.4(8)	C(38)-C(39)-C(52)-C(55)	-1.3(6)
C(16)-C(15)-C(27)-C(29')	-0.6(9)	C(45)-C(44)-C(56)-C(59')	54.2(11)
C(14)-C(15)-C(27)-C(28)	15.3(7)	C(43)-C(44)-C(56)-C(59')	-127.9(10)
C(16)-C(15)-C(27)-C(28)	-166.9(6)	C(45)-C(44)-C(56)-C(57)	-123.0(6)
C(14)-C(15)-C(27)-C(29)	128.0(5)	C(43)-C(44)-C(56)-C(57)	54.8(7)
C(16)-C(15)-C(27)-C(29)	-54.2(6)	C(45)-C(44)-C(56)-C(59)	7.8(8)
C(14)-C(15)-C(27)-C(30')	-64.3(7)	C(43)-C(44)-C(56)-C(59)	-174.3(7)
C(16)-C(15)-C(27)-C(30')	113.5(6)	C(45)-C(44)-C(56)-C(58')	-173.3(8)
C(18)-C(17)-C(31)-C(34)	-70.4(5)	C(43)-C(44)-C(56)-C(58')	4.6(9)
C(16)-C(17)-C(31)-C(34)	112.0(4)	C(45)-C(44)-C(56)-C(58)	121.7(5)
C(18)-C(17)-C(31)-C(33)	51.6(5)	C(43)-C(44)-C(56)-C(58)	-60.4(6)
C(16)-C(17)-C(31)-C(33)	-126.0(4)	C(45)-C(44)-C(56)-C(57')	-64.7(8)
C(18)-C(17)-C(31)-C(32)	170.0(4)	C(43)-C(44)-C(56)-C(57')	113.2(7)
C(16)-C(17)-C(31)-C(32)	-7.7(6)	C(45)-C(46)-C(60)-C(61')	-121.3(9)
P(2)-O(6)-C(36)-C(41)	-52.3(5)	C(47)-C(46)-C(60)-C(61')	55.6(10)
P(2)-O(6)-C(36)-C(37)	134.6(3)	C(45)-C(46)-C(60)-C(62)	55.7(6)
O(6)-C(36)-C(37)-C(38)	177.7(3)	C(47)-C(46)-C(60)-C(62)	-127.3(6)
C(41)-C(36)-C(37)-C(38)	4.9(6)	C(45)-C(46)-C(60)-C(63)	-177.0(6)

C(47)-C(46)-C(60)-C(63)	-0.1(8)	O(2B)-P(1B)-Rh(2)-C(64B)	-132.5(3)
C(45)-C(46)-C(60)-C(62')	0.4(12)	O(4B)-P(1B)-Rh(2)-C(64B)	-11.4(3)
C(47)-C(46)-C(60)-C(62')	177.3(11)	O(3B)-P(1B)-Rh(2)-C(64B)	106.5(3)
C(45)-C(46)-C(60)-C(61)	-61.5(6)	O(2B)-P(1B)-Rh(2)-C(67B)	163.3(2)
C(47)-C(46)-C(60)-C(61)	115.4(6)	O(4B)-P(1B)-Rh(2)-C(67B)	-75.6(2)
C(45)-C(46)-C(60)-C(63')	118.7(7)	O(3B)-P(1B)-Rh(2)-C(67B)	42.4(2)
C(47)-C(46)-C(60)-C(63')	-64.4(8)	O(2B)-P(1B)-Rh(2)-C(63B)	90.8(5)
P(1)-Rh(1)-C(64)-C(65)	95.9(3)	O(4B)-P(1B)-Rh(2)-C(63B)	-148.1(5)
P(2)-Rh(1)-C(64)-C(65)	-159.7(3)	O(3B)-P(1B)-Rh(2)-C(63B)	-30.1(5)
C(68)-Rh(1)-C(64)-C(65)	-65.1(3)	C(3B)-O(1B)-C(2B)-C(5B)	-148.8(5)
C(69)-Rh(1)-C(64)-C(65)	-95.2(3)	C(3B)-O(1B)-C(2B)-C(1B)	-25.2(6)
P(1)-Rh(1)-C(64)-C(71)	-138.0(3)	O(2B)-C(1B)-C(2B)-O(1B)	-124.2(4)
P(2)-Rh(1)-C(64)-C(71)	-33.6(6)	C(4B)-C(1B)-C(2B)-O(1B)	-2.3(5)
C(68)-Rh(1)-C(64)-C(71)	61.1(3)	O(2B)-C(1B)-C(2B)-C(5B)	-5.1(7)
C(65)-Rh(1)-C(64)-C(71)	126.2(5)	C(4B)-C(1B)-C(2B)-C(5B)	116.8(5)
C(69)-Rh(1)-C(64)-C(71)	31.0(3)	C(4B)-C(1B)-O(2B)-P(1B)	55.8(5)
C(71)-C(64)-C(65)-C(66)	7.4(9)	C(2B)-C(1B)-O(2B)-P(1B)	171.1(4)
Rh(1)-C(64)-C(65)-C(66)	105.0(5)	O(4B)-P(1B)-O(2B)-C(1B)	-100.0(4)
C(71)-C(64)-C(65)-Rh(1)	-97.6(6)	O(3B)-P(1B)-O(2B)-C(1B)	153.7(4)
P(1)-Rh(1)-C(65)-C(64)	-85.2(3)	Rh(2)-P(1B)-O(2B)-C(1B)	26.4(5)
P(2)-Rh(1)-C(65)-C(64)	154.1(4)	C(2B)-O(1B)-C(3B)-C(6B)	-79.9(5)
C(68)-Rh(1)-C(65)-C(64)	111.8(4)	C(2B)-O(1B)-C(3B)-C(4B)	41.8(5)
C(69)-Rh(1)-C(65)-C(64)	78.7(4)	O(2B)-P(1B)-O(3B)-C(7B)	31.0(4)
P(1)-Rh(1)-C(65)-C(66)	154.1(4)	O(4B)-P(1B)-O(3B)-C(7B)	-72.4(4)
P(2)-Rh(1)-C(65)-C(66)	33.3(8)	Rh(2)-P(1B)-O(3B)-C(7B)	164.9(4)
C(64)-Rh(1)-C(65)-C(66)	-120.7(6)	O(1B)-C(3B)-C(4B)-O(5B)	-167.4(4)
C(68)-Rh(1)-C(65)-C(66)	-8.9(4)	C(6B)-C(3B)-C(4B)-O(5B)	-45.6(6)
C(69)-Rh(1)-C(65)-C(66)	-42.0(4)	O(1B)-C(3B)-C(4B)-C(1B)	-41.6(5)
C(64)-C(65)-C(66)-C(67)	-95.2(6)	C(6B)-C(3B)-C(4B)-C(1B)	80.2(5)
Rh(1)-C(65)-C(66)-C(67)	-12.7(6)	O(2B)-C(1B)-C(4B)-O(5B)	-91.3(5)
C(65)-C(66)-C(67)-C(68)	40.0(7)	C(2B)-C(1B)-C(4B)-O(5B)	149.5(4)
C(66)-C(67)-C(68)-C(69)	36.4(8)	O(2B)-C(1B)-C(4B)-C(3B)	145.6(4)
C(66)-C(67)-C(68)-Rh(1)	-45.5(5)	C(2B)-C(1B)-C(4B)-C(3B)	26.4(5)
P(1)-Rh(1)-C(68)-C(69)	-158.5(3)	O(2B)-P(1B)-O(4B)-C(18B)	-108.9(4)
P(2)-Rh(1)-C(68)-C(69)	95.3(3)	O(3B)-P(1B)-O(4B)-C(18B)	-6.2(5)
C(64)-Rh(1)-C(68)-C(69)	-64.3(3)	Rh(2)-P(1B)-O(4B)-C(18B)	117.4(4)
C(65)-Rh(1)-C(68)-C(69)	-95.4(3)	P(1B)-Rh(2)-P(2B)-O(5B)	-29.97(14)
P(1)-Rh(1)-C(68)-C(67)	-35.3(6)	C(68B)-Rh(2)-P(2B)-O(5B)	-134.3(4)
P(2)-Rh(1)-C(68)-C(67)	-141.5(3)	C(64B)-Rh(2)-P(2B)-O(5B)	125.84(18)
C(64)-Rh(1)-C(68)-C(67)	58.9(4)	C(67B)-Rh(2)-P(2B)-O(5B)	79.4(5)
C(65)-Rh(1)-C(68)-C(67)	27.8(3)	C(63B)-Rh(2)-P(2B)-O(5B)	161.10(18)
C(69)-Rh(1)-C(68)-C(67)	123.2(5)	P(1B)-Rh(2)-P(2B)-O(6B)	-147.56(14)
C(67)-C(68)-C(69)-C(70)	5.9(9)	C(68B)-Rh(2)-P(2B)-O(6B)	108.1(4)
Rh(1)-C(68)-C(69)-C(70)	104.6(5)	C(64B)-Rh(2)-P(2B)-O(6B)	8.25(18)
C(67)-C(68)-C(69)-Rh(1)	-98.8(5)	C(67B)-Rh(2)-P(2B)-O(6B)	-38.2(5)
P(1)-Rh(1)-C(69)-C(68)	155.0(4)	C(63B)-Rh(2)-P(2B)-O(6B)	43.50(17)
P(2)-Rh(1)-C(69)-C(68)	-85.8(3)	P(1B)-Rh(2)-P(2B)-O(7B)	93.08(13)
C(64)-Rh(1)-C(69)-C(68)	112.7(3)	C(68B)-Rh(2)-P(2B)-O(7B)	-11.2(4)
C(65)-Rh(1)-C(69)-C(68)	78.7(3)	C(64B)-Rh(2)-P(2B)-O(7B)	-111.11(17)
P(1)-Rh(1)-C(69)-C(70)	31.0(7)	C(67B)-Rh(2)-P(2B)-O(7B)	-157.5(5)
P(2)-Rh(1)-C(69)-C(70)	150.2(3)	C(63B)-Rh(2)-P(2B)-O(7B)	-75.86(17)
C(64)-Rh(1)-C(69)-C(70)	-11.4(4)	C(3B)-C(4B)-O(5B)-P(2B)	129.6(4)
C(68)-Rh(1)-C(69)-C(70)	-124.0(5)	C(1B)-C(4B)-O(5B)-P(2B)	11.5(6)
C(65)-Rh(1)-C(69)-C(70)	-45.4(4)	O(6B)-P(2B)-O(5B)-C(4B)	-178.5(3)
C(68)-C(69)-C(70)-C(71)	-96.0(7)	O(7B)-P(2B)-O(5B)-C(4B)	-71.7(4)
Rh(1)-C(69)-C(70)-C(71)	-11.5(6)	Rh(2)-P(2B)-O(5B)-C(4B)	57.5(4)
C(69)-C(70)-C(71)-C(64)	41.7(7)	O(5B)-P(2B)-O(6B)-C(35B)	40.7(3)
C(65)-C(64)-C(71)-C(70)	33.0(8)	O(7B)-P(2B)-O(6B)-C(35B)	-64.0(3)
Rh(1)-C(64)-C(71)-C(70)	-49.4(5)	Rh(2)-P(2B)-O(6B)-C(35B)	170.6(2)
O(2B)-P(1B)-Rh(2)-P(2B)	-30.93(18)	P(1B)-O(3B)-C(7B)-C(8B)	-109.6(4)
O(4B)-P(1B)-Rh(2)-P(2B)	90.17(14)	P(1B)-O(3B)-C(7B)-C(12B)	68.8(5)
O(3B)-P(1B)-Rh(2)-P(2B)	-151.87(17)	O(5B)-P(2B)-O(7B)-C(46B)	-121.7(3)
O(2B)-P(1B)-Rh(2)-C(68B)	128.8(2)	O(6B)-P(2B)-O(7B)-C(46B)	-18.7(4)
O(4B)-P(1B)-Rh(2)-C(68B)	-110.1(2)	Rh(2)-P(2B)-O(7B)-C(46B)	105.2(3)
O(3B)-P(1B)-Rh(2)-C(68B)	7.9(2)	C(12B)-C(7B)-C(8B)-C(9B)	-5.8(7)

O(3B)-C(7B)-C(8B)-C(9B)	172.5(4)
C(12B)-C(7B)-C(8B)-C(19B)	172.2(5)
O(3B)-C(7B)-C(8B)-C(19B)	-9.4(7)
C(7B)-C(8B)-C(9B)-C(10B)	-0.1(7)
C(19B)-C(8B)-C(9B)-C(10B)	-178.3(5)
C(8B)-C(9B)-C(10B)-C(11B)	5.1(8)
C(8B)-C(9B)-C(10B)-C(23B)	-173.8(5)
C(9B)-C(10B)-C(11B)-C(12B)	-4.4(9)
C(23B)-C(10B)-C(11B)-C(12B)	174.5(5)
C(8B)-C(7B)-C(12B)-C(11B)	6.6(7)
O(3B)-C(7B)-C(12B)-C(11B)	-171.9(4)
C(8B)-C(7B)-C(12B)-C(13B)	-168.9(5)
O(3B)-C(7B)-C(12B)-C(13B)	12.7(7)
C(10B)-C(11B)-C(12B)-C(7B)	-1.2(8)
C(10B)-C(11B)-C(12B)-C(13B)	174.5(5)
C(7B)-C(12B)-C(13B)-C(14B)	131.0(6)
C(11B)-C(12B)-C(13B)-C(14B)	-44.4(8)
C(7B)-C(12B)-C(13B)-C(18B)	-49.8(8)
C(11B)-C(12B)-C(13B)-C(18B)	134.8(6)
C(18B)-C(13B)-C(14B)-C(15B)	-0.2(10)
C(12B)-C(13B)-C(14B)-C(15B)	179.1(6)
C(13B)-C(14B)-C(15B)-C(16B)	-2.2(11)
C(13B)-C(14B)-C(15B)-C(27B)	178.0(8)
C(14B)-C(15B)-C(16B)-C(17B)	0.4(11)
C(27B)-C(15B)-C(16B)-C(17B)	-179.7(7)
C(15B)-C(16B)-C(17B)-C(18B)	3.6(9)
C(15B)-C(16B)-C(17B)-C(31B)	-173.4(6)
C(16B)-C(17B)-C(18B)-O(4B)	-179.3(5)
C(31B)-C(17B)-C(18B)-O(4B)	-2.4(8)
C(16B)-C(17B)-C(18B)-C(13B)	-6.3(8)
C(31B)-C(17B)-C(18B)-C(13B)	170.6(5)
P(1B)-O(4B)-C(18B)-C(17B)	-140.9(4)
P(1B)-O(4B)-C(18B)-C(13B)	45.8(7)
C(14B)-C(13B)-C(18B)-C(17B)	4.6(9)
C(12B)-C(13B)-C(18B)-C(17B)	-174.5(5)
C(14B)-C(13B)-C(18B)-O(4B)	177.5(5)
C(12B)-C(13B)-C(18B)-O(4B)	-1.6(8)
C(7B)-C(8B)-C(19B)-C(22B)	-173.5(4)
C(9B)-C(8B)-C(19B)-C(22B)	4.5(6)
C(7B)-C(8B)-C(19B)-C(21B)	64.4(6)
C(9B)-C(8B)-C(19B)-C(21B)	-117.6(5)
C(7B)-C(8B)-C(19B)-C(20B)	-55.8(6)
C(9B)-C(8B)-C(19B)-C(20B)	122.2(5)
C(11B)-C(10B)-C(23B)-C(25B)	49.6(8)
C(9B)-C(10B)-C(23B)-C(25B)	-131.6(8)
C(11B)-C(10B)-C(23B)-C(26B)	-70.1(10)
C(9B)-C(10B)-C(23B)-C(26B)	108.7(8)
C(11B)-C(10B)-C(23B)-C(24B)	173.2(7)
C(9B)-C(10B)-C(23B)-C(24B)	-8.0(9)
C(14B)-C(15B)-C(27B)-C(30B)	-110.8(10)
C(16B)-C(15B)-C(27B)-C(30B)	69.4(9)
C(14B)-C(15B)-C(27B)-C(29B)	123.8(10)
C(16B)-C(15B)-C(27B)-C(29B)	-56.0(12)
C(14B)-C(15B)-C(27B)-C(28B)	7.3(12)
C(16B)-C(15B)-C(27B)-C(28B)	-172.5(8)
C(16B)-C(17B)-C(31B)-C(32B)	-2.5(8)
C(18B)-C(17B)-C(31B)-C(32B)	-179.3(5)
C(16B)-C(17B)-C(31B)-C(34B)	-123.5(6)
C(18B)-C(17B)-C(31B)-C(34B)	59.7(7)
C(16B)-C(17B)-C(31B)-C(33B)	115.8(6)
C(18B)-C(17B)-C(31B)-C(33B)	-61.0(7)
P(2B)-O(6B)-C(35B)-C(36B)	-113.9(3)
P(2B)-O(6B)-C(35B)-C(40B)	69.3(4)
C(40B)-C(35B)-C(36B)-C(37B)	-10.1(5)
O(6B)-C(35B)-C(36B)-C(37B)	173.4(3)
C(40B)-C(35B)-C(36B)-C(47B)	167.9(4)
O(6B)-C(35B)-C(36B)-C(47B)	-8.6(5)
C(35B)-C(36B)-C(37B)-C(38B)	2.9(5)
C(47B)-C(36B)-C(37B)-C(38B)	-175.2(3)
C(36B)-C(37B)-C(38B)-C(39B)	4.9(5)
C(36B)-C(37B)-C(38B)-C(51B)	-174.7(3)
C(37B)-C(38B)-C(39B)-C(40B)	-6.2(5)
C(51B)-C(38B)-C(39B)-C(40B)	173.4(3)
C(36B)-C(35B)-C(40B)-C(39B)	9.0(5)
O(6B)-C(35B)-C(40B)-C(39B)	-174.4(3)
C(36B)-C(35B)-C(40B)-C(41B)	-166.6(4)
O(6B)-C(35B)-C(40B)-C(41B)	10.1(5)
C(38B)-C(39B)-C(40B)-C(35B)	-0.4(5)
C(38B)-C(39B)-C(40B)-C(41B)	175.4(3)
C(35B)-C(40B)-C(41B)-C(46B)	-50.7(6)
C(39B)-C(40B)-C(41B)-C(46B)	133.8(4)
C(35B)-C(40B)-C(41B)-C(42B)	129.8(4)
C(39B)-C(40B)-C(41B)-C(42B)	-45.7(5)
C(46B)-C(41B)-C(42B)-C(43B)	-0.3(6)
C(40B)-C(41B)-C(42B)-C(43B)	179.2(4)
C(41B)-C(42B)-C(43B)-C(44B)	-3.6(6)
C(41B)-C(42B)-C(43B)-C(55B)	177.0(4)
C(42B)-C(43B)-C(44B)-C(45B)	3.2(7)
C(55B)-C(43B)-C(44B)-C(45B)	-177.3(4)
C(43B)-C(44B)-C(45B)-C(46B)	1.1(7)
C(43B)-C(44B)-C(45B)-C(59B)	-175.6(4)
C(42B)-C(41B)-C(46B)-O(7B)	178.8(3)
C(40B)-C(41B)-C(46B)-O(7B)	-0.7(6)
C(42B)-C(41B)-C(46B)-C(45B)	4.9(6)
C(40B)-C(41B)-C(46B)-C(45B)	-174.6(4)
P(2B)-O(7B)-C(46B)-C(41B)	54.3(5)
P(2B)-O(7B)-C(46B)-C(45B)	-131.6(4)
C(44B)-C(45B)-C(46B)-C(41B)	-5.2(6)
C(59B)-C(45B)-C(46B)-C(41B)	171.4(4)
C(44B)-C(45B)-C(46B)-O(7B)	-179.1(4)
C(59B)-C(45B)-C(46B)-O(7B)	-2.5(6)
C(35B)-C(36B)-C(47B)-C(50B)	-176.9(4)
C(37B)-C(36B)-C(47B)-C(50B)	1.0(5)
C(35B)-C(36B)-C(47B)-C(49B)	62.3(5)
C(37B)-C(36B)-C(47B)-C(49B)	-119.7(4)
C(35B)-C(36B)-C(47B)-C(48B)	-59.1(5)
C(37B)-C(36B)-C(47B)-C(48B)	118.8(4)
C(37B)-C(38B)-C(51B)-C(52B)	-10.7(5)
C(39B)-C(38B)-C(51B)-C(52B)	169.7(4)
C(37B)-C(38B)-C(51B)-C(54B)	108.3(4)
C(39B)-C(38B)-C(51B)-C(54B)	-71.2(5)
C(37B)-C(38B)-C(51B)-C(53B)	-132.3(4)
C(39B)-C(38B)-C(51B)-C(53B)	48.2(5)
C(42B)-C(43B)-C(55B)-C(57B)	-3.9(12)
C(44B)-C(43B)-C(55B)-C(57B)	176.6(11)
C(42B)-C(43B)-C(55B)-C(58B)	-115.1(10)
C(44B)-C(43B)-C(55B)-C(58B)	65.4(10)
C(42B)-C(43B)-C(55B)-C(56B)	120.7(8)
C(44B)-C(43B)-C(55B)-C(56B)	-58.8(9)
C(44B)-C(45B)-C(59B)-C(62B)	-119.4(5)
C(46B)-C(45B)-C(59B)-C(62B)	64.1(6)
C(44B)-C(45B)-C(59B)-C(60B)	115.5(5)
C(46B)-C(45B)-C(59B)-C(60B)	-61.0(6)
C(44B)-C(45B)-C(59B)-C(61B)	-2.0(6)
C(46B)-C(45B)-C(59B)-C(61B)	-178.5(4)
P(2B)-Rh(2)-C(63B)-C(64B)	-87.8(2)
P(1B)-Rh(2)-C(63B)-C(64B)	150.2(4)
C(68B)-Rh(2)-C(63B)-C(64B)	111.3(3)
C(67B)-Rh(2)-C(63B)-C(64B)	77.2(3)
P(2B)-Rh(2)-C(63B)-C(70B)	152.5(3)

P(1B)-Rh(2)-C(63B)-C(70B)	30.5(7)
C(68B)-Rh(2)-C(63B)-C(70B)	-8.4(3)
C(64B)-Rh(2)-C(63B)-C(70B)	-119.7(4)
C(67B)-Rh(2)-C(63B)-C(70B)	-42.5(3)
C(70B)-C(63B)-C(64B)-C(65B)	4.4(7)
Rh(2)-C(63B)-C(64B)-C(65B)	-99.6(4)
C(70B)-C(63B)-C(64B)-Rh(2)	104.0(4)
P(2B)-Rh(2)-C(64B)-C(63B)	93.0(2)
P(1B)-Rh(2)-C(64B)-C(63B)	-164.4(2)
C(68B)-Rh(2)-C(64B)-C(63B)	-66.4(3)
C(67B)-Rh(2)-C(64B)-C(63B)	-98.1(3)
P(2B)-Rh(2)-C(64B)-C(65B)	-142.6(3)
P(1B)-Rh(2)-C(64B)-C(65B)	-40.1(5)
C(68B)-Rh(2)-C(64B)-C(65B)	58.0(3)
C(67B)-Rh(2)-C(64B)-C(65B)	26.3(3)
C(63B)-Rh(2)-C(64B)-C(65B)	124.4(4)
C(63B)-C(64B)-C(65B)-C(66B)	40.2(6)
Rh(2)-C(64B)-C(65B)-C(66B)	-41.6(5)
C(64B)-C(65B)-C(66B)-C(67B)	36.3(6)
C(65B)-C(66B)-C(67B)-C(68B)	-93.1(6)
C(65B)-C(66B)-C(67B)-Rh(2)	-11.2(6)
P(2B)-Rh(2)-C(67B)-C(68B)	159.5(4)
P(1B)-Rh(2)-C(67B)-C(68B)	-90.5(3)
C(64B)-Rh(2)-C(67B)-C(68B)	112.0(3)
C(63B)-Rh(2)-C(67B)-C(68B)	77.0(3)
P(2B)-Rh(2)-C(67B)-C(66B)	39.2(8)
P(1B)-Rh(2)-C(67B)-C(66B)	149.2(4)
C(68B)-Rh(2)-C(67B)-C(66B)	-120.3(5)
C(64B)-Rh(2)-C(67B)-C(66B)	-8.3(4)
C(63B)-Rh(2)-C(67B)-C(66B)	-43.3(4)
C(66B)-C(67B)-C(68B)-C(69B)	4.6(7)
Rh(2)-C(67B)-C(68B)-C(69B)	-99.2(5)
C(66B)-C(67B)-C(68B)-Rh(2)	103.8(4)
P(2B)-Rh(2)-C(68B)-C(67B)	-165.2(3)
P(1B)-Rh(2)-C(68B)-C(67B)	89.8(3)
C(64B)-Rh(2)-C(68B)-C(67B)	-65.7(3)
C(63B)-Rh(2)-C(68B)-C(67B)	-98.3(3)
P(2B)-Rh(2)-C(68B)-C(69B)	-40.1(6)
P(1B)-Rh(2)-C(68B)-C(69B)	-145.1(3)
C(64B)-Rh(2)-C(68B)-C(69B)	59.4(4)
C(67B)-Rh(2)-C(68B)-C(69B)	125.1(5)
C(63B)-Rh(2)-C(68B)-C(69B)	26.8(3)
C(67B)-C(68B)-C(69B)-C(70B)	39.7(7)
Rh(2)-C(68B)-C(69B)-C(70B)	-42.5(5)
C(64B)-C(63B)-C(70B)-C(69B)	-92.9(5)
Rh(2)-C(63B)-C(70B)-C(69B)	-11.3(5)
C(68B)-C(69B)-C(70B)-C(63B)	37.2(6)

List of papers and meeting contributions

- List of papers:

Rui M.D. Nunes, Andreia F. Peixoto, M. Rosa Axet, Mariette M. Pereira, Maria José Moreno, László Kollár, Carmen Claver, Sergio Castillón
Selective hydrogenation of α,β-unsaturated oxosteroids with homogeneous rhodium catalysts
Journal of Molecular Catalysis A: Chemical, in press.

M. Rosa Axet, Sergio Castillón, Carmen Claver
Rhodium-diphosphite catalysed hydroformylation of allylbenzene and propenylbenzene derivatives
Inorganica Chimica Acta, in press. (Chapter 3)

M. Rosa Axet, Jordi Benet-Buchholz, Sergio Castillón, Carmen Claver
Carbohydrate derivative diphosphite ligands in asymmetric catalysis
To be submitted to Organometallics (Chapter 2)

- Meeting contributions:

M. Rosa Axet, Sergio Castillón, Carmen Claver
Ligandos quirales modificables para reacciones de hidrogenación e hidroformilación enantioselectiva
XXIX Reunión Biennal de la Sociedad Española de Química.
Madrid, Spain. 2003. Poster communication.

M. Rosa Axet, Sergio Castillón, Carmen Claver
New chiral diphosphites with sugar backbone and C_2-symmetry
14th International Symposium on Homogeneous Catalysis.
Munich, Germany. 2004. Poster communication.

M. Rosa Axet, Sergio Castillón, Carmen Claver, Karine Philippot, Bruno Chaudret
Stabilization of metal nanoparticles with carbohydrate

derivative ligands. Application in catalysis.
12th International Symposium on Relations between Homogeneous and Heteregeneous Catalysis.

Florence, Italy. 2005. Poster communication.
M. Rosa Axet, Sergio Castillón, Carmen Claver
Ligandos quirales modificables para reacciones de carbonilación enantioselectiva
Proyecto CYTED V.9. Reunion de coordinación
Huelva, Spain. 2003. Oral communication.

M. Rosa Axet, Sergio Castillón, Carmen Claver
Ligandos quirales modificables para reacciones de carbonilación enantioselectiva
Proyecto CYTED V.9. Reunion de coordinación
Coimbra, Portugal. 2004. Oral communication.

M. Rosa Axet, Sergio Castillón, Carmen Claver, Karine Philippot, Bruno Chaudret
Metal nanoparticles stabilized by chiral ligands with carbohydrate backbone
2nd NANOPARTICULES MÉTALLIQUES EN CATALYSE (NANOMETCAT).PICS meeting
Toulouse, France. 2004. Oral communication.

M. Rosa Axet, Sergio Castillón, Carmen Claver
Carbohydrate derivative ligands in asymmetric catalysis.
Application in stabilization of metal nanoparticles
Proyecto CYTED V.9. Reunion de coordinación
Salou, Spain. 2005. Oral communication.

M. Rosa Axet, Sergio Castillón, Carmen Claver, Karine Philippot, Bruno Chaudret
Stabilization of metal nanoparticles with carbohydrate derivative ligands.
Application in catalysis
3rd NANOPARTICULES MÉTALLIQUES EN CATALYSE (NANOMETCAT).PICS meeting
Tarragona, Spain. 2005. Oral communication.